SHOCK TUBE PYROLYSIS OF SELECTED LOW-MOLECULAR WEIGHT ALIPHATIC HYDROCARBONS

BY

EMENIKE NYECHE WAMI

A thesis submitted for the Degree of Doctor of Philosophy,
UNIVERSITY OF LONDON

Department of Chemical Engineering and Chemical Technology,
Imperial College of Science and Technology,
London, S.W.7.

December, 1979.

ABSTRACT

This thesis consists of parts A and B. Part A is a study of the pyrolysis of propane using the single-pulse shock tube technique. Part B deals with time resolved infrared spectroscopy applied to the pyrolysis of acetylene in a shock tube at a wavelength range of 2.0µm to 5.3µm.

A survey of the literature has been carried out on the pyrolysis of propane and acetylene, and on the use of the shock tube as a chemical reactor.

The pyrolysis of propane at temperatures between 1200 and 2800°K and 500 to 1500 KN/m^2 reaction zone pressure, showed that it is a first order reaction. The product distribution at these temperatures is quite different from those reported at lower temperatures. C_2H_2, C_2H_4, and CH_4 are the major reaction products in order of decreasing importance. C_2H_6 and C_3H_6 are present only at temperatures under 1500°K.

The effects of variation of reaction time, temperature and the total reaction zone pressure, on propane conversion to the major products showed that the maximum conversion of propane to methane and ethylene were only dependent on the temperature and not sensitive to variation in reaction times. Optimum propane conversion to acetylene was very sensitive to reaction time. At reaction times above 0.5ms, increase reaction pressure beyond 550 KN/m^2 does not favour the conversion of propane to acetylene.

Propane pyrolysis was accelerated by the addition of 0.1 to 0.9% of ethane due possibly to increase radical concentrations, especially methyl radicals and atomic hydrogen. Secondary reactions, involving radical dissociations and decomposition of the primary products were thought to be the

major factor influencing the kinetics between 1200°K and 2800°K temperatures.

Pyrolysis of acetylene was investigated as the reaction proceeds using an infrared spectroscopic technique which employed a rapid wavelength scanning device capable of 5000 scans per second. At temperatures between 1300 and 2760°K, the intensity of the infrared emission was maximal at wavelength positions which corresponded with the vibrations in the $\equiv CH$, $=CH-$, $=CH_2$ and $-C\equiv C$ groups. At wavelengths between 2.0 and 2.7μm, the infrared emission was preceeded by a pronounced induction time, the length of which decreased with an increase in both reaction temperature and the initial concentration of acetylene. A correlation was established between this induction time and that preceding carbon formation during the pyrolysis of acetylene. Arrhenius expression for second order rate of disappearance of acetylene yielded an activation energy, E_a = 139 KJ/mole, which falls within the lower scale of the value quoted in the literature.

A kinetic modelling program devoid of steady-state limitations was used to simulate concentration-time profiles of the major reaction products which matched the experimental infrared profiles. Comparisons between the experimental and theoretical results showed that no single reaction mechanism could explain the pyrolysis of acetylene over the wide temperature range studied. Two sets of mechanisms, involving an initial bimolecular reaction of acetylene to either $C_4H_3^\bullet$ or $C_2H^\bullet$ and $C_2H_3^\bullet$ radicals were proposed to explain the reactions at temperatures upto 1900°K, and above 1900°K respectively.

ACKNOWLEDGEMENTS

I wish to express my sincere and grateful thanks to Dr. D.H. Napier for his advice, supervision and encouragement throughout this research work.

Also to the Department of Chemical Engineering and Chemical Technology, Imperial College for the opportunity to carry out this work and for the provision of research equipment.

Grateful acknowledgement is made to the Rivers State Government of Nigeria for its financial assistance.

I am also indebted to my dear wife - Vicky for her patience, co-operation and finally typing of the thesis.

CONTENTS

EXPERIMENTAL SECTIONS

PART A

PART B

CHAPTER 1

GENERAL

I.I. INTRODUCTION

Simple aliphatic hydrocarbons are the most versatile raw material for the petrochemical industry. Their pyrolysis at high temperatures is a process of considerable industrial importance, forming the basis of so-called steam cracking and hydrogasification reactions. And nowadays with the increasing emphasis on air pollution control especially from the effluents of combustion engines and systems, high temperature pyrolysis of hydrocarbons has assumed an important role in elucidating the mechanism of fuel degradation prior to, and during combustion.

Pyrolysis of hydrocarbons involves the breakdown of relatively large molecules by the rupture of carbon-to-carbon and carbon-to-hydrogen bonds to form smaller molecules. The major reactions involve the generation and interactions of free radicals, and in certain cases the whole process is made very complex by the influence of the reactor surfaces. Therefore the understanding of the behaviour of the parent molecule, the factors which influence its conversion to different products and the fate of the intermediates is very crucial if a true and detailed formulation of its decomposition mechanism is to be achieved. It is in connection with this that the use of a 'wall-less' reactor - the shock tube - has become a very powerful tool in the field of chemical kinetics.

The absence of wall effects and the rapid generation of very high temperatures with the shock tube has made the shock tube technique a very attractive method for investigating homogeneous gas phase reactions of hydrocarbons at high temperatures. In employing the shock tube method for kinetic studies, various analytical techniques are available. For the single-pulse technique, the test gas mixture is rapidly heated to a desired temperature and then cooled suddenly. The shock treated mixture is analysed for reaction products by such methods as gas chromatography or mass spectrometry. This technique is adequate for investigating the formation of relatively stable products (for example, methane, ethane, ethylene, acetylene and others) and can give a large amount of information on the kinetics of the reaction; it is particularly suitable for studies aimed at defining the optimum conditions for the formation of the desired reaction products. However, for systems producing very reactive and unstable intermediate products - such as during the pyrolysis of acetylene - a detailed study can be achieved by using techniques which monitor changes in the concentrations of these intermediate species as the reaction proceeds. These include using photospectroscopic methods or the time of flight mass-spectrometer.

The availability of fast response infrared detectors has made it possible to follow the progress of the reaction by monitoring the changes in the emission intensities of certain molecular groupings of interest. And in recent years the development of high-speed wavelength scanning devices has allowed the emission intensity from more than one species to be measured at the same time. Such devices are suitable for studying the pyrolysis of shock-heated hydrocarbons. Measurements of the emission intensities of the species as a function of the reaction time could give valuable information about the kinetics of the system; this could be used in the kinetic modelling of the reactions.

I.2 Shock tube as a chemical reactor

The shock tube was first utilized by Vieille[1] in 1899 in the study of problems relating to flame propagation and later was used by Payman and Shepherd[2] in 1937 to study the detonation of methane-air mixtures. But it was not until in the early 1950's when Glick and his co-workers[3] developed the single-pulse shock tube for investigating chemical reactions, was there a major break through in the application of the shock tube technique to high temperature chemistry. Since then extensive modifications have been made and many new analytical techniques developed to give the shock tube a wider application in investigating various problems associated with gas phase reactions. This is evident from the numerous publications which had appeared within the last three decades in the fields of gas-dynamics and chemical kinetics. Chemical kineticists now regard the shock tube as an effective answer to many of the technical problems which confronted earlier investigators using the conventional reactors. In particular studies of reactions at temperatures around 1200°K, mainly by flow techniques, were subject to considerable uncertainties in all the important variables - particularly in the contact time and the mean reaction temperature, and there were always the inevitable heterogeneous side reactions occurring at the walls of the reactor.

Not only does the use of shock tube in chemical research offer a 'wall-free' reaction zone, but also with the shock tube, it has become possible to study reaction kinetics well beyond the temperature limits attainable with the conventional static and flow reactors. This is of prime importance since such very high temperatures are attained very rapidly. This is a unique feature which is very difficult to realize in conventional pyrolytic systems which empoly electric furnaces for heating.

Though the primary interest of using the shock tube lies in the understanding of the chemical behaviour of molecules at high temperatures, this technique is also valuable in providing additional information on lower temperature reaction mechanisms. The highly idealized conditions existing in the shock tube help in determining whether many of the assumptions used in interpreting low-temperature data from conventional systems are valid; and also to judge whether heterogeneous reactions are of any significance. Thus it has become possible to build-up a copious library of reliable kinetic data covering a wide range of temperatures for many gases.

A detailed account of the rapid progress in the use of the shock tube technique, its basic hydrodynamic theory and the overall shock tube performance have been treated in important texts by Bradley[4], Gaydon and Hurle[5], Greene and Toennies[6] and supplementary reviews due to Bauer[7], Bradley[8] and Belford and Strehlow[9].

1.3 Analytical techniques for chemical studies with the shock tube

In using the shock tube only small quantities of the reactant gas are involved and since all relaxation processes - vibrational, chemical reaction, electronic excitation and ionization - take place very fast, the requirements for the instrumentation for analytical purposes will combine the

the following:-
rapid time response, high sensitivity and small spatial dimension for optimum resolution. The instrumentation is also largely dictated by considerations of the shock wave cycle (incident, reflected, or quenched) to be studied and the property to be investigated.

Quantitative determination of rates of reaction could be made behind both the incident and reflected shock waves by measuring the time variation of such physical parameters as gas density, intensity of emission or absorption spectrum. While for the quenched shock wave the 'frozen' products are removed and analysed by normal laboratory methods. Various analytical techniques have been employed in high temperature studies of chemical reactions in the shock tube ; some of these may include:
(a) analysis by any of the conventional methods of the quenched reaction products,
(b) spectroscopic measurements for observing the emission or absorption spectra of the reacting species, and
(c) monitoring the history of the less stable intermediate compounds using the time of flight mass spectrometer.

I.3.I THE SINGLE-PULSE TECHNIQUE

This method closely parallels the usual laboratory methods used in gas phase kinetics at ordinary temperatures. The main contrast between the single-pulse technique and other shock tube methods ,which rely on optical or other means of following the course of chemical reactions as they proceed behind the shock wave , is that the single-pulse method is

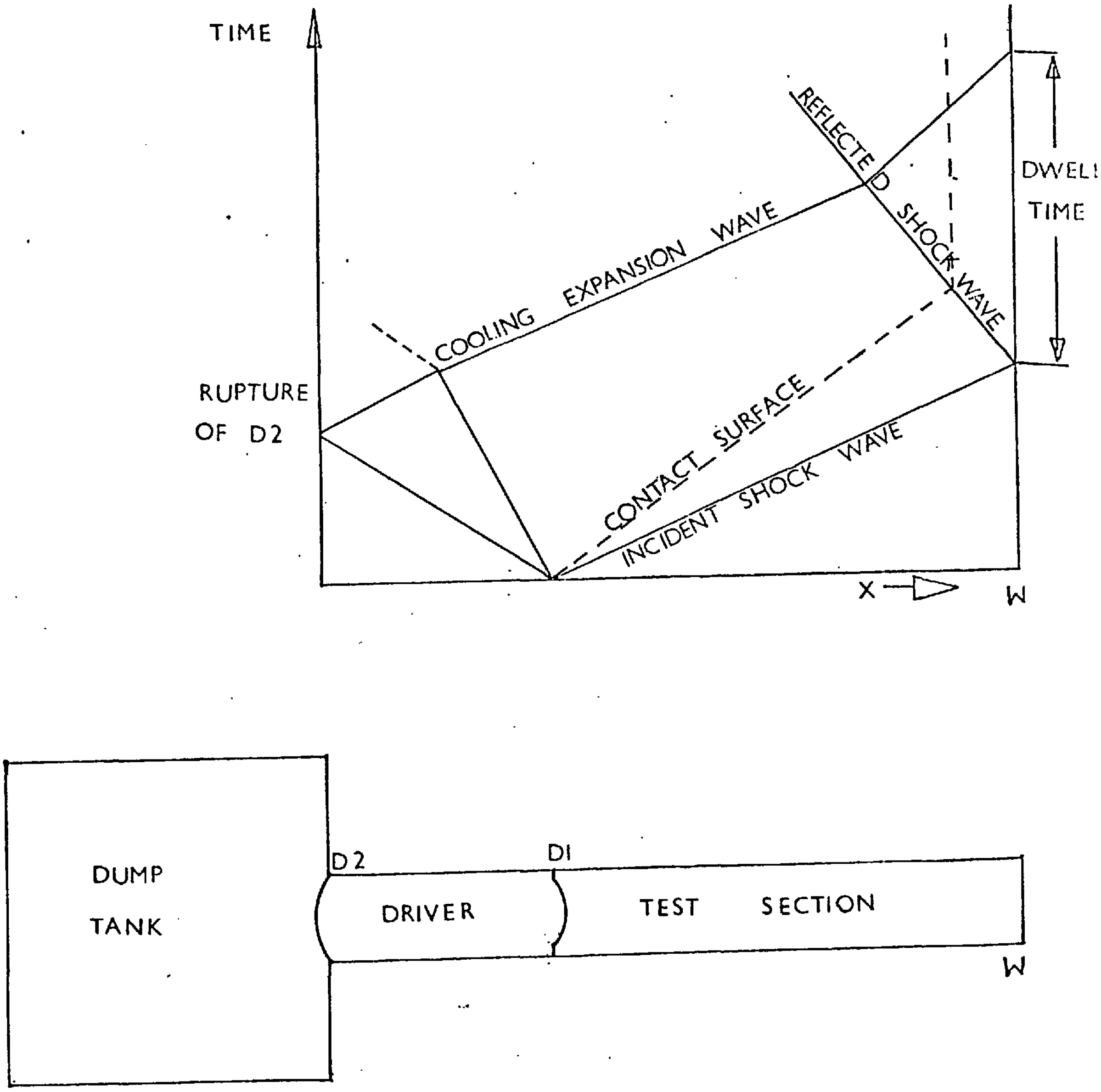

Figure 1.1 : A SINGLE-PULSE SHOCK TUBE

based on chemical analysis of the 'frozen' reaction products after the reactant gas had been shock treated. In the single-pulse method,gas sample is very rapidly raised to a calculable and constant temperature for a known period, after which the reaction is quenched by an expansion wave. The products are removed and then analysed.

The single-pulse heating and rapid cooling is achieved by a design due to Glick et al[3] (figure 1.1) which produces reflected shock and expansion waves by puncturing the diaphragms at D1 and D2. Bursting the diaphragm at D1 sets up an incident compressing shock wave which travels down the reaction section of the shock tube to reflect at the end wall, (W). This gives rise to a reflected shock wave which heats the compressed reactant gas as it travels upstream of the tube. The second diaphragm (at D2) is mechanically broken at a pre-determined time interval after puncturing the one at D1; since the diaphragm at D2 separates the high pressure end of the tube from a large evacuated dump tank an intensive expansion wave is generated by its breakage. The resulting expansion wave spreads back into the shock tube and quenches the reacting gas. After processing the gas sample, the reflected shock passes across the interface between the reactant and the driver gases. This results in general to shock-interface interactions during which two types of waves are formed - a transmitted shock wave (S_T) which propagates through the driver gases and a secondary reflected wave which may either heat or cool the reacting gas further. This is an important consideration in shock tube studies, as it is very essential that the cooled gas is brought to a standstill and prevented from undergoing stagnation heating.

Figure 1.2 illustrates three possible wave forms that can result from the interaction between the reflected shock (S_R) and the contact surface (CS). Because of the abrupt changes in the speed of sound (a) in the gases across the contact surface the secondary reflected wave could be either a shock or a rarefaction (an expansion) wave. Figure 1.3 shows the pressure variation at point X_1, near the end plate (W) for the corresponding wave systems.

The reflected wave at CS will be a shock (figure 1.2(i)) if $a_2 > a_3$,* and this will give rise to successively weakening multiple reflections between CS and the tube wall (W). Therefore in the region between W and CS both the pressure and temperature will increase with time in a stepwise fashion, but the increments after the first shock (S_1) are smaller. On the other hand, if $a_2 < a_3$ the reflected wave will be a rarefaction; this wave subsequently will reflect many times between the wall and CS. The type of wave reflected will alternate between a rarefaction and shock - as illustrated in figure 1.2 (ii). The pressure (as in figure 1.3 (ii)) and temperature will fall after the passage of the first rarefaction R_1 and then rise and fall to much lesser extents with subsequent weaker reflected disturbances.

Multiple shock reflections at the contact surface is undesirable if the gas is to be allowed to react for several milliseconds at conditions of constant enthalpy and pressure. The formation of secondary shock or rarefaction waves at the contact surface is prevented by a gas-dynamic technique called the 'tailored-interface' method[10,11]. Interface tailoring conditions are realized when $a_2 = a_3$ (figure 1.2(iii)) in

* The subscripts correspond to the shock regions as in figure 1.2.

Figure 1.2: Wave Systems formed by interaction between a reflected shock and the Contact surface.

Figure 1.3 : Pressure variation at position X'

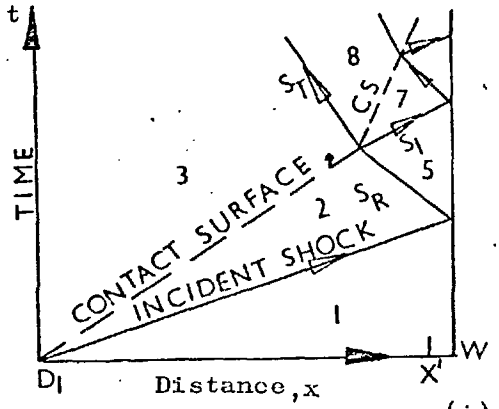

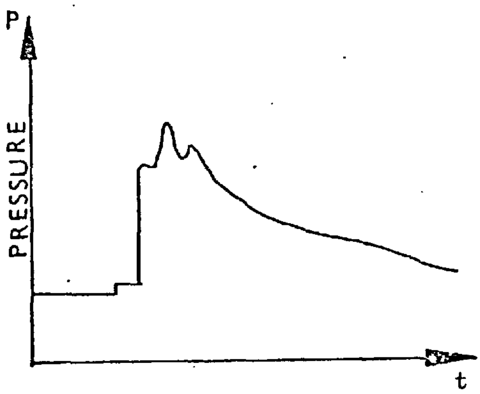

(i) $a_2 > a_3$
secondary shocks

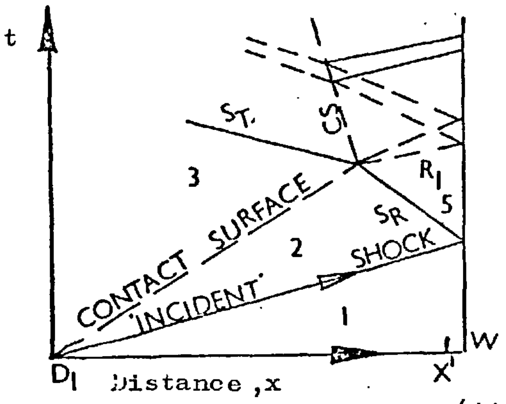

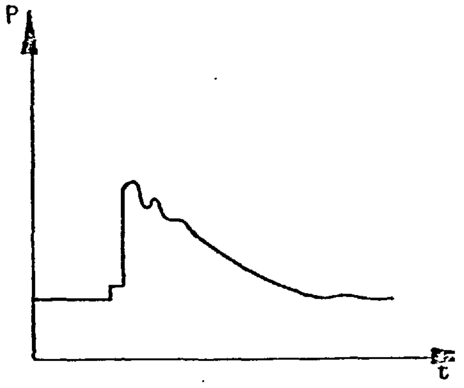

(ii) $a_2 < a_3$
Rarefaction waves

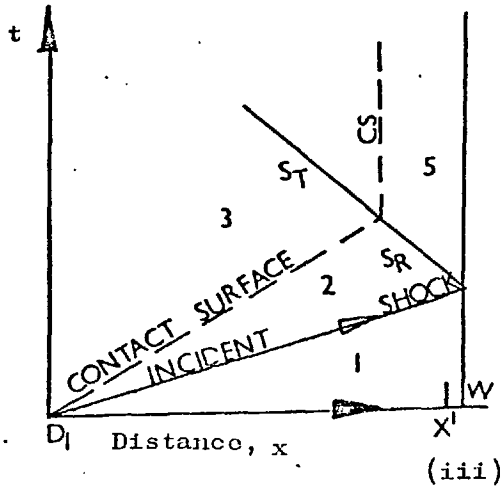

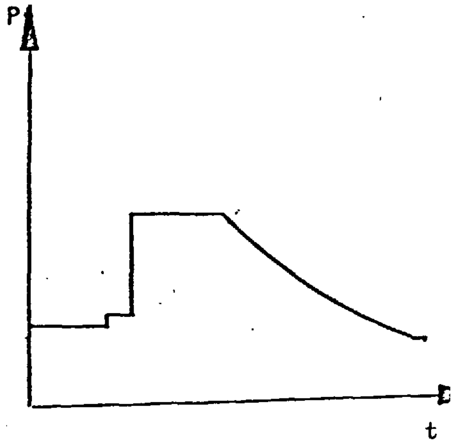

(iii) $a_2 = a_3$
Tailored Interface

which the reflected shock, S_R, passes through the contact surface without change of speed. Under this condition the contact surface is brought to rest abruptly and uniform conditions of pressure (figure 1. 2 & 1.3, (iii)) and temperature persist for a much longer time than in the two previous cases (as in (i) & (ii)) .

Unlike the single-pulse shock tube, shock tubes operating in simple mode form have no dump tank for generating intensive cooling expansion wave. And here quenching of the reaction products does not employ the technique of bursting a second diaphragm but is achieved by the formation of rarefaction wave at the contact surface as was described above and illustrated in (ii) in figures 1, 2 & 1.3. This method does not make any provision for preventing reheating of the gas sample after being processed by the primary reflected shock wave; its application relies on the assumption [12] that the reaction mixture is only reheated to a temperature much lower than T_5, the temperature behind the primary reflected shock wave. However, this assumption has been stated [13] to be invalid when the data obtained by Greene and co-workers [12] using this method of cooling are compared with results obtained from other shock tube investigations. It is believed that because of the diffuse nature of the contact surface the rarefaction so produced will be weakened [14]. Nevertheless a small drop in temperature will be sufficient to quench a chemical reaction in view of the strong dependence of chemical reaction rates on temperature and the high cooling rates of the order of 10^5 to 10^6 $^{o}K/s$ [3,13] attainable in the single-pulse shock tube.

The philosopy of using the single-pulse technique for chemical kinetics depends on the strong assumption that the whole gas sample is subjected to heating for the same length of time before quenching. However, this condition is not always met in practice. The x-t diagram for a single-pulse tube shows that the length of time the test gas is exposed to the high temperature pulse will vary along the length of the tube. Belford and Strehlow[9] have reviewed the several limitations inherent in the use of this technique. These limitations, especially the uncertainties in determining the true reaction times and the actual value of the reflected shock temperature, have led to the development of a number of modified methods for deriving reliable kinetic data from the single-pulse shock tube. The two major methods for evaluating kinetic data from the shock tube aimed at circumventing some of these limitations are the comparative rate method of Tsang [15,16] and the isolation section technique first reported by Johnston and Tschuikow-Roux [17].

In the comparative rate method a binary mixture of reactants in an inert carrier gas is used; the kinetics of one of the reactants (the standard) is well known while that of the second is being measured relative to the known kinetics of the first component. By using such technique the uncertainties in the value of the reflected shock temperature is largely removed [16]. In reference 16 the possible sources of errors in this type of approach and ways of minimizing them have been discussed.

Because the dwell time (reaction time) - that is the time during which the reaction mixture was subjected to the high temperature (T_5) - varies as a function of the distance from the end plate of the shock tube, calculations of experimental results are made using the average dwell time. Such average dwell. time represents only an approximation of the true value of the reaction time. An improved estimate of this value can be achieved if the reaction mixture were to be confined to within only a small length of the tube's test section. The isolation technique is based on this principle and therefore, it avoids the use of average values for the dwell time. This technique is accomplished by using two shutter [17] or pneumatically operated [20] valves usually located close to the end plate.

Evans et al [21] have recently compared the reliability of data obtained from both the comparative and isolation techniques. They obtained evidence in favour of the isolation technique; in addition, they suggested the importance of taking into account the deceleration of the shock front while calculating the reflected temperature, T_5.

One of the limitations of the reflected shock region for the study of chemical kinetics lies on calculating T_5. The most troublesome feature is the disagreement between the values of the reflected shock wave temperature (T_5) computed from measured reflected and/or incident shock velocities, based on a one-dimensional theory. The chief causes of such disagreements are the perturbations introduced by the nonideal opening of the diaphragm, and growing boundary layer generated by the incident shock. However, these difficulties associated with the calculation from measured velocities can be largely solved if this temperature is directly measured rather than calculated. Such option has been adopted by Napier and Subrahmanyam [22] and in the single-pulse experiments in this work.

On the whole, the use of the single-pulse shock tube technique in the study of chemical reactions at high temperatures has continued to enjoy much popularity amongst chemical kineticists since it was developed by Glick and co-workers. A host of other later investigators, such as references (15-17) to name but a few - have used this technique in the study of the pyrolysis of hydrocarbons.

I.3.2 Spectroscopic Technique

The application of the spectroscopic techniques in the study of the emission from shock-heated gases was pioneered by Gaydon and his co-workers [28], whose main interest was centered on the comparative study between the emission spectra from the shock-heated gas with those obtained in flames and discharge tubes. The spectrum of radiation from the shock-heated gases, as in flames and other systems which emit radiation, depends on the form of energy changes taking place within their molecules. Electronic transitions in molecules accompanied by simultaneous changes in the internal vibrational and rotational energies of the molecules are responsible for band spectra in the visible and ultra-violet regions. In the near infrared, the band spectra result from changes in the vibrational and rotational energy alone, while bands in the far infrared are due to only changes in the rotational energy. Emission continuum is usually attributed to the presence of hot solid particles; and studies in the shock tube of the kinetics of carbon formation [29-31] have utilized the appearance of emission continuum to identify the moment of incipient carbon deposition.

The availability of very sensitive and fast response photomultipliers has made the use of the spectroscopic techniques very attractive; and also there is that added advantage that optical techniques do not interfere significantly with the reacting gases. Numerous researches have been carried out in the ultra-violet, visible and infrared regions of the spectrum with both emission and absorption measurements. Emission measurements though simpler to conduct have a common defect in that measurements are obtained only for the concentrations of the excited state and any attempt to relate these to the groundstate concentrations of the principal constituents would require an accurate knowledge of the population distributions of the excited state. Fortunately certain compounds, for example acetylene, methane and ammonia, are capable of providing thermally excited emission in the infrared and this method has been used by Jacobs[32] and many others to obtain useful kinetic results by simply equating the intensity of the emission to be proportional to concentration of the compound.

Of greater utility is the absorption method since knowing the appropriate extinction co-efficients at the high temperatures of the shock tube, it is then easy to calculate the concentration of the reacting species from the amount of radiation absorbed.

The main difficulty inherent in the use of the spectroscopic techniques in shock tube studies is the small amount of light emitted and its short duration of few microseconds. While this could be a serious handicap for studies conducted in the primary shock waves, it is less serious in the reflected shock region where the period during which the light is emitted can be considerably pro-longed by using the interface - tailoring technique[33] and also the prevailing higher temperature and gas density lead to a considerable increase in the strength of the light emitted.

Of special interest in this work is the application of infrared spectroscopy, especially the ultra-rapid technique, to shock tube studies. This is discussed later in section 1.3.5 and 1.3.6.

1.3.3 Time of flight mass spectrometry

This is a novel technique of dynamic sampling behind the reflected shock through a pinhole. Essentially it is a simple mass spectrometer which operates on time of flight principles rather than on deflection in a magnetic field. It is incooperated with the shock tube via a small pinhole (about 0.05 - 0.127 mm in diameter[34,35]) made in the end plate which is lined with thin gold foil. The shock-heated gas leaks through this pinhole into the ionizing chamber, where the molecules are ionized before accelerating to the detecting system. Depending on the mass of the ions they will reach the detector at different times, the lighter ions reaching first since the velocity of ions of constant energy is proportional to the inverse square root of their mass.

The output signal from the detector is displayed on the oscilloscope at regular short intervals of about 50μs and can be photographed on a rotating drum camera. The main attraction of this method is that it has become possible to follow the course of chemical reaction as it proceeds, monitoring both the formation and disappearance of unstable intermediates. This method has been used by Kistiakowsky and co-workers [34, 41] to investigate the pyrolysis and oxidation of acetylene behind the reflected shock waves.

The major points for which this technique has often been criticized are the problems associated with the growth of thermal boundary layer and its aspiration into the sample jet, possible contamination of the sample by gas which has been treated by collisions with the walls of the leak, and possible self-rarefaction of the region from which sample is withdrawn.

I.3.4 Application of infrared spectroscopy to shock tube studies

Infrared spectroscopy enables the identification of certain functional groupings in a complex molecular structure and with the development of fast response infrared detectors the application of infrared spectroscopy in the study of fast reactions has become very popular. With the assumption of Beers Law that for a transparent gas the concentration of a reacting species is proportional to the intensity of the radiation it emits, it is then possible to make time - resolved measurements of the variation in the intensities of the various molecular groupings. Moreover, this method could be employed to follow processes occurring in the shock tube if it is assumed that radiative equilibruim is attained in short times compared with chemical decomposition.

The first application of high-speed infrared spectroscopy to shock tube studies was simultaneously reported by Hooker [29] and Windsor et al [36] at the seventh international symposium on combustion in 1959. Hooker detected infrared emission through sapphire window at 3.04 μm from shock-heated acetylene using a photoconductive indium antimonide cell, while Windsor et al used a lead sulphide detector to monitor the infrared emission of CO waveband at 2. 335 μm in their study of the vibrational relaxation of carbon monoxide. Useful kinetic results, some of which are discussed later, were obtained from these initial studies.

The first published data on reaction rate measurements using the infrared emission technique in a shock tube was reported at the 8th international symposuim on combustion by Jacobs[32]. He used a 0.7 µs time-constant gold-doped germanium infrared photoconductive detector to study the initial rate of ammonia decomposition in the range 2000 - 3000°K. By assuming that NH_3 behaves like a transparent gas, he measured the changes in ammonia concentration directly by following the infrared emission intensity as a function of time. Such measurements yielded a low value of 2I8.4 KJ/mole for the apparent activation energy, which is almost one half of the bond strength (44I KJ) in NH_2 - H. This was taken to be an indication that such measurements represent, not the initial decomposition rate but, a measure of the early rate of a chain process. However, in a later investigation [37] the same author obtained a more reliable kinetic data by measuring the rate over a period of time. The decomposition reaction of methane in the shock tube has been followed [38] by observing the infrared emission of methane at 3.5µm and those of the formed species at 2.9 - 3.0µm. It was shown that the first-order rate constant of its decomposition is dependent on the concentration of the carrier gas, argon. Wray and Feldman[39] in an extension of the work of Bott and Jacobs[40] on SF_6, used a liquid helium cooled copper-doped germanium detector in the study of the decomposition of SO_2F_2. They verified experimentally that the gas was transparent over a wide range of partial pressures of SO_2F_2, and hence calculated its decomposition rate at 1900°- 2300°K directly from the slope of the decay of the infrared emission. A comparison of their data with those of Bott and Jacobs[40] revealed that SF_6 decomposes about 10 times faster than does its oxidation product, SO_2F_2. Numerous other interesting result have been obtained in similar pyrolytic studies of various compounds carried out in the recent years. For example, Kuratani and Bauer[42] investigated exchange reaction between acetylene and deuterium at temperatures of 1300 - 1665°K. The rate of substitution of D for H was followed by recording the infrared emission intensity due to C_2HD (at 3.914 µm) and to C_2H_2 (at 3.129 µm). On the strength of their observation they were able to postulate the occurrence of two types of unstable intermediates;

a) a molecular complex, $C_2H_2.D_2$ between acetylene and deuterium; and

b) $C_2H_2D_2^*$ an excited molecule.

Also the use of infrared spectroscopic technique has become very useful in combustion studies of hydrocarbons in the shock tube. This involves the monitoring of the infrared emission from CO_2, CO, H_2O and the hydrocarbon species by using suitable narrow band filters and detectors. The oxidation products from the combustion of methane[43], and ethane[44] have been observed using this method.

I.3.5 Rapid scanning infrared technique

Studies utilizing high-speed infrared spectroscopy reviewed in the last section (I.3.4) were only used to observe the emission intensities at the characteristic vibrational frequencies of the bands of interest, Their application in investigating chemical reactions is very limited as the variation in the intensity of emission due to only one particular functional group (or groups if their emission bands are so close together that they cannot be resolved) could be followed at a time. In such attempts to monitor simultaneously the emission intensities due to more than one group involves the use of as many filters and detectors as there are functional groups; which is very expensive. Therefore the desire to limit cost, as well as to examine the progress of fast chemical reactions over a wider wavelength range in times as short as a few milliseconds, led to the development of rapid infrared scanning spectrometers.

The development commenced with the design by Bullock and Silverman[45] in 1950 of an instrument, based on the original ideas of Daly[46], which was capable of scanning across 2 micrometers in 2 milliseconds. In this and other later designs[47-50] which followed, rapid scanning across a wavelength interval at short times was achieved by the use of either fast rotating or oscillating littrow mirrors. The major problem associated with the use of rotating or oscillating mirrors in these designs are the mechanical strain placed on the mirror while in motion; this seriously limits the repetitive rate that can be achieved. These spectrometers lend themselves to kinetic studies of relatively slow chemical reactions and are not fast enough as to enable shock tube investigations to be carried out.

A decade later after Bullock and Silverman's initial attempt, Bethke[51] introduced a new design of ultra-rapid scanning infrared spectrometer which was capable of scanning upto 20,000 times per second over a scan width of 0.5 micrometers. This was achieved by changing the angle of incidence of the infrared radiation entering the monochromator by using a high speed rotating disc instead of a rotating mirror.

Figure 1.4[51] shows the layout of this instrument. The scan wheel D,has radial slits, located close to the edge, which acts as moving entrance slits for the monochromator. The infrared radiation emerging through the monochromator is picked up by a sufficiently fast response (rise time $<$ 0.2 ms) infrared photoconductive detector.

An ultra-rapid scanning spectrometer, based on this (Bethke's) design has been successfully used in this laboratory for the study of the pyrolysis of shock heated methane and ethylene[52] . The results from that study showed that the application of ultra-rapid scanning infrared spectroscopy to shock tube studies can be a valuable method of elucidating reaction mechanisms at high temperatures. And one of the objectives of the present investigation is to use this technique to elucidate the mechanism of acetylene pyrolysis behind the reflected shock waves.

Figure 1.4[51]**:** ULTRARAPID-SCAN SPECTROMETER

Optical schematic diagram of URSIS. The apparatus is a modified Perkin-Elmer model 83 single-pass monochromator. The light path is reverse that of an unmodified instrument. Both the axis of the scanning wheel and the scan trigger system (lamp, *L1*, *M8*, and *PM*) are mounted above the monochromator and its optics.

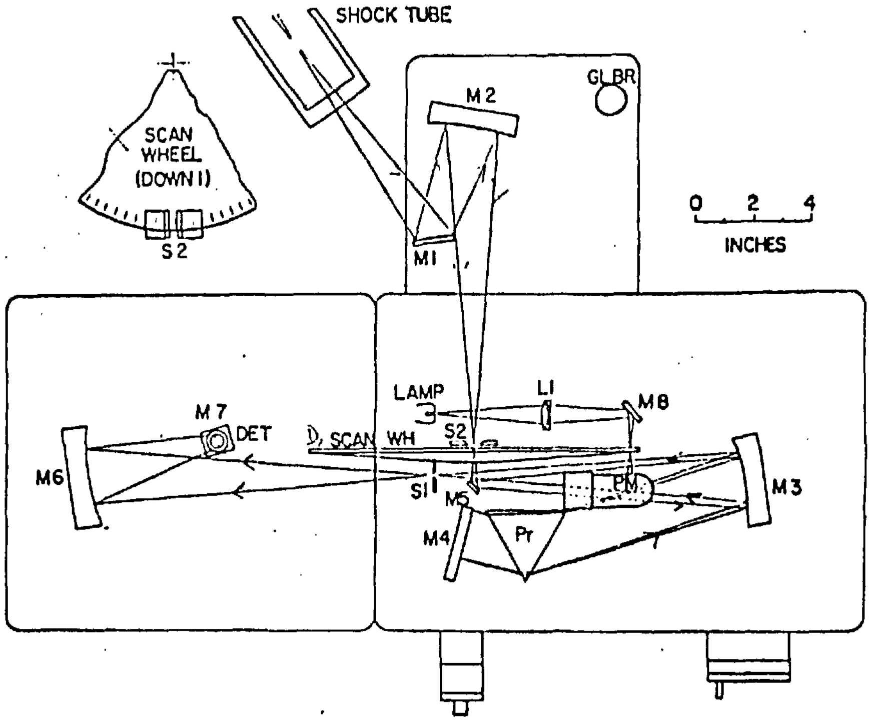

M1-8 - reflecting mirrors

S1 - Exit slit

S2 - Limiting slit

Pr - CaF_2 prism

DET - InSb Detector

Scan WH - Scanning wheel

1.4 The effect of boundary layer on shock tube kinetic data

The flow of viscous fluids through a tube very often results in the formation of a layer of fluid very close to the walls of the tube across which the flow velocity is progressively retarded until it finally becomes zero at the wall. The formation of such a layer called the boundary layer, in the shock tube has been extensively described in many texts[4 - 6, 59]. The presence of a wall boundary in shock tube can cause serious deviations in the test time, temperature and density histories of the shocked gas from those predicted by ideal theory. Duff[53] has observed that in a low-pressure shock tube (P_1 = 66.5 N/m^2) at a distance from the shock front corresponding to the position of the contact surface, the boundary layer thickness reaches as high as 20-53% of the radius of the tube.

The growth of boundary layer in the shock tube has been likened to an aerodynamic sink which removes gas from the region between the shock front and the contact surface; such mass removal causes the shock to decelerate while the contact surface is accelerated apparently because of the reduction in the cross-sectional area of the shock tube. The effects of the wall boundary layer becomes more pronounced as the length-to-diameter ratio of a shock tube is increased and as the initial pressure in the driven section is reduced.

The formation of a boundary layer, sometime after the rupture of the diaphragm, is shown schematically in (figure 1.5). The influence of boundary layer growth has been analytically treated in great detail by Mirrels[54-56]. Mirrels has suggested

Figure 1.5: Boundary layer formation

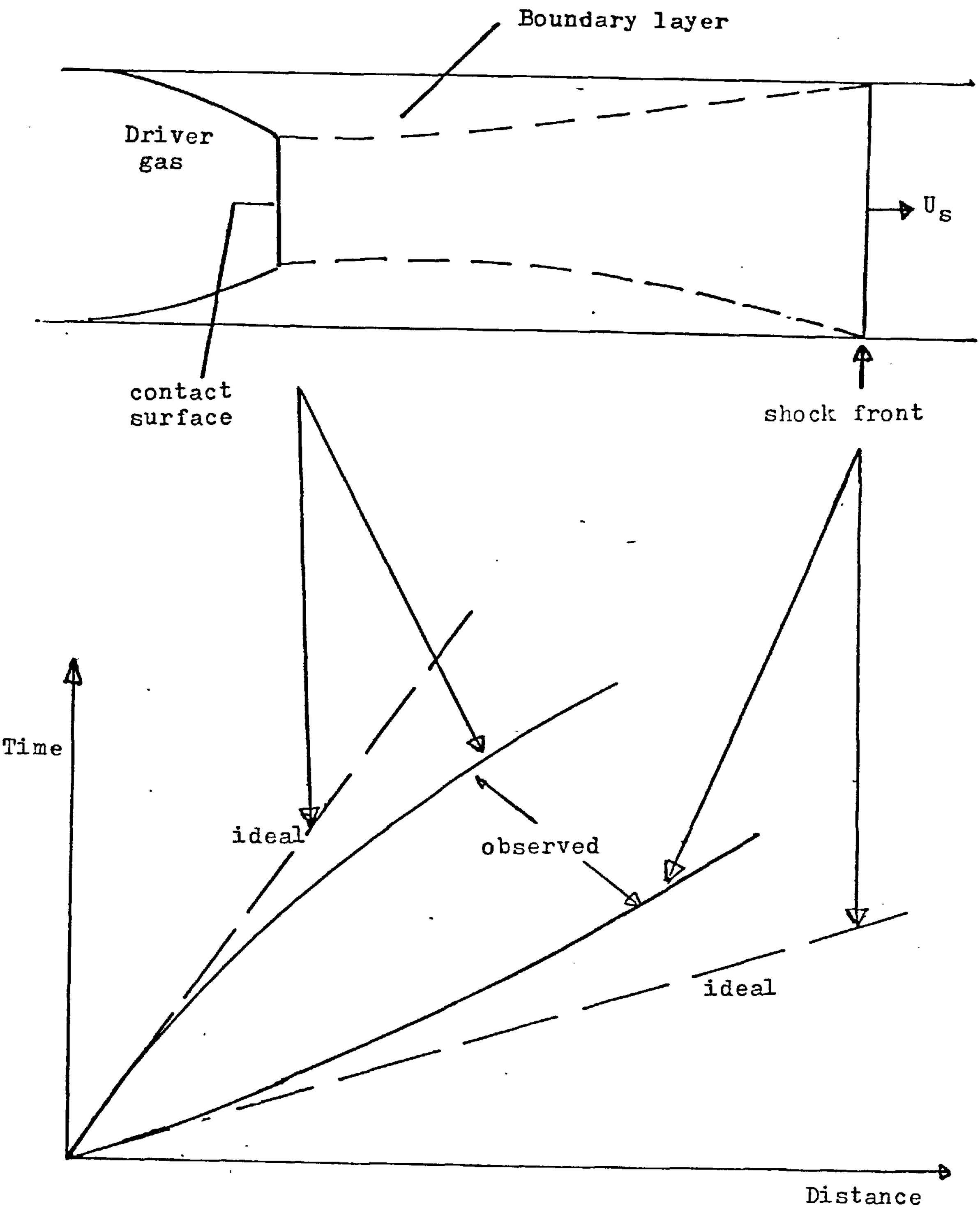

that flow non-uniformities associated with the boundary layer behind an incident shock may significantly affect shock tube studies of chemical kinetics. Brabbs and Bells[57,58], using the Mirrels equations, have experimentally confirmed that kinetic data from the shock tube are subject to, and must be corrected for, boundary layer induced non-uniformities for both turbulent and laminar flows. Warshay[63] has also examined the effects of boundary layer corrections on the measured rates of dissociation of 1% Br in argon using Mirrels' model for wholly turbulent boundary layer. A comparison of his kinetic data from two separate studies - without[62] and with [63] boundary layer corrections indicated that even under 'favourable' experimental conditions (M_s = 3-4, large tube diameter, 10.2cm, short reaction time, 10 to 50µs, and high P_1 = 18-72 torr*) where boundary layer corrections could be assumed to be unimportant, the application of such corrections produced a change of 20% in the rate constant at the lower temperatures with both the activation energy and the pre-exponiential constant decreasing. He also pointed out that the boundary layer effects on the apparent rate of dissociation of bromine was very significant at the lower temperatures (around 1264°K) but become negligible at high temperatures.

Mirrels' results[55,56] from the treatment of laminar flows in the boundary layer have been used by Strehlow and Belford[61] to evaluate some simple formulae which are very useful for estimating the magnitude of errors introduced by the boundary-

* 1 torr = 0.1333 KN/m^2

layer - induced non-idealities on kinetic parameters measured from shock tube studies. These formulae outline corrections for estimating:-

a) the actual observation time t_p, from the laboratory time t_l, using the equation:

$$t_p \cong t_l \; (\rho_2/\rho_1) \; (1 + 0.7 \, (t_l/t_m)^{\frac{1}{2}})$$

in the place of (1.4a)

$$t_p \cong t_l \; (\rho_2/\rho_1)$$

(1.4b) for an ideal flow with no boundary layer. Where:-

(ρ_2/ρ_1) = the density ratio across the shosk front

$t_m \cong$ the maximum hot flow transit time - defined as $t_m = 5.85 \, d^2 P_1/(M_s^{1.7} a_1) \; cm^{-1} torr^{-1}$, where d = hydraulic diameter (= 4 A/L, where A = tube area, and L = tube parameter), P_1 = initial pressure in the test section, M_s = shock mach number, and a_1 = velocity of sound in the gas ahead of the shock wave. Equation (1.4a) is an adquate approximation as long as $t_l/t_m < 0.1$; above this the correction is larger.

b) the temperature drift behind the incident shock (for a monatomic gas) is given as

$$\Delta T/T_2 \cong 0.2 \, (t_l/t_m)^{\frac{1}{2}} + 1.2 \, t_p \left[(M_s^2 - 1)/M_s^2 \times (M_s^2 + 3)\right]\left[d(\ln M_s)/dt\right] \quad (1.4c)$$

c) The density correction as:

$$\Delta\rho/\rho \approx \left(\Delta T/T\right) / (\gamma - 1)$$

$$\approx 1.5 \ (\Delta T/T) \qquad (1.4d)$$

The limits for the application of these corrections have been discussed in references (9, 61).

However, while these corrections are applicable to studies performed in the incident shock wave, there are no simple formulae yet available for making such estimations for boundary layer effects in the reflected shock waves because of the complexity of the flow pattern in the reflected shock region. The complication arises as the reflected wave travels against the on coming gas of the incident wave, it interacts with the boundary layer giving rise to bifurcation of the front [4, 5, 59]. This type of interaction leads to the thickening and the separation of the layer from the walls of the tube so that it extends more into the central region. The layer also becomes more turbulent and follows the front of the reflected shock up the tube at a lower velocity. This phenomenon will destroy the homogeneity of the reactant gas and introduce large gradients of gas properties transverse to the shock tube axis.

Both analysis and experiments indicate that monoatomic gases show little shock - boundary layer interaction, while gases composed primarily of complex molecules, for example, hydrocarbons, maybe seriously affected. Therefore, spectroscopic measurements of time variation properties, such as optical absorption or emission can be greatly affected by the growth of the boundary layer. It is therefore an important consideration in the present study since any changes in the gas density, resulting from non-uniformities in shock heating of the gas between the shock and the contact surface will be greatly magnified in the reflected shock region. Such changes in density could alter the strength of the emission and thus would invalidate any assumption of the dependence of concentration on the intensity of emission, except at low optical densities. However, under suitably controlled experimental conditions it is possible to keep the gas in the reflected shock region at an undisturbed state for up to several milliseconds; independent pressure and density measurements are usually useful in judging the reliability of measurements made in this region.

1.5 Tailoring of the interface

While it is desirable to conduct kinetic studies in the reflected shock region because of the accessibility to higher temperatures and the availability of longer observation times at which the hot gas is relatively static, as opposed to the conditions at the incident shock region where the gas is continually moving and the process may be studied during the passage of the shock down the tube before the onset of reflection, it might occur that the desired near ideal conditions behind the reflected shock are marred by interface instability arising from the generation of multiple reflected shock or rarefaction waves during the interaction between the reflected shock and the oncoming contact surface. This leads not only to reduction in the length of observation time behind the reflected shock but also the test gas is no longer subjected to a single isothermal pulse. References (4,5) have outlined various forms of wave pattern that could result from such interactions. This instability phenomenon occurs because of the differences in the speed of sound and specific heat ratio of the gases in the incident region from those behind the contact surface. Figures (1. 2 and 1. 3) show the various forms of interaction that do occur.

Instability at the interface can be arrested or at least minimized by the using the technique of interface tailoring. This technique relies on the principle of adjusting the conditions so that the sound speed and the specific heat ratio in the incident shock are matched to those in the region behind the contact surface, so that the reflected shock passes through the contact surface without any change in the shock strength. In such conditions the contact surface is brought to abrupt rest and the hot gas in the reflected shock region then remains stationary and uniform conditions persist for a greatly increased observation time until the reflected rarefaction wave arrives from the driver end of the tube.

The interface - tailoring conditions are usually achieved by adjusting the composition of the driver, or the test, gas and sometimes by electrically pre-heating the driver gas. In the present study the interface - tailoring technique was employed, and it was achieved by simultaneously varying the percentages of nitrogen in the pre-dominantly hydrogen driver gas and adjusting the initial pressures of the test gas. Calculations for tailoring conditions are outlined in section 2.3.5.

1.6 Pyrolysis of hydrocarbons

Pyrolysis of hydrocarbons proceed through a complex mechanism in which the degree of complexity increases with increasing molecular weight of the molecule being pyrolysed and with increasing conversion. The basic reactions occuring during the pyrolysis of hydrocarbons, especially for aliphatic hydrocarbons of paraffin series, are dehydrogenation reaction (I.I) and chain rupture reaction (1.2) resulting in the formation of olefines and lower molecular weight paraffins:

$$C_nH_{2n} + 2 \longrightarrow C_nH_{2n} + H_2 \qquad (1.1)$$

and

$$\underset{\text{Higher paraffin}}{C_{m+n}H_{2(m+n)+2}} \longrightarrow \underset{\text{olefin}}{C_mH_{2m}} + \underset{\text{lower paraffin}}{C_nH_{2n+2}} \qquad (1.2)$$

Which of these two reactions is favoured depends on thermodynamic considerations. The energy required to rupture a C - C bond (~ 209 - 344 KJ) is lower than those for C - H link (~293 - 418 KJ); this suggests that under non-catalytic conditions, the velocity of reaction (1.2) is greater than the velocity of dehydrogenation (I.I). However, different hydrocarbons differ in ease by which they undergo pyrolysis; in general the extent to which a compound decomposes at any temperature depends on its relative thermostability. Therefore the relative stabilities of different kinds of molecule are clearly of great significance.

Thermodynamics provides a useful definition of stability in terms of the standard free energy of formation of a compound from its elements, written as ΔG_F^o. With methane, for example, this is the standard free energy of the reaction (in equation 13)

$$C(solid) + 2H_2 (gas) \longrightarrow CH_4 \qquad (1.3)$$

Where ΔG_F^o is large and positive, the compound in question cannot readily be formed from its elements under the specified condition. A large positive value for ΔG_F^o for an existing compound indicates a marked readiness to decompose into the elements, or into other compounds of higher stability (i.e. with smaller positive or a negative ΔG_F^o). Figure (1.6) shows[70] the dependence of free energy of formation of gaseous hydrocarbons per carbon atom on temperature. The tendency for decomposition reaction to proceed at any temperature is from a higher to a lower curve in the figure. Hence, methane is the most stable of all the hydrocarbons over a wider temperature range. In general paraffins and naphthenes are relatively the more stable hydrocarbons at lower temperatures (below 500°K), whilst aromatics and olefins and acetylene show remarkable increase in relative stability at high temperatures. Acetylene, for example, is thermodynamically very unstable at ordinary temperatures but, being a highly endothermic compound, it becomes less unstable with rise in temperature.

At shock wave temperatures many investigators, amongst them Glick[64] and Skinner et al[65], have observed that during the pyrolysis of hydrocarbons paraffins quickly yield olefins (especially ethylene) which in turn is converted to acetylene (a more stable product at temperatures above 1500°K) and hydrogen. Consequently, a general and simplified decom-

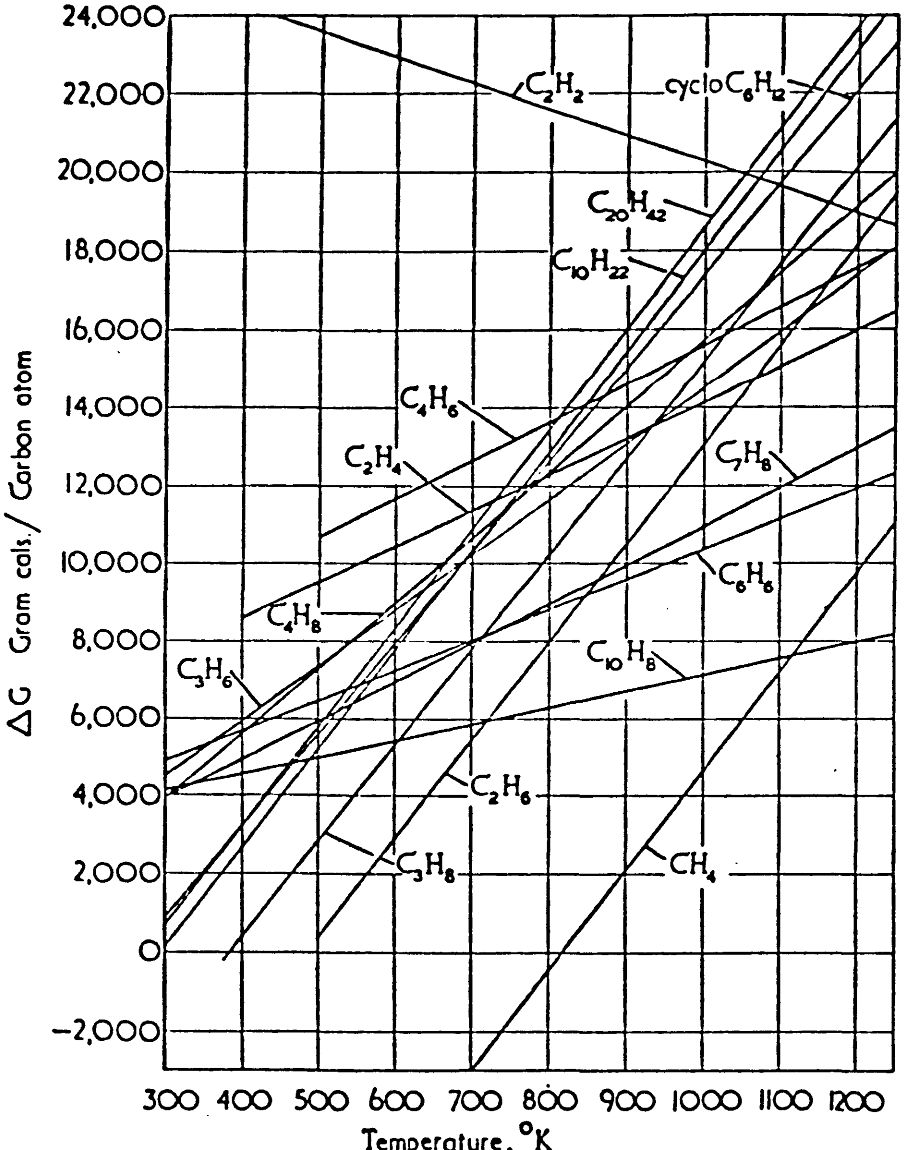

Figure (1.6)[70]

Free energy of formation of hydrocarbons position sequence for hydrocarbons can be represented as:-

$$C_{2n}H_{4n+2} \xrightarrow[-H_2]{K_1} C_{2n}H_{4n} \xrightarrow[-nH_2]{K_2} nC_2H_2 \xrightarrow[-nH_2]{K_3} 2nC$$

paraffin olefin acetylene carbon

in which $K_1 \gg K_2 \gg K_3$ are the rate constants, and n is the number of carbon atoms contained in the hydrocarbon.

This form of decomposition sequence illustrates that the higher molecular weight hydrocarbons are being systematically cracked to series of lower molecular weight products in which acetylene becomes a major reaction product at high temperatures[12, 22]. This is in keeping with Porter's[66] earlier suggestion that acetylene is the last stable hydrocarbon to be observed before carbon is formed during the pyrolysis of hydrocarbons. Deservedly, therefore particular attention has been paid to the study of the pyrolysis of the low molecular weight hydrocarbons since they form the bulk of the reaction products during the decomposition of higher hydrocarbons. Also of particular interest is the formation of the unsaturated intermediate products (olefins and acetylene) which are in great demand for the chemical industries.

For years, great research interest has been centred on the last step in the deomposition sequence of hydrocarbons, that is the pyrolysis of acetylene, since it is believed that it has direct bearing on the formation of carbon, a substance whose nuisance in combustion engines and systems is well known. Also of vital interest is the knowledge of the mechanism of acetylene pyrolysis which is very important with respect to the industrial hazards presented during acetylene manufacture and its wide use for chemical synthesis[67-69].

1.6.1 Free Radical Mechanism

In pyrolytic reactions there is a complex sequence of elementary steps intervening between reactants and the products as a result of formation of very reactive intermediates(atoms and free radicals)[71] in the course of the reaction. The involvement of free radicals and atoms during pyrolytic reactions has led to serious difficulties in formulating the reaction mechanism of even the simpliest hydrocarbon. By posulating the free radical mechanism, Rice and Herzfeld[72] have demonstrated how very complex reaction mechanism may still lead to simple overall kinetics. The Rice-Herzfeld free radical mechanism distinguishes three types of elementary reactions - initiation, propagation and termination- as the chain processes occurring during pyrolysis.

(a) <u>Chain Initiation:</u>

The initiation step is the formation of free radicals from a valence-saturated molecule. This can result from a number of ways depending on the reactant(s) involved and the method employed in investigating the reaction. Initiation can occur during pyrolysis by any of the following ways:-

i) by the unimolecular splitting of the parent molecule at its weakest link; for example, during the pyrolysis of most aliphatic paraffins, such ethane, propane, the decomposition starts with the rupture of the C - C bond to yield radicals; for example,

$$C_2H_6 \longrightarrow CH_3^{\bullet} + CH_3^{\bullet} \qquad 2.1.(3)$$

$$C_3H_8 \longrightarrow CH_3^{\bullet} + C_2H_5^{\bullet} \qquad 2.1.(4)$$

ii) by molecular interactions between the molecules of the reactant(s), as in the initiation of acetylene pyrolysis:

$$C_2H_2 + C_2H_2 \longrightarrow C_4H_3^{\bullet} + H^{\bullet} \qquad 2.1.(5)$$

or

$$C_2H_2 + C_2H_2 \longrightarrow C_2H_3^{\bullet} + C_2H^{\bullet} \qquad 2.1.(6)$$

iii) Reaction can also be heterogeneously initiated at the walls of the reaction vessel. The last initiation method (iii), is only applicable to situations where reactor surfaces play important role, as in most studies conducted in static and flow apparatus; but it is of no significance when the shock tube is used. The magnitude of the rate of chain initiation depends on the number of the active centres involved. Generally, the initiation steps are show and endothermic.

b) Chain Propagation

The radicals once formed, propagate the reaction by generating other new radicals. In this reaction-step product-molecules are formed while the total number of radical intermediates, or chain centres remain constant. In applying Rice-Herzfield chain mechanism to the pyrolysis of hydrocarbons, the chain propagation reactions can be classified into three distinct groups:

i) attack by the free radicals on the parent molecule(s) to form an end product and a new free radical or atom; for example,

$C_2H_6 + H^\bullet \longrightarrow H_2 + C_2H_5^\bullet$ 2.1.(7)

$C_2H_2 + {}^\bullet C_2H \longrightarrow C_2H_4 + C_2H^\bullet$ 2.1.(8)

ii) unimolecular conversion of one free radical into another;

$i\ C_3H_7^\bullet \longrightarrow n C_3H_7^\bullet$

iii) the unimolecular decomposition of a free radical to form a product and a new free radical or atom: for example;

$C_2H_5^\bullet \longrightarrow C_2H_4 + H^\bullet$ 2.1.(9)

$C_3H_7^\bullet \longrightarrow C_2H_4 + CH_3^\bullet$ 2.1.(10)

$C_4H_3^\bullet \longrightarrow C_4H_2 + H^\bullet$ 2.1.(II)

Propagation reactions are usually fast and thermo-neutral or exothermic

(c) Chain termination

The chain process in terminated when all the generated free radicals in the system are consumed. Chain may be terminated either by the capture of the radicals by the vessel walls (for reactions conducted in convectional systems), or by the recombination and disproportionation reactions of the free radicals;

$$\left.\begin{array}{lllll} CH_3^{\bullet} & + & CH_3^{\bullet} & \longrightarrow & C_2H_6 \\ C_4H_3^{\bullet} & + & C_4H_3^{\bullet} & \longrightarrow & C_8H_6 \end{array}\right\} \text{recombination} \qquad \begin{array}{r} 2.1.(12) \\ 2.1.(13) \end{array}$$

or

$$C_2H_5^{\bullet} + C_2H_5^{\bullet} \longrightarrow C_2H_4 + C_2H_6 \quad \text{disproportionation} \qquad 2.1.(14)$$

Also chain may be broken by the addition of inhibitors - special substances which replace the active free radicals by radicals of low activity, incapable of propagating the chain process. Chain breaking process can be either linear or quadratic reactions. In the linear chain breaking reaction the rate of breaking is proportional to the first power of the free radical concentration, here the chain could be terminated at the walls; whereas in a quadratic chain breaking, the rate is proportional to the product of the concentration of two free radicals or to the square of the concentration of any of the free radicals, and are usually the result of termination by either a recombination or disproportionation reaction. Quadratic termination reactions in the gas phase must have high rate constants to compete since the radical concentrations are usually small.

The nature of the initiation, propagation and termination steps are of very important consideration in relating the reaction mechanism to the overall kinetic behaviour of a system. The overall order of a reaction is mainly determined by the manner in which the chains are broken. Goldfinger et al[73] have studied this relationship and have classified free radicals into two major groups, β- and μ-radicals, judging from the standpoint of the types of propagation steps in which they participate. The β- radicals are those that only participate in second-order propagation steps; for example in equations 2.1.(7) and 2.1.(8) CH_3, $H^\bullet$ atom and the ethynyl radical in the pyrolysis of ethane and acetylene respectively are β- radicals. Whereas in equations 2.1. (9 - 11), the radicals $C_2H_5^\bullet$, $C_3H_7^\bullet$ and $C_4H_3^\bullet$ are termed μ-radicals as they mainly participate in first - order propagation steps.

A careful choice of possible combinations between these radicals in the chain breaking reaction can resolve the question posed by the experimental observation that some unimolecular reactions have a non-integer overall reaction order. Goldfinger and co-workers[73] have formulated a table of possible combinations between β- and μ- radicals inorder to explain such discrepancies. Summary of such various combination possibilities, and including the conditions in which termination steps involve the participation of third bodies are generally available in standard texts on reaction kinetics, such as references[74 - 77]. Such summary has been outlined in table 1.

Table 1: Overall orders of reactions for various types of initiation and termination reactions

First order Initiation		2nd - order Initiation		Overall order
simple termination	3rd body termination	simple termination	3rd body termination	
-	-	$\beta\beta$	-	2
$\beta\beta$	-	$\beta\mu$	$\beta\beta M$	$3/2$
$\beta\mu$	$\beta\beta M$	$\mu\mu$	$\beta\mu M$	1
$\mu\mu$	$\beta\mu M$	-	$\mu\mu M$	$\frac{1}{2}$
-	$\mu\mu M$	-	-	0

This analysis shows that if the chain initiating reaction is bimolecular rather than first-order, the overall orders are higher by one-half, and where the termination steps involve a third body, the tendency is for the order to be reduced by one-half. However, several factors influence the form a termination step takes in a reaction. Since the combination of free radicals requires little or no activation energy, their rate coefficients are mostly dependent on the frequency factors; these themselves do not vary greatly, therefore the relative concentrations of the radicals are very significant determining factors that influence the type of termination process that takes place. Higher concentrations of β-radicals will favour $\beta\beta$- and $\beta\beta M$ termination steps, while the abundance of μ-radicals results in $\mu\mu$ and $\mu\mu M$ combinations. The general importance of table (2.1) is underlined by the fact that it is very helpful in deciding a reaction mechanism without having to solve the complex steady-state equations in each case.

1.6.2 Review of the pyrolysis of some selected hydrocarbons

Pyrolysis of the individual hydrocarbons have been extensively studied and it will be too cumbersone to attempt to undertake a detailed review of all of them. Hence the literature survey will be limited only to those hydrocarbons - propane and acetylene - which are of major interest to the current study.

1.6.2.1 Pyrolysis of propane

The commercial importance of propane for the production of olefins-ethylene and propylene - led to up surge of interest in the kinetics of its pyrolysis. Considerable work has been carried out in this respect at low temperatures ($300^{o}K-900^{o}K$) using static systems and the results of such researches have been discussed extensively [79-84]. Also extensive studies of propane decomposition at moderately high temperatures ($950-1300^{o}K$), aimed at simulating the industrial pyrolyzing conditions using tubular flow reactors [85-91], while only very few experimental investigations have been reported to date using the shock tube techniques. Works prior to about 1954 has been reviewed by Steacie[93] while a recent review by Volkan and April[94] has comprehensively covered much of the latter studies.

The pioneering researches on propane pyrolysis were conducted at low temperatures using conventional static systems; notable among these which dealt with reaction rate and reaction mechanism include studies by: Pease and Durgan[95], Steacie and Puddington[96], Marek and McCluer[97], and Ingold et al[98]. These studies showed the decomposition of propane to be largely a homogenous gas-phase reaction proceeding with a radical chain mechanism; the reaction was reported to be first - order relative to the concentration of propane with the activation energy varying from 209 - 293 KJ. The major decomposition products of propane pyrolysis are hydrogen, methane, ethylene and propylene all of which are found to be present in nearly equal amounts and at low conversions, and are thought to be formed according to the stoichiometry;

$$C_3H_8 \longrightarrow CH_4 + C_2H_4 \qquad (a)$$

$$C_3H_8 \longrightarrow H_2 + C_3H_6 \qquad (b)$$

Laidler et al[79] have re-examined the foregoing results by investigating the exact nature of the initiation and termination reactions at temperatures between 800 - 900°K and at pressures up to 79.8 KN/m^2. They arrived at similar conclusion that the reaction is homogenous and proceeds by a free radical mechanism in which the initiating step was the self-dissociation of propane to a methyl and an ethyl radical; they also observed in addition that a transition in the reaction order from first to $^3/_2$ occurred at higher temperatures (> 920°K) and low pressures. Laidler and co-workers[79] therefore proposed the following eight step reaction mechanism,

Initiation $$C_3H_8 \longrightarrow CH_3^{\bullet} + C_2H_5^{\bullet} \qquad (1)$$

$$C_2H_5^{\bullet} + C_3H_8 \longrightarrow C_3H_7^{\bullet} + C_2H_6 \qquad (2)$$

$$H^{\bullet} + C_3H_8 \longrightarrow C_3H_7^{\bullet} + H_2 \qquad (3)$$

$$CH_3^{\bullet} + C_3H_8 \longrightarrow C_3H_7^{\bullet} + CH_4 \qquad (4)$$

$$C_3H_7^{\bullet} \longrightarrow CH_3^{\bullet} + C_2H_4 \qquad (5)$$

$$C_3H_7^{\bullet} \longrightarrow H^{\bullet} + C_3H_6 \qquad (6)$$

$$C_3H_7^{\bullet} + CH_3^{\bullet} \longrightarrow CH_4 + C_3H_6 \qquad (7)$$

termination $$2\,CH_3^{\bullet} \longrightarrow C_2H_6 \qquad (8)$$

which explains the basis why the order is closer to $^{3}/_{2}$ at lower pressures and higher temperatures, and closer to unity at higher pressures and lower temperatures. Here, the $\beta\mu$ termination reaction (7) is important in the first order region, whereas reaction (8) a $\beta\beta$ radical recombination is an important step in the $^{3}/2$ order region. The transition of the reaction order from first to $^{3}/2$ was accompanied by a decrease in the activation energy from 280 - 227.8 KJ.

Studies at higher temperatures using the flow technique[85 - 90] have detected the presence of some secondary products like ethane, acetylene, C_4 and some heavier hydrocarbons in addition to the major products. Several of the primary products, especially propylene, are relatively unstable. At higher conversions of propane yields of ethylene and methane increase relative to those of propylene and hydrogen.

Both Buekens and Froment [88] and Crynes and Albright[89] have indicated that the overall rate of propane decomposition is not well described by either first-order or other simple-order equations. They observed that the activation energy ~~de~~increases with increasing propane conversion. Similarly, Kershenbaum and Martin[86] who used a theoretical model to determine the order of the reactions and the reaction rate constants from their experimental results on non-isothermal propane decomposition at 1070 - 1270°K also found that the overall order of the reaction lies between 1.0 and 1.2, although they processed their data assuming a first-order kinetics and obtained

$$K_{overall} = 2.4 \times 10^{11} \exp(-\ 52{,}100/_{RT_{max}})\ s^{-1}.$$

On the other hand Kunugi et al[85] taking the decomposition rate to be 3/2 as proposed by Laidler et al obtained the rate constant as;

$$K = 5.5x10^{13} \exp(-51,500/RT) \text{ ml}^{\frac{1}{2}} \text{ mol}^{-\frac{1}{2}} \text{ sec}^{-1}$$

Both results therefore seem to agree, within the limits of experimental error, with the prediction that the order of propane pyrolysis lies between 1.0 and 1.5.

Effects of various diluents on the course of propane pyrolysis have been investigated. Dilution of the pyrolyzing propane with hydrogen accelerates the decomposition rate. Its accelerating influence increases with increasing extent of dilution. The addition of hydrogen also increases the selectivity of the formation of methane and ethane, while those of propylene and ethylene decreases. This has been explained[85] in terms of secondary hydrogenolytic demethylation of propylene - which enhances the yield of methane and ethylene.

$$C_3H_6 + H_2 \longrightarrow C_2H_4 + CH_4$$

The ethylene so formed is in turn hydrogenated to ethane. The addition of propylene[87,91] and nitric oxide[80,99,100] shows marked inihibitory effects on the rate of propane pyrolysis. Herriot et al[90] and Crynes and Albright[89] have studied the effects of steam dilution. Steam accelerated propane decomposition though not as effectively as O_2. At high conversions increase in steam concentration significantly increases the selectivity of ethylene, while those of methane, ethane and propylene decreased by about 1%.

Although the pyrolysis of propane is at least implicitly assumed in many cases to be a completely homogeneous gas phase reaction, the influence of reactor surfaces has been frequently demonstrated. Laidler et al[79], and Poltorak et al[101] used the static reactor at subatomspheric pressures and found that the surface acts both to initiate and terminate the reaction. Fusy et al[103] and Martin et al[102] claim that the wall is effective in terminating the chains. Similarly, Leathard and Purnell[81] have suggested that heterogeneous deactivation of hydrogen radicals at the walls,

$$H^{\bullet} \xrightarrow{\text{wall}} \text{product}$$

is an important reaction when explaining the self-inhibition reactions of propane. Treatment of the inside walls of the reactor surface by H_2S and various other gases has been reported by workers[89,90] using flow reactors. Contacting H_2S with the reactor for several minutes at temperature from 373° - $1073^{\circ}K$, resulted in the formation of metal sulphide film on the reactor walls. These metal sulphides are gradually converted to metal oxides when oxygen or steam comes in contact with the reactors. The metal oxides promote coking reactions and the formation of large quantities of hydrogen. Herriot et al[90] have confirmed qualitatively that reactor history is an important factor in the overall pyrolysis process since it affects the types of heterogeneous wall reactions which are especially important relative to coke and hydrogen formation. Hence, the residence times in reactors are of important consideration in kinetic studies of high temperature pyrolysis. The residence times in static and flow reactors are relatively high and surface effects enormous, these invariably result in the loss of many pyrolysis products which if not observed hinder the formulation of an accurate pyrolysis mechanism. The shock tube technique has the ability to restrict the residence times of the reaction mixture to micro-seconds and to embrace a higher temperature range. As a result the immediate products of the reaction can be observed and an accurate mechanism can be proposed.

Unfortunately, very little work has been done on propane pyrolysis using the shock tube. Benson[92] in 1967 studied the pyrolysis of propane at temperature range between 1100°-1450°K using a chemical shock tube. Both uncatalyzed and hydrogen sulphide catalyzed homogeneous decomposition was investigated. His values for a first order constants for the uncatalyzed reaction were in excellent agreement with lower temperature data[85,86] obtained from other convectional techniques. However, at this temperature range, the product distribution differed from those obtained at other studies, though the trend, that propane pyrolyzes via two routes, at equal rates, one route leading to propylene and hydrogen, the other to ethylene and methane or ethane, was still maintained. He observed that the production of propylene falls with increasing conversion, while methane and ethane formations were substantially unchanged. The yield of ethylene and acetylene rose at the expense of propylene; and at high temperatures; propylene was thought[92] to be subsequently converted, almost stoichiometrically into ethylene and acetylene. This result contrasted to the observations at lower temperatures [85,95] where decreased propylene selectivities were accompanied by sharp rises in the selectivity for methane and ethane.

The presence of hydrogen sulphide accelerated the initial decomposition, and maintained a high propylene selectivity at high propane conversion which normally decreases as ethylene selectivity increases. Hydrogen sulphide also enhanced the formation of methane at the expense of ethane. Change in the reaction (reflected shock) pressure from 811 to 507 KN/m^2 had no effect on the observed selectivity pattern. The gross features of the pyrolysis was explained by a free radical mechanism in which a two channel initiation reaction involved unimolecular decomposition of propane to a methyl and an ethyl radical on one hand, and to a propyl radical and hydrogen atom on the other. The mechanism discussed was essentially similar to the low temperature scheme, though suggestions for the inclusion of steps of propylene conversion to ethylene were made, but not followed up.

Lifshitz et al[27] studied the decomposition of propane at temperature range between 1050-1650°K, at initial pressures of 50-200 KN/m^2 using a single-pulse shock tube. The average reaction time was 700 μs and they analysed the reaction mixture for both primary and secondary products. The rate of production of each of the primary products was defined as:

$$\frac{d\left[P_i\right]}{dt} = 10^{\alpha_i} \exp\left[-E_i/RT\right] \left[C_3H_8\right]_0^{\beta_i}$$

This showed that the activation energies lie between 209-293 KJ and that the power dependence of the initial rates of the formation of those products on the initial concentration of propane vary from 1.2 to 1.6. They also investigated the isotope distribution by pyrolyzing a mixture of C_3H_8 and C_3D_8

in argon. They had inferred from such results that ethane was produced predominantly via the reaction,

$$CH_3^\bullet + CH_3^\bullet \longrightarrow C_2H_6$$

In a later mechanistic analysis based on the results of that investigation, Lifshitz and Frenklach[104] proposed an 11-step reaction scheme which they believed was adquate to explain the mechanism of high temperature pyrolysis of propane. However, one should have thought that for such a mechanism to be capable of explaining the reaction mechanism of propane pyrolysis at high temperatures, and indeed to reflect the pattern of the product distribution observed in that study, it ought to include the secondary decomposition reactions of some of the primary products such as ethylene and propylene to give prominent secondary products like acetylene, allene, etc. But no account was given for the appearance of these secondary product in their experimental results[27].

As far as the author of this current work is aware, the only reported investigators to have studied the pyrolysis of propane in a chemical shock tube at temperatures beyond 2000°K, are Shirotsuka et al[106]. Their study covered a very wide temperature range from 1000 - 5000°K, and reaction times of 0.8 - 1.5ms at high reaction zone pressure of $\sim$ 981 KN/m^2. Although they had processed their data by assuming a first order kinetics, on the grounds that a better correlation was obtained for a first order than a second order treatment, yet their analysis demonstrated that Arrhenius plot for a first order rate kinetics cannot be extrapolated beyond 1300°K.

A sharp drop in both the values of the activation energy and the frequency factor occurred at temperatures above 1300°K, thus yielding two separate first order rate expressions;

$$K_1 = 1.1\times10^{13} \exp(-61000/RT)\ s^{-1} \text{ at } 1000\text{-}1300^{o}K$$

and

$$K_1' = 10^{4} \exp(-6550/RT)\ s^{-1} \text{ at } 1310\text{-}5000^{o}K.$$

Although no appearent reason was given for such rapid fall in the value of the activation energy from 255 KJ/mole to 27.4 KJ/mole, and the frequency factor change from 10^{13} to 10^{4}, but it is believed[86,87] that this fall in rate of reaction with increase in temperature indicates the involvement of secondary reactions which inhibit propane pyrolysis. Also the results from other shock tube investigations[27,107] have shown that even at moderately high temperatures (1200-1680°K) a first order kinetics is not appropriate to describe propane pyrolysis, rather there is a change to a three-halves order kinetics. But at temperatures as high as 3000°K and above, it would be expected that other processes apart from pyrolysis, for example ionization, may be taking place and these would undoubtedly alter the kinetics of the reaction.

Hence it is obvious that there has not been sufficient experiments at high temperatures to determine the kinetics of propane pyrolysis. Even the pattern of product distribution during its pyrolysis is still in question, and the few investigations[27,107] so far conducted at high temperatures do not show any agreement as regards the overall order of the kinetics of the process. This is apparent from the Arrhenius plot shown in figure 1.6 . 1.

It is however , essential that in investigating the pyrolysis of propane at high temperatures, the experimental conditions are limited to temperature ranges where other processes apart from the 'simple chemistry' will not greatly affect the result .

Figure 1.6·1: First-order Arrhenius plot for propane pyrolysis obtained by authors at temperatures > 1100°K

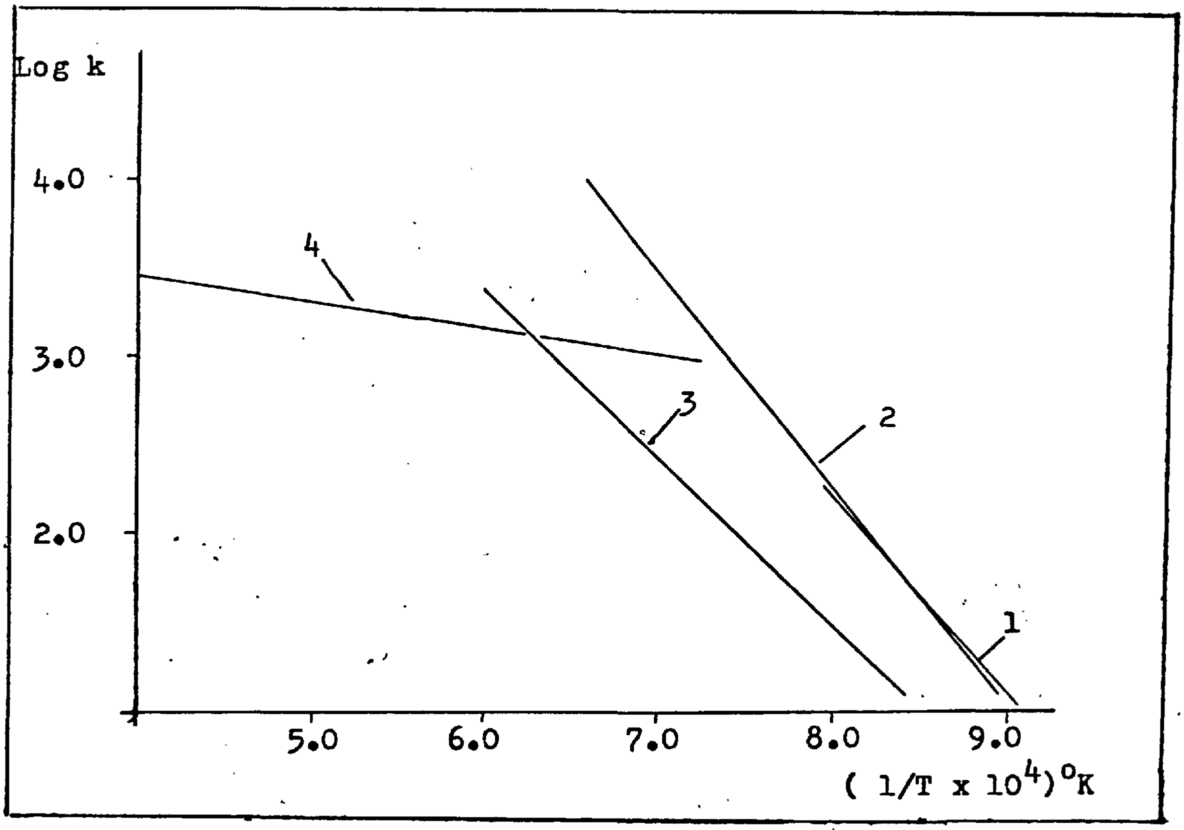

1	-	Kershenbaum and Martins[86]	(1070 - 1270°K)
2	-	Benson[92]	(1100 - 1450°K)
3	--	recalculated Frend's data[107] assuming first-order kinetics	(1210 - 1680°K)
4	-	Shirotsuka et al[106]	(1310 - 5000°K

1.6.2.2 Pyrolysis of acetylene

Thermal decomposition of acetylene has been extensively studied apparently because of its extremely important features in the pyrolysis of other hydrocarbons. Knox et al[108] have obtained evidence that some hydrocarbons originally react to form acetylene and that it is through this compound that the final products, hydrogen and carbon, are formed. Later studies of hydrocarbon pyrolysis including investigations using the shock tube, have confirmed that breakdown to acetylene eventually occurs as this is the most stable species at high temperatures. Much of the earlier works on acetylene pyrolysis have been summarized by Steacie[109]. These were low temperature studies carried out either in static or flow systems. Since that review numerous investigations has been undertaken using variaties of novel techniques and covering the temperature range from (580° - 2900°K).

In general at low temperatures, about 900°K, polymerization is almost the only principal reaction of acetylene, the product being predominantly aromatic hydrocarbons; and also small quantities of hydrogen, methane, ethylene and higher olefinic and acetylenic hydrocarbons and possibly carboneous solid are produced. At high temperatures, in the region of 900°- 2900°K, both polymerization and decomposition reactions occur, the product being carbon, hydrogen and acetylenic hydrocarbons - like vinylacetylene, diacetylene, and higher molecular weight triple-bonded structures, the latter being present in minor quantities.

Suggestions have been put forward as to the nature of the initial products in acetylene pyrolysis. Silcocks[110] observed that at 640 - 740°K, the polymer was initially C_4H_4 and the mean molecular weight increased slowly as the reaction proceeded. Cullis et al[111] using infrared spectrosiopic method, at 673°- 873°K, observed that acetylene was initially converted to polymers and benzene which slowly decomposed to give methane. At a wider temperature interval (773 - 1273°K), Cullis and Franklin[112] studied acetylene pyrolysis employing both static and flow reactors. Their analysis also showed that both polymerization and decomposition occurred, and they found vinylacetylene to be the sole initial product, whereas methane was the predominant final gaseous product. They also observed that vinylacetylene was being converted to C_4H_2 and H_2. In contrast, Read[113] found that vinylacetylene is not an important intermediate in the formation of either diacetylene or carbon from acetylene. This contradicts the results of Munson and Anderson[114] at 773° - 1120°K, that bimolecular reaction to form vinylacetylene, followed by reaction with other molecules of acetylene, is one process which leads to carbon formation from acetylene. Frank - Kamenetsky[115] deduced from pressure measurements that there is first an induction period, followed by dimerization to $(C_2H_2)_2$, with a heterogeneous reaction occurring after 50% of the acetylene had reacted.

Silcocks[110] also demonstrated the importance of heterogeneous reactions during acetylene pyrolysis; while Minkoff et al[116] found that the rate of decomposition was influenced by unclean surface of the reaction vessel. For example, they[116] observed that the decomposition rate was increased from about (1.28 to 2.20)x10^{-4} mole/cc-s by the deposit from previous experiments. Hence no clear mechanism has emerged, as to how acetylene decomposes from these works employing conventional experimental techniques. The difficulty in understanding the mechanism of the reaction seems partly from the analytical difficulties involved in obtaining reliable data because of the high reactive nature of acetylene and most of it products. For example, Bone and Coward[117] experienced that at 1073°K and higher temperatures acetylene always flashed on being admitted to the reaction vessel unless it was largely diluted with nitrogen or hydrogen; and this explosive characteristics make any accurate determination of the rate of reaction under isothermal conditions very difficult. Also the time lag between sample collection and its analysis has been shown[112] to cause remarkable increase in diacetylene - vinylacetylene ratio. However, at present, some of these problems have been largely overcome by use of modern techniques such as the shock tube coupled with the use of spectroscopic methods.

Although many of the early studies were confused by the presence of heterogeneous reactions, shock tube studies also revealed the presence of polymers under circumstances where heterogeneous reactions are highly improbable. Aten and Greene[23, 24] investigated acetylene pyrolysis in the temperature range 1400 to 2500°K using shock wave heating. They employed a combination of time resolved emission and absorption measurements in the visible region of the spectrum and analysis of the quenched reaction products; and they had related the formation of polymer products, in this case mainly diacetylene and some vinylacetylene, to the change in turbidity of the gas. Green et al[12], Skinner and Sokoloski[118],Kozlov and Knorre [25] and Mar'yasin and Nabutovskii[31,119], also analysed the quenched reaction products from shock heated acetylene using more conventional techniques and they all detected the presence of either vinylacetylene or diacetylene or both. However, though there has been speculations that some of these products might have been formed during the cooling process; later studies [34,41]in similar temperature range using time of flight (T.O.F)mass spectrometer have confirmed the presence of not only C_4 acetylenic hydrocarbons but also C_6, C_8 and even higher polyacetylenes. The spectroscopic work of Bauer et al[120] has indicated that aromatic polymers are formed at high temperatures as their characteristic absorption spectra were obtained from the shock heated gas.

However, there are contradictory reports on the role of these acetylenic compounds during the pyrolysis reactions of acetylene. Skinner and Sokoloski [118], Mar'yasin and Nabutovskii [31,119] , and to some extent Bradley and Kistiakowsky[34] have identified vinylacetylene to be the major primary product while others [12,24]have reported that diacetylene is the only prominent C_4 intermediate at 1400 - 2500°K. Gay et al [41] , using a shock tube coupled to a high resolution T.O.F mass spectrometer, which was capable of displaying spectra every 20 μs found C_4H_3 to be the first "neutral species" formed. This species readily attained a steady-state concentration and was then followed by subsequent formation of C_4H_2 , C_6H_2

and C_8H_2 - in this order. This finding disagrees with the concept of Bradley and Kistiakowsky which suggests that the polymers (C_4H_4, C_6H_6 and C_8H_8) are simultaneously formed and instead of polymerization proceeding until all the acetylene had been consumed, they attain a state of equilibrium with acetylene after about 30% conversion. The relative ratios of the equilibrium concentrations of polymers remained constant during the experiment. Gay et al[41] also noticed that the steady state concentration of C_4H_3 increased very little with temperature, while that of C_4H_2 increased rapidly and hence from this and other observations they concluded that reactions (1) and (2) are not reversible and that

$$2C_2H_2 \longrightarrow C_4H_3 + H \qquad (1)$$

$$2C_2H_2 \longrightarrow C_4H_2 + H_2 \qquad (2)$$

the decomposition sequence of acetylene proceeds in the following forward direction:

$$C_2H_2 \longrightarrow C_4H_3 \longrightarrow C_4H_2 \longrightarrow C_6H_2 \longrightarrow C_8H_2 \longrightarrow \underset{\text{carbon}}{C} + H_2$$

It is therefore apparent that there is considerable conflicting evidence and suggestions as to how acetylene decomposes, and as such it has been difficult to formulate a single reaction mechanism which could describe the overall kinetic behaviour of acetylene. Furthermore, from the fact that the dilution of reacting acetylene with either vinylacetylene, diacetylene or methylacetylene accelerates its consumption [112,116,121], it seems probable that these polymers, once formed, react further with acetylene and may be playing significant role in the overall decomposition of acetylene to carbon. Hence many different mechanisms have been, from time to time, postulated. The various suggested mechanisms as to how acetylene decomposes to carbon can be classified broadly into two groups;

i) those which involve polymerization[122,123] to high molecular weight hydrocarbons, usually aromatic in nature, which then lose hydrogen but leave the carbon nucleus intact,

and ii) those in which the removal of hydrogen[16] is the primary step, the labile species formed then combining in some way to give solid carbon.

The first group is usually associated with a bimolecular reaction whereas the latter is more often attributed to free radical mechanism. Actually according to later theories, these two processes, polymerization and dehydrogenation, are not truly independent and neither occurs as a distinct preliminary to the other. Thus Porter[66] advanced the "acetylenic theory", whose concept of "simultaneous" polymerization and dehydrogenation is now widely accepted. This concept has been greatly clarified by the work of Bonne et al[124], and Kistiakowsky and his co-workers[34,41]. It would appear that the mechanism of acetylene decomposition to the final products, carbon and hydrogen, involves the intermediate formation of polyacetylenes.

Bonne, Hamman and Wagner[124], investigated the mechanism of carbon formation in premixed C_2H_2/oxygen flames, whilst Kistiakowsky and co-workers[34,41] studied the pyrolysis of acetylene in shock waves. Even though the two systems are

Figure 1.7: Formation of polyacetylenes during the pyrolysis of acetylene.[41, 124]

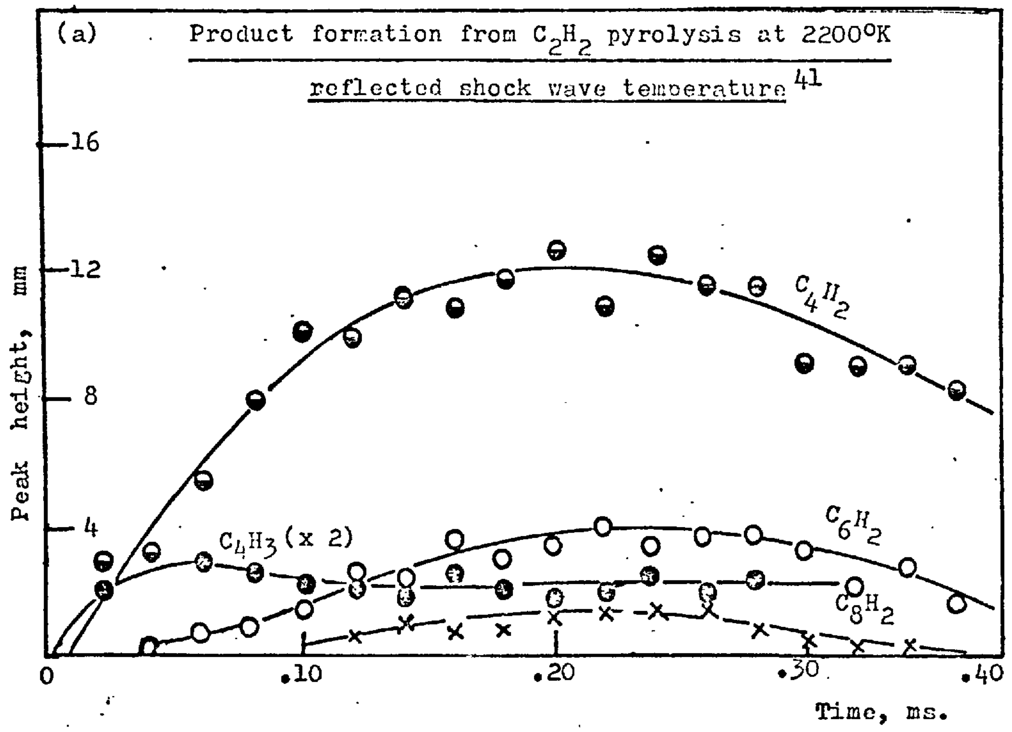

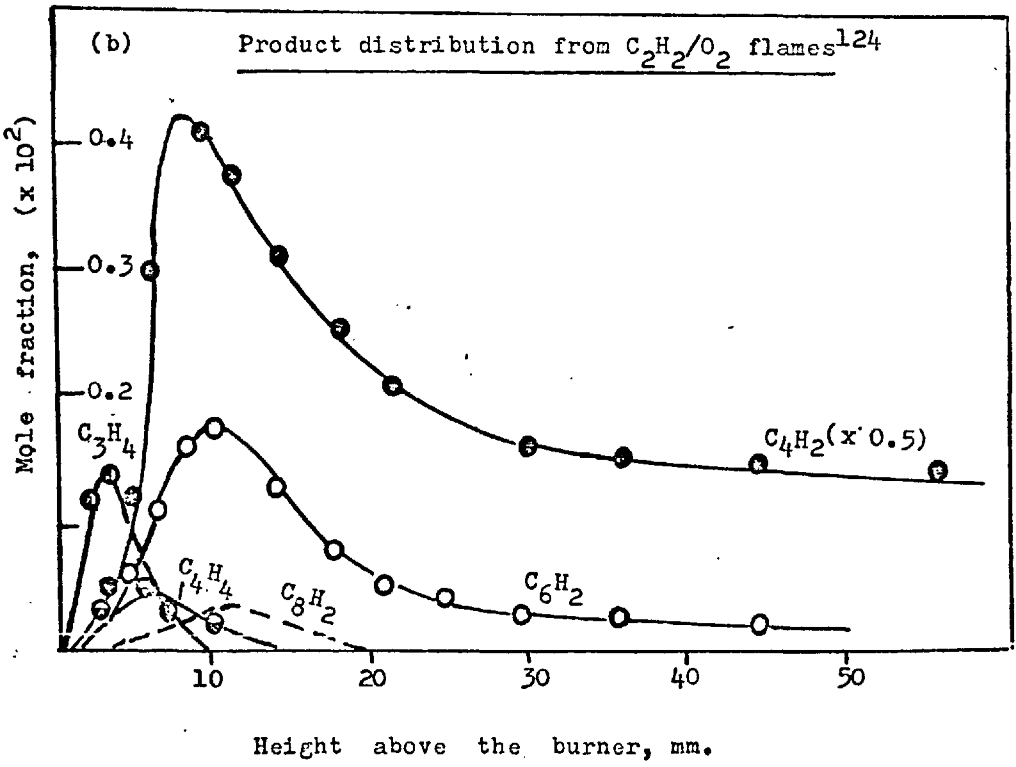

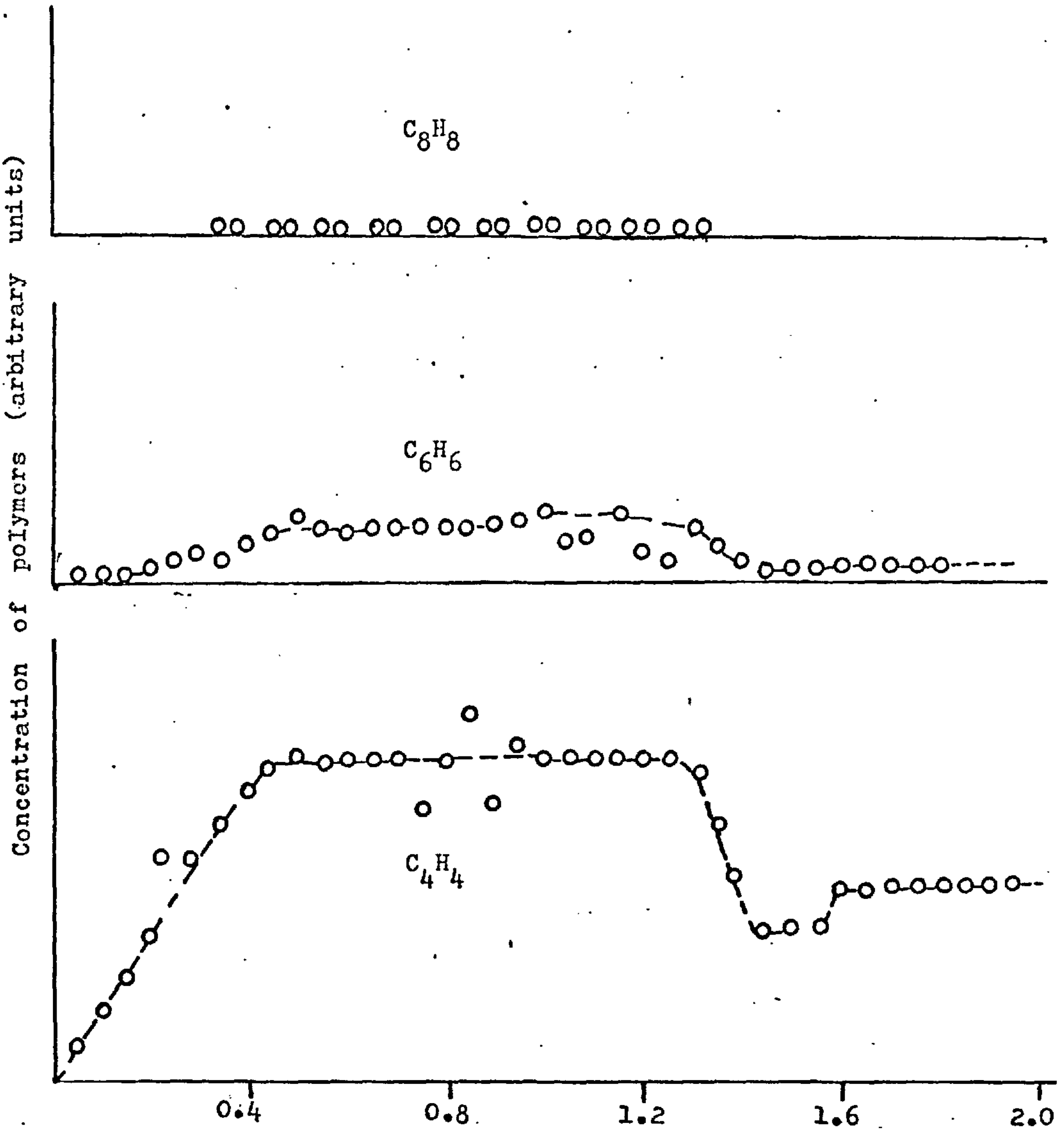

FIGURE 1.8: FORMATION[31] OF POLYACETYLENES FROM THE PYROLYSIS OF C_2H_2 AT REFLECTED SHOCK TEMPERATURE OF 1870°K.

very different, the results obtained are remarkably similiar (figures 1.7, (a) and (b)), and in each case it was possible to identify and follow the concentrations of the polyacetylenes- C_4H_2, C_6H_2, C_8H_2 and $C_{10}H_2$ - throughout the entire course of reaction. From their [34,41] time-resolved measurement (as in figures 1.7 (a) and 1.8 it is evident that the formation of the higher polyacetylenes was characterized by an induction period, whose length seems to increase with increasing molecular weight of the species. Similarly, several investigators on carbon formation during the pyrolysis of acetylene in shock waves using emission spectroscopic[29, 31] or other methods have also recorded pronounced induction time before the onset of carbon particle deposition. A good correlation has been known[34] to exist between the induction period for carbon formation and the characteristic times, for the polyacetylenes to decay. Carbon starts to form as the concentrations of these polymers pass through maxima. Such findings undoubtedly present evidence that the polyacetylenes are carbon precursors during thermal decomposition of acetylene, and it seems that useful kinetic data could be obtained from both the rate of formation and decay of these polymers.

The rate of carbon formation from shock heated acetylene has been measured by Hooker[29], Mar'yasin and Nabutovskii[31] and Gospling et al[30] using optical method. They had characterized the induction period as the time before the onset of emission from the solid carbon particles in the visible spectrum region. Though their techniques were similar, nevertheless the values of E_{ind}, activation energy for carbon formation varied widely from 54.34 KJ/mole[29] - 209 KJ/mole[31].

Mar'yasin and Nabutovskii[119] had also used a different method and obtained E_{ind} = 125KJ/mole. In this case, their method of determining the induction period consisted of passing a plug of cotton wool through the reaction chamber of the shock tube after each experimental run, and the colour of this cotton wool indicated the presence or absence of carbon black. For confirmatory purposes in the doubtful cases, a liquid extraction of the cotton wool plug was carried out by means of benzene, and the presence of black colour after the extraction was regarded as a positive indication of carbon black formation. The reaction times, determined from the reflected shock pressure trace, was taken to be the induction period of carbon formation in the cases where the first positive indentification was noticed. However, the accuracy of such method is not only subjective and doubtful but lacks precision as to the very instant when carbon formation starts, and therefore it is important that each data can only be assessed and compared depending on the similarities of the technique used and the method of data processing employed in the investigation.

A number of experimental results appear to favour a simple bimolecular reaction for the removal of acetylene. In many investigations covering wide temperature ranges (620-2450^{O}K) it has been shown that the decomposition of acetylene is dominated by a single reaction mechanism which obeys a second order kinetic law. An Arrhenius plot of second-order rate constans for this wide temperature range fall approximately in a single straight line, which can be represented by the expression[41]

$$\log K = 10.8 - 173900/2.3RT$$

where K is (1/mol sec).

Such remarkable features do suggest that to a great extent the rate controlling step is bimolecular - with the combination of two molecules of C_2H_2 to form vinylacetylene. However, such reaction as;

$$2C_2H_2 \longrightarrow C_4H_4$$

alone cannot explain all the other features of the acetylene pyrolysis; - for example, the presence of an induction period as reported by[23,24,29-31,111,115,119] which is eliminated by the addition of substances, such as diacetyl and ethylene oxide [111] which readily generate free radicals; whereas the presence of about 1% nitric oxide (an inhibitor) greatly lengthens the induction period (by a factor of 100 or more)[109].

The activation energy of the reaction of C_2H_2 decomposition is low, between 100 - 209KJ/mole. Such low value of activation energy would not favour the two possible simple modes of unimolecular decomposition of acetylene into radicals, such as;

1) $C_2H_2 \longrightarrow 2CH\cdot$ - originally proposed by Bone and Coward[117]

and 2) $C_2H_2 \longrightarrow C_2H^\bullet + H^\bullet$ by Silcocks[110]

Both reactions - (1) and (2) - are very endothermic, about 961.4 and 506KJ, respectively[125]. Many authors have therefore, favoured a biradical mechanism which gives an excited molecule of acetylene in triplet state[126,127] or a triplet and biradical species $C_4H_4^{*}$[128]. Minkoff [126,127] suggested mechanism based on the assumptions that both chain initiation and termination are surface dependent, and that the chain carriers are acetylene or polymeric molecules in the triplet state, viz:

$$2C_2H_2 \longrightarrow 2C_2H_2^{*}$$

$$C_2H_2^{*} + C_2H_2 \longrightarrow (C_2H_2^{*})_2$$

$$(C_2H_2^{*})_n + C_2H_2 \longrightarrow (C_2H_2^{*})_{n+1} \text{ or } C_2H_2^{*} + M_n$$

$$(C_2H_2^{*})_n + (C_2H_2^{*})_n \longrightarrow \text{products}$$

$$\text{or} \qquad (C_2H_2^{*})_n \longrightarrow M_n$$

where $(C_2H_2^{*})$, $(C_2H_2^{*})_2$, etc are triplet molecules and M_n = "dead" polymer.

It is believed that at lower temperatures, the trans configuration of the triplet state leads to the formation of straight-chain polymers, whilst at higher temperatures the presence of radicals in the cis configuration would account for the elimination of hydrogen; for example,

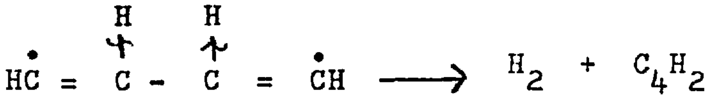

$$\dot{H}C = \overset{H}{C} - \overset{H}{C} = \dot{C}H \longrightarrow H_2 + C_4H_2$$

thus explaining the formation of aromatic hydrocarbons and carbon. Palmer and Dormish[128] later modified Minkoff's triplet mechanism. Instead of C_2H_2 undergoing initially double excitation, $2C_2H_2 \longrightarrow 2C_2H_2^*$ they proposed a unimolecular excitation of acetylene to its lowest lying state;

$$C_2H_2 \quad + \quad C_2H_2 \quad \longrightarrow \quad C_2H_2^* \quad + \quad C_2H_2$$

where the second molecule of acetylene is present only as a collision partner. The triplet acetylene on further collision with a fresh molecule of acetylene gives a triplet dimer which in turn undergoes further collisions to give stable products such as benzene;

$$C_2H_2^* \quad + \quad C_2H_2 \quad \longrightarrow \quad C_4H_4^*$$

$$C_4H_4^* \quad + \quad C_2H_2 \quad \longrightarrow \quad \text{product.}$$

Since the generation of stable species from the excited states must take place at the surfaces, the triplet state mechanism might seem adquate in explaining the acetylene reactions in the conventional systems where surface effects are apparent. But with very fast reactions and in cases where surface effects are absent or quite negligible (for example in shock tubes) its authenticity might be questionable. A new dimension to the whole question of the mechanism of acetylene pyrolysis was given by the application of rapid sampling technique in conjunction with the shock tube. The detection of $C_4H_3^{\bullet}$ radical[41] which remained in a steady state concentration throughout the entire course of the reaction has led to the suggestion[41,129] that this species is formed from acetylene by a reaction such as;

$$2C_2H_2 \quad \longrightarrow \quad C_4H_3^{\bullet} \quad + \quad H^{\bullet}$$

and that, subsequently, other polyacetylenes are formed by the reactions:

$$C_4H_3^{\bullet} \ (+ M) \longrightarrow C_4H_2 + H^{\bullet} \ (+M)$$

$$C_4H_2 + C_2H_2 \longrightarrow C_6H_3^{\bullet} + H^{\bullet}$$

$$C_6H_3^{\bullet} \ (+ M) \longrightarrow C_6H_2 + H^{\bullet} \ (+M) \quad \text{etc}$$

Bonne et al[148] proposed a very similar mechanism. It differs only in that formation of higher polyacetylenes is thought to occur via the reaction of acetylene with $C_4H_3^{\bullet}$ and $C_6H_3^{\bullet}$ radicals rather than with tht polyacetylenes themselves.

Another possible route via which the radical $C_4H_3^{\bullet}$ could be produced is by the reactions.

$$C_2H_2 + C_2H^{\bullet} \longrightarrow C_4H_3^{\bullet}$$

Cullis, Hucknall and Shepherd[130] have suggested that the initial nucleus in carbon-forming system is the $C_2H^{\bullet}$ radical, and that the initial stage of the carbon-forming process from acetylene involves the reaction.

$C_2H^{\bullet} + C_2H_2 \longrightarrow C_4H_2 + H^{\bullet}$ in which both the acetylene and polyacetylenes are said to act as the growth species.

An alternative free radical mechanism in which the possible initiation reaction includes the bimolecular reaction of acetylene to give a vinyl and ethynyl radical has been suggested by Stehling et al [121] and theoretically developed in detail by Back [131].

The Back's mechanism is based on bimolecular disproportionation reaction of two molecules of acetylene into radicals;

$$C_2H_2 + C_2H_2 \longrightarrow C_2H^{\bullet} + C_2H_3^{\bullet}$$

This initiation step is followed by series of radical addition, abstraction and decomposition reactions - which accounted for the formation of the generally observed reaction products of acetylene pyrolysis over the entire temperature range from (700 - 2400°K). This mechanism presupposes that the products are distributed as follows:

diacetylene - is the major product at high temperatures
vinylacetylene- is the major product intermediate temperature,

while aromatics and polymers are the dominant products at the lower temperatures.

The Back's mechanism consists of 17 reaction steps, and assumes that at high temperatures, as found in shock tubes, the vinyl radical formed at the initiation step will be largely dissociated and the chain will be carried by hydrogen atom and $C_2H^{\bullet}$ radicals. Since the relative concentration of these radicals is a complex function of a number of competing reactions, it is possible that changes in the product distribution with temperatures follow the change in the relative concentration of the radicals, but this cannot be ascertained without any exact knowledge of the rate constants for the elementary reactions involved. Therefore, the problem involved in adopting this and other complex mechanistic schemes in kinetic modelling to reproduce the experimentally observed time dependent parameters, such as in concentration - time profiles of the species, lies in the choice of accurate rate constants for each of the steps - a task which is not easy since most of these reactions involve (uncommon) high-molecular weight radicals.

From the above review, therefore, it is obvious that due to the complexity of the pyrolysis reaction of acetylene the mechanism is still not very clear. Inorder to understand more of its complex reaction mechanism which involves simultaneous polymerization and dehydrogenation reactions, studies are still required - especially in investigating the early stages of the reaction at high temperatures under homogeneous conditions - using fast detecting techniques to monitor the rapid building-up and the decaying of the numerous intermediates present in the system.

1.7: The present work

Following the review on section 1.6, the current studies were undertaken to elucidate the mechanism of high temperature pyrolysis of hydrocarbons with reference to propane and acetylene. To accomplish this, it was necessary to use a reactor which is free from 'wall-effect' - the shock tube and to proceed as follows:-

(i) To investigate the pyrolysis of propane at temperatures from 1200°K to 2800°K and to determine the pattern of product distribution using gas chromatograph.

(ii) To examine in details the effects of variation of such parameters as time, temperature and pressure on the optimum conversion of propane to the major reaction products; especially the effect of increases in the reaction zone pressure on the yield of acetylene at high temperatures.

(iii) To investigate the effect of addition of some quantities of ethane - a known product of propane pyrolysis and also an important source of radicals ($CH_3^\bullet$, $C_2H_5^\bullet$ and $H^\bullet$) - on the decomposition of propane.

(iv) To suggest mechanism for high temperature pyrolysis of propane based on the product distribution.

(v) To study acetylene pyrolysis at temperatures between 1400 to 2760°K by monitoring the formation and decay of intermediate species and products using an ultra-rapid scan infrared spectrometer.

(vi) To elucidate mechanism of the reaction by using a kinetic modelling program, devoid of steady state assumptions, to generate concentration - time profiles for reaction products which could match with the experimental infrared emission profiles.

CHAPTER 2

CALCULATION OF SHOCK PARAMETERS

2.1 Shock wave formation and propagation

A classic illustration by Becker[132] for a gas confined in a cylinder equipped with a freely movable piston gives an elegant description of wave formation and its propagation in a tube. If sudden impulse is applied to the piston it accelerates, and the entire motion is thought to consist of many small successive movements. Each such movement generates a corresponding pressure pulse which propagates through the gas ahead of the piston. This will travel at the sound speed of the gas as a compression wave with a velocity (a_n), characterized by the temperature T_n of the gas;

$$a_n = \sqrt{\frac{\gamma R T_n}{m}} \qquad 2.I.0$$

where

a is the sound speed of the gas

γ = the specific heat ratio

R = the universal gas constant

m = the molecular weight of the gas

The compression is rapid and assumed to be adiabatic, so that the passage of the first wave raises the temperature of the gas to T_2. The next small movement of the piston generates a further compression wavelet which will travel at the velocity, a_2, characterized by T_2. Since each successive compression wavelet increases the temperature of the gas (i.e. $T_n > T_{n-1}$) and the sound velocity increases with temperature (equation (2.I.0)), therefore there is the tendency for the later pulses to overtake the preceeding ones. Naturally, it is not possible for pulses to actually overtake one another since any pulse attempting to overtaking its predecessor will enter gas at a lower temperature T_{n-1} and will therefore decelerate immediately. Consequently, the pulses coalesce to form an abrupt discontinuity in pressure, temperature and density.

This discontinuity, once formed, moves with a constant velocity intermediate between the sound speeds of the hot and the undistured cold gas ahead. In a real shock tube the driver gas acts as the piston and the face of this 'gaseous piston' is called the contact surface, while the accumulation of the compressed gas moving at supersonic velocity into the uncompressed gas is the shock wave. The boundary between the shock wave and the uncompressed test gas ahead of it is the shock front.

2.2 Shock tube coordinates

A simple shock tube, illustrated in figure 2.0(A), is essentially a long tube separated by a thin diaphragm into two sections - the high pressure driver section and the low pressure driven section. When the diaphragm is suddenly broken and instanteously removed a shock wave travels away from it at a supersonic speed into the test gas while a rarefaction wave travels in the opposite direction with a sonic velocity into the driver gas. The nature of the driver gas and the pressure ratio (P_4/P_1) across the diaphragm dictates the strength of the shock to be realized.

An idealized pressure distribution along the shock tube after a time, t' has elapsed after the bursting of the diaphragm is shown in figure 2.0(B); while the shock history is plotted in the x - t diagram in figure 2.0(C).

The advancing shock front is halted at the end wall of the shock tube and it is reflected back into the already

FIGURE 2.0: Idealized wave diagram for the shock tube at time t' after bursting the diaphragm.

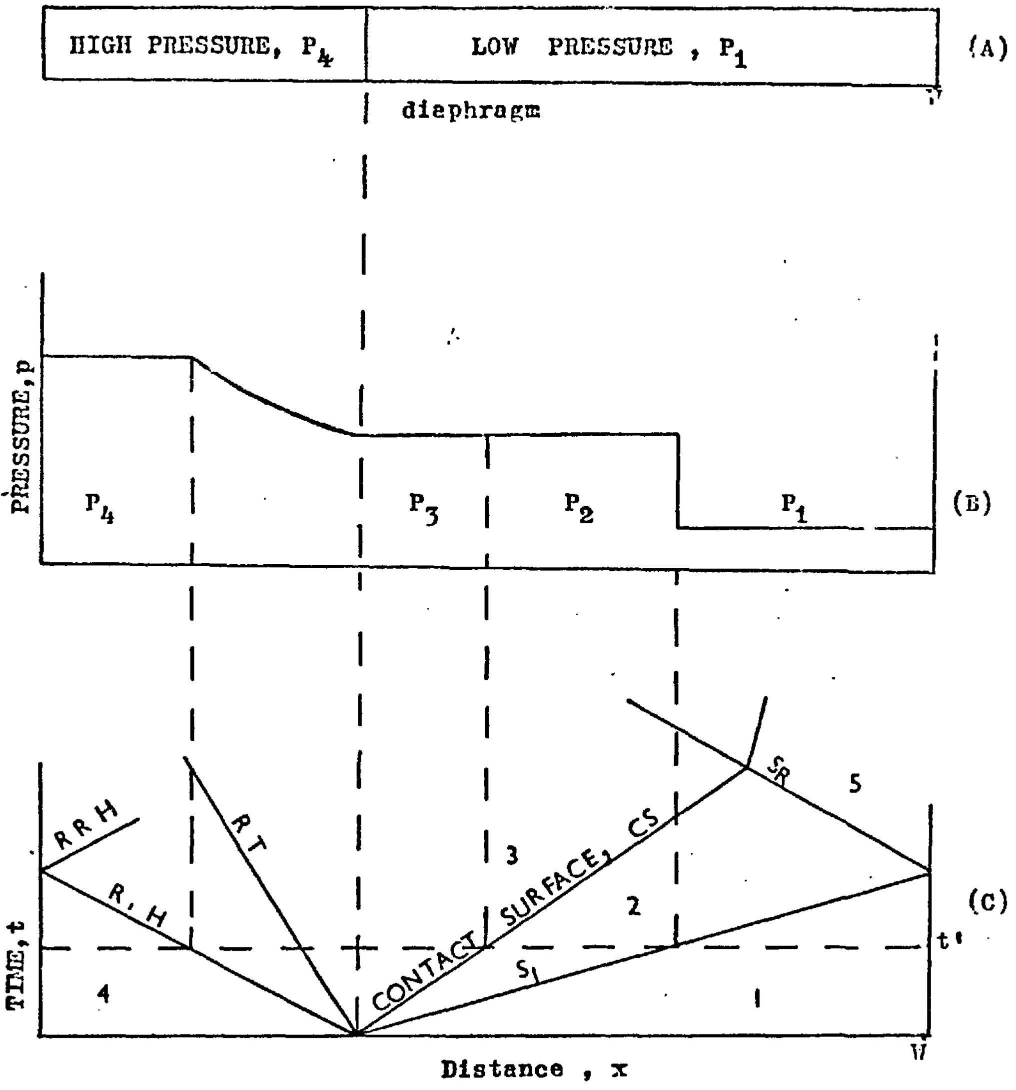

S_I - Incident Shock Wave
S_R - Reflected Shock Wave
RH - Rarefaction Head
RRH - Reflected Rarefaction Head
RT - Rarefaction Tail

SHOCK COORDINATE SYSTEMS IN THE SHOCK TUBE.*

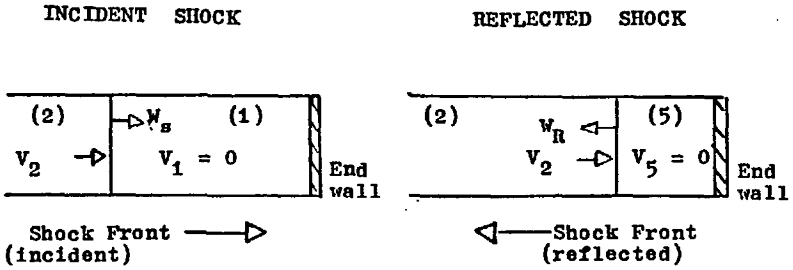

Figure (2.1) - For laboratory-fixed coordinates (shock tube at rest)

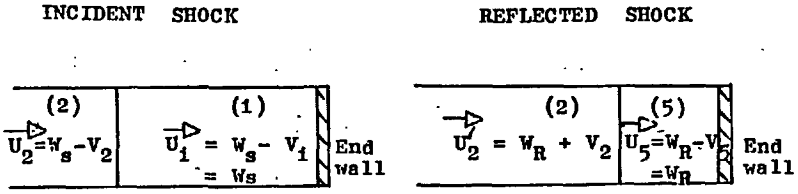

Figure (2.2) - Shock - fixed coordinate (shock front at rest)

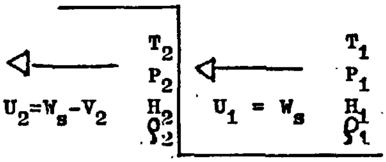

Figure (2.3) - Translational changes of gas properties across the incident shock front for system in fig.(2.2).

heated region (2). The result of this is that the gas in the reflected shock region (5) is compressed twice and as such temperatures higher than those in region (2) are produced.

To solve the resultant hydrodynamic equations of the gas motion in the shock tube, two basic coordinate systems are used. For the first system, the shock tube is taken to be at rest while the velocities of the gas molecules (V) and the shock front (W) are measured relative to it (figure 2.1). Figure 2.2 shows the second system in which the gas is regarded as flowing with a velocity (U_1 or U_2') into a stationary shock front, to emerge at the other side with a lower velocity (U_2 or U_5 for the incident and reflected waves respectively).

The gas ahead of the incident and behind the reflected waves are assumed to be stationary ($V_1 = 0$, $V_5 = 0$), and hence the following general relationships are obtained:

$$U_1 = W_S - V_1 = W_S \qquad 2.1.1$$

$$U_2 = W_S - V_2 \qquad 2.1.2$$

$$U_5 = W_R - V_5 = W_R \qquad 2.1.3$$

$$U_2' = W_R + V_2 \qquad 2.1.4$$

The transitional changes in the properties of the test gas across the incident shock front, for a shock fixed co-ordinate can be illustrated, as in figure 2.3. Therefore writing the conservation equations for mass, momentum and energy respectively for gas passing through a unit area of a stationary shock front, we obtain:-

$$\rho_1 U_1 = \rho_2 U_2 \qquad \text{for mass} \qquad 2.1.5$$

$$\rho_1 U_1{}^2 = \rho_2 U_2{}^2 \qquad \text{for momentum} \qquad 2.1.6$$

$$H_1 + \tfrac{1}{2} U_1{}^2 = H_2 + \tfrac{1}{2} U_2{}^2 \qquad \text{for energy} \qquad 2.1.7$$

In formulating the energy conservation equation (equtn.2.1.7) it is assumed that there is no heat exchanges in the shock wave since the duration of flow in the shock tube is only a few milliseconds; and heat losses by conduction, convection and radiation are neglected.

The momenclature and the symbols used in this and related sections are given in section 2.3.1 and in appendix A1.

2.3 Calculation of shock parameters

The conservation equations 2.1.5 to 2.1.7 given in section 2.2 are true generally for conditions in the shock waves in any gas. The solution of these equations are obtained in terms of the ratios of the pressure, density and temperature across the shock front. Since the initial conditions ahead of the shock are known, P_2, ρ_2 and T_2 can be evaluated. For an ideal gas the exact solution of these equations is fairly straight forward since the specific heats, C_p and C_v, are constant and independent of temperature, and the enthalpy which by definition is:

$$H = E + RT$$

where E is the internal energy and R is the gas constant per unit mass of gas, becomes simply, $H = C_p T$. But in the case of a real polyatomic gas the specific heats are temperature dependent, and furthermore dissociation and ionization - both of which are dependent on temperature and pressure - may occur at elevated shock temperatures and the solution conservation equations are best carried out by interative method.

In this chapter is outlined the procedures for calculating shock parameters for an ideal and real gas conditions. Also the calculation for tailoring interface conditions assuming ideal gas conditions are given in section (2. 3.5).

2.3.1 Nomenclature

ρ = gas density

P = pressure

T = Temperature

C_p = Specific heat at constant pressure

C_v = Specific heat at constant volume

γ = Specific heat ratio, C_p/C_v

a = Speed of sound in the gas mixture

α = $(\gamma + 1)/(\gamma - 1)$

β = $(\gamma - 1)/2\gamma$

X = mole fraction of the lower molecular component of the driver gas - Hydrogen.

M = molecular weights of the gases.

f = percentage of hydro-carbon in argon

H = Enthalpy per unit mass

E = C_v.xT, the internal energy per unit mass

M_s = mach number

W = velocity of the shock front

V = the actual velocity of the gases in the S/T

U = the velocity of the gases relative to W and V

P_{ij} = P_i/P_j

T_{ij} = T_i/T_j

E_{ij} = E_i/E_j

Subscripts correspond to the different gas regions in fig.(2.0).

1 = initial conditions in the test section of the shock tube

4 = initial conditions in the driver section of the " "

2 = incident shock region

5 = conditions behind the reflected shock wave.

2.3.2 Calculation of shock parameters for ideal gas conditions

2.3.2.1 Equations.

For ideal gases having constant specific heats, expression (3.2.0) has been given[5] as:

$$P_{21} = \frac{2\gamma M_{s1}^{2} - (\gamma - 1)}{(\gamma + 1)} \qquad 3.\ 2.\ 0$$

where M_{s1} - the mach number is equal to W_s / a_1

and $a_1 = \sqrt{\frac{\rho_1}{\gamma P_1}}$

Napier and Simonson[133] have derived the following relationships, known as the Rankine - Hugoniot equations, from the conservation equations (2.1.5 - 2.1.7):

(a) Diaphragm pressure :

$$P_{41} = P_{21} / \left\{ 1 - (P_{21} - 1) \left[B_4 E_{14} / (\alpha_1 P_{21} + 1) \right]^{\frac{1}{2}} \right\}^{1/B_4} \qquad (3.2.1)$$

(b) $\frac{\text{incident temperature}}{\text{initial temperature}} = T_{21} = P_{21} (\alpha_1 + P_{21})/(\alpha_1 P_{21} + 1) \qquad (3.2.2)$

(c) $\frac{\text{Incident Density}}{\text{Initial Density}} = \rho_{21} = P_{21} / T_{21} \qquad (3.2.3)$

(d) $\frac{\text{Reflected Pressure}}{\text{Incident Pressure}} = P_{52} = (\alpha_1 + 2 - P_{12})/(\alpha_1 P_{12} + 1) \qquad (3.2.4)$

(e) $\frac{\text{Reflected Temperature}}{\text{Incident Temperature}} = T_{52} = P_{52} (\alpha_1 + P_{52})/({}_1 P_{52} + 1) \qquad (3.2.5)$

(f) $\frac{\text{Reflected Density}}{\text{Incident Density}} = \rho_{52} = P_{52} / T_{52} \qquad (3.2.6)$

and the following relationships are easily obtained.

(g) $\frac{\text{Reflected Temperature}}{\text{Initial Temperature}} = T_{51} = T_{52} \times T_{21}$ (3.2.7)

(h) $\frac{\text{Reflected Pressure}}{\text{Initial Pressure}} = P_{51} = P_{52} \times P_{21}$ (3.2.8)

(i) $\frac{\text{Reflected Density}}{\text{Initial Density}} = \rho_{51} = \rho_{52} \times \rho_{21}$ (3.2.9)

These equations (3.2.0 - 3.2.9) are easily solved for the parameters behind the reflected shock wave once the initial conditions in the shock tube are known and the shock speed is measured. Alternatively a theoretical solution is carried out in terms of diaphragm pressure ratio by assigning values to P_{21} , in this case the knowledge of the shock speed is not necessary but could be used for comparison between measured and computed values for the shock speed.

2.3.2.2 Procedure for calculation

Tables of the data used in the calculations have been extracted from various sources. All calculations were carried out by using the college CDC 6400 computer in the following sequence:

(1) Read in values of X, f, W_s, T_1, P_1, and M, C_p, C_v, for each gas.

(2) Calculate C_{v4}, C_{p4}, and C_{v1}, C_{p1}, ρ_1 and hence γ_4 and γ_1, for gas mixtures.

(3) Calculate α_4, β_4, E_4, α_1, β_1, E_1 and a_1 and M_{SI}

(4) Assign a value to the incident pressure ratio P_{21} or calculate it from equation (3.2.0) if W_s is measured.

(5) Calculate the diaphragm pressure ratio, P_{41} from equation (3.2.1).

(6) Calculate T_{21} from equation (3.2.2)

(7) Calculate the incident density ratio, ρ_{21} from equation (3.2.3)

(8) Calculate P_{52} from equation (3.2.4)

(9) Calculate T_{52} and ρ_{52} from equations (3.2.5) and (3.2.6) respectively.

10) Calculate T_{51}, P_{51} and ρ_{51} from equations (3.2.6 to 3.2.7).

I1) Calculate the incident shock temperature

$$T_2 = T_{21} \times T_1 \text{ and } P_1 = \frac{P_4}{P_{41}} \text{ and } \rho_2 = \rho_{21} \times \rho_1$$

I2) Calculate the reflected shock parameters from:-

reflected shock temperature, $T_5 = T_{51} \times T_1$

reflected shock Pressure, $P_5 = P_{51} \times P_1$

reflected shock Density, $\rho_5 = \rho_{51} \times \rho_1$

I3) WRITE out the values of W_s, P_{21}, P_{41}, T_2, ρ_{21}, ρ_{51}, P_{51} and T_5.

2.3.3 Calculation of shock parameters considering real gas effects.

At higher shock temperatures chemical reactions will be taking place and the ideal gas conditions will no longer be applicable. And because of the larger heat content of a real gas, the temperature in a shock-wave through a real gas is considerably lower than in a corresponding shock through an idea one, whilst the density is appreciably higher. These effects are discussed later.

Unlike the idea of gas, a real gas possess the modes of energy which are excited to a degree that depends on the temperature. An amount of energy equal to $\frac{1}{2}KT$ (where K is Boltzmann's constant) is allotted to each degree of freedom in the modes of translation, rotation and vibration associated with a molecule for the classical partition energy. But in the quantum partition of energy both the translational and rotational modes usually have this value at approximately room temperature, whereas the energy of vibration only approaches it at much higher temperatures. Thus the specific heats of polyatomic gas increase with temperature.

It is thus clear that those equations derived for an ideal gas will not serve to predict the corresponding behaviour of a real gas. The variation of the specific heats with temperature must be taken into consideration.

2.3.3.1 Valid shock relations for a real gas

The basic conservation equations describing the incident conditions are exactly those given by equations (2.1.5 - 2.1.7), and for a dissociating gas, the gas law also holds. For iterative purposes, these equations have been conveniently reduced to the following forms:

$$H_2 - H_1 = \frac{1}{2}\,\frac{U_1^2}{10^7 J}\left[1 - \left(\rho_1/\rho_2\right)^2\right] \qquad (3.3.0)$$

$$P_2/P_1 = 1 + \frac{M_1 U_1^2}{RT_1}\left(1 - \rho_1/\rho_2\right) \qquad (3.3.1)$$

$$\frac{P_2}{P_1} = \rho_2/\rho_1 \times \left(\frac{T_2}{T_1}\right) \times \left(\frac{M_1}{M_2}\right) \qquad (3.3.2)$$

where

J = mechanical equivalent of heat and the factor $10^7 J$, is to convert ergs to calories

R = The gas constant expressed in ergs per degree

M_1, M_2 = are the initial and final molecular weights of the gas in regions 1 and 2.

If it is assumed that there is no change in weight between regions 1 and 2 which is reasonable since the hydrocarbon mixture is largely diluted with argon, then $M_1 = M_2$.

For the reflected shock the conservation equations can be written in a manner similar to equations (2.1.5 - 2.1.7) in which the relations in equations (2.1.2 to 2.1.4) has been used to obtained the following equations:

$$\rho_5 W_R = \rho_2 (V_2 + W_R) \qquad (3.3.3)$$

$$P_5 + \rho_5 W_R^2 = P_2 + \rho_2 (V_2 + W_R)^2 \qquad (3.3.4)$$

$$H_5 + \tfrac{1}{2} W_R^2 = H_2 + \tfrac{1}{2} (V_2 + W_R)^2 \qquad (3.3.5)$$

Inorder to solve these equations by iterative method they are reduced to forms similar to equations 3.3.0 to 3.3.2.

$$H_5 = H_2 + \left(\frac{1}{2} \frac{V_2^2}{10^7 J} \right) \left[1 + \frac{2}{(P_5/\rho_2 - 1)} \right] \qquad (3.3.6$$

$$P_{52} = 1 + \frac{M_2 V_2^2}{RT_2} \left[\frac{\rho_{52}}{\rho_{52} - 1} \right] \qquad (3.3.7)$$

and

$$P_{52} = \rho_{52} \times T_{52} \times M_{25} \qquad (3.3.8$$

Solution to equations (3.3.0 to 3.3.2) was carried out using the method of Gaydon and Hurle, while the reflected shock conditions were obtained by applying the same principle. The method outlined below assumes the knowledge of the measured shock speed U_1, and the variation of enthalpy with temperature. The temperature in the driven section of the shock tube, T_1 was set to be 300 °K, and $H_1 = 0$.

2.3.3.2. Calculation Procedure

All calculations were performed using the college C.D.C. 6400 computer as in section 2.3.2.2. Thermodynamic data for acetylene, propane, ethane and argon were taken from Janaf tables[134,135]. The computational sequence was as follows:

1) Read in the percentages of the hydrocarbons, and argon, the enthalpies of these gases as a function of temperature, and the incident shock velocity, U_1.

2) Calculate the enthalpy of the test mixture in question as a function of temperature from the following relationship:

- H(T) for test mixture = f x H (T) of the hydrocarbon
  + (1 - f) x H(T) of argon;

where f is the fraction of the hydrocarbon being investigated in the test mixture.

3) Curve fit enthalpy of the test mixture as a function of temperature using curve fitting subroutine.

4) Guess a value for ρ_{21}, approximately equal to α_1.

5) Calculate H_2 from equation (3.3.0), using this value of ρ_{21} and U_1.

6) With this value of H_2, obtain T_2 from the curve fit.

7) Using the guessed value for ρ_{21}, and the T_2 obtained in step (6), calculate a first value for the incident pressure ratio, $P_{21} = (P_{21})1$ from equation (3.3.2), setting $M_1 = M_2$.

8) Calculate a second value $(P_{21})2$ for the incident pressure using the same assigned value for density

ratio ρ_{21} and U_1 from equation (3.3.1).

9) Compare both values $(P_{21})1$ and $(P_{21})2$ for incident pressure ratio, obtained in steps (7) and (8).

10) If $\left| (P_{21})1 - (P_{21})2 \right| > \Delta$

where Δ is the tolerant error limit, go back to step (4) and assign another value to ρ_{21} and repeat steps (5) to (10). Iterations from step (4) to (10) are repeated until the values of $(P_{21})1$ and $(P_{21})2$ converge, i.e. $\Delta \approx 0$. In the present study Δ was set to 0.01.

11) At the convergence of $(P_{21})1$ and $(P_{21})2$, calculate

$$P_{21} = \frac{(P_{21})1 + (P_{21})2}{2}$$

12) Calculate U_2 from equation (2.1.5), i.e.

$$U_2 = U_1 / \rho_{21} ,$$

and V_2 - the gas velocity in region 2 from equation (2.1.2), to obtain $V_2 = U_1 - U_2$.

The reflected shock parameters are obtained similar procedure by solving equations (3.3.6 to 3.3.8) as follows;

13) Guess a value for ρ_{52}, approximately equal to twice ρ_{21}.

14) Calculate H_5 from equation (3.3.6) by substituting the values of H_2 and V_2 obtained in steps (5) and (12) respectively.

15) From the curve fit, obtain a value for T_5 corresponding to H_5.

16) Calculate $(P_{52})1$ from equation 3.3.8, again setting $M_2 = M_5$, i.e. assumming no dissociation took place.

(17) Calculate $(P_{52})2$ from equation (3.3.7),

(18) Compare $(P_{52})1$ and $(P_{52})2$ obtained in steps (16) and (17); and test for $\left| (P_{52})1 - (P_{52})2 \right| < \Delta$

(19) If (18) is outside the specific error limit, then the Iteration was repeated by gradually reducing the values assigned to ρ_{52} in step (13), until $(P_{52})1$ and $(P_{52})2$ satisfied the error condition.

(20) When step (18) is satisfied, calculate

$$P_{52} = \frac{(P_{52})1 + (P_{52})2}{2}$$

(21) Calculate $\rho_{51} = \rho_{52} \times \rho_{21}$

$P_{51} = P_{52} \times P_{21}$, and $P_5 = P_{51} \times P_1$

$T_5 = T_{52} \times T_{21} \times T_1$

(22) Write out the name of the test gas and f.

(23) Write out U_1, P_{51}, ρ_{51}, T_2, T_5.

The results of such calculation for both ideal and real gas conditions are discussed latter.

2.3.4 Results of calculation of shock parameters for both ideal and real gas conditions.

Calculation of the shock parameters in both the incident and reflected shock regions were carried out respectively for mixtures of C_2H_2 and propane in argon using the procedures outlined above in sections 2.3.2.2 and 2.3.3.2. The results are presented graphically in figure (2.4.1. to 2.4.4) for mixtures of 2% and 5% C_2H_2 in argon and 4% propane in Argon. The parameters were calculated in the units indicated in the figures, and the units are consistent with those used in the experimental section of the current study. The pressure units are in KN/m^2 and the shock velocity in cm/s. Figures (2.4.I to 2.4.3 a) show the variation of both the incident and reflected shock temperatures with shock velocity. The temperatures in both the incident and reflected shock regions are seem to increase with increasing shock velocity. As expected, shock heating by the reflected wave results in much higher temperatures (nearly twice as much) than heating from the incident shock. In all cases, both for acetylene and propane mixtures in argon the predicted temperatures for the real gas are less than those for an ideal one under similar experimental conditions. This is because for ideal gas it is assumed that specific heats are independent of temperature whereas actually at high shock speeds the heat capacity of the gas is increased due to the excitation of vibration; this would lead to the temperature rise predicted by the real gas lagging behind that predicted at ideal conditions. This lag is expected to become more pronounced as dissociation begins to occur and heat is being absorbed. The actual shock temperature will probably be lower than that predicted by real gas [22] as the effect of chemical reactions has not been considered in these calculations. This is clearly illustrated in figures (2.4.3b) in which the measured shock temperature for propane - argon mixtures obtained in this work (as has been described in section 3.3.3) have been compased to the calculated values.

As anticipated the variation of density ratio, ρ_{51} and the pressure ratio (P_{51}), with reflected shock temperature are higher for a real gas than for an ideal one.

Figure 2.4.1: Shock temperature vs. incident shock velocity for H_2/N_2 driver gas in 5% C_2H_2/Ar. mixture.

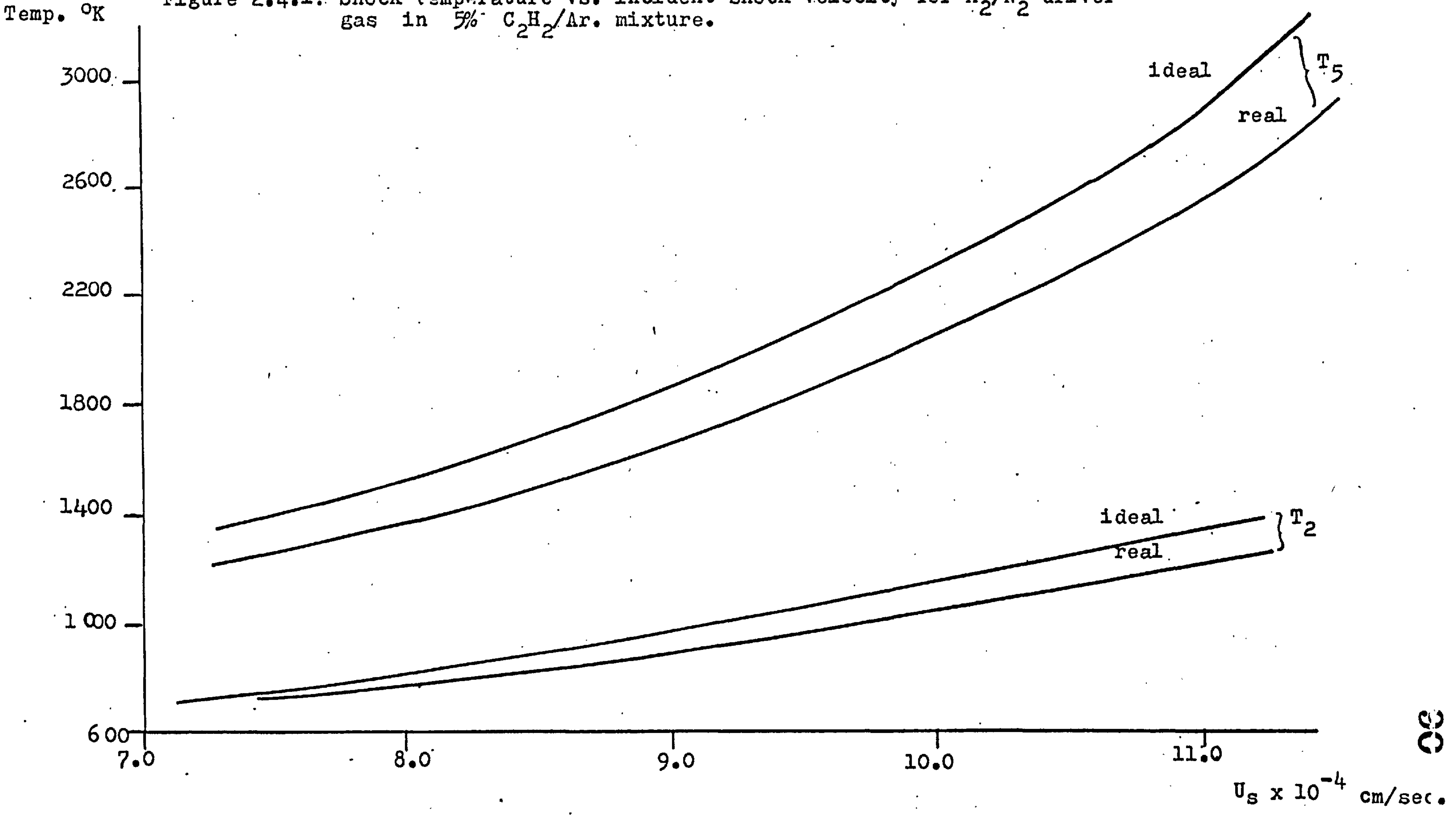

Figure 2.4.2: Shock temperature vs. incident shock velocity for H_2/N_2 driver gas in 2% C_2H_2/Ar. mixture.

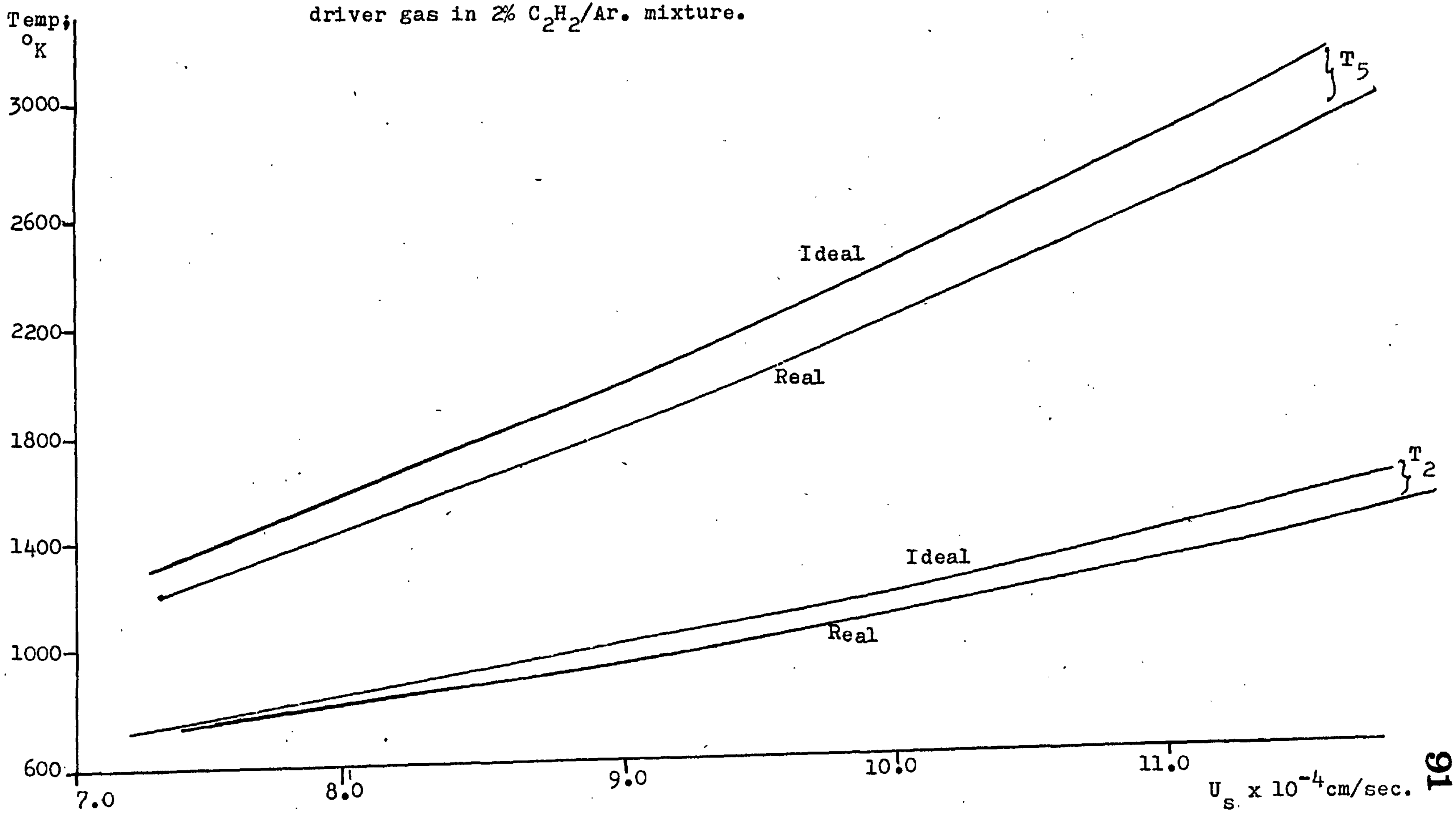

Figure 2.4.3a: Shock temperature vs. incident shock velocity for H_2/N_2 driver gas in 4% $C_3H_8/Ar.$ mixture

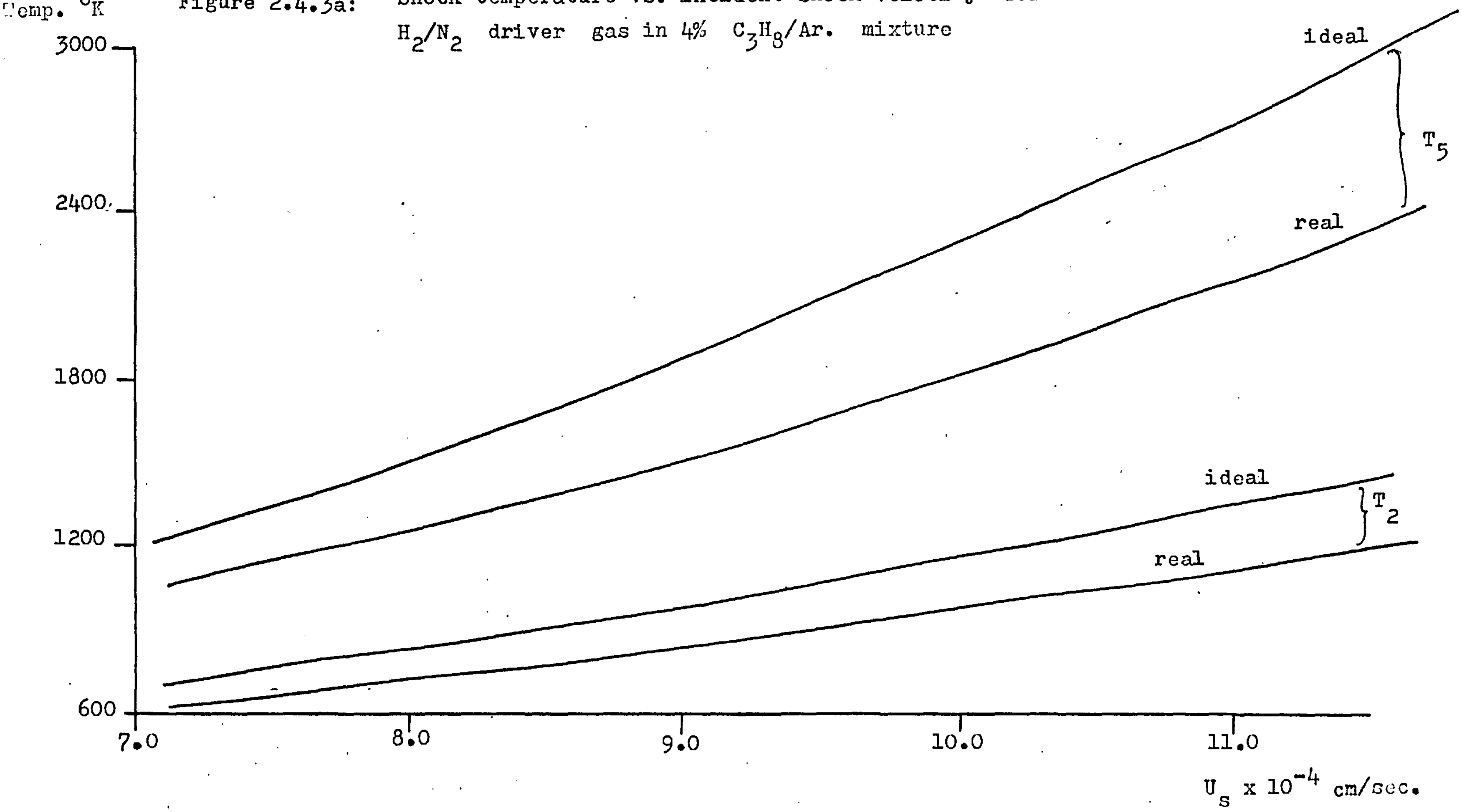

Figure 2.4.3b: Incident shock velocity versus reflected shock temperature for 4% C_3H_8/Ar. mixture

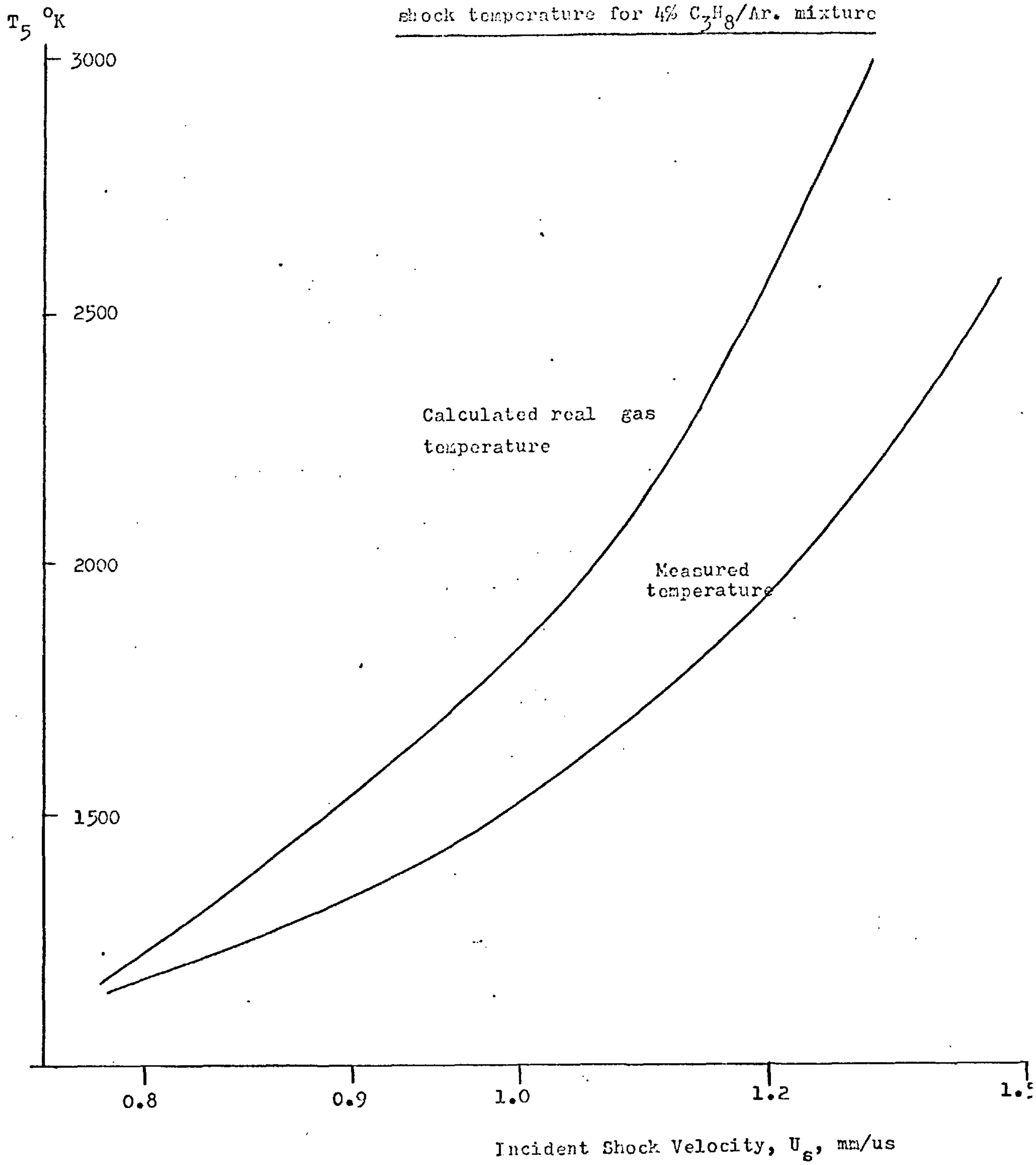

Figure 2.4.4:

Density Ratio vs. Reflected Shock Temperature for mixture of 5% C_2H_2/Ar.

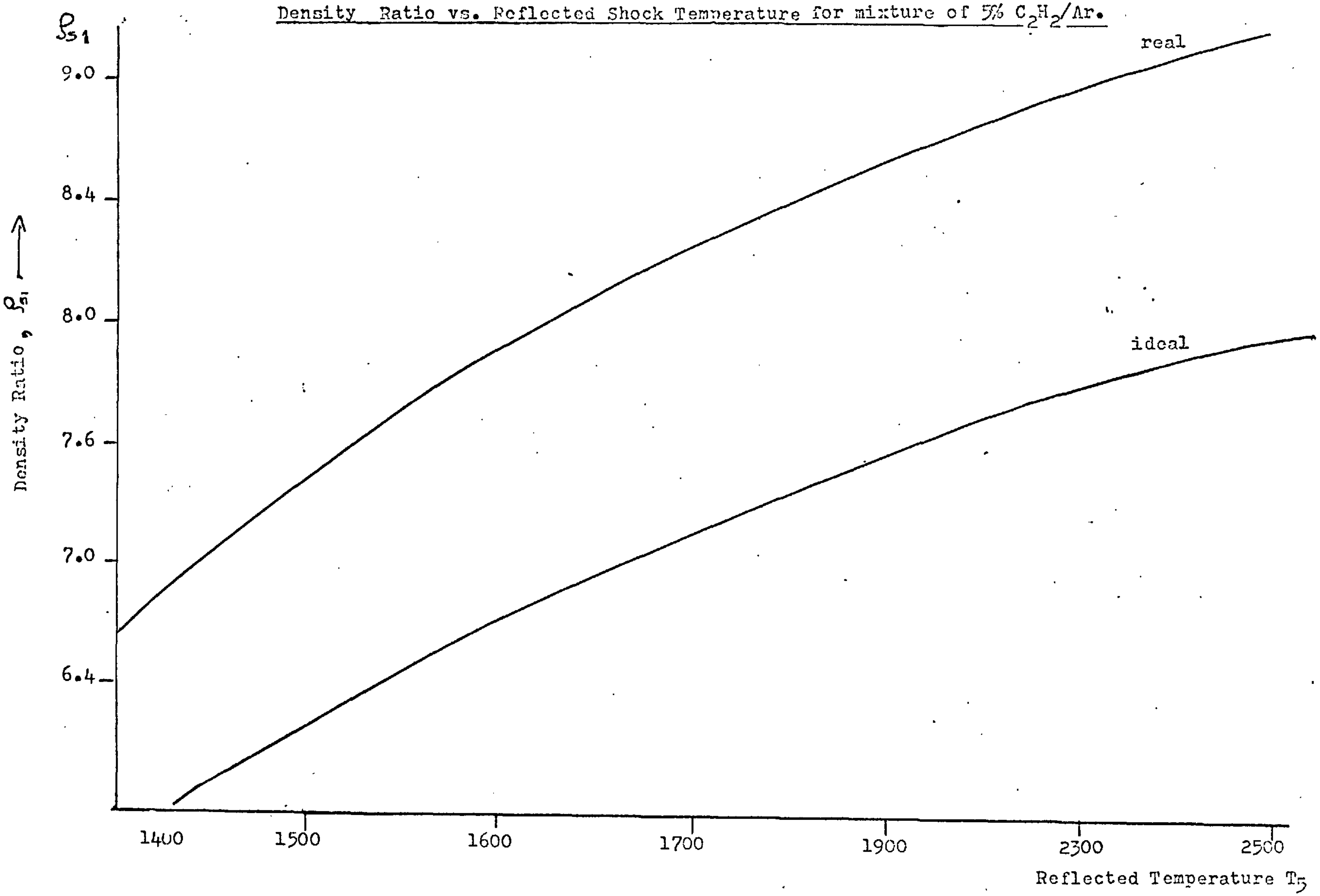

Figure 2.4.5:

Dependence of computed reflected pressure on reflected shock temperature for mixture of 5% C_2H_2 in Argon

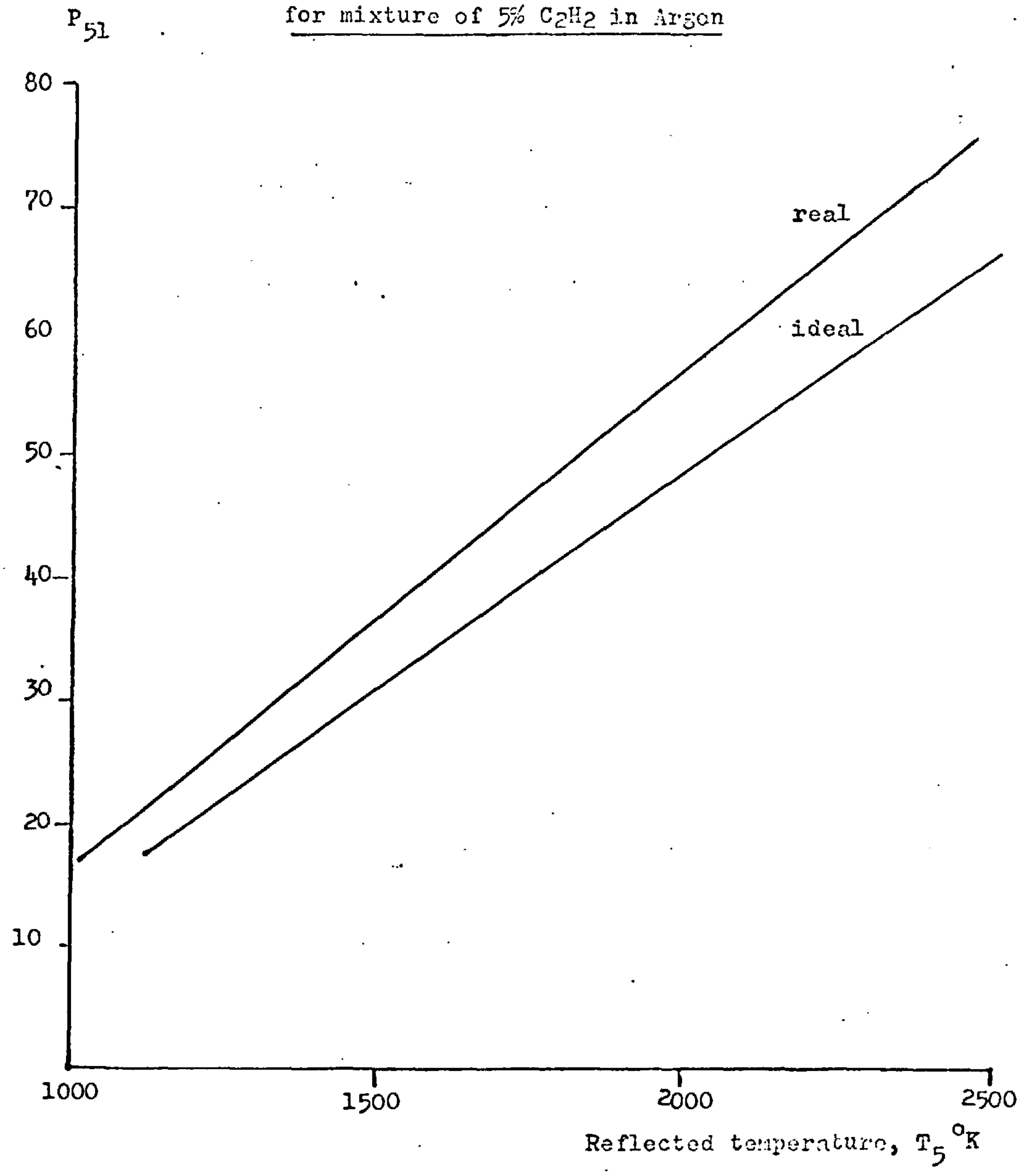

This is shown in figures (2.4.4) and (2.4.5) for 5% C_2H_2/argon, similar dependence are also true for mixtures of 2% C_2H_2 in argon and 4% propane in argon and were therefore not shown graphically. The behaviour of P_{51} is predicted from the combination of equations (2.3.1) and (2.3.7) from which the final pressure is seen to be mainly dependent on the initial gas density and the shock speed. The variation of density ratio ρ_{51} is predicted from a consideration of the equation of state, $P = \rho RT/M$ in which the density increases above the ideal value due to the fall in temperature resulting from the excitation vibrational energy; also for a real gas, the occurrence of dissociation leads to a pronounced increase in the predicted real value of ρ_{51} since the real gas temperature is decreased as heat is being absorbed.

2.3.5 Calculation of interface - tailoring conditions [136,137]

As was pointed out in section 1.5, it is desirable to 'tailor' the contact surface so as to prevent multiple shock reflections. A convenient tailoring procedure adopted was that of adjusting the composition of the driver gas. Calculations were based on finding the percentage dilution of hydrogen with nitrogen necessary to produce tailored conditions for a given initial pressure of the test gas.

Computation was carried out by assuming ideal shock tube conditions: that is:-

a) an ideal bursting of the diaphragm.

b) the boundary layer and shock wave attenuation are negligible.

c) all heat capacities of the gases are independent of temperature.

The condition for achieving a tailored contact surface for the reflected shock passing from region 2 to 3 (as in figures (1.2), is that the specific internal energy ratio of the gases in these regions obey the following relation

$$E_{32} = \left[\frac{C_{v_3} T_3}{M_3}\right] \Big/ \left[C_{v2} T_2 / M_2\right] = \left(\alpha_3 P_{52} + 1\right) \Big/ \left(\alpha_2 P_{52} + 1\right) \qquad (3.5.0)$$

In addition, equations (3.2.1 to 3 .2.9) still hold and including,

$$T_{43} = \left(P_{41} / P_{21}\right)^{2\beta 4} \qquad (3.5.1)$$

With the initial temperatures in both the driver and driven sections the same, i.e. $T_1 = T_4$, and by making the assumptions that the gas before and immediately after the incident shock wave are the same; and also that the gas behind the contact surface (region 3) is the same as the driver gas (in region 4), i.e.

$$M_1 = M_2 \; ; \; C_{v1} = C_{v2}, \text{ and } M_3 = M_4 \text{ and } C_{v_3} = C_{v4}.$$

equation 3.5.0 can be rewritten to the form[136],

$$M_4 / M_1 = \left(C_{v4} / C_{v_1}\right) x \; T_{34} \; x \; T_{12} \; x \left(\alpha_1 P_{52} + 1\right) \Big/ \left(\alpha_4 P_{52} + 1\right)$$

or more conveniently for iterative purposes to

$$Z \; x \; M_{N2} + \left(1 - Z\right) M_{H2} = M_1 \left(\frac{C_{v4}}{C_{v1}}\right) x \; T_{34} \; x \; T_{12} \times \left[\frac{\left(\alpha_1 P_{52} + 1\right)}{\left(\alpha_4 P_{52} + 1\right)}\right] \qquad (3.5.$$

where Z, is the fraction of nitrogen in the driver gas. Solution of equation (3.5.2) gives the required conditions for achieving tailored contact surface. The solution of the above equation was carried using iteration method with the aid of a computer programme based on the procedure described below;

2.3.5.1 Computing procedure

1) Read in the initial temperatures ($T_1 = T_4$), specific heats of argon, hydrogen, nitrogen and of the hydrocarbon in question.
2) For a given mixture strength (%) of the test gas (hydrocarbon) is argon, calculate α_1, β_1, C_{V1} and A_1
3) Choose a value for P_{21} (corresponding to the desired temperature of investigation).
4) Calculate, T_{21}, P_{52}, and T_{52} from equations 3.2.2 , 3.2.4 and 3.2.5, respectively.
5) Calculate the corresponding value of the reflected shock temperature, T_5 from

$$T_5 = T_{52} \times T_{21} \times T_1$$

6) Guess a value for Z, the percentage fraction of nitrogen in the driver gas; starting from $Z = 0$.
7) Calculate C_{v4}, α_4 and β_4 for the driver gas.
8) Using the values from steps (2), (3) and (7), calculate both sides of equation (3.5.2).
9) Compare the R.H.S. and L.H.S. of equation (3.5.2) and if the difference is greater than a fixed tolerable error bound, Z is gradually increased by small increments and steps (6) to (8) repeated at each increment of Z , until the desired error limit is obtained. The exact solution occurs when the difference between both sides of equation (3.5.2)

passes through zero

IO) When this condition is fulfilled, the tailoring condition has been achieved and the diaphragm pressure is calculated from equation 2.2.I

11) Write out the values of P_{41}, U_5, Z, T_2, T_5 P_{51} and ρ_{51}

I2) Thus for a given diaphragm bursting pressure, P_4, the initial pressure of the gas in the test section P_1 is calculated from $P_1 = \frac{P_4}{P_{41}}$.

Inorder to facilitate computation, figures (2.5.1) is plotted based on the results from 2.3.2.2.This figure shows the relationship between the reflected shock temperature and the pressure ratios P_{21} and P_{41}; and it acts as a quick guideline to the choice of P_{21} corresponding to the desired reflected shock temperature andthe diagraphm pressure ratio.

2.3.5.2 Results of calculation for interface tailoring conditions.

The results of calculation performed by the procedure outlined above are shown in tables [2.5.1 to 2.5.3] and presented graphically in figures (2.5.2 - 2.5.5).

Figures (2.5.2 and 2.5.3) show the variation of the diagraphm pressure ratio with the composition of the driver gas in acetylene mixtures (2% and 5%) in argon and 4% propane in argon. As the pressure ratio, P_{41} increases, the higher the percentage of hydrogen in the driver gas necessary for achieving interface tailoring. The same relationship is true for the dependence of reflected shock temperature on the percentage of hydrogen in the driver gas

Table 2.5.1: Tailoring conditions for a mixture of 2% C_2H_2 in argon

P_{21}	P_{41}	X_{H_2}(%)	U_s x10^{-4} cm/sec.	ρ_{51}	P_{51}	T_5, ^oK
5.0	16.54	51.4	6.54	4.56	16.12	1075
5.5	19.10	55.4	6.85	4.77	18.54	1166
6.0	21.70	58.8	7.14	5.01	21.0	1258
6.5	24.37	61.8	7.42	5.24	23.5	1348
7.0	27.13	64.4	7.69	5.44	26.1	1439
7.5	29.89	66.8	7.95	5.63	28.7	1530
8.0	32.63	69.0	8.20	5.81	31.36	1620
8.5	35.55	70.8	8.45	5.97	34.03	1711
9.0	38.36	72.6	8.68	6.12	36.72	1801
9.5	41.4	74.0	8.92	6.26	39.44	1891
10.0	44.2	75.6	9.14	6.39	42.18	1982
10.5	47.27	76.8	9.36	6.51	44.94	2072
11.0	50.26	78.0	9.58	6.62	47.7	2162
11.5	53.1	79.2	9.79	6.73	50.5	2252
12.0	56.2	80.2	9.99	6.83	53.3	2342
12.5	59.0	81.2	10.19	6.922	56.12	2432
13.0	62.4	82.0	10.39	7.01	58.9	2522
13.5	65.55	82.8	10.59	7.095	61.78	2612
14.0	68.6	83.6	10.78	7.17	64.6	2702
14.5	71.52	84.4	10.97	7.25	67.48	2792
15.0	74.9	85.0	11.15	7.32	70.34	2882
15.5	78.20	85.6	11.33	7.39	73.21	2972
16.50	84.46	86.8	11.69	7.52	79.0	3152

Table 2.5.2: Tailoring conditions for a mixture of 5% C_2H_2 in argon

P_{21}	P_{41}	X_{H_2} (%)	U_s, x10^{-4} cm/sec	ρ_{51}	P_{51}	T_5, °K
5.0	16.56	53.4	6.55	4.54	16.16	1068
5.5	19.11	57.2	6.86	4.81	18.58	1158
6.0	21.77	60.4	7.15	5.06	21.07	1248
6.5	24.42	63.4	7.43	5.29	23.61	1338
7.0	27.14	66.0	7.70	5.50	26.19	1428
7.5	30.0	68.2	7.96	5.70	28.8	1518
8.0	32.80	70.2	8.21	5.87	31.46	1607
8.5	35.69	72.0	8.46	6.04	34.14	1697
9.0	38.64	73.6	8.70	6.19	36.85	1786
9.5	41.48	75.2	8.93	6.33	39.58	1876
10.0	44.4	76.6	9.16	6.46	42.3	1965
10.5	47.47	77.8	9.38	6.59	45.10	2054
11.0	50.4	79.0	9.59	6.70	47.9	2143
11.5	53.57	80.0	9.80	6.81	50.70	2232
12.0	56.6	81.0	10.00	6.92	53.5	2322
12.5	59.53	82.0	10.21	7.01	56.34	2411
13.0	62.7	82.8	10.41	7.10	59.2	2500
13.5	65.86	83.6	10.61	7.19	62.0	2590
14.0	68.85	84.4	10.80	7.27	64.89	2678
14.5	72.28	85.0	10.98	7.35	67.76	2767
15.0	75.0	85.8	11.17	7.42	7064	2856
15.5	78.25	86.4	11.35	7.49	73.53	2945
16.50	84.4	87.6	11.70	7.62	79.3	3123

Table 2.5.3: Tailoring conditions for 4% propane in argon

P_{21}	P_{41}	X_{H_2}	U_s $\times 10^{-4}$ cm/sec	51	P_{51}	T_5 °K
4.0	11.14	0.502	5.90	3.93	11.55	880
5.0	16.6	0.542	6.55	4.58	16.20	1060
5.5	19.16	0.580	6.86	4.86	18.6	1150
6.0	21.8	0.612	7.15	5.11	21.1	1240
6.5	24.5	0.640	7.43	5.35	23.7	1329
7.0	27.2	0.66	7.70	5.56	26.26	1417
7.5	30.0	0.688	7.96	5.75	28.90	1506
8.0	32.9	0.708	8.22	5.94	31.60	1595
8.5	35.7	0.726	8.46	6.10	34.25	1683
9.0	38.70	0.742	8.70	6.26	36.97	1772
9.5	41.7	0.756	8.93	6.40	39.7	1861
10.0	44.6	0.770	9.16	6.54	42.5	1949
10.5	47.7	0.782	9.38	6.67	45.3	2037
11.0	50.6	0.794	9.60	6.78	48.0	2126
11.5	53.77	0.804	9.81	6.90	50.88	2214
12.0	56.8	0.814	10.0	7.0	53.7	2302
12.5	59.7	0.824	10.22	7.10	56.6	2390
13.0	62.9	0.832	10.42	7.19	59.4	2479
13.5	66.0	0.840	10.61	7.28	62.3	2567
14.0	68.9	0.848	10.80	7.36	65.2	2655
14.50	72.4	0.854	10.99	7.44	68.0	2743
15.0	76.0	0.860	11.17	7.51	70.9	2831
15.5	78.9	0.866	11.36	7.59	73.8	2920
16.5	85.0	0.878	11.71	7.72	79.7	3096

Figure 2.5.1: Relationship between P_{21}, P_{41} and T_5 for tailoring conditions for a mixture of 5% C_2H_2/Ar.

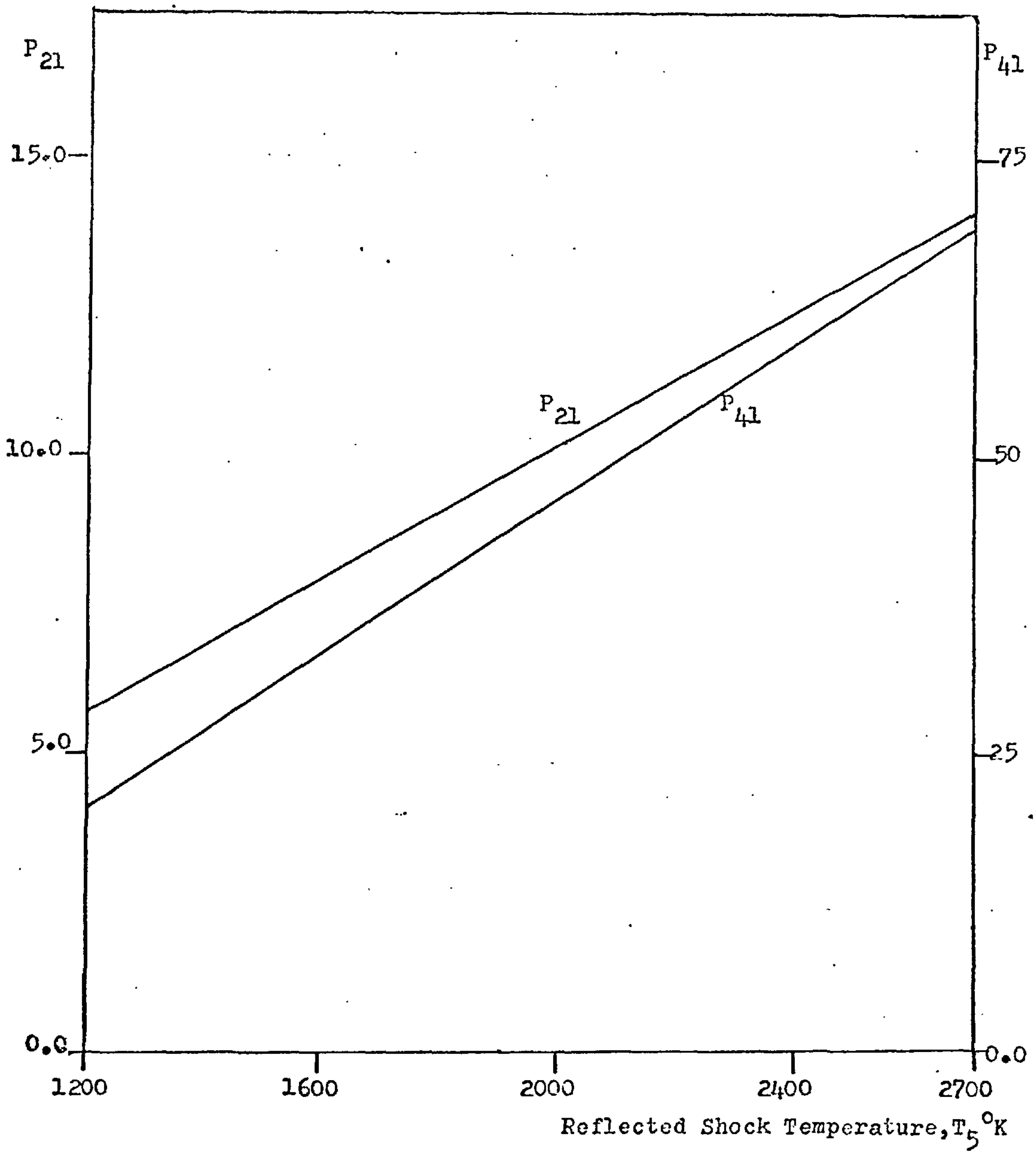

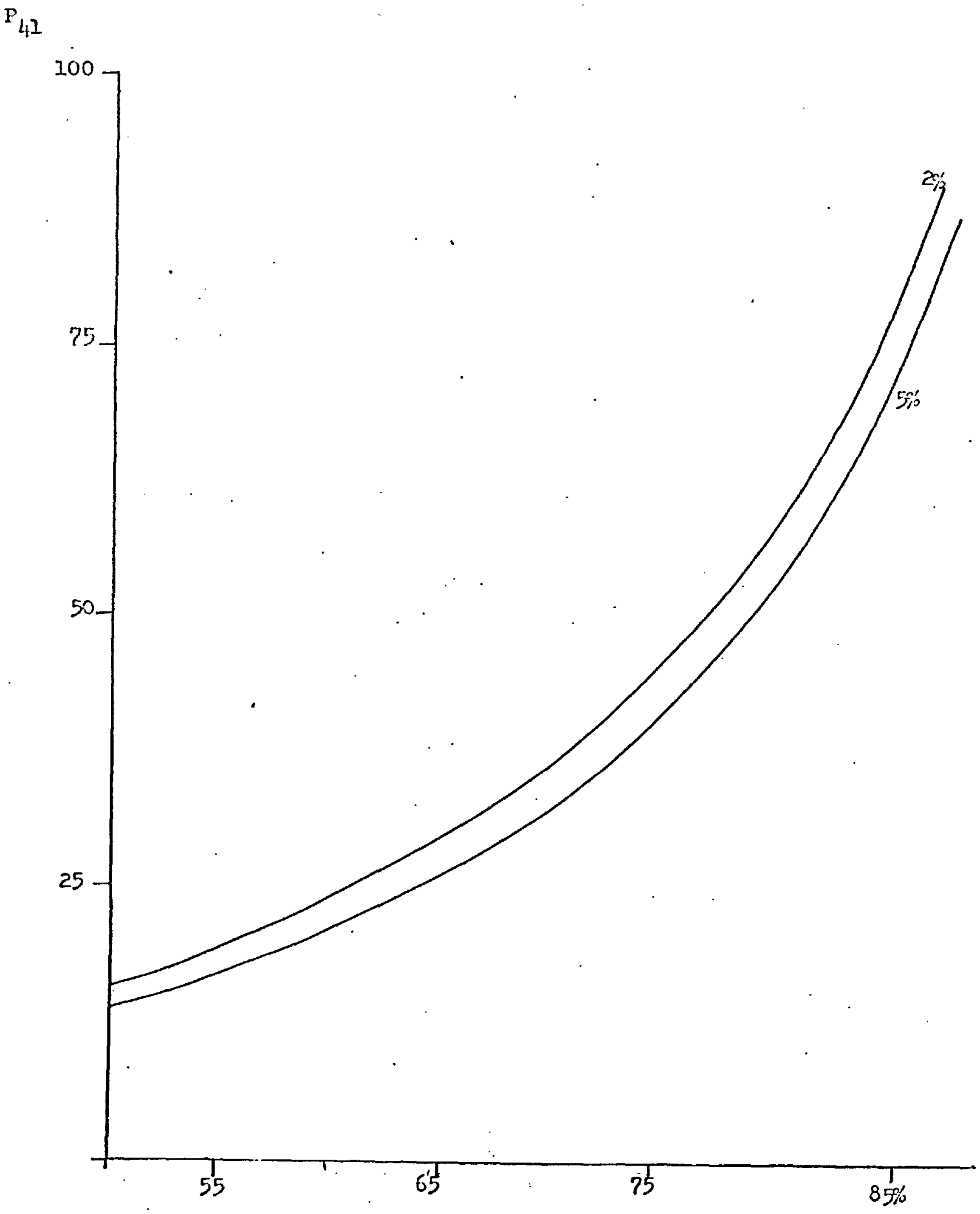

Figure 2.5.2: Tailoring Conditions for C_2H_2/Ar. mixtures at various Pressure Ratios across the Diaphragm.

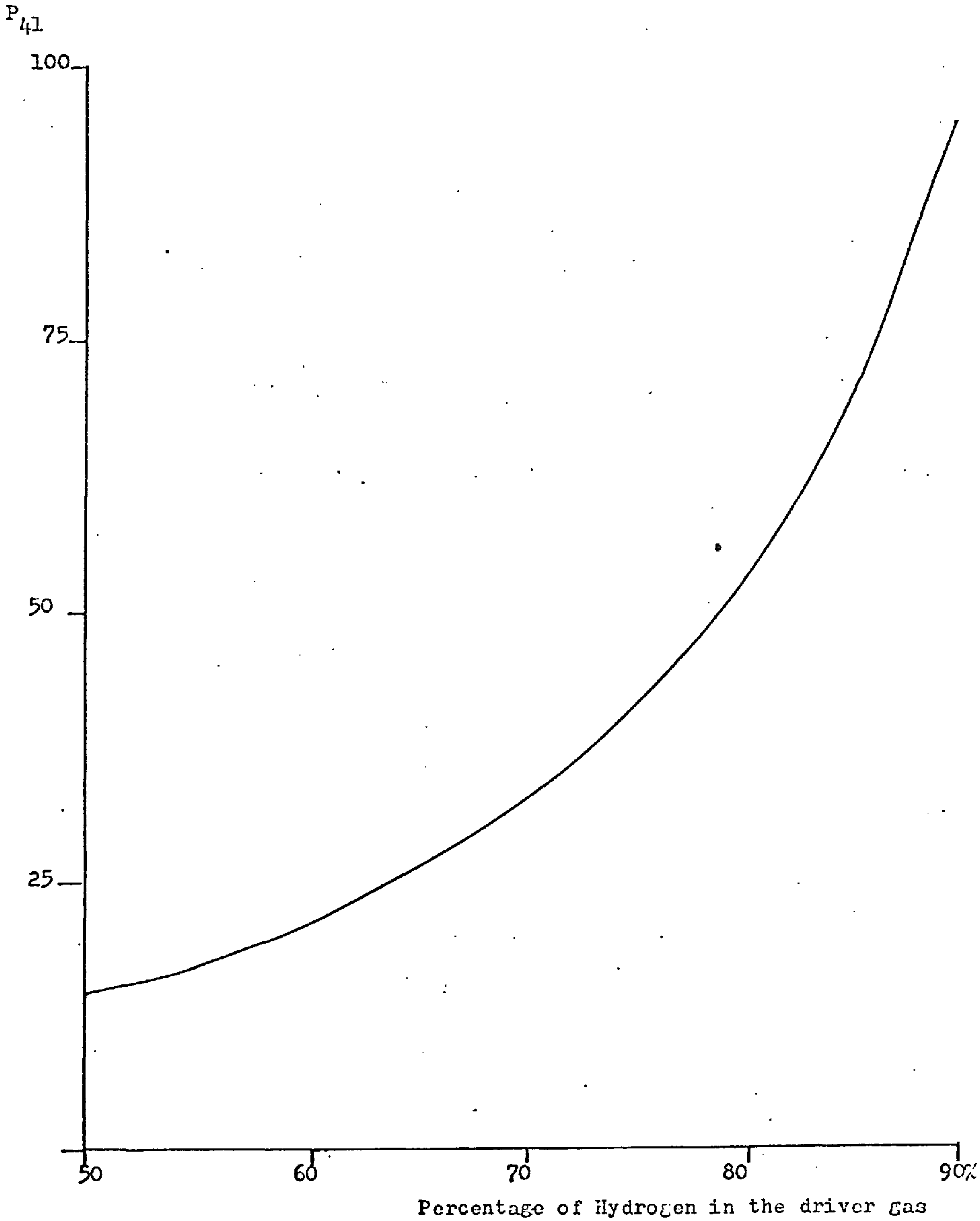

Figure 2.5.3: Tailoring Conditions for 4% C_3H_8/Ar. mixtures at various Pressure Ratios across the Diaphragm.

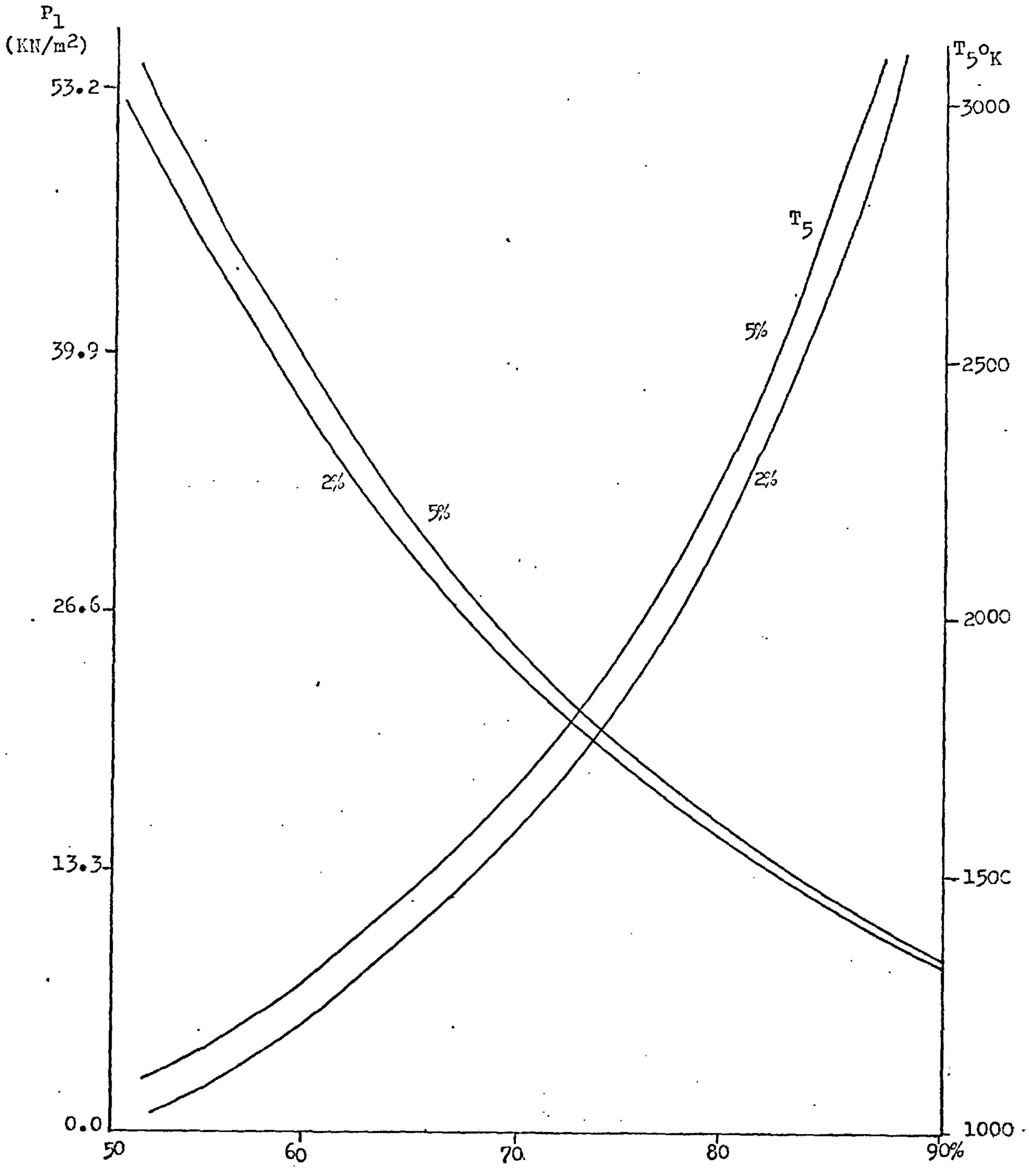

Figure 2.5.4: Tailoring Conditions for C_2H_2/Ar. mixtures at constant Diaphragm bursting Pressure (P_4) = 830 KN/m^2.

Figure 2.5.5 : Reflected Shock Temperature, T_5 vs Percentage of Hydrogen content in the H_2/N_2 Driver gas at tailoring conditions for a mixture of 4% C_3H_8/Ar.

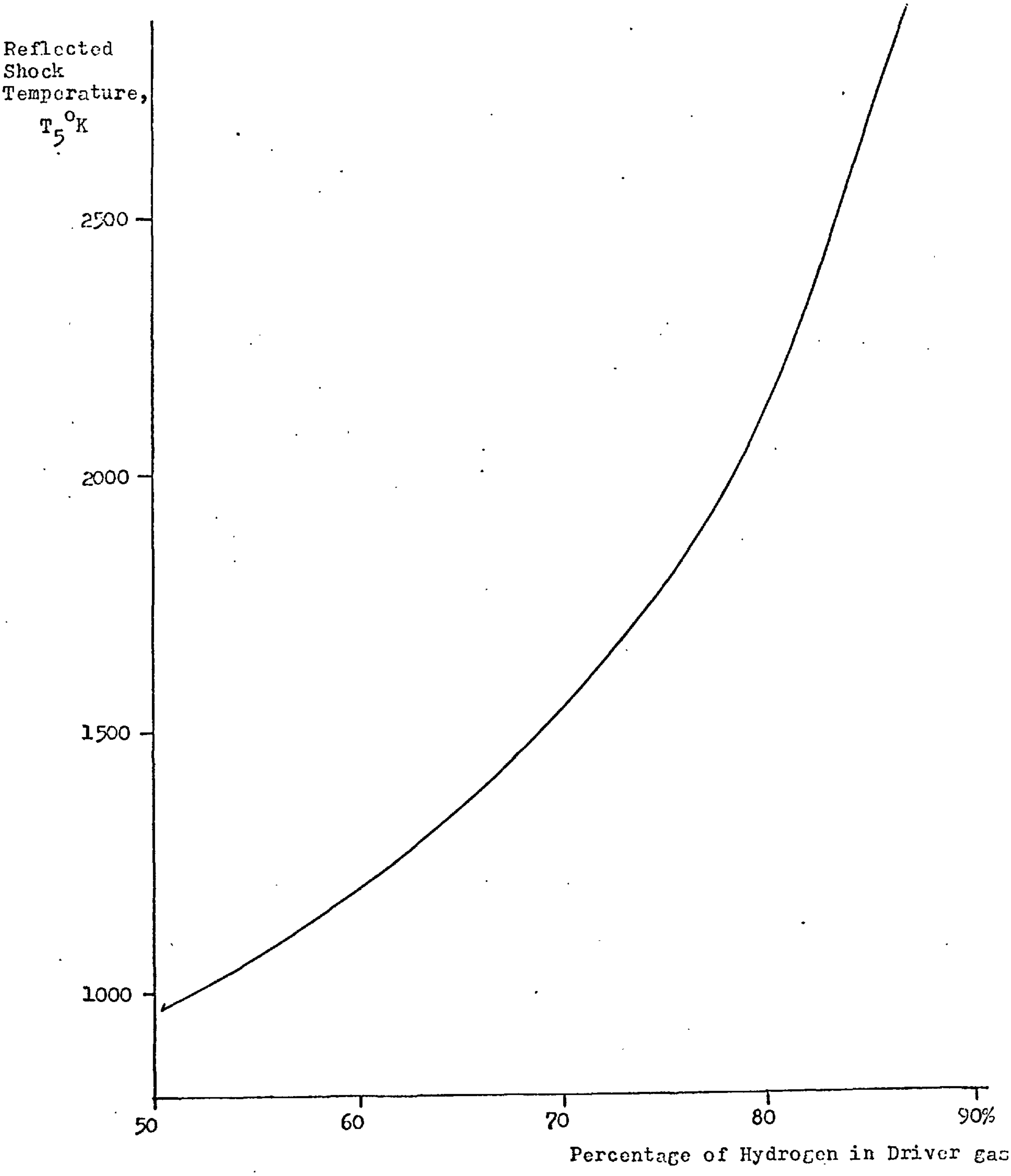

(figures (2.5.4 and 2.5.5)).

These plots (figures 2.5.2 - 2.5.5) reveal that, even at high shock temperatures upto 3000°K, it is still essential to dilute hydrogen with small quantities of nitrogen inorder to avoid instability in the interface.

The initial shock tube conditions for tailoring conditions are easily determined from figures (2.5.2 - 2.5.5) once the desired reflected shock temperature is known. For experiments conducted at constant diaphragm bursting pressures, plot of the type figures (2.5.4) is prepared and hence the initial pressure in the driven section (P_1) and the percentage of dilution of the driver gas with nitrogen are readily obtained.

The validity of these theoretically derived values for tailoring conditions, are only ascertained by experimentally observing the constancy of the trace of the reflected pressure.

PART A

THE SINGLE - PULSE SHOCK TUBE PYROLYSIS OF PROPANE.

CHAPTER 3

THE SINGLE-PULSE SHOCK TUBE EXPERIMENTS

CHAPTER 3

THE SINGLE-PULSE SHOCK TUBE EXPERIMENTS

3.1. The Single - Pulse Shock Tube

This shock tube is of conventional single-pulse design and was built at Vickers' Research Establishment, Ascot. The design was based on that described originally by Glick[64]. The shock tube was constructed from a heavy wall copper tubing; the tube has uniform section of 7.62cm internal diameter. The dump tank was fabricated in stainless steel. The entire shock tube was mounted on very rigid support 122cm high.

A diagrammatic representation of the shock tube is given in figure 3.1 and marked on it are some of characteristic features which have been described in detail elsewhere[22]. Only a brief description of the apparatus and these features are given below.

3.1.1. The driver section and the dump tank

The driver section is 183cm long and is separated at both ends by diaphragms at positions D1 and D2 from the experimental section of the shock tube and the dump tank respectively. The driver section has connected to it variable length delay times - tube B which has eight ports; each of these ports is capable of being blanked off and to each of which an auxiliary tube C could be fixed. The auxiliary tube C is 38cm long and 5cm in internal diameter; its function is to create strong shocks to operate the plungers for piercing the diaphragms at D1 and D2. The time interval between the bursting of the diaphragms is closely controlled by changing the connections of tube C to any of the ports in B.

FIGURE 3.1: SCHEMATIC DIAGRAM OF THE LAYOUT OF THE SINGLE - PULSE SHOCK TUBE

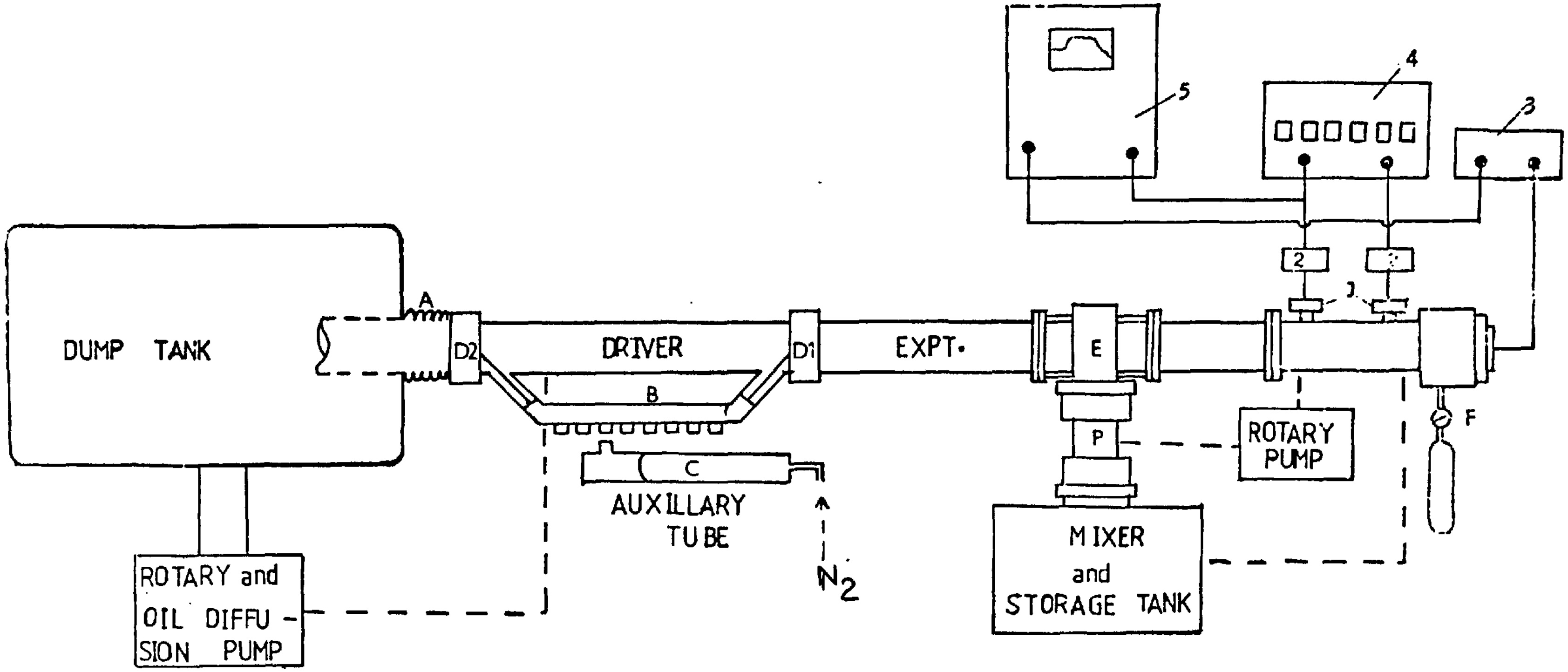

The joint of the shock tube to the dump tank is of special construction to facilitate alignment of the tube. A stainless steel bellows, A was welded to the flange of the diaphragm station at D2 and to the dump tank. The shock tube was attached to this flange at D2 and passed through the bellows. It was supported at the other end by a three - armed, spring-loaded spider in the dump tank. This arrangement afforded a considerable degree of flexibility in the alignment of the shock tube sections by drawing together the flanges at D2.

3.1.2. The experimental or test section

This section of the tube is 366cm long and is bolted to the driver section by means of a large threaded collar which houses the diaphragm holder at D1. Almost halfway along this section at E, is attached a wide aperture construction 'the swinging tube' section[138] which permits rapid evacuation of the test section via an oil diffusion pump P.

Measuring devices such as the platinum gauges, and the pressure gauge as well as the observation window are mounted on the tube flush with the inside wall.

3.1.3. Diaphragm Mount

The diaphragms at D1 and D2 were housed in diaphragm holders into which a recess was machined so that the petals formed as a result of bursting the diaphragms could bend back further than the diameter of the shock tube and hence beyond the flow of the gas. This type of mount is very effective[22] in preventing multiple reflections which would have otherwise occurred using plain mounts in which case the petals occupy a large proportion of the cross - section of the tube and therefore would hinder free gas flow.

3.1.4. Diaphragm Material.

The diaphragms were made from oxygen-free, high conductivity copper sheet. The diaphragms were cut from the sheet using a blanking tool mounted in a flypress, cruciformed to the desired thickness and then annealed in a furnance at 900^{o}K. The depth to which the diaphragm was cruciformed depended on the required range of bursting pressures (830-1690 KN/m^{2}) since the temperature behind the shock wave is approximately determined by selection of appropriate driver to driven gas pressure ratios. However, due to non-idealities associated with the rupture of the diaphragm, the final temperature cannot always be accurately predicted.

One method by which reproducibility can be achieved is to prestress the diaphragm to within about 10% of its natural bursting pressure and then to finally rupture it mechanically. This option has been employed in the present investigation.

A safety diaphragm (3.8cm pre-domed aluminium disc) was located in the swinging tube section. This diaphragm relieves at a pressure of 386 KN/m^{2} inorder to protect the baffle valve from excess pressure; it was normally replaced after about 10 runs as the stress imposed on it by the continual evacuation and pressurization of the tube caused it to split. At higher values of the reflected shock pressure it was observed that the safety diaphragm repeatedly relieved.

3.2 Evacuation of the shock tube.

Rapid evacuation of the shock tube was accomplished by using an oil diffusion (Speedivac Model F603) fitted to the dump tank, and halfway along the experimental section, at E. The oil diffusion pumps were backed respectively by an Edward one stage rotary type vacuum pump. At E a wide aperture valve making connection to the swinging tube section was built in to provide an increased effective cross-section of the port through which pumping took place. The extent of evacuation attained in the dump tank and the driver section was measured with a Pirani gauge (Edwards Head M6A, Meter B5 Model, measurable range $(500\text{-}10^3)\text{x}133$ N/m^2. The dump tank and the driver section could be pumped down to 0.133 N/m^2. The test section and the sample reservoir tube were evacuated down to $0.133\text{x}10^{-3}$ N/m^2 and this was measured using a Penning gauge (Edwards Model 6, Meter Model 7) and a leak rate of $6.55\text{x}10^{-5}$ $N/m^2/\text{min}$ was allowed. The approximate time for achieving the mentioned vacuum levels was about 30 minutes.

3.3 Instrumentation - Diagonistics

The shock parameters measured are the following:-

a) The incident shock velocity

b) reflected shock pressure

c) reflected shock temperature and

d) the dwell time.

These parameters were measured in the usual way applicable to shock tube experiments. Given below are brief outlines of the instruments and methods of measuring these parameters.

3.3.1. Measurement of shock velocity.

The velocity of the incident shock was measured by timing the passage of the shock front across the film platinum gauges positioned at known distance(s) apart. The arrival of the shock front at the locations of the platinum gauges is detected by the increase in the resistance of the platinum film due to the temperature rise induced in it by heat transfer from the shock-wave. The stepwise rise in temperature due to the passage of the shock front induces a small rapid voltage across the film when a constant current is passed through it. The voltage signal is amplified by specially designed circuits such as that shown in figure A 3.1 in the appendix.

The platinum gauges were made by closely following the method outlined by Gaydon and Hurle (reference 5 page 113)- which in essence is painting a thin film (about 0.5mm wide) of bright liquid platinum on a fire-polished flat end of a glass rod (about 6mm in diameter and 2.0cm long) and extended a short way around the polished edges. The rod was then oven-heated for about 20 minutes at temperature (~950°K) a little above the softening point of the rod material so as to obtain a firm bond between the platinum and the glass. The rod was withdrawn and then cooled; the process was repeated so as to obtain an even strip of the film whose resistence was about 50 - 80 ohms. Two current-carrying leads were attached to the two edges of the platinum strip using silver conducting pastes - (X - 351 and X - 353). The glass rod with the conducting leads was housed in a copper mount such that the flat end of the rod with the strip of the platinum film was exposed. The glass rod was held in position and sealed with

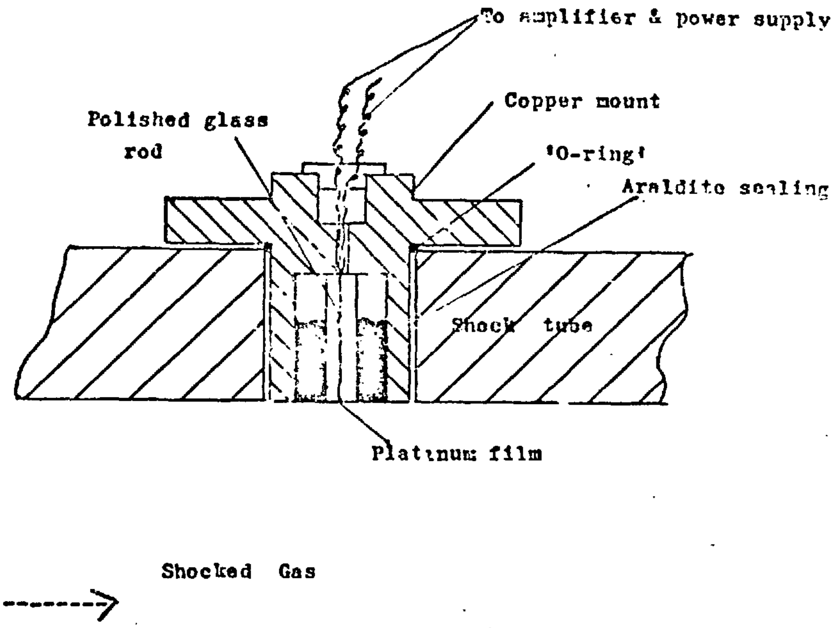

Figure 3.2: Platinum Gauge Mount

Araldite. The copper mount was inserted in the wall of the shock tube with the platinum film being flush with the inner wall of the tube and its narrow dimension parallel to the shock flow. Figure 3.2 shows the mounting of the gauge.

In this study, two platinum gauges were used and they were positioned 0.305m (i.e. 1 foot) apart towards the end plate of the tube. The gauge positions are marked 1 in figure 3.1. The time taken by the shock front to traverse this distance was read on a microsecond Counter Chronometer (Scientific Systems Ltd.); this was triggered and stopped by amplified signals from the first and second gauges respectively.

The shock velocity was calculated by dividing the distance between the gauges (0.305m) by the counter reading.

3.3.2. Measurement of the Reflected shock Pressure

The pressure history behind the reflected shock was monitored using a quartz S.L.M.PZ6 piezo-electric gauge which was mounted at the end plate of the experimental section of the shock tube.

Quartz or other similar crystals without centre of symmetry are'piezo-active' - that is they become polarized when subjected to unidirectional stress; pressure gauges made from such crystals depend on the change of charge distribution on the faces of these crystals when subjected to deforming pressure. For pressure measurements in the shock tubes the piezo-electric gauge functions in the following way:- the compression of the crystal by the shock wave induces an electric charge - whose magnitude is directly proportional to the compressing pressure. The charge is amplified using suitable charge amplifier and the resulting signal measured. In the current experiments the output of the pressure transducer was amplified using Kistler (Model 566) charge amplifier and the signal was displayed on the oscilloscope from which photographic records were made.

In the design of the mount for the crystal special precautions to provide sufficient reduction in the response of the gauge to mechanical shock such as transmitted through the wall of the shock tube was taken by using antivibrational mounting. The face of the transducer was flush with the inner wall of the shock tube; and direct metal-to-metal contact was avoided by using 'O'-rings - which also served for vacuum sealing.

The pressure gauge was previously calibrated in terms of pressure versus the output of the amplifier; this gave a linear relationship for evaluating the pressure. This calibration was re-checked by measuring the trace deflections displayed on the oscilloscope when the tube was pressurized to different values by direct supply of nitrogen gas from the cylinder. The following expression was obtained for the evaluating the pressure;

$$P_5 = \text{constant} \times {}^{V}/_{K}$$

where V = trace deflection of the oscilloscope, measured in volts.

K = setting of the charge amplifier, volts/Pcb.

and the constant has a numerical value of 12.32 KN/m^2/Pcb.

From the pressure trace recorded, the reaction time was measured, and the trace also served as an indicator of whether the interface was properly matched.

3.3.3. Temperature Measurement

The measurements of the reaction temperatures were carried out in the single-pulse shock tube exactly in the manner described by Napier and co-workers[22, 139, 140] using both Na-line and C_2 - reversal methods. Two pairs of silica windows, placed in a copper-lined steel housing in the position G, as in figure 3.1, were aligned in diametrical opposition so that a double beam method was used and the "fairing-in" to the contour of the shock tube minimized the degree of turbulence produced in the gas behind the reflected shock. Tungsten ribbon lamp was used as the background source. The optics, filters and the photomultipliers of the measuring systems in a light-tight box were conveniently mounted as described in reference 22 and arranged[5] as in figure 3.3.

The double-beam method was achieved using the optical arrangement shown in figure 3.3 in which a system of mirrors M_1 and M_2 enabled the same source P to be used for both beams. A neutral filter NF was used in one of the beams to reduce the brightness temperature of P by a known amount. Light from the back-ground tungsten ribbon lamp P was reflected off the front-surfaced aluminised mirrors M_1 and M_2 through the shock tube S on to the photomultipliers PM_1 and PM_2. Lenses L_1 and L_3 served to focus the light into the shock tube, and lenses L_2 and L_4 then form images on the photomultipliers. Apertures A limit the light beam so that the photomultipliers receive the same cone of light from the lamp as from the shock-heated gases. The required wavelength spectrum line was isolated using interference filters IF.

Figure 3.3: Optical arrangement for double-beam measurement of spectrum-line reversal temperature.[5]

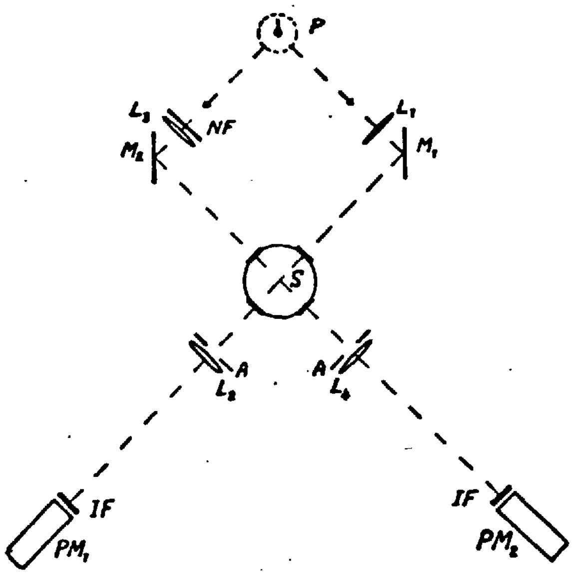

The measurement was made mostly by C_2 reversal method against the tungsten ribbon lamp (5165Å) (0,0) Swan band). This method has the advantage that no additions to the reacting gases are needed. The principle of its operation lies in the comparison of the temperatures of the shock-heated gas and that of the back-ground source; if the reacting gas is cooler than the lamp then the resonance lines of the spectrum appear as dark absorption lines; whereas, if it is hotter, then the spectrum is visible in the emission as bright lines superimposed on the continuum. But when both the source and the reacting gas are the same temperature, the spectrum lines just disappears, that is at the reversal point.

From the recorded oscillograph traces the gas temperature can be estimated. For example, if the temperature of the shock-heated gas in between the full brightness temperature of the lamp, T_L, and the reduced brightness temperature in the beam with the neutral filter, T_r, so that one trace of the oscillograph records absorption by deflection a and the other beam gives an emission deflection e, from such measurements the gas temperature, T_g, is accurately estimately by using the interpolation formula [5];

$$T_g = T_r + e(T_L - T_r) \Big/ (a + e)$$

where

T_g = reaction temperature, °K

T_L = full brightness temperature of the lamp, °K

T_r = reduced brightness temperature of the lamp in the beam with neutral filter, °K

Calibration curves (as in figure A 3.2 in the appendix) of the lamp current versus tungsten ribbon lamp temperatures with and without neutral filter were carried out in the preliminary runs and this facilitated extrapolation of the reaction temperatures.

3.3.4. Oscilloscope

Tektronix oscilloscope type 549 was used with variety of plug-in units to display the output from the Kistler charge amplifier. The oscilloscope was fitted with a built-in delay system, suitable for delaying the single sweep of the oscilloscope after the receipt of an external triggering pulse. The oscilloscope was usually triggered by a signal from the position of the first platinum gauge, this enabled the sweeping of the oscilloscope to commence just before the onset of the shock reflection at the end plate. As the pressure gauge was located in the vicinity of the reacting gas, it served to display the time for which the gas was maintained at high temperature - the 'dwell time'.

The pressure signal was usually displayed at 0.05v/cm and the oscilloscope sweeping rate at 500µs/cm. The single sweep trace was photographed using an Ilford film and developed using Kodak high contrast D19 developer. Figure 3.4 shows a typical photographic record of the pressure trace obtained from the single-pulse shock tube experiments.

3.4. Sampling of Reaction Products.

The reaction products were collected in a pyrex sample reservoir tube having volume of 250ml. The sample tube is separated from the shock tube by a pneumatically operated

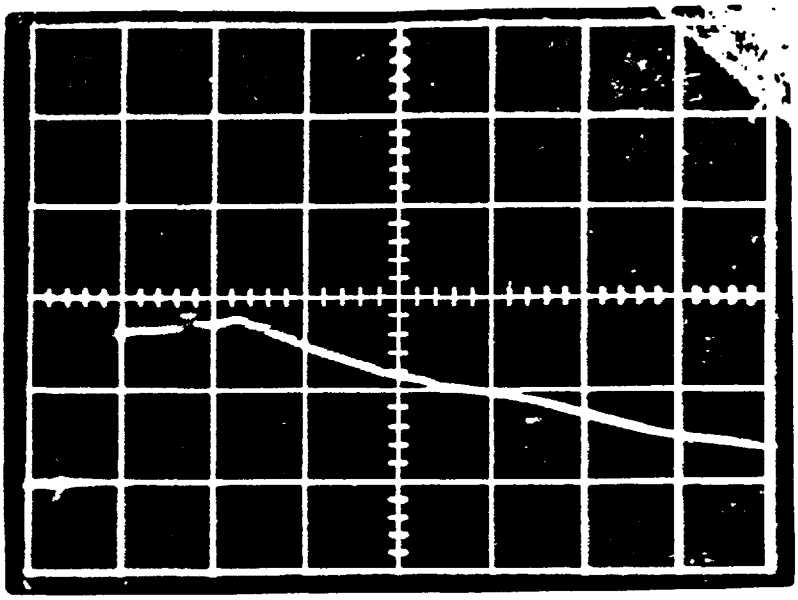

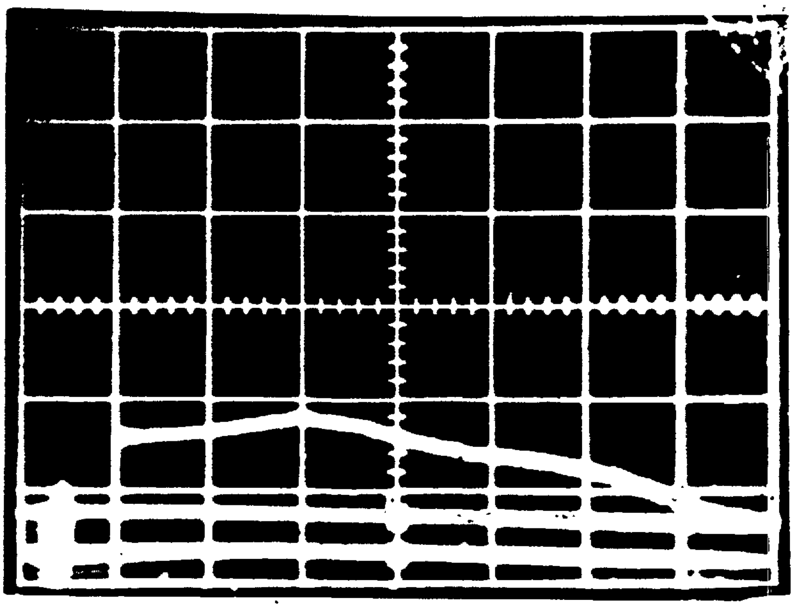

FIGURE 3.4: TRACE OF REFLECTED SHOCK PRESSURE, P_5.

valve, F. This valve was connected to the head of the auxiliary tube by a coil of tungum tube about 10.6m long acting as a delay line. The pressure pulse generated after the bursting of the diaphragm in the auxiliary tube travelled down the tungum tube to open F. It was estimated that the valve F opens within 50ms of the rupture of the auxiliary tube's diaphragm, and as such was very effective in preventing back mixing of the sample with the content of the shock tube during the short interval ($\sim 1/2$ sec.) before the valve was closed and the sample removed for analysis.

3.4.1. Sampling Proceedure

Figure 3.5 shows the sampling system, Tap T_1 was closed immediately after shutting valve F. The sample reservoir tube was disconnected from the shock tube beyond F, and connected to a pre-evacuated 50ml sample loop via a B10 cone and socket joint. The sample loop was constructed with three way taps, T_2 and T_3; this allowed air to be removed from the loop arms before introducing the mixture into the loop and to the chromatograph via a sample valve. The sample was compressed into the column. A current of nitrogen carrier gas was used to purge the content of the loop into the columns.

Samples at constant pressure and volume were always injected onto the column each time, and this considerably facilitated analytical calculations.

3.4.2. Product Analysis

Composition of the reaction mixture was analysized using Phase Sep Chromatograph (model LC - 2) equipped with a Gow-Mac katharometer detector. The detector formed a part of a wheatstone bridge network and also incorporated an inbuilt D.C.

Figure 3.5: <u>Sampling System</u>

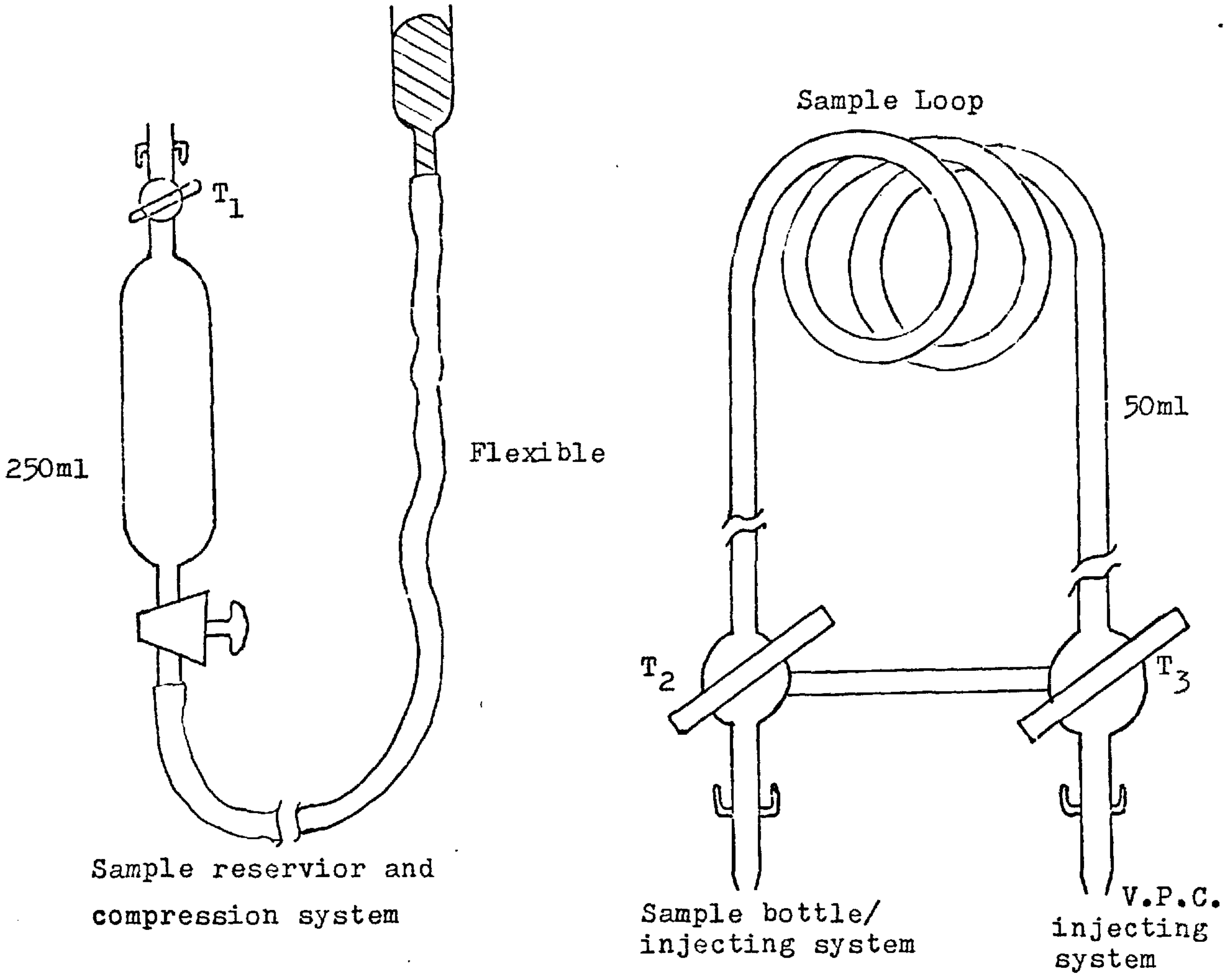

(b)

(a)

amplifier. The output from the bridge was fed into the amplifier and the resulting signal displayed on a potentiometric ventor recorder.

The separation of the hydrocarbons took place in two copper columns coupled to each other in series. The columns were of uniform 0.635cm internal diameter and were packed with porasil and porapak R materials respectively. This arrangement ensured good peak resolution for the C_3 and C_2 hydrocarbons. 'Oxygen-free nitrogen' was used as the carrier gas and was admitted to the system via a pressure controller and a needle valve. The carrier gas flow rate was measured using a soap bubble flow meter. The response of the detecting system to each of the following hydrocarbons - methane, ethane, ethylene, acetylene, propane and propylene - was determined by injecting known pressure of each hydrocarbon. Both the retention time and the response for each hydrocarbon was recorded. The response for each hydrocarbon was found to be linear over the range of sample injections used. Known mixtures of each hydrocarbon in turn were made using propane as a diluent. This was introduced into the chromatograph using the gas sampling valve. Response factors for the hydrocarbons, relative to propane, were determined at the optimum analytical conditions - column lengths were 2.0m and 1.5m for porasil and Porapak R columns respectively, column temperature of $373^{o}K$ and carrier gas flow rate of 52ml/min.

The response of the detecting system to the various hydrocarbons is listed in table 3.0. A standard hydrocarbon gas mixture (BOC special gases) was analysed, using the determined response factors and found to give good agreement with the specified composition.

Table 3.0: Response of the detecting system to various hydrocarbon gases

Hydrocarbon	Retention time, min.	Determined Response factor
Methane	1.0	3.32
Ethane	2.0	1.70
Ethylene	2.20	1.65
Acetylene	2.75	1.35
Propane	3.5	-
Propylene	4.30	0.96

3.4.3. Materials for the experiment

(a) Driver Gases:

Hydrogen and nitrogen:	supplied by BOC and used without further purification.

(b) Experimental Gases:

Argon:	supplied by BOC as 99.995%
Hydrocarbons:	supplied by BOC special gases; all at least 99.0% purity

3.4.4. Typical experimental procedure

An outline of the procedures necessary to produce and utilize a shock wave in the apparatus previously described is given here.

The test gas mixture (propane heavily diluted by argon) was prepared in a 200 litre stainless steel tank and stored here under 207 KN/m^2 pressure for several days before use to allow for proper mixing.

The diaphragms at D1 and D2 were mounted in the diaphragm holders and bolted in place on the shock tube. The diaphragm in the auxiliary tube was also located in position. The dump tank, the driver and test sections and the sample reservoir tube were evacuated simultaneously to the appropriate vacuum levels. The pressures in the dump tank and the driver section reached 0.133 N/m^2 and 0.133×10^{-3} N/m^2 in the experimental section within 30 minutes. At these pressure levels, the dump tank and the driver section were isolated from the pumping line. The driver gas mixture was made up to the appropriate pressure P_4 in the driver section, the percentage of nitrogen in hydrogen being varied so as to obtain tailored - interface conditions with the experimental test gas pressure P_1. The oscilloscope, shock speed counter and the triggering system were set ready. Valve F was shut i.e. isolating the sample reservoir tube, and the test section isolated from the vacuum system. The test section were loaded to the required pressure P_1 with test gas mixture from the storage tank. The pressure gauges for reading P_4 and P_1 were shut off, and the shutter of the camera was opened. The auxiliary tube was fired by direct supply of nitrogen from the cylinder. The shock generated from the auxiliary tube pushed the plunger to pierce the diaphragm at D_1, and a shock wave travelled down and was reflected from the end-wall of the experimental section, the second diaphragm at D_2 broke and the reaction was quenched. The valve F, which was opened pneumatically by the pressure pulse from the bursting of the diaphragm in the auxiliary tube was closed as soon as possible ($\sim 1/2$ sec.) after firing the auxiliary tube. The camera shutter was closed; the counter readings was noted. The sample reservoir tube was disconnected from the shock tube and the sample taken for gas chromatographic analysis. The photograph of the pressure trace was developed, fixed and dried. Thus for each experiment a photograph giving the reaction time and the value of the reflected shock pressure was obtained. From the measured shock velocity, the reflected shock temperature, T_5 was computed and compared with the measured value obtained from C_2 reversal method. The result of product analysis for each run gave a chromatogram from which kinetic results were compiled.

CHAPTER 4

RESULTS OF PROPANE PYROLYSIS IN A SINGLE-PULSE SHOCK TUBE

4.0: Results of Propane Pyrolysis in a Single Pulse Shock Tube

Data obtained from the analysis of the shock treated reaction mixtures provided information on the product distribution. With knowledge of the temperature and the reaction time, and together with the analysis of the chromatogram, the overall order and the activation energy of thermal decomposition of propane could be determined.

4.1: GENERAL FEATURES

4.1.1: Product distribution.

Pyrolysis of mixture of 4% propane in argon was extensively investigated over a wide temperature range of 1200 - 2700^{o}K at reaction times varying from 0.1ms. to 3.5ms and total reaction pressures of 500 - 1500 KN/m^{2}. The reacted mixtures were analysed for hydrogen, methane, ethane, ethylene, acetylene, propane and propylene. The sample was not analysed for the presence of higher molecular weight ($>C_4$) hydrocarbons.

The main products detected were methane, ethylene, acetylene and hydrogen. Propylene and ethane were only detected at the lower temperature ranges. Table 4.1 shows the detailed initial experimental conditions and the experimental results in which the percentage of the individual product present was determined from the peak area of the chromatogram applying the necessary calibration factor. Over the entire temperature range covered in this investigation extremely high degree of decompositions of propane were obtained; even at temperatures as low as 1400^{o}K, and at reaction times as short as 0.2ms. no less than 35% of the propane was converted to products.

Table 4.1: Experimental conditions and Results of the pyrolysis of a mixture of 4% Propane Argon

Run no.	P_1	P_{41}	H_2 in Driver gas	Temperature (measured)	Reaction Time	Yield of products i.e. mole % of propane converted to:-					Propane Decomposed
	torr		%	°K	ms	CH_4	C_2H_4	C_2H_2	C_2H_6	C_3H_6	%
91	250	52	80	1300	0.2	16.78	53.28	3.20	5.06	15.98	40.3
90	210	60.2	80	1400	0.2	18.75	53.97	8.46	3.77	8.0	34.8
89	180	70	80	1500	0.2	18.78	49.81	15.8	1.98	4.45	43.92
88	180	70	80	1500	0.7	20.26	46.58	20.82	1.97	-	46.6
24	170	77.6	85	1740	0.8	19.3	45.4	27.0	-	-	48.0
12	"	71.5	85	1740	3.5	20.6	35.3	28.6	-	-	51.6
63	"	74.5	85	1760	0.8	19.3	34.9	37.5	-	-	46.3
87	180	70.0	80	1760	2.0	20.3	35.6	30.0	-	-	44.58
11	170	71.5	85	1760	3.5	18.0	29.0	23.3	-	-	52.7
10	170	71.5	85	1760	3.8	23.2	49.4	53.7	-	-	65.6
92	160	79	83	1830	0.1	16.4	56.2	21.7	-	-	54.9
37	175	72.4	100	1800	0.5	20.9	44.6	23.9	1.95	-	48.9
23	150	81.0	85	1800	0.7	18.4	29.0	39.4	-	-	52.5
86	160	79	83	1800	2.0	19.7	30.6	37.0	-	-	52.9
14	150	81.6	85	1800	3.5	18.0	23.2	34.2	-	-	60.2
85	150	84	85	1820	2.0	14.9	14.7	35.8	-	-	66.33

Table 4.1 contd.

Run no	P_1 torr	P_{41}	% H_2 in P_4	T_5, °K	t, ms	Yield of products - mole %					%Propane decomposed
						CH_4	C_2H_4	C_2H_2	C_2H_6	C_3H_6	
4	160	77.5	86	1840	2.0	13.0	18.4	27.6	-	-	67.5
133	90	74.5	90	1860	0.4	16.8	21.2	53.9	-	-	96.4
22	130	93.5	85	1860	0.7	18.5	26.3	43.3	-	-	68.65
83	125	"	"	1860	2.0	11.3	8.61	34.1	-	-	82.0
15	130	93.5	"	1860	3.5	14.0	12.5	34.6	-	-	73.9
21	130	93.5	"	1870	0.7	18.1	23.0	44.0	-	-	64.6
61	130	97.4	"	1870	0.7	3.7	11.7	64.5	-	-	66.9
60	130	"	"	1870	1.0	17.5	19.5	51.0	-	-	65.2
62	130	"	"	1870	1.1	5.05	8.5	57.7	-	-	64.8
16	130	93.5	"	1890	3.5	10.5	10.6	26.0	-	-	95.4
94	100	126	"	1923	0.2	13.5	9.94	57.9	-	-	38.0
38	115	110	100	1923	0.6	16.2	11.8	52.6	-	-	73.7
39	115	"	100	1923	0.7	17.8	15.3	49.9	-	-	75.[illegible]
40	119	106.7	"	1923	2.2	8.34	7.84	29.9	-	-	93.7
19	110	110.5	85	1945	1.0	17.5	16.0	53.0	-	-	76.4
18	110	"	"	1945	3.5	14.6	15.4	37.4	-	-	62.3
131	100	67	100	1950	0.3	8.2	6.5	66.2	-	-	91.6
132	100	"	"	1950	0.3	8.0	6.7	68.2	-	-	89.0
97	90	140	87	1990	0.4	5.4	6.7	58.4	-	-	96.7

Table 4.1: contd.

Run no	P_1	P_{41}	H_2 %	T_5, °K	Reaction time	CH_4	C_2H_4	C_2H_2	C_2H_6	C_3H_6	% C_3H_8 decomposed
107	37	182	87	1990	0.7	1.98	6.7	65.6	-	-	*
95	90	140	"	2000	0.4	5.2	6.5	54.2	-	-	*
26	100	121.2	90	2000	0.8	7.2	7.6	45.6	-	-	85.8
77	90	140	87	2000	2.3	2.3	3.4	16.1	-	-	*
29	105	121	90	2020	0.4	8.9	7.9	54.5	-	-	76.4
30	90	140.7	94	2075	0.5	2.4	6.1	60.0	-	-	94.2
98	75	169	87	2080	0.4	2.9	5.7	49.0	-	-	*
115	33	202	96	2100	0.3	2.3	-	66.4	-	-	*
109	75	182	94	2100	0.4	1.9	5.4	47.8	-	-	*
108	75	182	"	2100	0.6	1.1	-	65.9	-	-	*
112	33	202	"	2135	0.3	1.2	4.8	53.8	-	-	*
130	80	84	100	2135	0.3	1.86	5.0	79.3	-	-	*
129	80	"	100	2135	0.3	0.0	0.0	80.2	-	-	*
128	60	11.2	"	2135	0.4	0.0	0.0	86.3	-	-	*
135	45	155	90	2135	0.8	1.1	2.1	27.3	-	-	*
136	58	177	"	2135	1.0	0.3	2.2	19.2	-	-	*
31	90	140.7	94	2153	0.5	2.9	6.3	65.4	-	-	99.2
57	75	169	100	2160	0.4	1.8	4.4	58.6	-	-	*

Table 4.1 contd.

Run no.	P_1 torr	P_{41}	% H_2 in P_4	T_5, °K	t, ms	Yield of products - mole %					% C_3H_8 decomposed
						CH_4	C_2H_4	C_2H_2	C_2H_6	C_3H_6	
64	80	140.7	94	2160	0.4	1.4	5.2	61.2	-	-	*
32	90	140.7	"	2172	0.5	3.3	6.9	64.6	-	-	93.3
66	"	"	"	2160	1.0	2.6	4.4	29.9	-	-	*
67	"	"	"	"	1.5	2.3	4.9	28.4	-	-	*
104	37	182	90	2200	0.3	3.1	-	65.3	-	-	*
116	33	202	96	2208	0.3	4.9	-	37.4	-	-	*
65	80	158.3	94	2200	1.5	1.15	3.64	22.4	-	-	*
105	37	181.6	90	2235	0.2	7.4	9.57	36.3	-	-	*
117	35	192	100	2275	0.4	-	-	81.5	-	-	*
33	80	158.3	97	2306	0.45	0.9	7.8	75.1	-	-	99.5
34	80	"	97	2335	0.45	1.4	7.7	74.3	-	-	*
41	"	"	100	2355	0.7	2.18	4.5	31.8	-	-	*
69	"	"	97	2355	"	1.7	5.6	38.7	-	-	*
70	75	168.9	97	"	"	1.2	4.8	39.5	-	-	*
71	68	186.2	90	"	2.0	2.0	5.1	18.4	-	-	*
72	67	"	90	"	2.0	0.8	2.3	11.1	-	-	*
43	85	158.3	100	2455	0.4	1.64	5.68	47.1	-	-	*
42	75	168.9	100	2455	0.7	1.6	5.0	31.1	-	-	*
50	80	158.3	100	2515	0.4	2.0	6.1	56.9	-	-	*
58	80	"	100	"	"	1.2	4.3	38.7	-	-	*

Table 4.1 contd.

Run no	P_1 torr	P_{41}	H_2 % in P_4	T_5 °K	Reaction time, ms	Yield of Products - mole, %					%, Propane decomposed
						CH_4	C_2H_4	C_2H_2	C_2H_6	C_3H_6	
73	60	211	92	2515	1.2	1.35	4.1	14.1	-	-	*
54	75	169	90	2560	0.3	0.4	5.7	62.5	-	-	*
52	80	"	100	"	0.3	0.2	5.0	72.4	-	-	*
32	75	"	"	2560	0.4	0.9	6.4	70.9	-	-	*
127	45	149	90	2630	0.2	-	-	60.1	-	-	*
126	35	191	100	2630	0.4	-	-	55.1	-	-	*
120	30	224	"	2630	0.4	-	3.4	64.7	-	-	*

At any constant temperature the percentage of propane converted was increased by increasing the reaction time. In figure 4.0 the dependence of propane conversion on the length of the reaction time is shown. At very high temperatures ($>2200^{o}$K) no propane was recovered in the reaction mixture, thereby indicating that total decomposition of propane was achieved.

Figures 4.1 and 4.2 show the distribution of the major products of propane pyrolysis at reaction times of $\sim$0.7ms. The percentage of each product was calculated on the basis of moles of carbon in that product per 100 moles of carbon in the propane converted. These figures (figure 4.1 and 4.2) show that product distributions at the high temperature range covered in this study are considerably different from those reported by investigators at low temperatures. Here it was observed that the yields of propylene, ethane and ethylene rapidly passed through maximum and declined, while the formation of methane showed a continuous and steady increase. The yield of acetylene increased gradually from near zero at 1200^{o}K, but rose very sharply after $\sim 1450^{o}$K. The appearance of acetylene in the reaction mixture corresponded with the temperature range at which the yields of propylene and ethane, and to a lesser extent ethylene, showed rapid decline. At higher temperatures the percentage yield of methane and ethylene decreased with increase in temperature and attained a minimum value ($< 5\%$), whereas the yield of acetylene continued to increase and passed through a broad maximum at the same temperature region where the yield in ethylene and methane had minimum value.

FIGURE 4.0 : Percentage of propane conversion as a function of reaction and temperature.

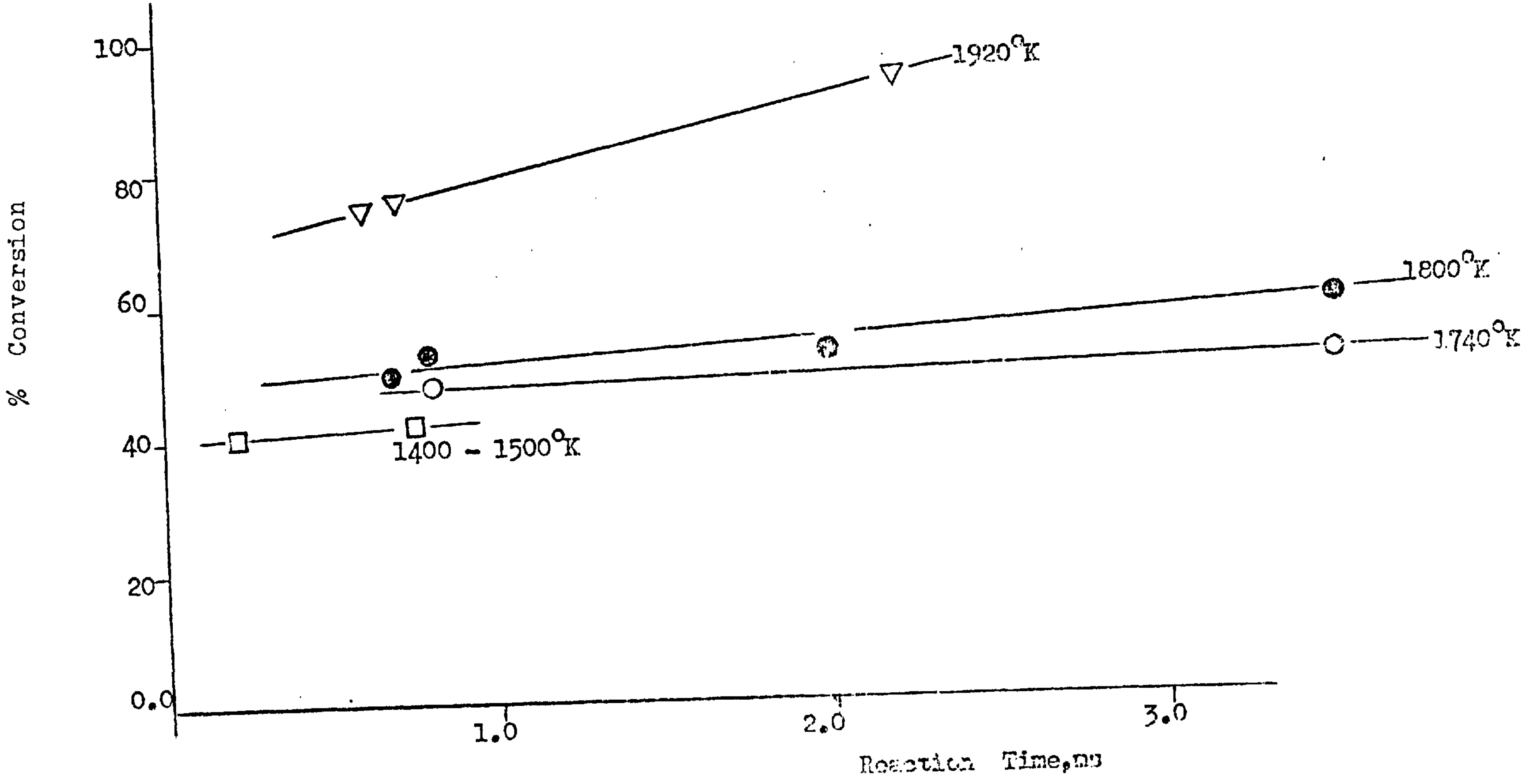

FIGURE 4.1: Product distribution from propane pyrolysis at reaction time up to 0.8ms.

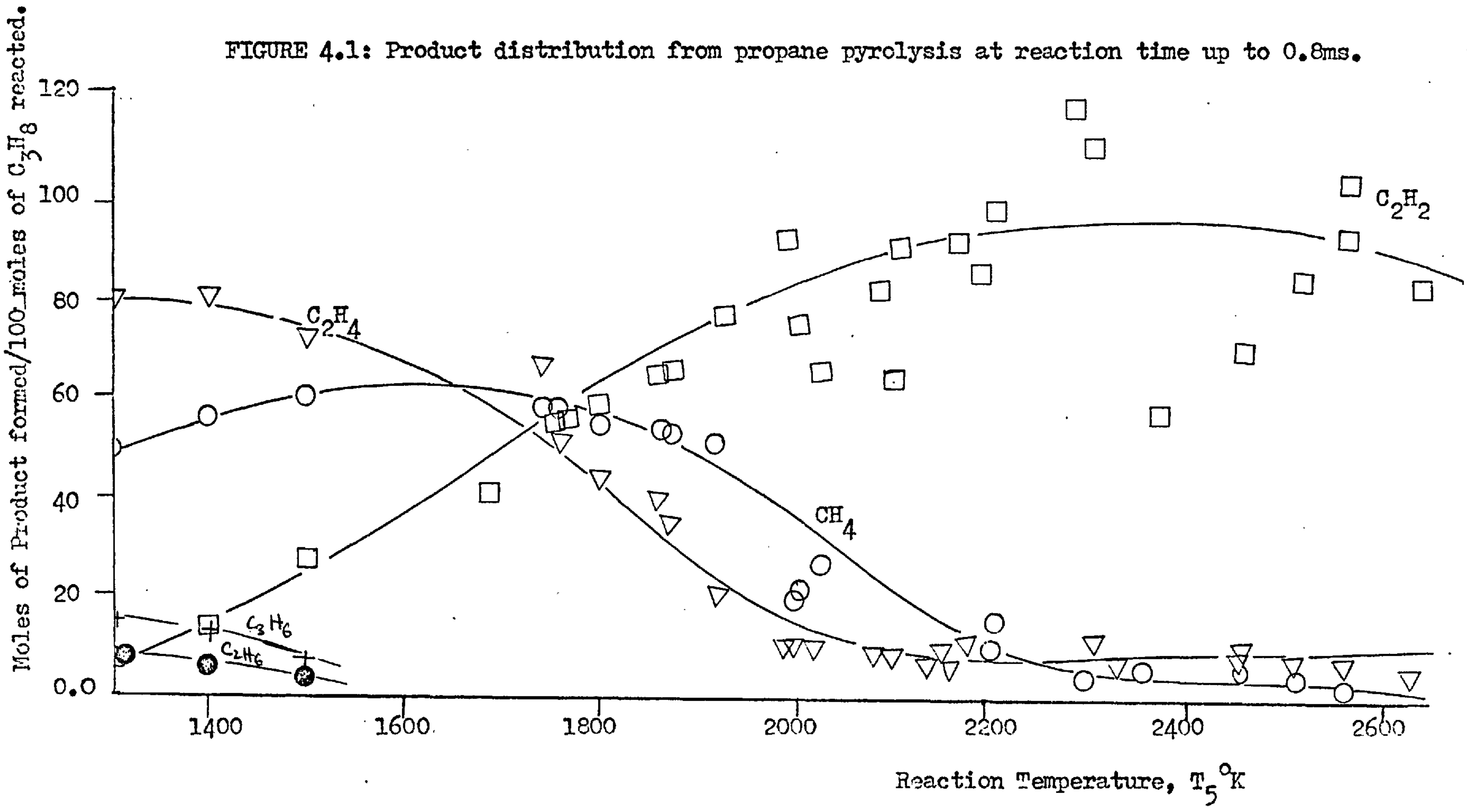

FIGURE 4.2: Percentage of propane converted to carbonecous Materials ('carbon').

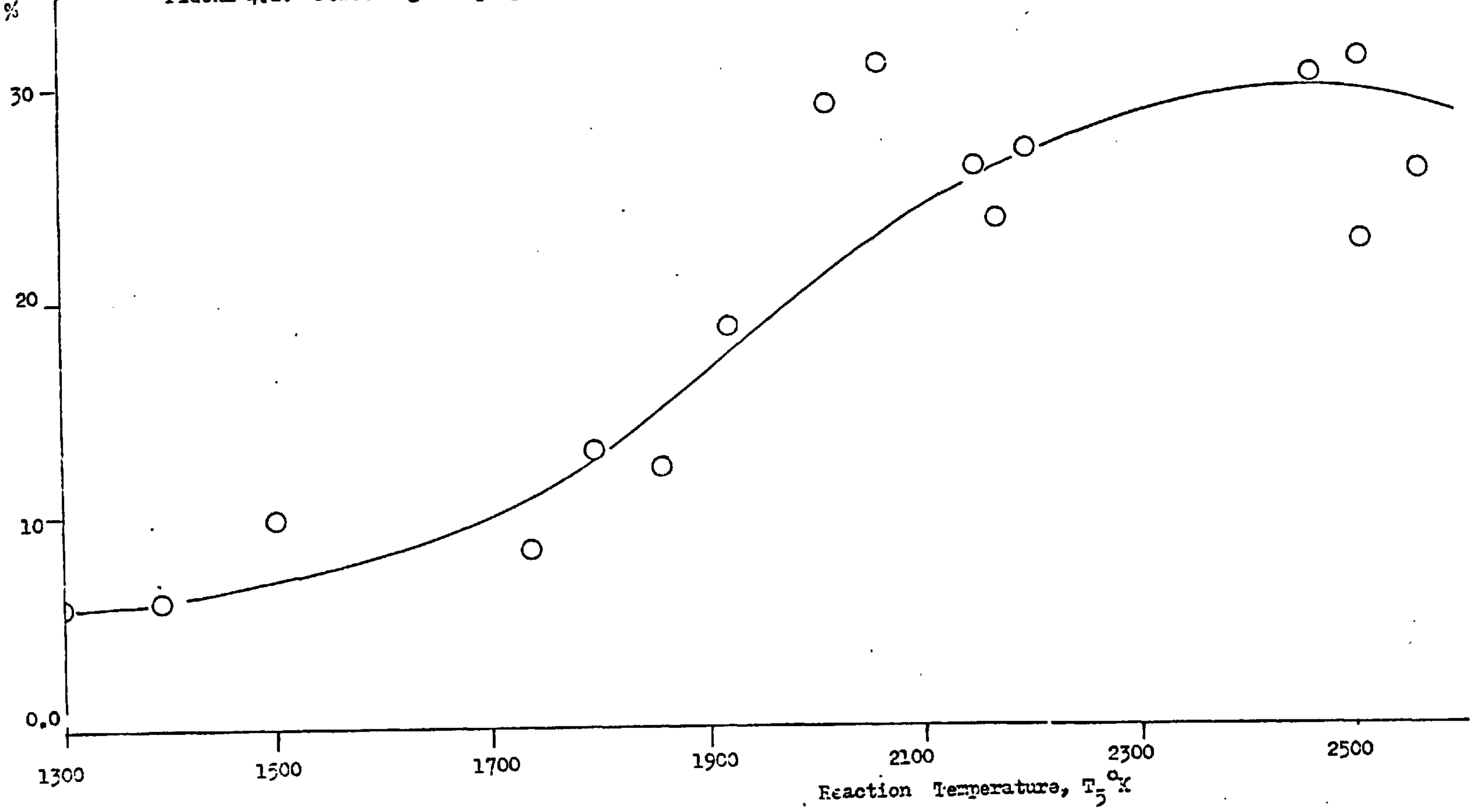

The conversion of propane to carbonaceous materials - that is high carbon - content substances - at the temperatures of this investigation was determined by mass balance from the total carbon/hydrogen ratio. The formation of these substances followed a similar trend to that of acetylene but it continued to rise even when the yield of acetylene started to decline slowly.

For detailed examination of the distribution of the major reaction products over the entire temperature range and for all the reaction times, table 4.1 was arranged on temperature/reaction time bases. The table shows the dependence of the yield of the various products, that is moles of the product formed per 100 moles of propane converted, on the variation of both the reaction time and temperature.

The effects of simultaneous variation of temperature and reaction times on the conversion of propane into methane, ethylene and acetylene are shown on figures 4.3 and 4.4 which are based[78] on table 4.1. These figures show 'iso-conversion' curves which demonstrate under what experimental conditions a desired degree of conversion of propane into any of those products can be achieved. The highest yield of methane (~20 - 15%) was achieved between 1450°-1650°K for reaction time up to 3.5ms. Outside this temperature-time range, the percentage of conversion of propane into methane gradually decreased; the rate of decrease was faster at the higher temperature side of the maximum iso-conversion contour. The conversion of propane to ethylene was higher than its conversion to methane. Highest conversions of propane into

Figure 4.3: Conversion of Propane to Methane and Ethylene

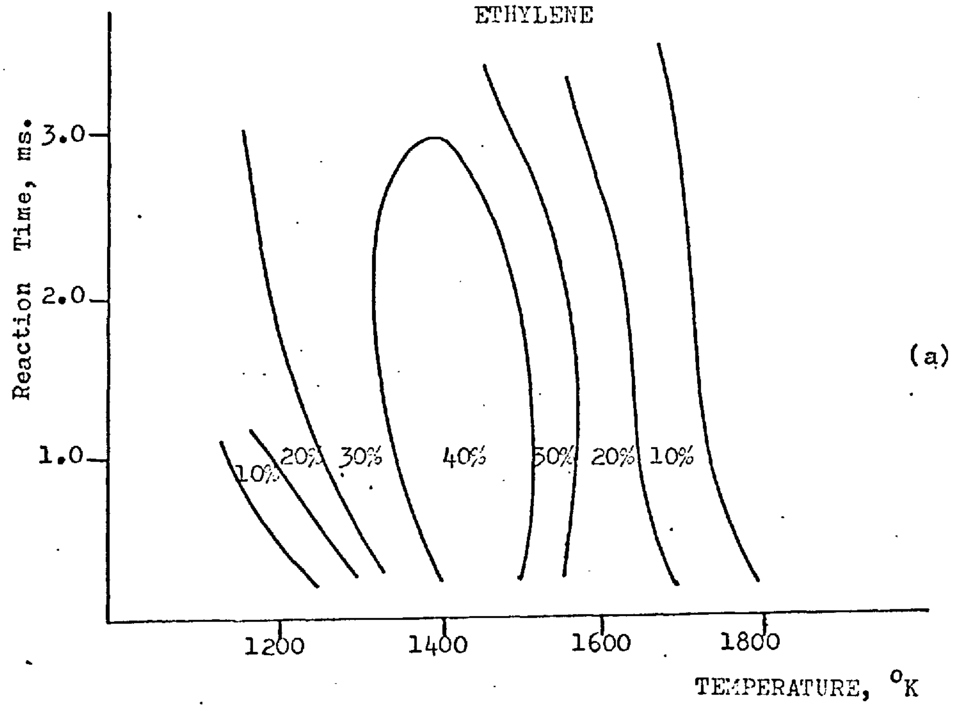

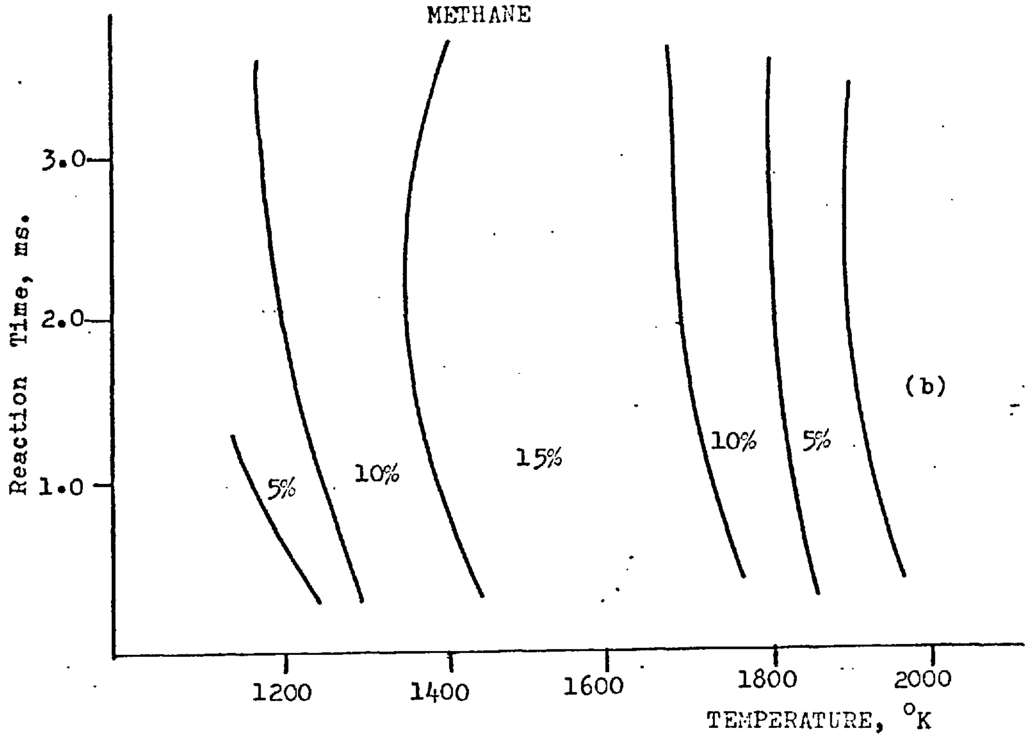

FIGURE 4.4: Conversion of Propane to Acetylene (partial pressure of propane = 55 KN/m^2)

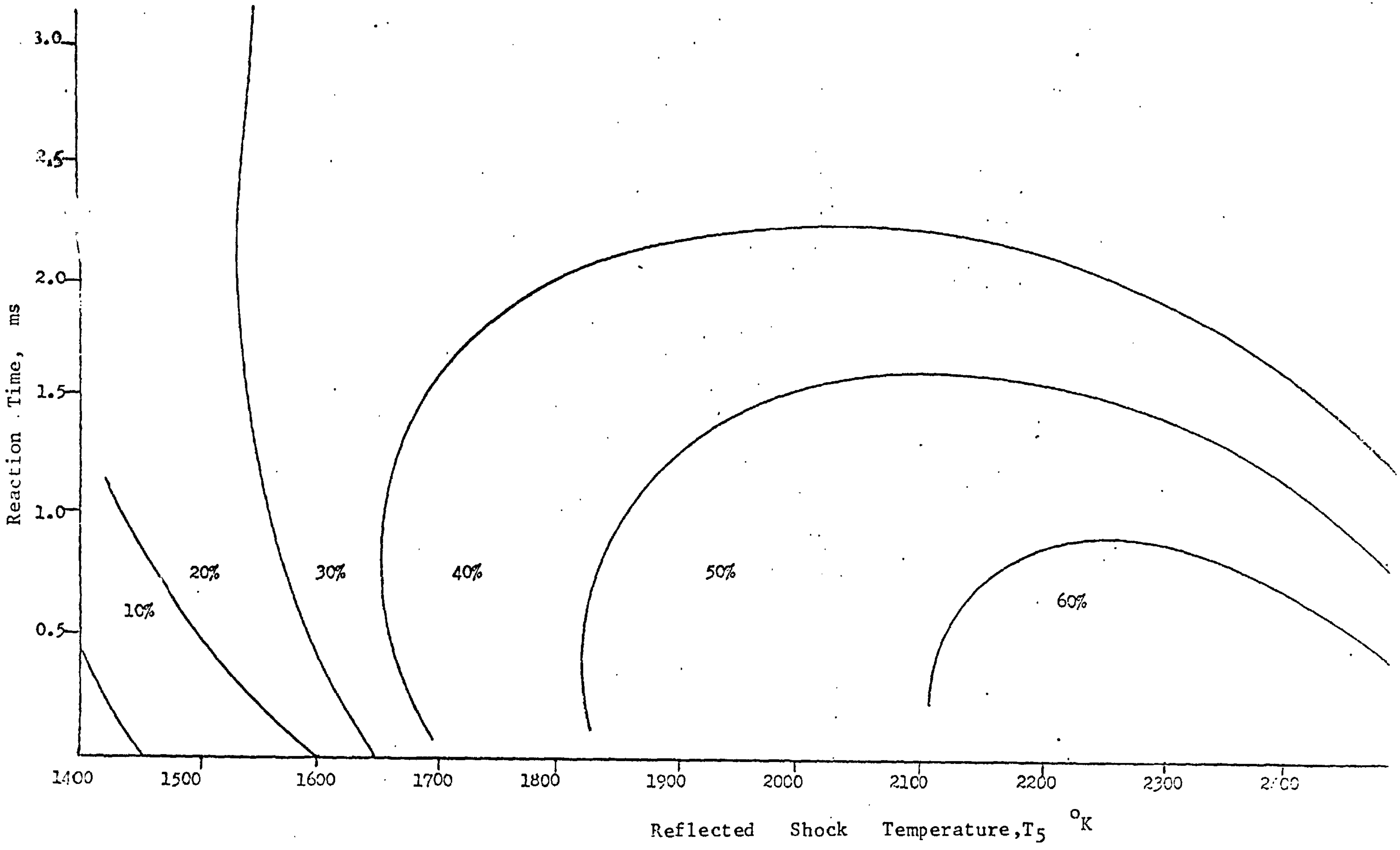

ethylene range from 40 - 50% and its contour enveloped an area bounded by temperature interval 1380° - 1500°K and reaction time upto 3ms. Outside this interval the conversion decreased gradually as was noted in the case of methane. Figure 4.3 (a and b) indicate that maximum conversion of propane into both methane and ethylene occurred within the same temperature.

The iso-conversion curves of propane into acetylene, (figure 4.4) covers a wider temperature but narrower reaction time range than those of methane and ethylene. At those temperatures where the conversions into methane and ethylene reached maxima and seemed less dependent on the length of the reaction time, the conversion into acetylene was at a minimum. At conversions into acetylene less than 30%, increase in reaction times above 1.5ms does not result in an appreciably change in the conversion value. At higher conversions of propane into acetylene the influence of reaction time variation becomes very pronounced. The yield of acetylene becomes more sensitive to prolonged shock-heating time at higher conversions of propane. The maximum iso-conversion curve ($>$ 60%) of propane into acetylene occurred between 2100° - 2500°K at reaction times under 0.8ms.

4.1.2: Effect of Reflected Pressure on Conversion to Acetylene.

Figure 4.5 and 4.6, show the effects of pressure variation on propane conversion to acetylene. In figure 4.5 the percentage of propane conversion to acetylene has been plotted against the reflected shock pressure P_5, for three different reaction times - 0.4ms, 2.0ms. and 3.0ms. The plot shows

Figure 4.5 : Effect of pressure variation on the conversion of propane into acetylene at different reaction times

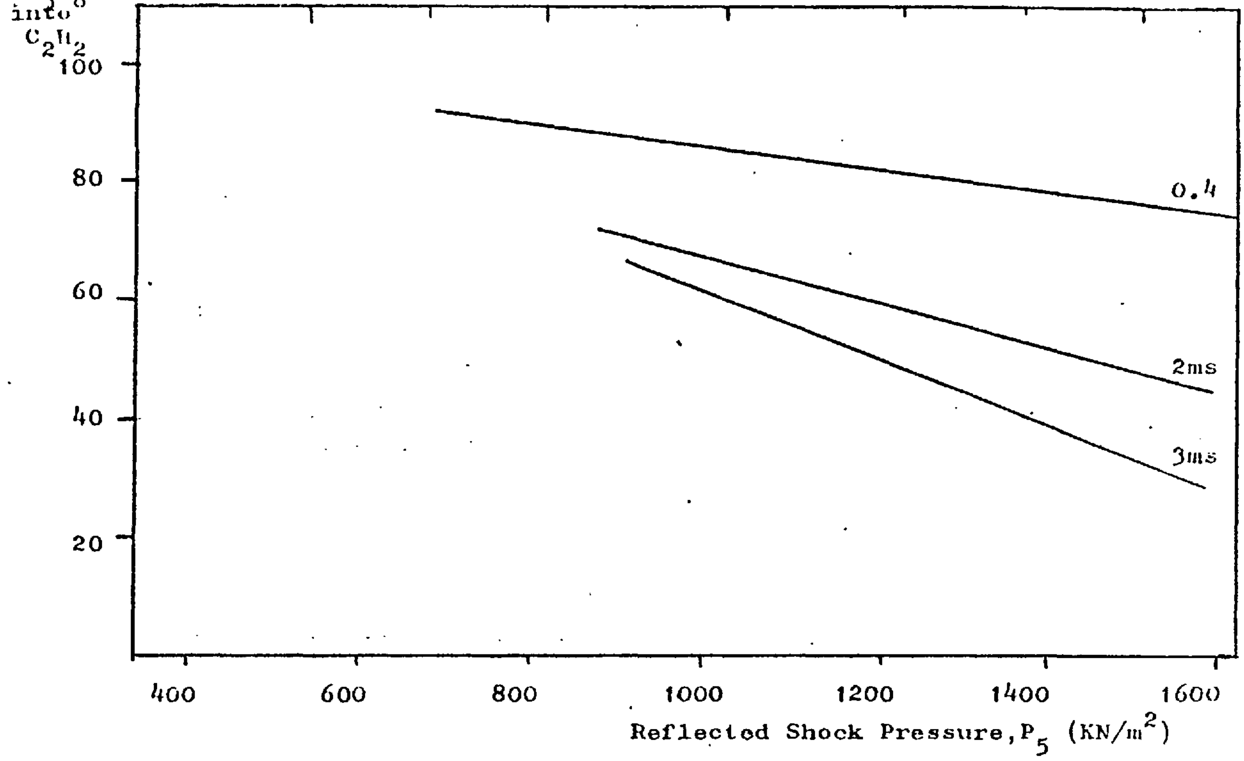

Figure 4.6 : The effect of pressure on the conversion of propane into acetylene; conversion vs reaction time

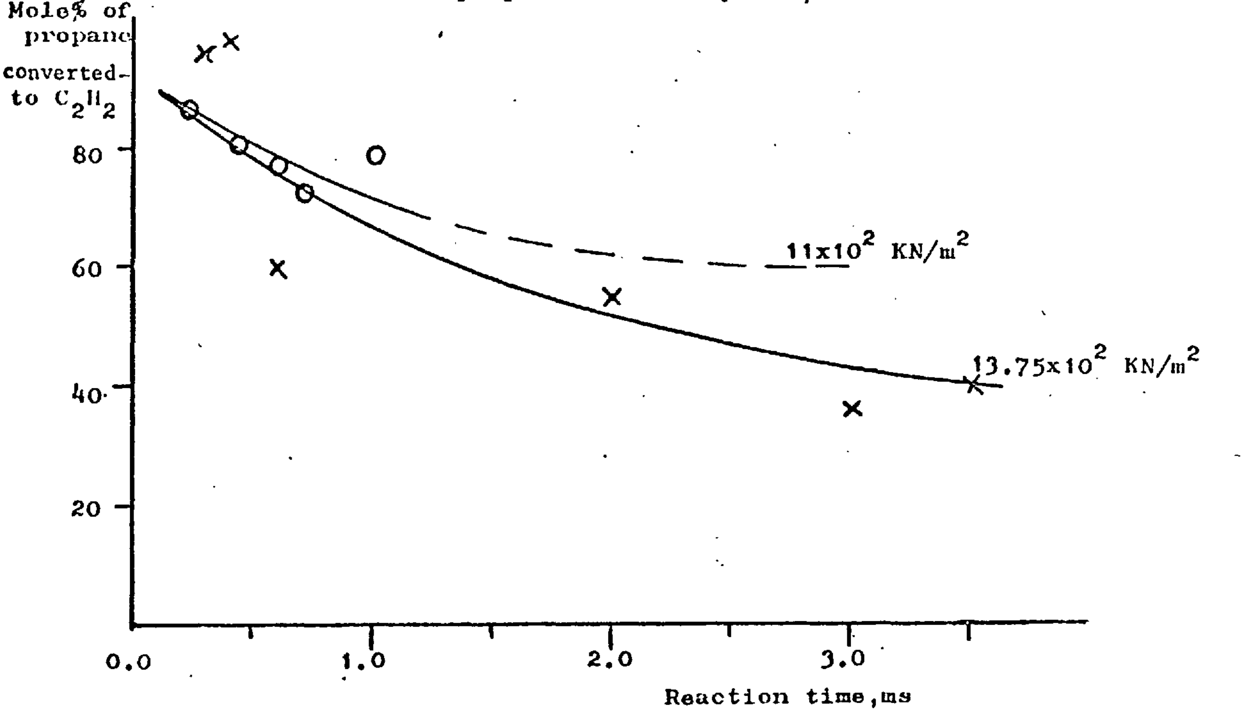

that if the reaction time was held constant, and the pressure changed, the percentage of propane converted to acetylene decreased as the pressure was increased. Such decrease in conversion to acetylene was linear, and the slope of the decrease became steeper with increasing reaction time. For example, at reaction time, $t \leq 0.4$ms high conversions of propane to acetylene were maintained and these were less sensitive to variations in the reflected shock pressures than conversions at t = 2.0ms and 3.0ms. Increasing the reaction pressure by two folds resulted in decrease of conversion of propane to acetylene by the following percentages:-

5%, 25%, and 45% for t = 0.4ms., 2.0ms. and 3. ms respectively.

This is further confirmed by figure 4.6 in which the variation in propane conversion to acetylene versus reaction times, has been plotted for two close values of reflected shock pressures. It can be seen in this figure that the two pressure curves converged at reaction times less than 0.5ms, whereas at longer reaction times the curves were separated. The vertical distance separating the pressure curves increased as the value of the reaction time became larger.

Although results are not available at lower pressure, the lines in figure 4.5 are not parallel and are likely to converge at lower values of reflected shock pressure (probably in the region under 550 KN/m^2 at reaction times, $t > 1.0$) indicating that higher conversions could be achieved at lower pressures independent of the reaction time. Therefore the reaction pressure P_5, has significant effect on the optimum conversion of propane to acetylene, and figures 4.5 and 4.6, demonstrate the necessity for controlling both the reaction time and the pressure. The decrease in the conversion of propane to acetylene with increasing pressure is to be expected if it is assumed that the reaction occurs via the establishment of the following chemical equilibrium,

$$2C_3H_8 \rightleftharpoons 3C_2H_2 + 5H_2 \qquad (4.0)$$

in which case the reaction proceeds with a considerable increase in volume. The influence of reaction pressure on the position of the equilibrium can be explained in terms of le Chatellier's Principle - which requires that an increase in pressure should shift the equilibruim in the direction which reduces the volume of the system as a whole. Hence in equation (4.0), increase in pressure will shift the equilibruim towards the left, and consequently the conversion of propane to acetylene will diminish with increasing pressure. Also, there is the tendency for the acetylene so formed to polymerize, since elevated pressure favours its polymerization. Figures 4.5 and 4.6, together with figure 4.4 show that for optimum conversion of propane to acetylene, it is necessary to conduct the experiments at short reaction times, low reaction pressure and high temperatures; but at reaction pressures under about 550 KN/m^2 the length of the reaction time is no longer very crucial.

4.1.3: The Effect of Addition of Ethane

In an attempt to elucidate the effect of increased radical concentration in the yield of the primary products at high temperatures, small quantities of ethane were added to the mixture of propane in argon. Because ethane readily generates methyl and ethyl radicals and hydrogen atoms its presence ought to influence the pattern of product distribution in the pyrolysis of propane.

The results of pyrolysing mixtures of propane/ethane in argon (C_3H_8: C_2H_6: Ar) in the following ratio 3.9:0.1:96 and 3.7:0.9:95.4) are shown in table 4.2. Inorder to examine the effects of the addition of ethane to the pyrolysis of propane, the convenient parameter chosen for the assessement of this effect was the percentage of propane converted. It is well-known that during the pyrolysis of pure ethane/argon mixtures the yield of propane is quite negligible, therefore in pyrolysing propane/ethane/argon mixtures, the difference between the amount of propane introduced into the shock tube and the amount recovered from the shock treated mixture represents the net change due to reaction. The quantity of ethane contained in the shock-treated mixture consists of:-

(a) unreacted ethane from the propane/ethane/argon mixture and

(b) ethane derived from the decomposition of propane.

The method of calculating the yield of ethane from propane/ethane/argon mixture was based on mass balance and is shown in appendix A4.

The effects of the addition of ethane to the pyrolysis of propane, is shown in table 4.1 and in figure 4.7.

Table 4.2: Results of pyrolysis of mixture of propane/ethane in argon.

(a) mixture B, C_3H_8: C_2H_6: Ar = 3.9:0.1:96.0

Run No.	Temperature	Reaction time	Yield of Products, i.e mole % i.e. mole % of C_3H_8 converted to:-					% Propane
	°K	t, ms	CH_4	C_2H_4	C_2H_2	C_2H_6	C_3H_6	Conversions
251	1200	3.0	10.49	29.96	0.0	3.00	8.99	51.8
253	1200	3.0	11.09	32.91	0.0	2.77	5.55	35.8
250	1200	3.2	9.95	31.52	0.83	3.32	7.47	47.7
252	"	3.5	9.95	33.46	0.00	3.39	3.39	29.3
245	1250	0.10	9.48	28.21	0.00	4.41	13.22	18.27
244	1300	0.10	8.06	29.75	0.00	5.56	20.86	30.7
247	1300	0.10	8.42	30.12	0.00	5.32	15.95	49.6
248	1350	3.0	10.25	30.17	2.12	3.31	5.95	59.7
246	1400	0.10	8.96	32.11	1.87	4.68	9.35	52.0
223	1450	0.10	9.72	35.2	3.0	1.94	7.50	72.5
236	1500	0.80	18.9	41.8	25.3	-	-	99.6
240	1600	0.20	8.72	31.96	2.1	4.36	8.72	72.0
238	1600	0.40	13.5	23.4	22.4	-	-	79.8
229	1700	0.40	9.9	14.0	33.6	-	-	-
219	1700	0.50	16.4	11.9	35.3	-	-	99.3
221	1750	0.40	12.7	8.75	43.9	-	-	*
226	1750	0.40	16.15	8.13	45.1	-	-	*
220	1800	0.50	9.64	6.97	34.2	-	-	*
217	1900	0.50	3.7	3.37	20.6	-	-	*
248	1900	0.50	1.73	1.75	12.2	-	-	*

Table 4.2 contd.

(b) mixture C, C_3H_8: C_2H_6: Ar = 3.7 : 0.9 : 95.4

Run No.	Temperature ^oK	Reaction time ,ms	Yield of products - i.e. mole % converted to:-					% Propane Conversions
			CH_4	C_2H_4	C_2H_2	C_2H_6	C_3H_6	
211	1500	0.5	20.6	30.8	27.2	-	-	50.8
212	1550	0.5	18.5	11.7	27.2	-	-	59.25
207	1860	"	18.8	30.7	31.1	-	-	78.0
209	1880	"	17.5	29.2	29.7	-	-	78.89
210	1890	"	16.3	25.2	28.7	-	-	89.60
208	1900	"	16.5	17.5	39.6	-	-	83.8
203	1930	1.0	3.5	2.9	1.7	-	-	*
204	1975	0.5	5.3	5.0	25.3	-	-	*
205	1978	0.5	5.2	5.1	26.0	-	-	*

Table 4.3: Percentage decomposition of propane at reaction time upto 0.7ms for mixtures with and without added ethane

Temperature ^oK	% decomposition of propane in mixtures:	
	4% C_3H_8 + 96% Ar A	3.7% C_3H_8 + 0.9% C_2H_6 95.4%Ar C
1400	34.9	-
1500	46.6	50.8
1550	-	59.3
1740	48.0	-
1860	68.6	78.2
1880	65.0	78.8

Figure 4.7: Effect of ethane on decomposition of propane at reaction times < 1ms.

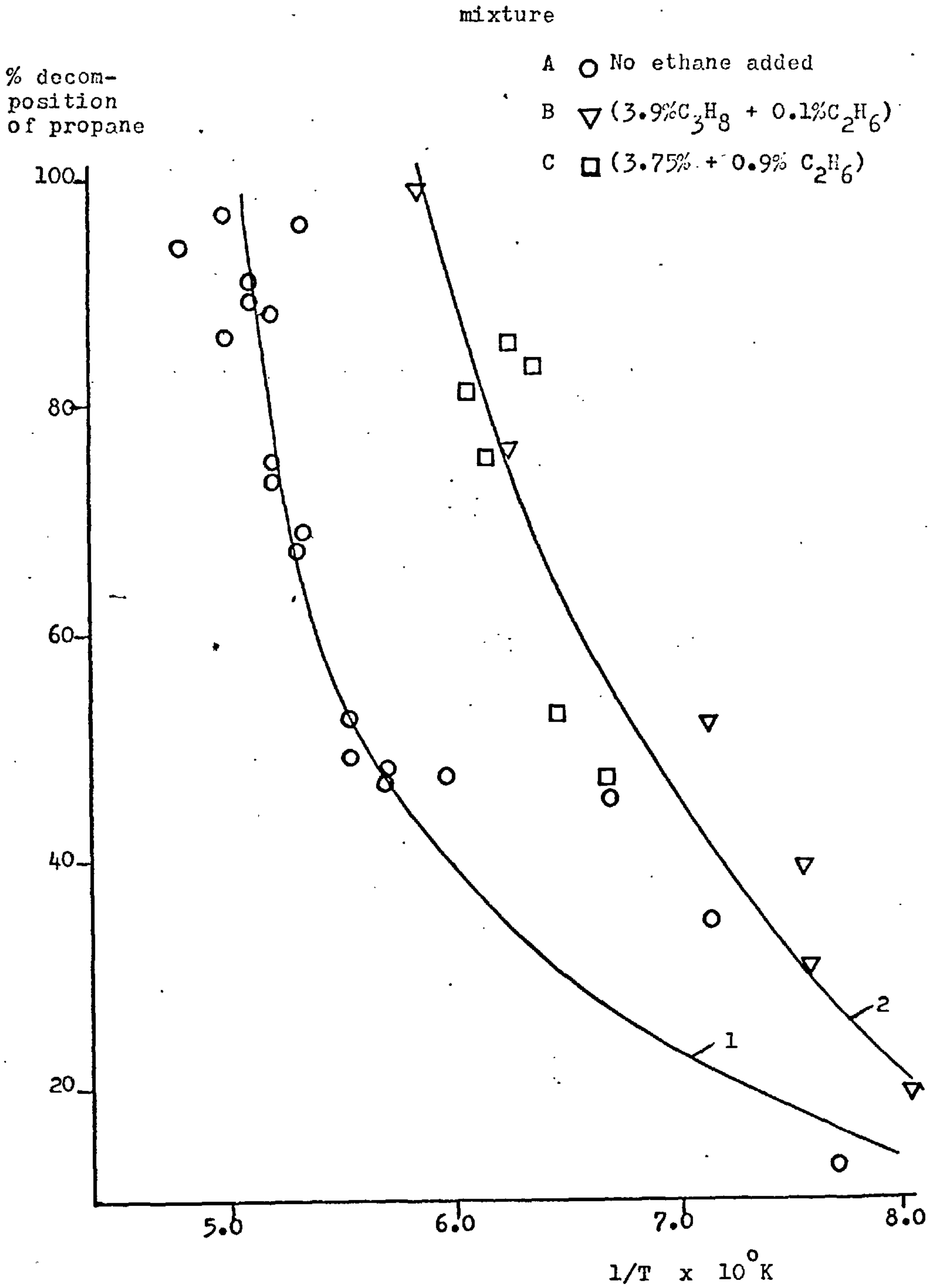

Both the table and figure 4.7 are based on the values extracted from the results in tables 4.1 and 4.2 in which mixtures have the following percentage compositions:

Mixture B has C_3H_8: C_2H_6: Ar = 3.90:0.1:96.0
" C " " " " = 3.70:0.9:95.4
and mixture A contains C_3H_8 in Ar. in the ratio 4:96.0

Generally, the values indicated in table 4.3 and in figure 4.7 , show that the addition of ethane increased propane decomposition. It can be seen that ethane when present even in trace amount greatly accelerated propane decomposition especially at high temperatures, but increase in the quantity of ethane added to the propane/argon mixture did not result in an equal increase in its accelerating influence. Within the limits of the scatter in the experimental points, it can be seen that mixture C, which contains almost 10 times as much quantity of ethane as in mixture B, produced nearly the same degree of acceleration. At lower temperatures, the points on the two curves (1 and 2) in figure 4.7 lie much closer together - indicating that at low temperatures the accelerating influence of ethane addition on the decomposition of propane is not as pronounced as at high temperatures. This might be attributed to changes in the concentration levels of the radicals and hydrogen atoms involved in the reaction - this will be discussed further at the end of this section.

Figure 4.8 shows the variation in the yields of the reaction products as a function of propane conversion in the presence of ethane a constant reaction time of 0.1ms in the temperature range of 1250°- 1450°K. Here it was observed that

Figure 4.8: Product yield as a function of variation in propane conversion at T = 1300 - 1400°K for reaction time <0.2ms.

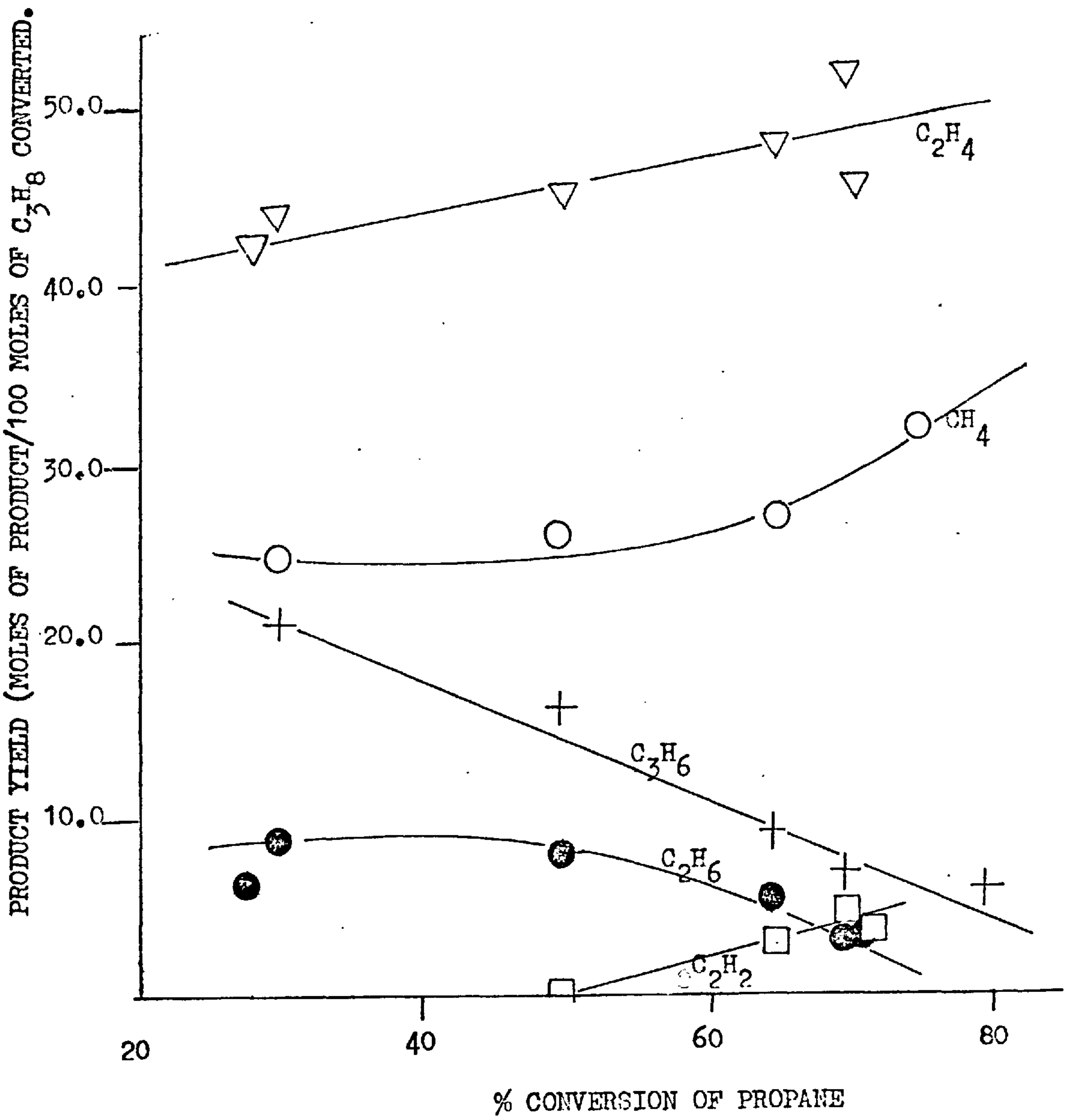

in the presence of ethane increases in propane decomposition greatly enhanced the yields of ethylene and methane, while those of propylene and ethane declined. Acetylene appeared among the reaction products only at higher ($>$ 40%) propane conversions. The shape of the curves in figure 4.8 show two distinct patterns:

a) for the olefins (C_2H_4 and C_3H_6); the increase in the yield of ethylene was linear and this corresponded to a linear decrease in the formation of propylene;

b) in the case of the paraffins, the increase in methane formation as well as the decrease in the yield of ethane exhibited curvatures in their profiles.

These seems to indicate that ethylene increased at the expense of propylene and methane at the expense of ethane.

Some investigators[141, 142], have also observed that the addition of ethane to pyrolysing feedstocks, greatly promoted the yield of ethylene at the expense of propylene. It has been suggested[141], that ethane enters the reaction by increasing the concentration of atomic hydrogen, which can react with the relatively unreactive propylene to yield ethylene. This occurs probably via propyl radicals[88] through the following reactions:

$$
\begin{aligned}
C_3H_6 + H^{\bullet} &\longrightarrow iC_3H_7^{\bullet} \\
iC_3H_7^{\bullet} &\longrightarrow nC_3H_7^{\bullet} \\
nC_3H_7^{\bullet} &\longrightarrow C_2H_4 + CH_3^{\bullet} \\
CH_3^{\bullet} + R &\longrightarrow CH_4 + R^{\bullet}
\end{aligned}
$$

where R could be C_2H_6, C_3H_8 or radical.

Similar observation by Kunugi et al[85], who studied the pyrolysis of propane in the presence of hydrogen showed that the yields of ethylene and methane were enhanced at the expense of propylene.

The yield of acetylene in the presence of ethane was relatively very low and it is believed that its formation occurs as a result of the decomposition of vinyl radicals which are formed at higher conversions through ethyl radicals or the decomposition of propylene[26].

A comparative study of the effects of the addition of ethane to pyrolysing propane on the average rates of the formation of the major reaction products is shown in table 4.4 and these values have been plotted in figures 4.9 to 4.12. The comparison was based on the rate of the yield of the individual product per 100 moles of propane reacted. The average rate R, was defined as:

$$\bar{R}_i = \frac{[\text{Product}_i]_t}{t}$$

where $[\text{Product}_i]_t$ - is the total moles of product i formed at time t for 100 moles of propane converted.

The relative rate, RR_i, was defined as the average rate of formation of the product i from a mixture with added ethane relative to that of the formation of the same product from 4% propane in argon under similar experimental conditions; this was evaluated as

$$RR_i = \frac{\bar{R}_i \text{ in mixture (B)}}{\bar{R}_i \text{ in mixture (A)}}$$

TABLE 4. 4: Log Rate of product formation - $\log_{10} \frac{(\text{Product})}{t}$

PRODUCTS	CH_4		C_2H_4		C_2H_2	
MIXTURE* / TEMP. °K	A	B	A	B	A	B
1300	2.402	2.398	2.602	2.653	1.38	-
1400	2.436	2.431	2.593	2.682	1.789	1.450
1450	2.458	2.438	2.571	2.696	2.072	1.629
1500	1.94	1.86	2.00	1.895	1.643	1.676
1600	-	2.34	-	2.25	-	1.924
1700	-	1.94	-	1.636	-	2.06
1750	2.190	2.033	2.233	1.49	1.909	2.222
1800	2.098	1.763	2.127	1.301	1.855	2.011
1900	1.908	1.346	1.463	1.00	2.119	1.791
1950	1.908	-	1.52	-	2.53	-

* Mixture A = 4% C_3H_8 in argon

" B = (3.9% C_3H_8 + 0.1% C_2H_6) in argon

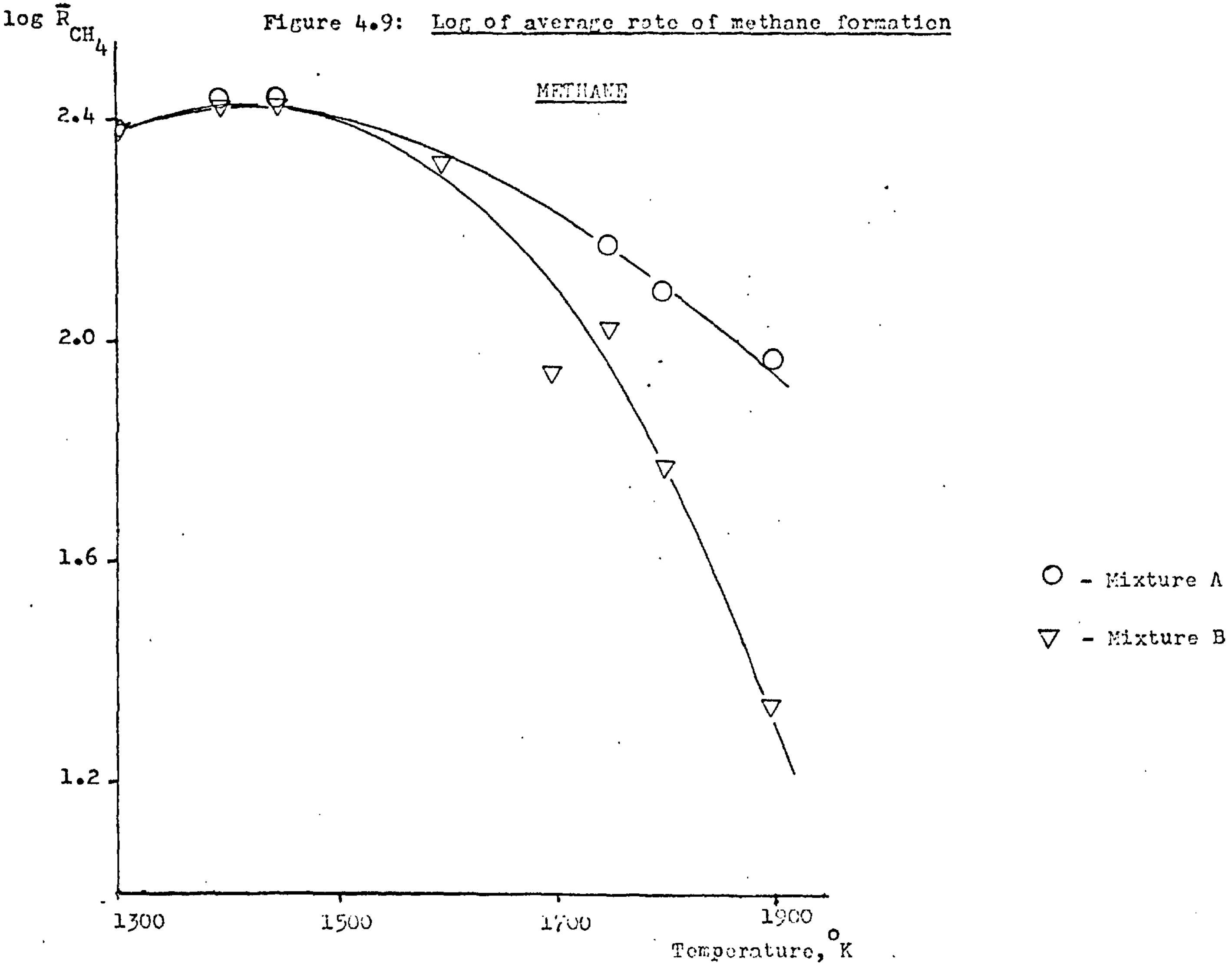

Figure 4.9: Log of average rate of methane formation

Figure 4.10: Average rate of ethylene formation.

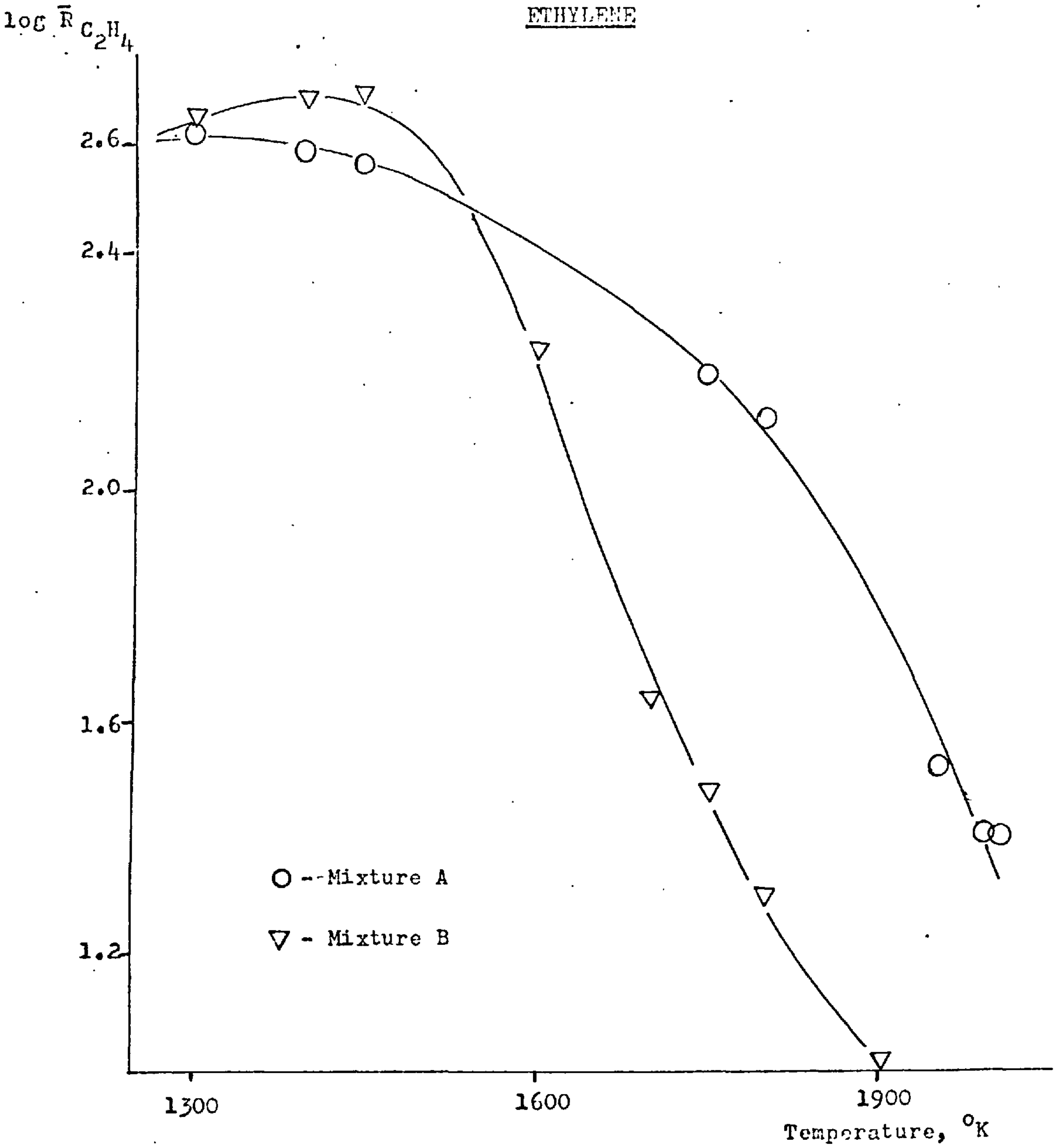

FIGURE 4.11: Logarithm of Average Rate of C_2H_2 formation.

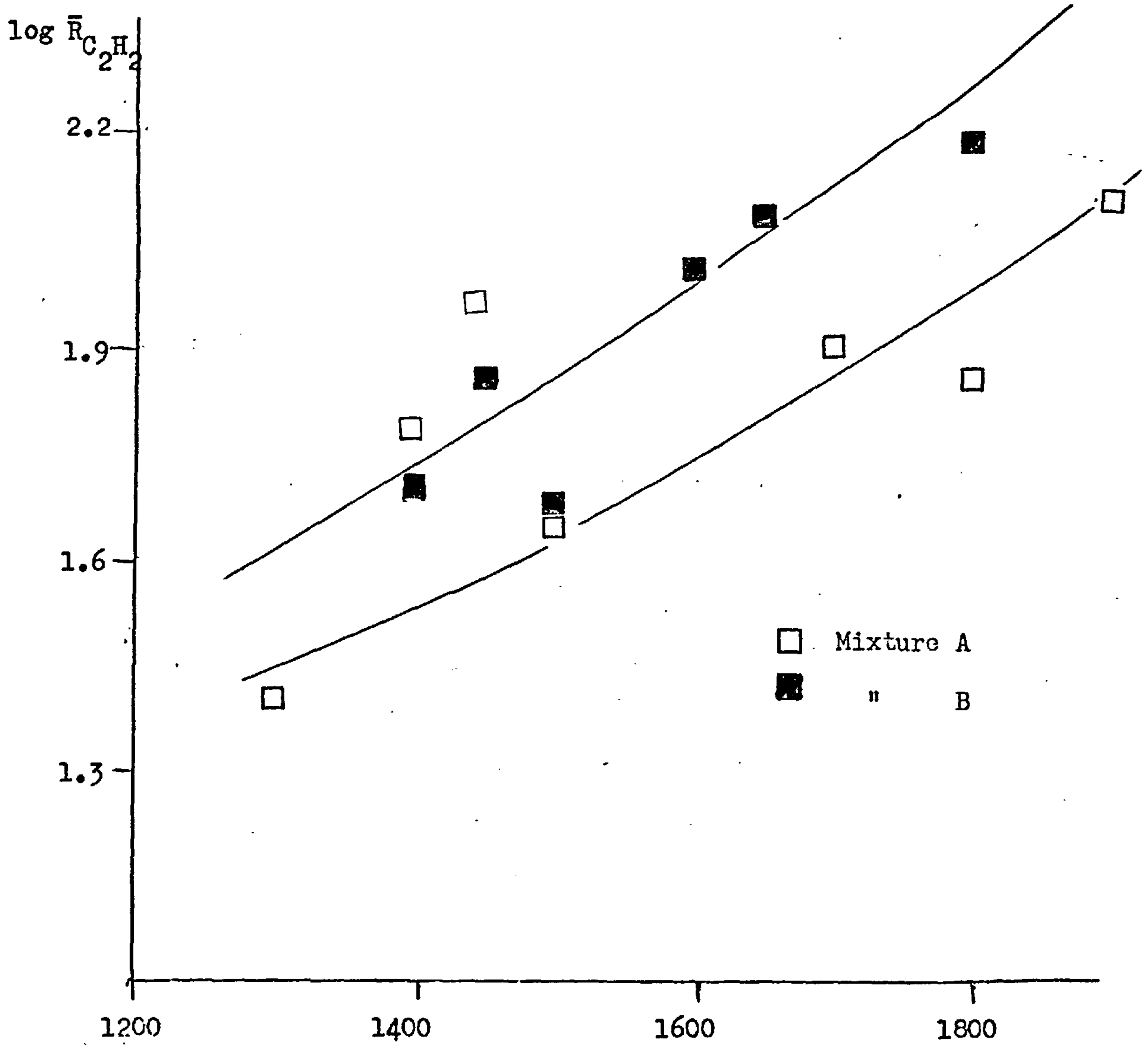

FIGURE 4.12: Relative Rates of product formation.

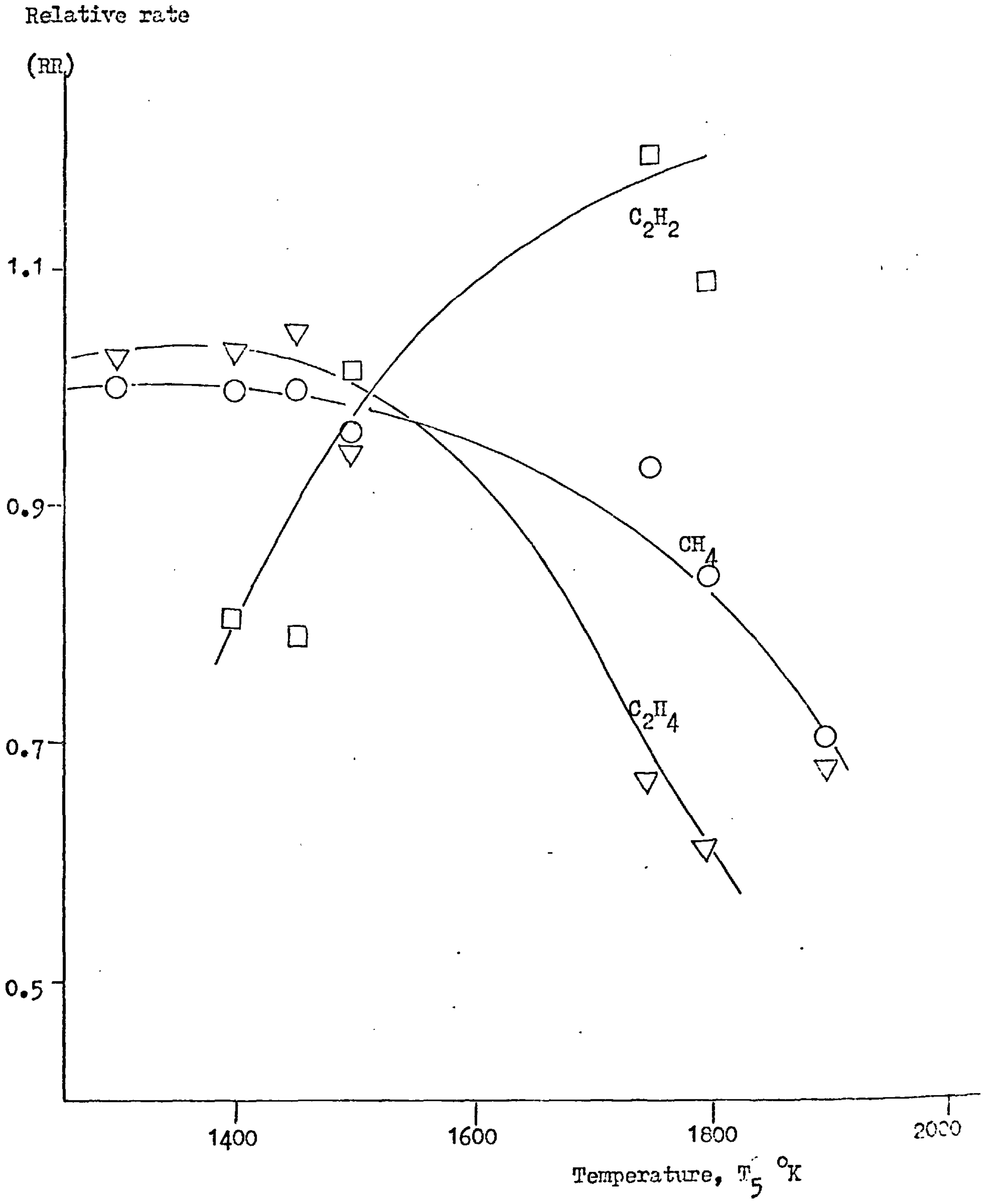

where mixture (A) is pure propane/argon mixture and mixture (B) - propane/ethane/argon mixture.
For each temperature at which these evaluations were carried out, the difference in reaction times for both mixtures was not more than ± 0.1ms.

Generally, the addition of ethane did not change the overall trend of the dependence of the average rates of formation of the products on temperature. At all the temperatures the curves for both mixtures exhibited the same characteristic shapes. At temperatures under 1600°K, the rates of formation of methane and ethylene was essentially the same for both mixture A (i.e. reaction mixture with no ethane added) and mixture B(with added ethane). Above this temperature the addition of ethane retarded the rate of the formation of both ethylene and methane. Figure 4.11 shows the effect of the addition of ethane on the average rate of formation of acetylene. Ethane accelerated the formation of acetylene; the rate was slightly increased by increasing the reaction temperature.

It can be seen in figures 4.12 that there was no change in the relative rates of formation of methane and ethylene at temperatures upto 1600°K, but above this temperature the relative rates decreased with increasing temperature. On the other hand the relative rate of propane conversion to acetylene increased with temperature.

4.2: Discussion of propane results.

The above observed effects of the addition of ethane on the pyrolysis of propane might be explained in terms of changes in the concentrations of the radicals. The non-significant effect of the addition of ethane at lower temperatures ($<1200^{o}K$), could be due to the fact the C-C bond in ethane is stronger than that in propane, so propane dissociates more readily to methyl and ethyl radicals,

$$C_3H_8 \longrightarrow CH_3^{\bullet} + C_2H_5^{\bullet} \qquad (5.1)$$

whereas ethane will remain largely undissociated. If propane were pyrolysed alone, it will be mostly consumed by the combination reactions between it and these radicals, via the reactions,

$$CH_3^{\bullet} + C_3H_8 \longrightarrow CH_4 + C_3H_7^{\prime} \qquad (5.2)$$

$$C_2H_5^{\bullet} + C_3H_8 \longrightarrow C_2H_6 + C_3H_7^{\prime} \qquad (5.3)$$

but in the presence of small quantity of ethane which is largely undissociated (relative to propane) at lower temperatures, these radicals will also react with ethane molecule to produce similar products, as in reactions (5.4) and (5.5).

$$CH_3^{\bullet} + C_2H_6 \longrightarrow CH_4 + C_2H_5^{\bullet} \qquad (5.4)$$

$$C_2H_5^{\bullet} + C_2H_6 \longrightarrow C_2H_6 + C_2H_5^{\bullet} \qquad (5.5)$$

But the net effect of reaction (5.5) is zero, so only the reaction involving the methyl radical will be of important consideration in the presence of undissociated ethane. At temperatures around $1000^{o}K$, the rate constants of the combination reactions of methyl radicals with propane and ethane are in the same order of magnitude. For example, at T = 1000°K, these rate constants are[91]

$$K_{5.2} = 1.5\text{x}10^6 \quad (\text{l/mole.s})$$

and

$$K_{5.4} = 1.07\text{x}10^6 \quad (\text{l/mole.s})$$

so there will be no appreciable change in the decomposition behaviour of propane at low temperatures, especially as regards product distribution since reaction (5.1) is the only source of methyl radical and reactions (5.2) and (5.4) compete for this radical at almost the same rate. This fact is borne out in figure 4.7 where curves 1 and 2 lie closer to each other towards the lower temperature region. Figure 4.12 confirms this trend - since the curves for the relative rates of formation of methane and ethylene at temperatures under 1600°K did not change and their values were almost equal to unity.

At increased temperatures (above 1500°K), ethane will also dissociate thereby increasing the radical concentrations of methyl and ethyl and hydrogen atom. Since methyl radical is an important chain-carrier in propane pyrolysis, increase in its concentration will result in the acceleration of the consumption of propane. Increase in the concentration of hydrogen atom will also promote propane pyrolysis since the former is known[79, 88] to react to reduce the self-inhibiting characteristics of propane decomposition. On the other hand at elevated temperature of this magnitude, ethyl radicals will be involved in secondary reactions. Ethyl radicals will, like other hydrocarbon radicals higher than $CH_3^{\bullet}$, decompose rapidly to lower species and hence will not participate to any significant extent in bimolecular reactions with other species present. The decomposition of ethyl radicals will occur via the following reaction steps

$$C_2H_5^{\bullet} \longrightarrow C_2H_3^{\bullet} + H_2$$

$$C_2H_3^{\bullet} \longrightarrow C_2H_2 + H^{\bullet}$$

which will also lead to increase in the concentrations of hydrogen atoms and acetylene. Figures 4.9 - 4.12 show the significance of 1500°K, which could be explained in terms of ethyl radicals dissociating to form acetylene via vinyl radicals instead of

$$C_2H_5^{\bullet} \longrightarrow C_2H_4 + H_2.$$

This fact is borne out by reference 26 where the ratio $[C_2H_2]$ to $[C_2H_4]$ increased very sharply after 1500°K. For example, at 1500°K, this ratio was 6.5 times higher than its value at 1300°K.

Previous investigators of the pyrolysis of propane at temperatures lower than those encountered in the present study have indicated that acetylene is a minor product; but as was illustrated in figure 4.1, acetylene was a major reaction product, and its yield was considerably higher than those of the other hydrocarbons. On the other hand propylene which is usually regarded as a major primary product of propane pyrolysis at lower temperatures was not detected in the reaction mixtures at temperatures above 1500°K. Hence the product distribution at temperature range from 1200 - 2700°K covered in this study showed a marked difference from the lower temperature data.

In another shock tube investigation[27] of the pyrolysis of propane behind the reflected shock waves at 1050 - 1650°K, it was also reported that the product distribution was considerably different from the one at the lower temperature range, and that at temperatures above 1300°K the pyrolysis of the primary products towards the production of acetylene, propyne and allene begins to occur at a considerable rate. It is apparent, therefore, that during the pyrolysis of propane at high temperatures, many other reactions, normally not considered or termed insignificant at the lower temperature investigations, emerge to prominence and thereby alter the product distribution pattern.

It has been suggested that the pyrolysis of propane becomes very complex at high conversions due to the occurrence of secondary decomposition reactions. The present investigation maintained very high propane conversion, reaching almost 100% at temperatures above 2000°K and hence the explanation of the observed product distribution is not simple. At the experimental conditions of this work, it is not possible to suggest an overall stoichiometry of the major reactions leading to the observed product distributions because of the high levels of propane conversion achieved. The usual assumption that the propane decomposition occurred via two routes with roughly equal importance;

$$C_3H_8 \longrightarrow C_3H_6 + H_2 \qquad 5.6a$$

and

$$C_3H_8 \longrightarrow C_2H_4 + CH_4 \qquad 5.6b$$

can only be applicable at very low conversions (about 10%) and low temperatures. The rapid fall in the yield of the so-called primary products at high temperatures, suggest a possible change in reaction mechanism, and that reactions 5.6 (a & b) represent rather a simplification of the true process. This point is discussed further in section 4.3 on reaction mechanism.

As was pointed out in section (1.6.2) most investigators (92, 96-7, 105-6) found that the decomposition of propane obeys a first order rate law, but many later investigators (79, 85, 107) have indicated that the reaction order varies from 1.2 to 1.5. The experimental data obtained from the present investigation were therefore analysed assuming both first and $^3/_2$ order kinetics.

The Arrhenius plot for a three halves order analysis of data obtained between 1300 - 2300°K revealed that the data points were largely scattered especially at the lower temperatures. Analysis based on first order kinetics gave a better fit to the data points than a $^3/_2$ order reaction. Figure 4.13 shows the Arrhenius plot for a first-order reaction rate in the temperature range between 1600 - 2300°K, and the generalized rate expression obtained by least squares analysis is;

$$k = 1.79\text{x}10^8 \exp(-\ 176.2\ \text{KJ/RT})\ s^{-1}.$$

The values obtained for the frequency factor, A and the activation energy, E_a are compared in table 4.5 with other literature values. The value for activation energy obtained in the current investigation is lower than the values outlined in the table but nearer Frend's[107] recalculated data assuming a first order reaction; generally (as in figure 4.14) it compares favourably with the observed 'fall' in activation

Table 4.5: Kinetic parameters from previous shock tube studies on propane pyrolysis

Authors	Temperature °K	A	E (KJ/mole)
Benson[92]	1100 - 1450	2.7×10^{12}	256.2
Frend recalculated data[107]	1210 - 1680	10^{8}	180.3
Shirotsuka et al[106]	1000 - 1310	1.1×10^{13}	255
"	1310 - 500	10^{4}	27.5
Present study	1200 - 2800	1.79×10^{8}	176.2

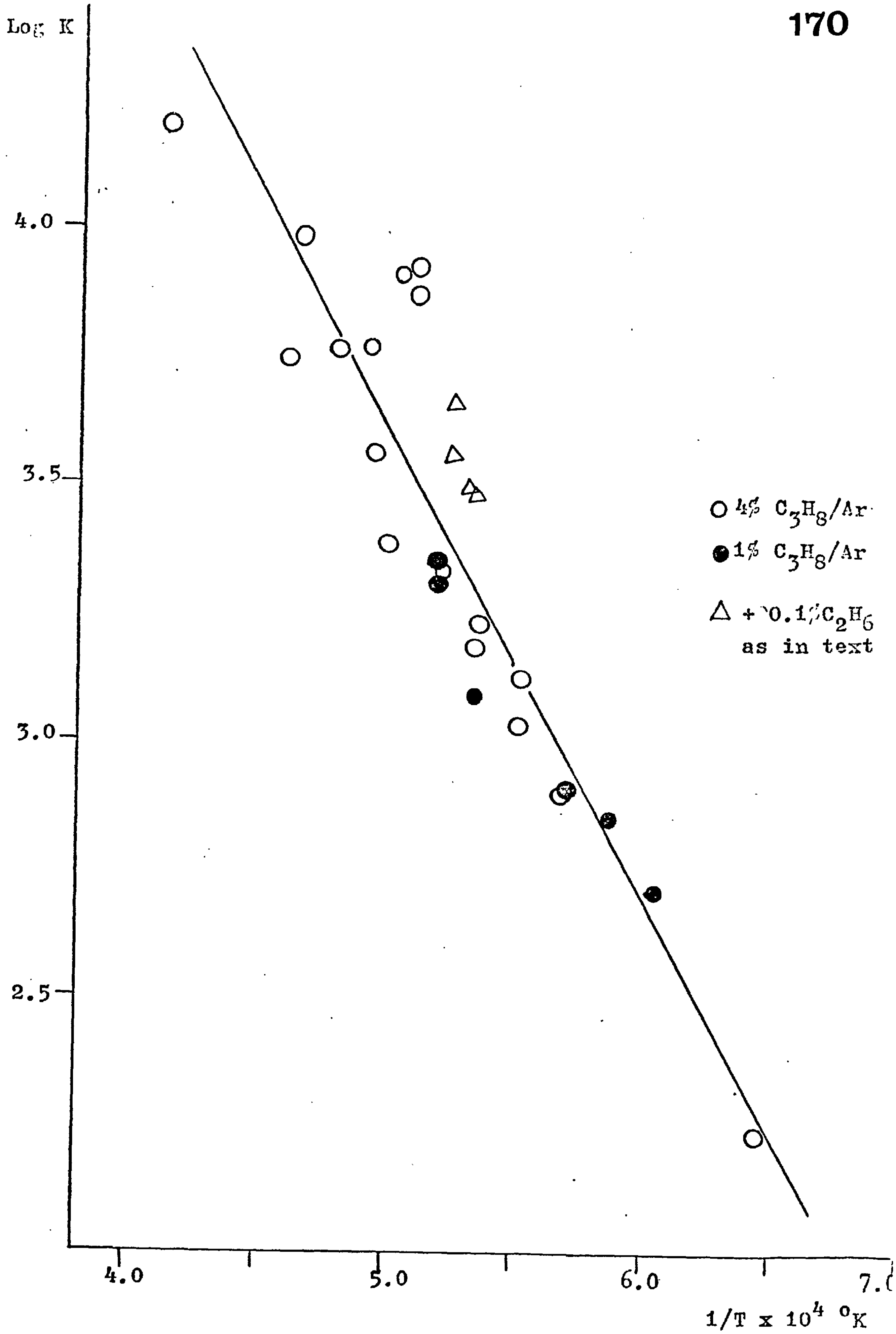

Figure 4.13 : First Order Arrhenius plot for propane pyrolysis.

Figure 4.14: Comparison of 1st order Rate constants of Propane Pyrolysis

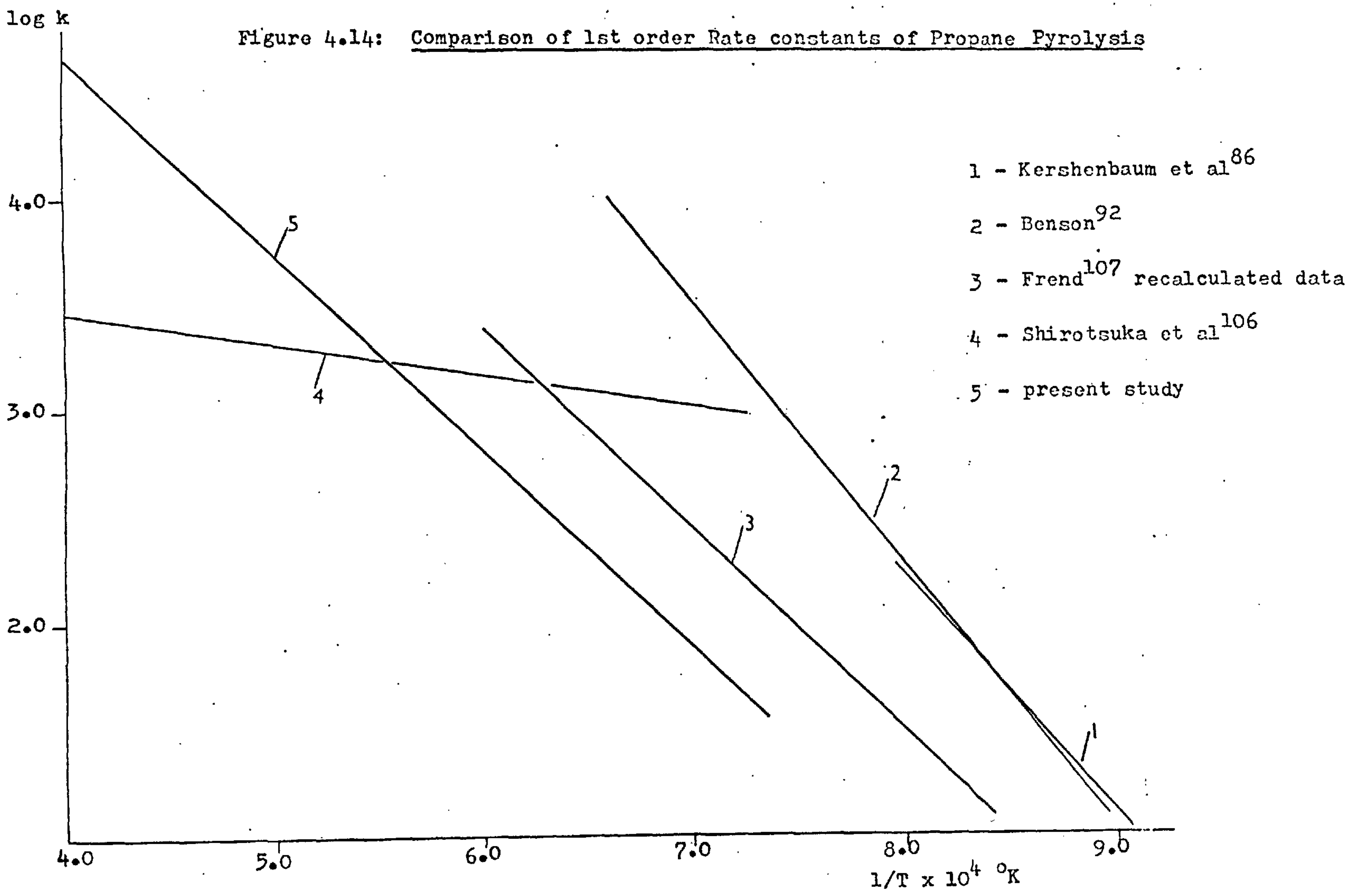

energy with increase in temperature. Figure 4.14 compares most of the published high temperature kinetic data for first order propane pyrolysis. The current result exhibits fairly good agreement with the literature data. While it is true that the other studies (see table 4.7) have indicated higher activation energies, usually between 200 - 296 KJ/mole, the discrepancies can be explained by the differences in temperature and the conversion levels of propane. Of all the literature values used in assessing these parameters, that of Frend[107] is the most relevant on the grounds that he had used similar (shock tube) technique and the temperature range covered by the present investigation overlapped the temperature region studied by Frend. An value for the activation energy (180.3 KJ/ mole obtained from his data assuming a first order kinetics is very close to E_a= 176.2 KJ/mole of the current investigation. However, the current work was conducted at a much higher conversions (>95% maximum) as opposed to a maximum of ~60% employed by Frend. The latter worked at rather lower total pressure ~ 80 KN/m^2.

The only reported investigation of propane pyrolysis at temperatures exceeding those of the present investigation using a chemical shock tube is that due to Shirotsuka et al[106]. Their study covered a wider temperature range (1000° - 5000°K), but had employed similar experimental conditions of high total reaction zone pressure of ~10^3 KN/m^2, and very high propane conversions. Their first-order kinetic data at the reaction temperature between 1310°K and 5000°K had very low values for both the frequency factor ($A = 10^4$) and the activation energy (E = 27.5KJ/ mole). In orderwards there was a rapid drop in the reaction

Table 4.7: Literature values for constants rate of propane decomposition

Author	Method	Temp. range, ^{o}K	1st order rate constant, K (sec. $^{-1}$)	Reference
Laidler et al (1962)	static reactor	800-880	2.58×10^{14} exp (- 67100/RT)	79
Marek et al (1931)	static reactor	870-970	2.55×10^{13} exp (- 62100/RT)	97
Paul et al (1934)	"	830-920	4.0×10^{16} exp (- 74900/RT)	172
Steacie and Puddington (1938)	"	820-930	2.88×10^{13} exp (- 61000/RT)	96
Besthy (1978)	flow reactor	920-1020	4.8×10^{10} exp (- 48600/RT)	105
Kershenbaum et al (1967	non-isothermal flow reactor	1070-1270	2.4×10^{11} exp (- 52100/RT)	86
Benson, A.M. (1967)	shock tube	1100-1450	2.72×10^{12} exp (- 56000/RT)	92
Shirotsuka et al (1969)	shock tube	1000-1310	1.1×10^{13} exp (- 61000/RT)	106
Shirotsuka et al (1969)	"	1310-5000	1.0×10^{4} exp (- 6550/RT)	106

rate in this temperature range. However, comparison between the current results and those obtained by Shirotsuka et al[106] would be incorrect because of the enormous temperature difference; and moreover the reliability of such results obtained at extreme high temperatures around 5000°K is very questionable. At 5000°K processes like ionization are likely to become increasingly important and this would undoubtedly affect their result.

However, in discussing the discrepance in the values of the rate constants reported in literature, it is important that one should note that most of these research were conducted on different systems, and at different extents of reaction and temperatures. In the instances of high temperatures and high conversions, secondary reactions could be a major determining factor. The discrepancies in the values of the activation energy and the pre-exponential factors obtained by different investigators have been attributed to various causes ranging from the involvement of heterogeneous catalytic reactions at the walls of the reactor[105] to purely mechanistic effects. However, in the circumstances of the current investigation heterogeneous reaction is insignificant on the grounds that for reactions in the shock tube the wall has no effect, the heating is instantaneous and the reaction times are very short. Therefore an explanation of such low values of activation energy is sought in the mechanism of the process.

The rate expression obtained in this work shows that both the activation energy and the frequency factor are low relative to literature values, which means that the rate of the reaction was decreasing at the temperature range from 1300 - 2300°K. Such a decrease in the rate of propane pyrolysis could be attributed to the breakdown of some intermediates by reaction which does not help the main reaction. Propylene which is usually a major product of propane pyrolysis at moderate temperature, is a known[79, 86, 87] inhibitor and its characteristics are responsible for the decrease in the reaction rate at high temperatures.

4.3: Mechanism

Pyrolysis of propane is known to be initiated by the rupture of C - C bond to generate methyl and ethyl radicals.

$$C_3H_8 \longrightarrow CH_3^{\bullet} + C_2H_5^{\bullet} \qquad (5.1)$$

At temperatures around 800°K and lower, the level of the concentration of these radicals is extremely low because $K_{5.1}$ is very small due to very high activation energy (E_a = 353.2 KJ/mole)[94] of this step. As such there will be little tendency for these radicals to recombine. Also the unimolecular dissociation reaction,

$$C_2H_5^{\bullet} \longrightarrow C_2H_4 + H^{\bullet} \qquad (5.7)$$

is slow ($A = 10^{14}$, E_a = 167.2 KJ/mole)[94, 104]. Hence the only channels for the removal of these radicals at low temperature regimes will be their attack on propane to yield propyl radicals, methane and ethane.

$$CH_3^{\bullet} + C_3H_8 \longrightarrow CH_4 + C_3H_7 \ (i,n) \qquad (5.2)$$

$$C_2H_5^{\bullet} + C_3H_8 \longrightarrow C_2H_6 + C_3H_7 \text{ (i,n)} \quad (5.3)$$

Also at low temperatures, the formation of propylene and ethylene are essentially obtained from unimolecular dissociation of the propyl radicals,

$$n - C_3H_7^{\bullet} \longrightarrow CH_3^{\bullet} + C_2H_4 \quad (5.8)$$

$$i - C_3H_7^{\bullet} \longrightarrow H^{\bullet} + C_3H_6 \quad (5.9)$$

while hydrogen is formed from by abstraction reaction,

$$H^{\bullet} + C_3H_8 \longrightarrow H_2 + \text{(i,n)}\ C_3H_7^{\bullet} \quad (5.10)$$

These reactions (5.1 to 5.4; and 5.8 - 5.10) have been shown[79,82] to be adquate in explaining the details of the product distribution at low temperatures by the fact that $[H_2] = [C_3H_6]$ and $[CH_4] = [C_2H_4]$. However the change in the product distribution pattern in the high temperature regime employed in the current study does indicate that other reactions become important at elevated temperatures.

Although reaction (5.1) is still thermodynamically favoured at high temperatures, an alternative initial step[91],

$$C_3H_8 \longrightarrow C_3H_7^{\bullet} + H^{\bullet} \quad (5.1b)$$

may become important at elevated temperatures and hence a number of variations in the consecutive reactions will follow the initiation. At these temperatures, the initiation rates become very much faster and therefore the initial levels of the concentration of radicals are much higher than at low temperatures; also the rate of unimolecular dissociation of ethyl radical proceeds faster than combination reaction (5.3) Both radical recombination and dissociation will readily occur at higher temperatures,

$$C_2H_5^{\bullet} \longrightarrow C_2H_4 \quad + \quad H^{\bullet} \qquad (5.7)$$

$$CH_3^{\bullet} + CH_3^{\bullet} \longrightarrow C_2H_6 \qquad (5.11)$$

Reactions (5.7) and (5.11) will therefore be competing with (5.3) and (5.2) for $C_2H_5^{\bullet}$ and $CH_3^{\bullet}$ radicals. Reactions (5.3), (5.11), and (5.9) are the main sources of ethane and propylene formation. But since these products are present only in small quantities at temperatures under 1500°K, and are negligible or totally absent at higher temperatures, it seems to suggest that either reaction (5.7) is considerably faster than (5.3) or that these products (C_2H_6 and C_3H_6) are subjected to immediate secondary reactions by the attack of the abundant free radicals and hydrogen atoms.

The importance of secondary reactions at high temperature regimes and high conversions of propane is emphasized by the rapid increase in the yield of the acetylene - a 'secondary' reaction product, which had been hitherto absent, or present only in trace amount at lower temperatures. Table (4.8) shows changes in the product distribution at temperatures upto 1900°K. It is evident from this table that of all the 'primary' products of propane decomposition at moderate temperatures ($1200 < T < 1500$°K); propylene is the most vulnerable to prolonged reaction time. Above 1500°K, propylene was not detected in the reaction mixture. The steep fall in the yield of propylene corresponded to a very rapid increase in the yield of acetylene. Between 1300°K and 1400°K, the yield of propylene dropped by as much as 72%, followed by that of ethane with 60% drop, while on

Changes in product formation with reaction temperature

Table 4.8

Reflected shock Temp. °K	% conversion of Propane	Reaction time, ms	Mole % of Propane converted into:					
			CH_4	C_2H_4	C_2H_2	C_2H_6	C_3H_6	C *
1300	13.0	0.2	16.8	53.3	3.2	5.06	16.0	5.69
1400	34.9	0.2	18.2	52.0	8.2	3.8	8.0	6.35
1500	43.9	0.2	19.7	50.0	15.8	2.00	4.45	9.17
1500	46.6	0.7	20.3	44.7	21.0	1.96	0.0	10.39
1740	51.6	3.5	20.6	35.3	28.6	0.0	0.0	15.49
1800	52.50	0.7	18.4	29.0	39.4	0.0	0.0	12.74
1923	73.7	0.6	16.2	11.8	52.6	0.0	0.0	19.6

* gm - atom

the other hand the yield of acetylene rose by about 400%. At this same temperature range the yield of methane increase by 17% while that of ethylene slightly decrease by ~6.0%. The rapid decrease in the yields of both propylene and ethane at this temperature interval is a strong indication that these products (C_3H_6 and C_2H_6) are themselves undergoing rapid decomposition reactions. The primary mode of propylene decomposition could be[163],

$$C_3H_6 \longrightarrow C_2H_3^{\bullet} + CH_3^{\bullet} \qquad (5.12)$$

which may be followed by reactions

$$C_2H_3^{\bullet} \longrightarrow C_2H_2 + H^{\bullet} \qquad (5.13)$$

$$C_2H_3^{\bullet} + C_3H_6 \longrightarrow C_2H_4 + C_3H_5^{\bullet} \qquad (5.14)$$

Also ethane decomposes[26,27,107] to methyl radicals,

$$C_2H_6 \longrightarrow CH_3^{\bullet} + CH_3^{\bullet} \qquad (5.15)$$

and followed by

$$CH_3^{\bullet} + C_2H_6 \longrightarrow C_2H_5^{\bullet} + CH_4 \qquad (5.4)$$

$$C_2H_5^{\bullet} \longrightarrow C_2H_4 + H^{\bullet} \qquad (5.7)$$

$$\phantom{C_2H_5^{\bullet}} \longrightarrow C_2H_3^{\bullet} + H_2 \qquad (5.16)$$

The presence of vinyl radicals, $C_2H_3^{\bullet}$ in relatively large quantities in the system is undoubted since acetylene became the most prominent hydrocarbon in the reaction mixture at high temperatures. Acetylene was formed probably via reaction (5.13) and (5.17)

$$C_2H_3^{\bullet} \longrightarrow C_2H_2 + H^{\bullet} \qquad (5.13)$$

and

$$C_2H_3^{\bullet} + C_3H_5^{\bullet} \longrightarrow C_2H_2 + C_3H_6 \qquad (5.17)$$

Another source of vinyl radical may be reactions

$$C_2H_4 + H^\bullet \rightarrow C_2H_3^\bullet + H_2 \quad (5.18)$$

$$CH_3^\bullet + C_2H_4 \rightarrow CH_4 + C_2H_3^\bullet \quad (5.19)$$

Reaction (5.18) is considered to be very important at high temperatures.

The relationship between the rapid decline in the yields of both propylene and ethane and the corresponding rapid rise in the yield of acetylene, as seen in table (4.8), suggests an active involvement of propylene and to some extent ethane in the formation of acetylene at temperatures between 1200 and 1500°K. Benson [92] had made a similar observation in the relationship between propylene and acetylene at identical temperature region (1100 - 1450°K), and had concluded that at high temperatures propylene so formed from propane (at lower temperatures) is converted almost stoichiometrically to ethylene and acetylene. However, in the present investigation no enhancement of ethylene at temperatures above 1300°K (e.g. see as in table (4.8)was found, but rather a steady slow fall, whose rate of decrease increased rapidly at temperatures above 1700°K, was observed. It is rather the yield of methane that was slightly favoured by the disappearance of propylene and C_2H_6 from the product spectrum. Thus indicating that reactions (5.12) and (5.19) are more favoured than reaction (5.14).

Product distribution at temperatures above 1700°K, (fig.4.1) illustrates that the maximum yield of C_2H_2 corresponded to the minimum yields of ethylene and methane, also the formation of "carbon" was quite substantial at this temperature region. From the product distribution pattern, it could therefore be suggested that ethylene and methane also undergo secondary decomposition reactions, which contribute substantially to the overall yield of acetylene and 'carbon' at the temperatures between 1700 - 2700°K. Other investigators[165, 166] using high temperature a argon plasma jet had inferred from the products of propane processing that ethylene is the major precursor to acetylene formation, thus stressing the significance of reaction (5.18). However it may be added that at temperatures above 2000°K these hydrocarbons (CH_4 and C_2H_4) are being converted in a similar fashion to acetylene and 'carbon', and that reactions ($C_2H_4 \rightarrow 2C + 2H_2$, and $CH_4 \rightarrow C + 2H_2$) are definitely taking place probably through some intermediates like acetylene.

Since the formation of methane and ethylene is not favoured at extremely high temperatures, and C_3H_4, even when present[86, 107] is liable to be in a very small amount, reaction (5.14) and other reactions leading to the formation of C_3H_4, for example,

$$CH_3^{\bullet} + C_3H_6 \rightarrow CH_4 + C_3H_5^{\bullet}$$

and

$$C_3H_5^{\bullet} \longrightarrow C_3H_4 + H^{\bullet}$$

are considered to be af little importance. In which case only reaction (5.16) is left as the effective source[107] of vinyl radicals since in principle reaction (5.18) will be equivalent to a one-step mechanism of reactions (5.7) and (5.16).

Chain termination steps at high temperatures, such as encountered in this investigation, may become very complex and are open to some question. Conventionally, biradical termination

$$R\bullet + R_1^{\bullet} \longrightarrow R - R,$$

is considered the major termination reactions and depending on the type of radicals (μ or β) involved in the reaction of the overall order of the reaction will vary between unity and two. And for a complex system such as the pyrolysis of propane at high temperatures in which the chain reaction could be carried by as many as five radicals - $H^\bullet$, $CH_3^\bullet$, $C_2H_5^\bullet$, i and n- $C_3H_7^\bullet$, there are at least 15 possible radical recombination reactions which in principle could lead in termination.

However, at the temperatures of this investigation most of these reactions are easily eliminated either on the grounds that the concentration levels of some of the radicals participating in such reactions are very low or that their recombination steps are too slow to compete with the other channels of disappearance. For instance, a computational analysis carried out by Lifshitz and Frenklach[104] for experimental results obtained[27] at $P_1 = 26.6$ KN/m^2 and at reflected shock temperatures around 1250°K (which is analogous to the conditions at the lower end of the temperatures employed in this work), showed that the steady state concentrations of the radicals decreased in the following order;

$$CH_3^\bullet,\quad H^\bullet,\quad C_2H_5^\bullet,\quad iC_3H_7^\bullet \text{ and } nC_3H_7^\bullet.$$

In quantitative terms, their computation showed that the concentration of the methyl radical was approximately greater than those for $H^\bullet$, $C_2H_5^\bullet$, i - and n- $C_3H_7^\bullet$ radicals by factors of 15, 10^2, $7.5\text{x}10^2$ and $5\text{x}10^3$ respectively. Such a wide disparity in the concentration levels of the radicals suggests that the only meaningful reaction capable of being an effective termination step must be between radicals that are in highest concentrations. Hence at high temperatures the system is predominated by β-radicals ($CH_3^\bullet$ and H°), recombination reactions involving $CH_3^\bullet$ and $H^\bullet$ will be the most likely termination step.

Indeed the rate of recombination of two methyl radicals,

$$2CH_3 \longrightarrow C_2H_6 \qquad (5.19)$$

is $2.4x10^{13}$ cc mol/s,[104] whereas that for

$$2C_2H_5 \longrightarrow C_4H_{10} \qquad (5.20)$$

is $3x10^{11}$ cc mol/s[164] - showing that reaction (5.19) is about 100 times faster than (5.20).

Reaction,

$$CH_3^\bullet + H^\bullet \longrightarrow CH_4 \qquad (5.21)$$

has $K = 2.4x10^{12}$ cc mol sec^{-1} which is only 10 times slower than reaction (5.19). In the present system, figure (5.2) ethane production is very low and is totally absent at $T > 1500^\circ K$, inferring that recombination reaction (5.21) is more likely to be the termination step in preference to (5.19). And moreover reaction (5.21) is likely to be in a third order region under the present experimental conditions, hence a ββM termination will result in an overall first order reaction. It would therefore appear that from the experimentally obtained first order kinetics, reaction (5.21) is quite a feasible as a termination step.

PART B

INFRARED SPECTROSCOPY OF SHOCK HEATED ACETYLENE.

CHAPTER 5

APPARATUS AND EXPERIMENTAL METHOD

5.0. Apparatus

The apparatus consisted of the single mode shock tube and its evacuating system, instruments for measuring the incident shock velocity and the reflected shock pressure, and the scanning system for monitoring the infrared emission from the shock heated acetylene.

5.1. The Shock Tube

A schematic diagram of the shock tube and the associated instruments used in the spectroscopic study is shown in figure 5.1. This shock tube is dimensionally the same as that described in section 3.0, except that it has been converted to operate as a simple mode shock tube. This was accomplished by removing the dump tank (as shown in figure 3.1) from the position of the location of the second diaphragm D2, and the tube was blanked off.

5.2.0. Instrumentation

Measurements of both the shock velocity and the reflected shock pressure were made using the same equipment as those described previously in sections 3.3.1 and 3.3.2. Only those additional instruments not outlined in chapter 3 are described below.

5.2.1. The Infrared System

5.2.1.1. The Optical Window

The infrared window was made from Irtan-2, this is the Eastman-Kodak trade name for hot pressed polycrystalline zinc sulphide. The material was shaped to form and mounted as was described in reference[140]. The mounted window was fitted into the wall of the shock tube at the window location close to the

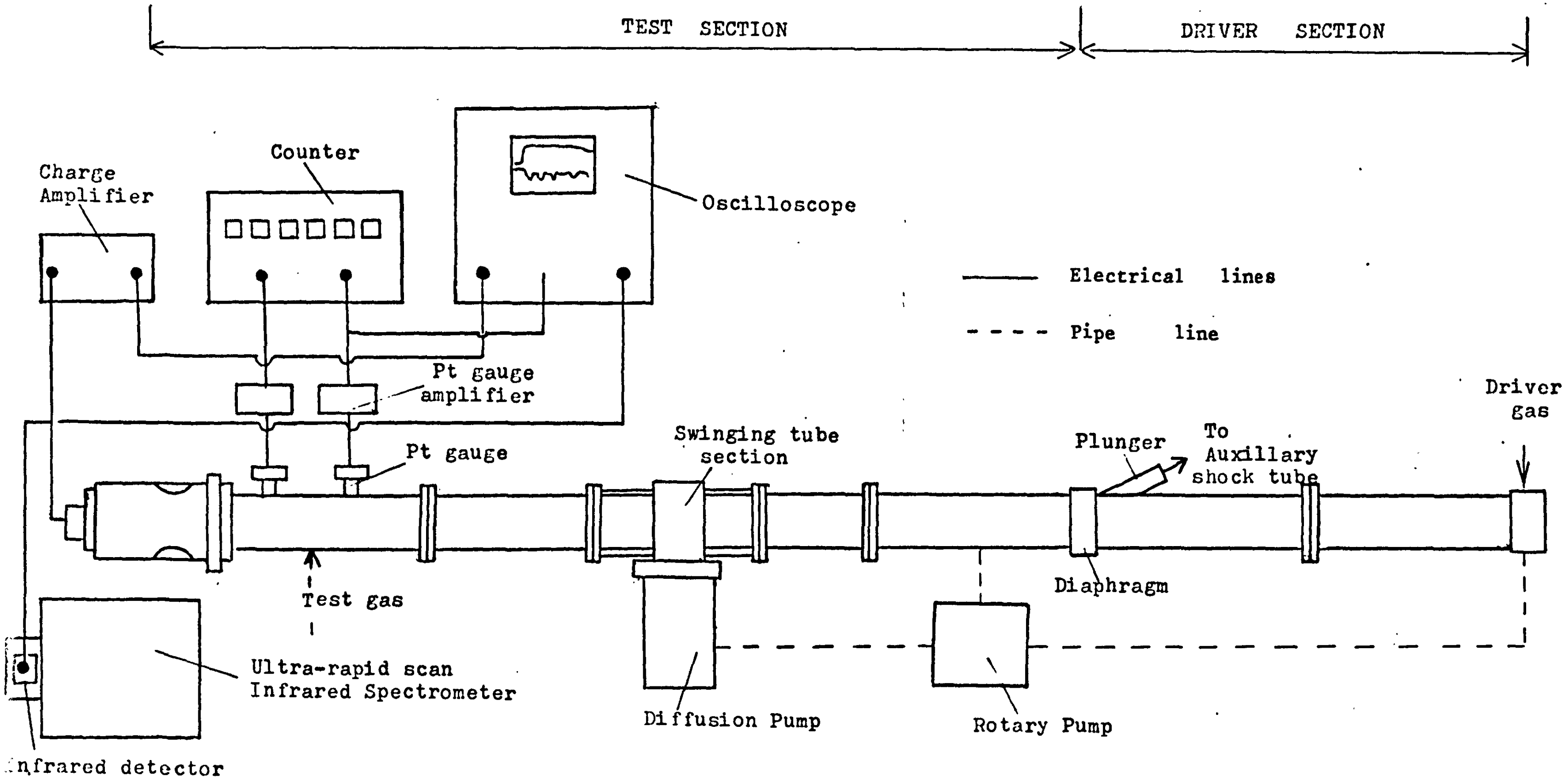

FIGURE 5.1: SCHEMATIC DIAGRAM OF THE SIMPLE MODE SHOCK TUBE.

end cap. When in position the optical window was flush with the inner walls of the shock tube. Vacuum sealing between the shock tube and the window mount was made using O-ring. Figure 5·2 shows the location of the optical window in the shock tube.

5.2.1.2. The Ultra-rapid Scan Spectrometer

The design of this instrument was based on the idea of Bethke.[51] Essentially this is the adaptation of a simple monochromator into an ultra-rapid scanning device by replacing the entrance slit of the monochromator with moving slits. A schematic diagram of the ultra-rapid scan infrared spectrometer is shown in figure 5.2. The ultra-rapid scanning system consists of the following components:-

(i) Monochromator

This was a Grubb-Parson single-pass type instrument equipped with reflecting mirrors (M3 to M5) and a calcium fluoride prism which transmits over 85% of infrared radiation in the wavelength range from 2µm to 6µm[143]. The wavelength setting of the monochromator was altered by changing the angle between the mirror (M3) and the prism by means of a mechanism for driving the wavelength drum (D_1).

(ii) Scanning Wheel

This was a rotating disc 29.2cm in diameter made from an aluminium alloy. The disc had 120 equally spaced radial slits of 10x1.0mm machined close to its edge. The disc was driven at speed up to 5000 rpm by a 1.5 horse power synchronous a.c. electric motor. The scan wheel was mounted such that at its lowest point the position of the radial slits was almost flush with the limiting slit (S1) of the monochromator. As the wheel was rotated the radial slits moved across S1 in turns thus permitting only one scan wheel slit at a time to come into view.

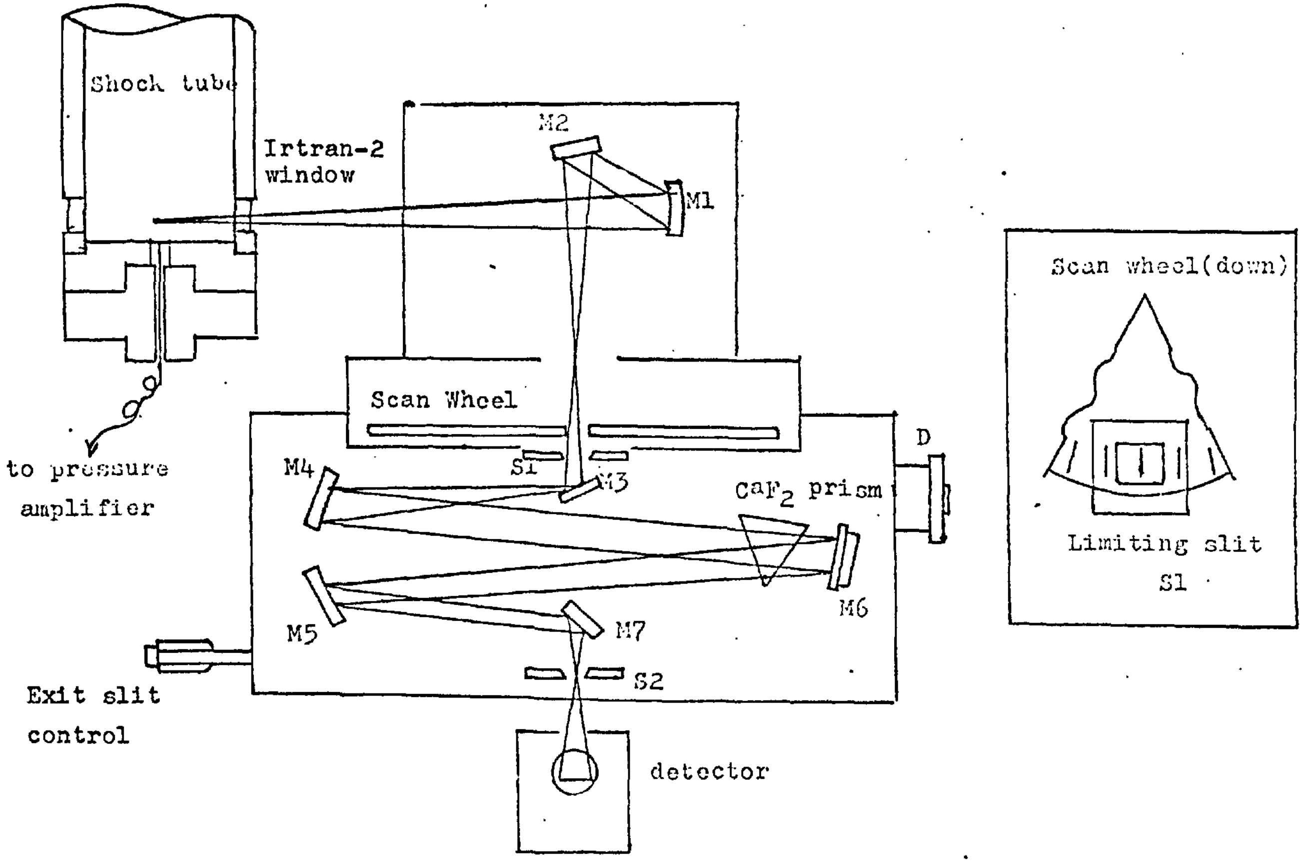

Figure 5.2: Layout of the ultra-rapid scan infrared spectrometer

(iii) The reflecting Mirrors - M1 and M 2

M1 was a concave mirror which focussed the infrared radiation from the shock heated gas onto the position of S1 via the reflecting mirror M2. Both mirrors were surface aluminised glasses which absorbed less than 5% of the infrared radiation in the range 2 to 8μm.

5.2.1.3 Infrared Detector

A fast response indium antimonide photoconductive detector (Mullard type ORP 13)[150] was used. The photoconductive element was 6.0x 0.5 mm. in dimension and was mounted on a glass dewar vessel. The detector was cooled with liquid nitrogen. The detector is sensitive to radiation from visible up to 5.6 μm. in the infrared and has maximum response at 5.3 μm. At the operating conditions of 77°K it has a fast response time constant of less than 5 μs. The response characteristics of the Indium antimonide has been given in reference 150.

5.2.1.4 Infrared Filters

Several narrow band pass infrared filters whose transmission characteristics are shown in figure A5.0 in the appendix were kindly loaned from the Astronomical Department of the College. These filters were originally supplied by the Optical Coating Laboratory, Inc; Santa Rosa, California.

5.2.1.5 Infrared Source

The monochromator was initially calibrated using the infrared emission provided by a Perkin Elmer black body radiator (model Ser. 149, Pat. 521 - 0400) with a temperature controller unit (model 521 - 5). The source was also equipped with beam chopper.

5.2.2 Oscilloscopes and Cameras

Dual beam Tektronix storage oscilloscope (type 549) and a EM 102 dual beam (SE Lab. Engineering Ltd.) oscilloscope were used. Both oscilloscopes have an in-built time delay system, suitable for delaying the single sweep of the oscilloscope after the receipt of an external triggering pulse from the trigger unit. However, in most cases the delay setting was set at zero since the oscilloscopes were triggered from a position less than 60 cm from the end plate by signal from the first platinum gauge which was also used for measuring the incident shock velocity.

The oscilloscopes were used to display the output from the pressure gauge and the infrared detector. The storage oscilloscope when used in the storage mode enabled measurements to be taken directly from the screen of the oscilloscope. However the use of the storage mode was limited mostly to the preliminary runs as it does not always meet the required very high standard of signal resolution needed in this type of investigation. The EM 102 oscilloscope, with EM 530 plug - in unit, was used for bulk of the investigation. The traces displayed on the oscilloscope were photographed using either a Shackman Polaroid PL 7A oscilloscope camera for instantaneous results or a Zenit E camera loaded with a role of Ilford HP5 film. The film was developed later in a high contrast developer (D 19) and fixed and then printed. The photographs were analysed and the results recorded.

5.3 Gas handling system

5.3.1 The Mixing Tank

The mixing tank was a cylindrical vessel of 30.0cm internal diameter, built from thick (0.5cm) pyrex glass. Figures 5.3 shows the mixing tank and its connecting system. The tank was constructed in two parts - an upper shorter (25.0cm high) section and a longer lower half (50.0cm high). The edges of both halves of the mixing tank were flanged so as to obtain an increased surface of contact between them. The edges were greased using high vacuum apezion 'M' grease and then held together.

The upper part of the tank has three glass cone and socket joints through which connections were made to the gas supply systems and a manometer. A stirrer fitted with paddles was let into the tank through a centrally located metallic cone and socket joint which was made from an aluminium alloy. The aluminium socket was joined to the glass wall with araldite. Vacuum seal at the glass joints were made using high vacuum apezion 'M' grease, while oil-seal rings were used for sealing between the rotating shaft of the stirrer and the metallic cone; this ensured free rotation of the shaft without air leaking into the tank. The shaft was driven by an electric motor which was held in position by a rigid support. The assembled mixing tank was supported on a wooden frame-work and protected with a safety wire gauze.

Mixing was carried out such that the total pressure in the tank, P_{total}, was less the atmospheric. The desired mixture strength was prepared manometrically by varying the partial pressure of acetylene in the total pressure of the mixture.

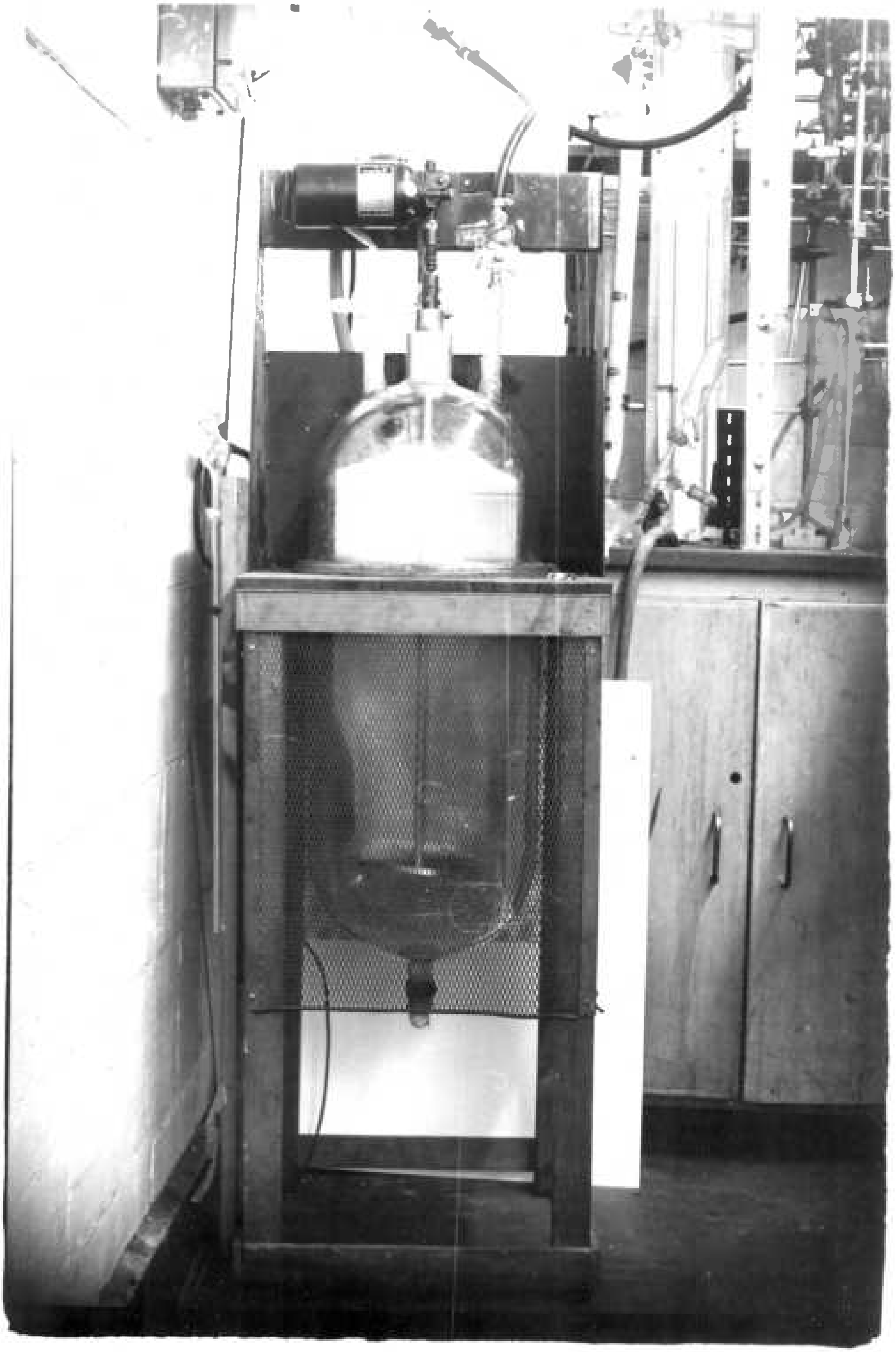

FIGURE 5.3 :THE MIXING TANK.

5.3.2 Gas purification train

Acetylene which is available commercially in cylinders is stored under pressurein acetone and therefore acetone is the main impurity. Other impurities, such as[68,69] air (1.0%), CO_2 (0.01%), sulphur compounds (0.0001% as H_2S), phosphorus compounds (0.0001% PH_3) and moisture (0.1%) may also be present. The elimination of these impurities from acetylene was achieved by passing the gas through a purification train shown in figure 5.4. This consists of the following:-

i) Two U - tubes immersed in a cold trap (CT1, CT2) of dry-ice in methyl-chloride bath (at 198°K) to freeze off the bulk of the acetone contained in the gas released from the cylinder.

ii) two dreschel bottles (B1, B2) containing concentrated (70%) suphuric acid to remove ~~any acetone not~~ PH_3 and other hydride impurities (AsH_3, H_2S etc) from the acetone free gas from (i) ~~removed in (i)~~;

iii) one dreschel bottle (B3) containing aqueous 15% potasium hydroxide solution to remove CO_2 and acidic impurities; and ~~bottle~~ bubbler (B4) containing potassuim permanagate solution to remove oxygen impurities; oxidise further any impurities - especially non-metallic hydrides - not removed in (ii)

iv) two drying columns 46 cm. high by 3.0 cm. internal diameter (D1, D2) containing anhydrous phosphorous pentoxide.

v) three 5 litre pyrex flask (S1, S2, S3) for storing the purified acetylene gas;

vi) one detatchable sample bottle (SB) used for withdrawing samples for analysis;

vii) one mercury manometer (M), and a flow meter F;

viii) a rotary pump for evacuating the system.

FIGURE 5.4: PURIFICATION TRAIN FOR ACETYLENE.

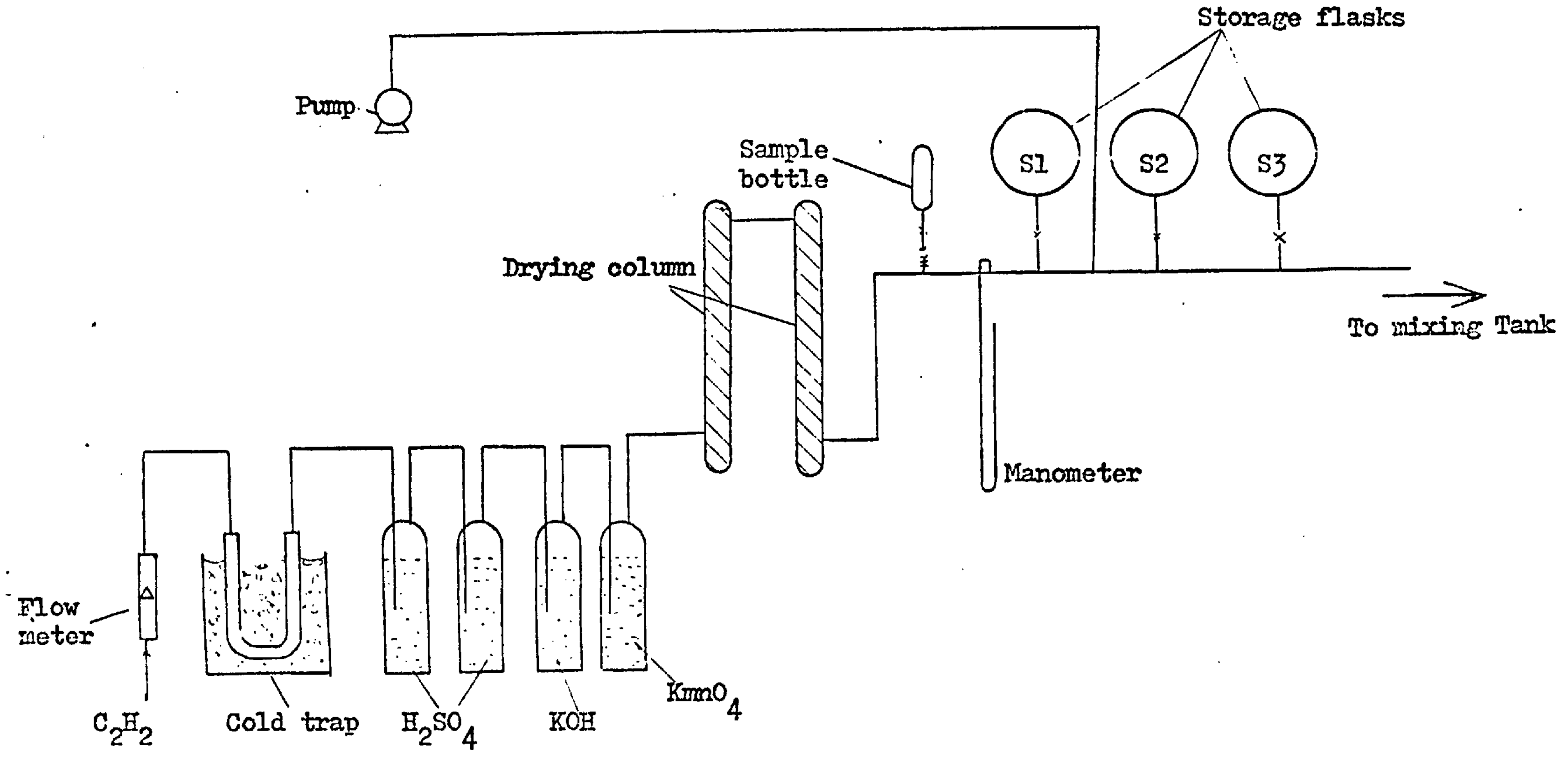

The entire purification rig was constructed with pyrex glass and connections to the gas cylinders and the shock tube were made using glass/metal flexible joints.

The purification process was carried out as follows; the purification train was first evacuated and the storage flasks (S1 - S3) were flushed for about 3 minutes with 'oxygen-free' nitrogen to exclude air, and then evacuated again. The storage flasks and the sample bottle were isolated by closing the taps. The gas supply of acetylene from the cylinder was then passed through the purification train. The purified gas was stored in the storage flasks.

The extent of purification achieved was tested by drawing off samples with the detatchable sample bottle and analysed using a Perkin-Elmer double beam infrared spectrophotometer Model 700. Spectra of samples before and after purification were compared; the conspicious absence of the very strong C=O band of acetone at 5.8μm and its strong CH_3 deforming frequency at 8.32μm in the purified sample indicated the elimination of acetone. Figures 5.5 show the infrared spectra of samples drawn directly from the cylinder and of that after purification. The spectrum of the purified acetylene was counter checked with that obtained from standard calibration mixture of 1% C_2H_2 in N_2. This mixture was kindly supplied by EDT Supplies Ltd. A quantitative assessement of the degree of purification achieved was obtained by using gas chromatographic analysis. The acetylene was shown to have a purity of above 99.98%.

Figure 5.5a : Infrared Spectrum of unpurified Acetylene obtained directly from obtained directly from the commercial cylinder.

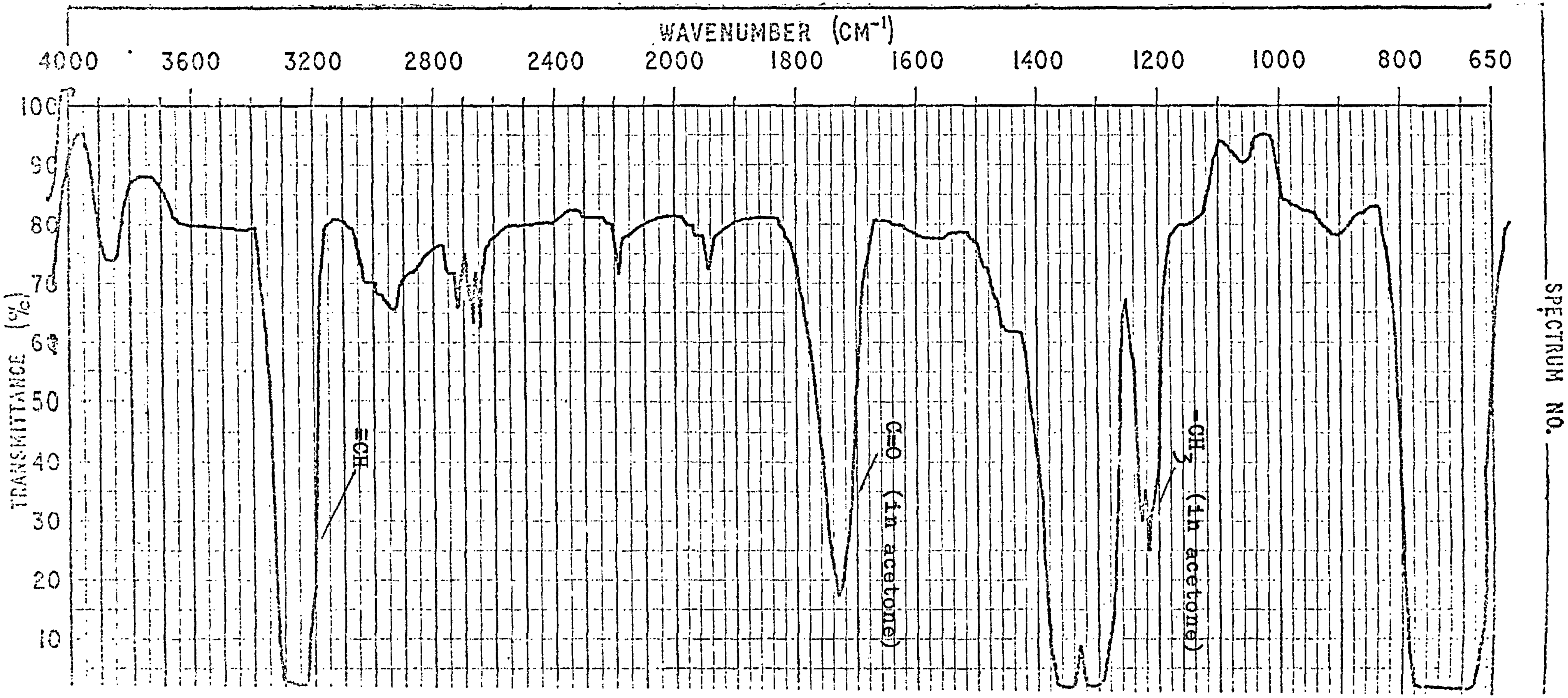

Figure 5.5b : Infrared Spectrum of Acetylene after purification.

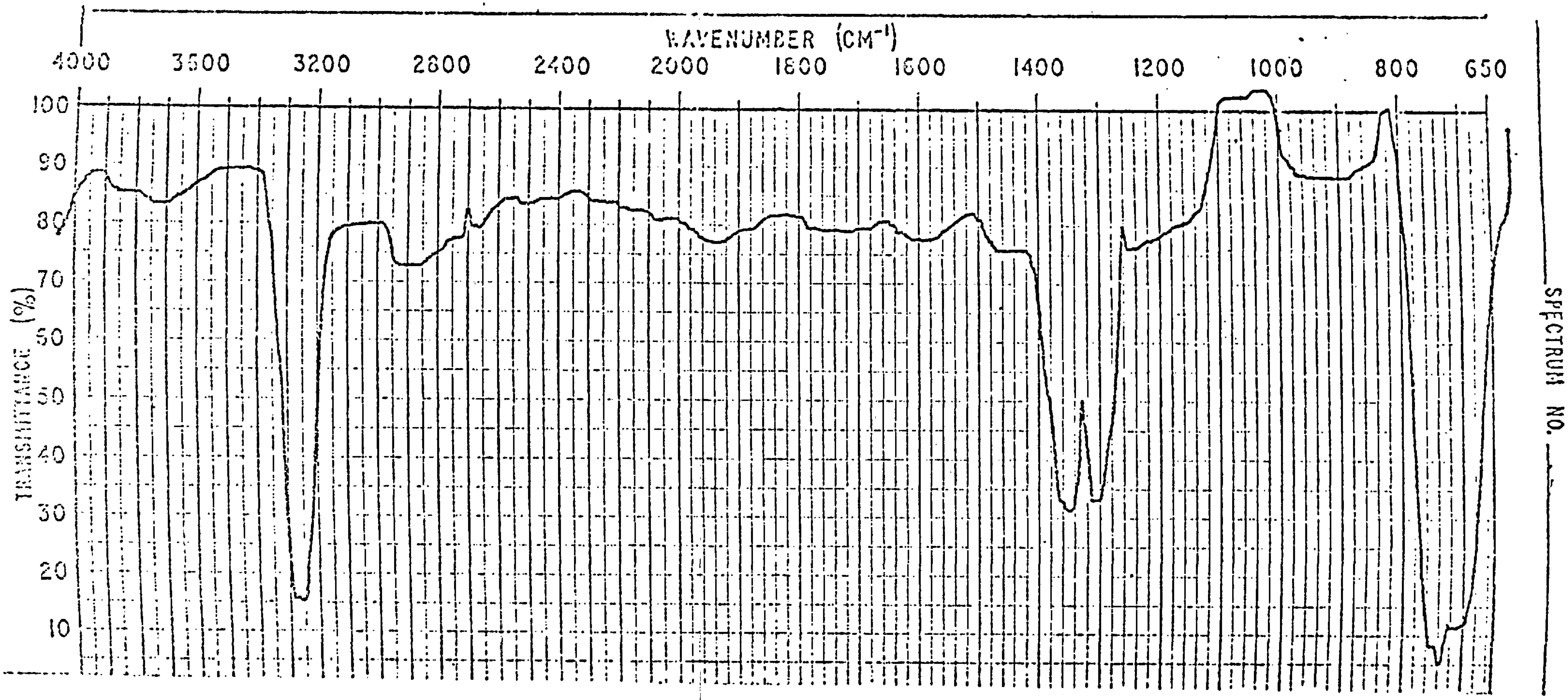

5.4: Diaphragm material

The plastic film - Melinex - available in various nominal gauges (supplied by Imperial Chemicals Industry, Plastic Division) was used for the diaphragm. Mostly two types of melinex - gauge 500 (type'S') and gauge 700 (type'O') of thickness 0.130mm and 0.180mm respectively were used. These had natural bursting pressures of ~ 620 KN/m^2 and 827 KN/m^2 respectively.

Melinex has a special advantage over other types of diaphragms (in particular metallic sheets) in that when over pressurized, it tears thus giving 'neat' bursting and the diaphragm fragments do not usually travel down the driven section of the shock tube. If the driver pressure, is close to or equals its natural bursting pressure tearing is very rapid and the diaphragm rupture occurs in a manner analogous to the bursting of a balloon by over pressurization. Reproducible shocks can be obtained using Melinex as long as the diaphragm is first pressurized to within~80% its natural bursting pressure on the driver side and then mechanically ruptured by a sharp plunger. Unfortunately, however, small fluctuations in the strength of any given gauge of melinex were reflected in small variations in the natural bursting pressures. Nevertheless, shocks exhibiting attentuation or acceleration due to poor diaphragm rupture were easily recognizable both from the reflected pressure trace and inconsistency in the value of the measured transit time between the positions of the platinum gauges.

5.5. Setting up the infrared spectrometer

5.5.1 Preliminary calibration of the monochromator

The calibration of the single pass monochromator was undertaken by using narrow band infrared filters. For such calibration it was essential that a narrow pencil of radiation was used and both the entrance and exit slits were set at minimum width value of 0.1mm inorder to ensure very high resolution. A blackbody radiator (Perkin Elmer, Model Ser. 149, Pat. 521 - 400) operating at 2000°K was used as an infrared source. The blackbody radiator unit was equipped with both a beam chopper and a temperature controlling unit. The infrared radiation was focussed on the entrance slit of the monochromator by means of a mirror system and the radiation emerging from the monochromator was detected by the detector positioned at a suitable distance from the exit slit. The filters were mounted and secured into different slots in a specially designed filter holder -this permitted a quick and safe handling of these fragile filters. The filter holder was then interposed in between the exit slit and the detector such that the filters were parallel to and as close as possible to the window of the detector. Such mounting arrangements permitted any radiation emerging from the monochromator through the exit slit that passes through the filters to be picked up by the detector. The output of the detector was amplified and channelled into two separate measuring devices. One channel was connected to the oscilloscope which served for visual observation of the amplitude of the transmitted infrared signal; the second channel was connected to a digital voltmeter which displayed the values of the output at different settings of the wavelength drum. As the drum setting was gradually changed, the corresponding readings of the voltmeter was recorded. From such recordings, it was quite easy to detect the wavelength drum positions which corresponded to the maximum transmission (or any fraction of it) for the filter. The same procedure was repeated for each of the filters used.

The calibration points chosen for each filter were the drum settings that corresponded to maximum (100%) transmission and 50% transmission on both sides of the peak value. By using six different narrow band filters whose peak transmissions ranged from 2.2 µm to 5.0µm, it was possible to calibrate the instrument accurately throughout the entire range within the detection limits of the detector.

5.5.2: Optical alignment and calibration of the spectrometer for centre of scan wavelength.

The monochromator, scan wheel and the mirror system M1 and M2 were assembled and properly positioned. Provisional alignment of the optical system was carried by using a 100 watt lamp bulb and visually following the colours of the visible light emerging through the system at the exit slit S2. This was accomplished by removing the two (diametrically opposite) shock tube windows directly facing the optical mirror M1 and placing the lamp bulb at a position close to the location of the window furthermost from M1. In such arrangement the rays from the bulb had to transverse the shock tube via the locations of the windows before falling on M1. After the provisional alignment the lamp bulb was replaced by the infrared radiator and the infrared detector was positioned close to the exit slit S2. The exit slit was set to the same width as the scan wheel slits. The position of the detector was correctly adjusted by watching the output on the oscilloscope.

The scan wheel was then set into motion at a speed such that a reasonable number of scans could be seen on the oscilloscope for an average observation time of 3ms.. This speed was set permanently at 2500 rpm which gave 5000 scans per second. Measurements of the output of the detector as a function of both the width of the exit slit and the distance of the detector from the monochromator were made. Such measurements showed that at a fixed distance from the monochromator and at constant radiation intensity, the response of the detector was proportional to the area of the photoconductive element that was exposed to the radiation. No loss in rise time or resolution was experienced. The detector was therefore positioned at a fixed distance from the monochromator and the exit slit was set back to a minimum value (0.1mm).

The shock tube windows were replaced and the shock tube evacuated, then loaded with acetylene/argon mixture to appropriate pressure and the shocks fired. The width of the exit slit was successively increased by small increaments until an appreciable signal was displayed on the oscilloscope. This process was repeated at other wavelength settings and the detector responce examined. Once the optimum experimental condition had been established, the spectrometric system was covered to avoid the incidence on the detector of excessive ambient radiation. The exit slit was set to 0.35mm and this remained constant throughout the study. At this setting, the resolution of the spectrometer was approximately 0.01 µm[52].

In the scanning conditions, the entrance slit is no longer stationary but has been replaced by the slits in the scan wheel which moves across the limiting slit S1. As a result the conditions under which the previous calibration was carried out - i.e. using a narrow pencil of light, is no longer applicable and the spectrometer had to be recalibrated so as to determine the centre of scan wavelength at corresponding setting of wavelength drum, D1. This calibration was carried out by using narrow band infrared filters and the blackbody source. The scan wheel was set in motion at the appropriate speed; the shock tube windows were removed and the black-body radiator was placed in position as described earlier. The filters were interposed in between the exit slit and the detector one at a time and the output displayed on the double beam storage oscilloscope. The sweep rate of the oscilloscope was set so that about 3 to 5 scans were displayed when it was triggered manually. For each filter, the drum setting was gradually altered until a transmitted infrared signal was seen on the oscilloscope. Adjustment of the drum setting was continued until the peak of the transmitted radiation became central with respect to the zero intensity levels between scans. Hence by comparing traces the centre- of-scan wavelength was determined. The calibration points thus obtained were rechecked by replacing the infrared windows and firing shocks into acetylene/argon mixtures. Figure 5.7 shows the result obtained by shock heating a mixture of 2% C_2H_2 in Ar at a temperature of 2300°K using a 3.0 μm infrared filter. The upper trace is the pressure and the lower is the infrared emission transmitted through the filter. The intensity of the emission increases downwards. The zero-signal points between scans was used to measure the scan width. The scan width increases

FIGURE 5.7 : INFRARED EMISSION RECORD FROM SHOCK-HEATED MIXTURE OF 2% C_2H_2/Ar AT 2300°K USING A NARROW BAND - PASS 3.0 μm FILTER.

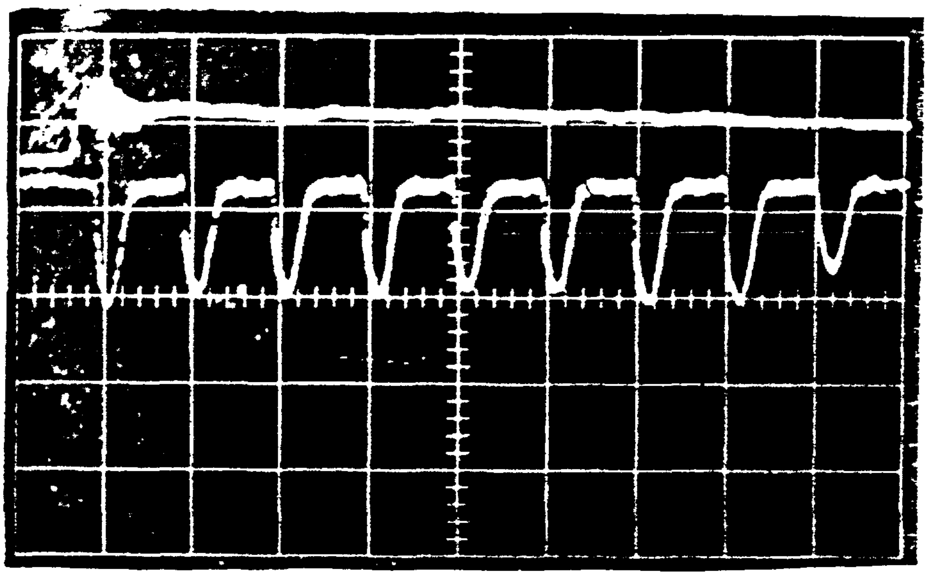

With the wavelength and a chart given the relationship between the scan width and the centre of scan wavelength was available from a previous study[52].

The calibration curve for a given centre of scan wavelength versus the wavelength drum setting is shown in figure 5.8.

5.6 Identification of spectral regions

The present investigation was undertaken relying on the fact that at the range of temperatures covered in this work the majority of the principal products of acetylene pyrolysis are known. And from the literature the fundamental vibrational frequencies for acetylene and these products are available. By carrying out investigations at these wavelength regions, it would be possible, within the resolution limitations of the instrument, to identify the structural groups that are present and to follow the time variation characteristics of their emission intensities.

The major stable products of acetylene pyrolysis at high shock temperatures[24, 34, 41] are vinylacetylene, diacetylene, higher polyacetylenes (e.g. C_6H_2 and C_8H_2), 'carbon' and hydrogen. These products with the exception of carboneous compounds and hydrogen, are acetylenic hydrocarbons. The two stretching vibrations in acetylenic molecules involve $-C \equiv C-$ and $\equiv C-H$ stretching. All $\equiv CH$ groups show a strong, sharp and characteristic C - H stretching vibration at 2.95 - 3.04µm. The $-C \equiv C-$ stretching mode is inactive in acetylene itself on symmetry grounds. For monosubstituted acetylene,[146, 147] e.g. as in vinylacetylene, it is found at 4.67-4.76µm and in disubstituted acetylenes between 4.43-4.57µm. This correlation has been found also to apply to cyclic acetylenes[148,149].

Figure 5.8: Calibration curve for infrared spectrometer.

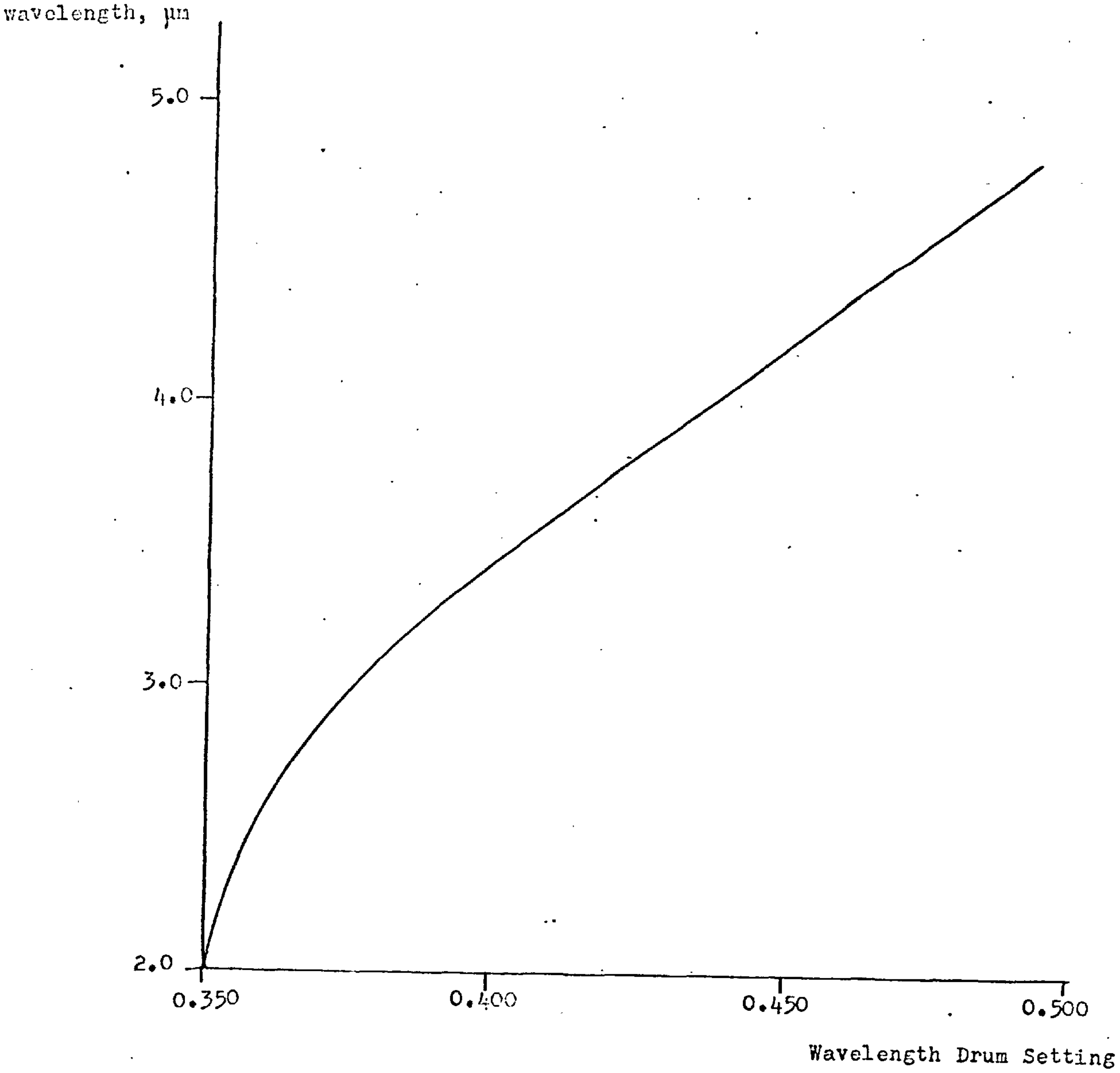

In addition for vinylacetylenes, the characteristic vibration frequencies of the vinyl group is also involved. Petrov et al[145] have assigned vibrational frequencies to the various stretching modes in vinylacetylene hydrocarbons. From these references, table 5.1 has been prepared.

Table 5.I <u>Characteristic vibrational frequencies for different structural groups</u>

Structural group	As compound	Wavelength, µm
≡ CH	C_2H_2	3.04
≡CH	C_4H_4, and other vinylacetylene hydrocarbons	3.0I2
≡ CH	C_4H_2	2.985
= CH_2	C_4H_4 and in other vinylacetylene hydrocarbons	3.22
= CH-	C_4H_4	3.30
− CH_3	CH_4, C_2H_6	3.40
- C≡ C-	C_4H_4	4.73
- C≡ C-	C_4H_2	4.94

Composite frequencies of CH_2 are also found in other spectra regions. For example[145], olefinic hydrocarbons are characterised by the presence of a fairly intensive frequency in 1800 - 1850 cm^{-1} (5.4 - 5.55 μm), and in vinylacetylene hydrocarbons at 5.29μm.

With the wavelength values assigned to each of the structural groups as a guide, shocks were fired into mixtures of acetylene in argon and the results obtained at different drum settings analysed. Figures 5.9 (a,b, and c) show typical photographic records of such experimental runs. The position of the peaks were measured from the right of the scan; and in each scan the wavelength is increasing from right to left. The length of each scan as measured from the photographic records was 1.0cm, but in certain cases, for example as can be seen in figure 5.9 (a), this value is reduced to 0.85cm due to slit 'tilting' effect which occurs as the slit was just coming into view. In figure 5.9 (a), all the scans except the first two from the left of the scope, clearly show a peak position at 0.57cm from the right of the scan; this corresponds to $\equiv$ CH structure at 2.95μm. The second scan from the left in figure 5.9 (b) also contains the $\equiv$ CH acetylene peak at 3.03μm and $=CH_2$ group at 3.22μm at 0.3cm and 0.56cm respectively. The second scan in figure 5.9 (c) contains the acetylenic -C≡C- structure at 4.84μm and $=CH_2$ peak at 5.2μm which are positioned at 0.60cm and 0.9cm respectively from the right of the scan.

Table 5.2, gives the values of the various positions of these peaks and the centre of scan wavelengths for the corresponding wavelength drum settings.

FIGURE 5.9: INFRARED EMISSION RECORDS USED FOR IDENTIFING THE PEAK POSITIONS.

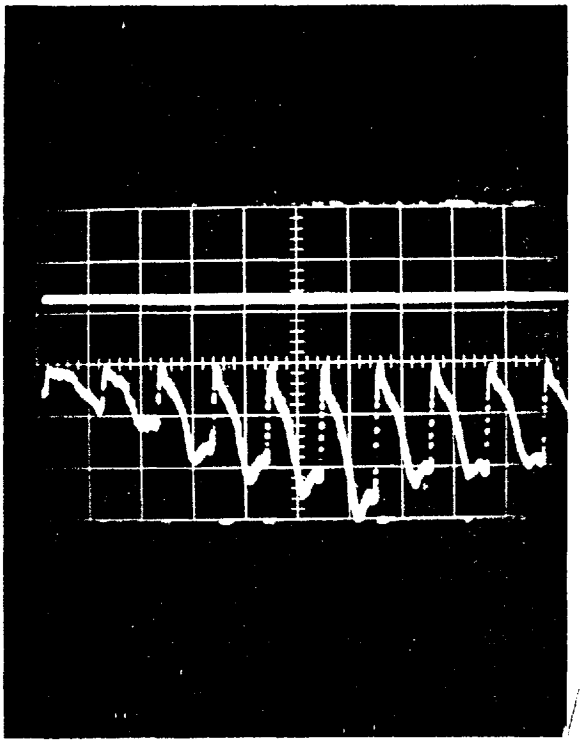

(a)

RUN NO. 350

P_1 = 3.99 KN/m^2 (5% C_2H_2/Ar)

P_{41} = 206.6

% H_2 = 95

TEMPERATURE (T_5) = 2700°K

SCOPE SETTING Y = 1.0V/cm.

X = 0.2ms/cm.

DRUM SETTING = 0.364

CENTRE OF SCAN WAVELENGTH = 2.9μm.

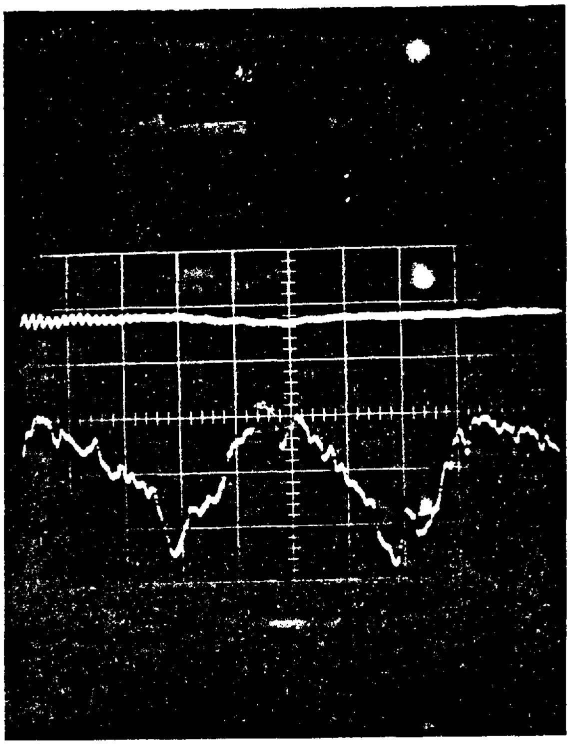

(b)

RUN NO. 371

P_1 = 15.96KN/m^2 (5% C_2H_2/Ar)

P_{41} = 60.3

% H_2 = 80.35

TEMPERATURE (T_5) = 2000°K

SCOPE SETTING Y = 0.05V/cm.

X = 50μs/cm.

DRUM SETTING = 0.375

CENTRE OF SCAN WAVELENGTH = 3.0μm

FIGURE 5.9: CONTD.

(c)

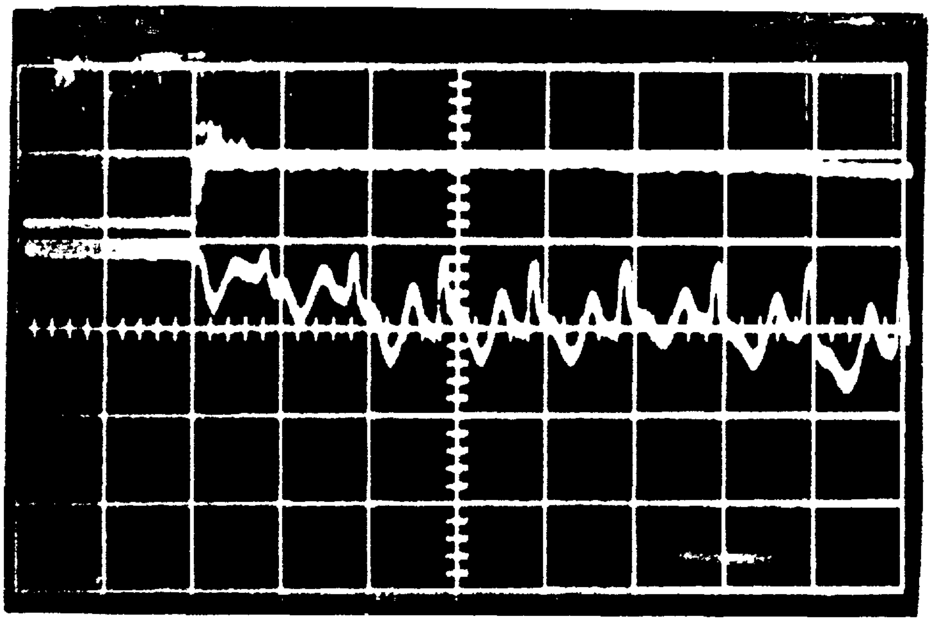

RUN NO. 410

P_1 = 12.37 KN/m^2 (5% C_2H_2/Ar)

P_{41} = 75.0;

% H_2 = 85.20 ; T_5 = 2224.°K

SCOPE SETTING: Y = 1.0 V/cm.

X = 0.2 ms/cm.

DRUM SETTING = 0.465

CENTRE OF SCAN WAVELENGTH = 4.40μm

Table 5.2: Wavelength positions on oscilloscope records for calibrating the spectrometer

Run No.	P_1 KN/m^2	P_{41}	%H_2 in driver gas	Temp. ^oK	Drum setting	Centre of scan wavelength µm	Distance form the right of the scan where peaks were sited, cm			
							≡CH 2.95-3.04	=CH_2 3.22µm	=CH- 3.30µm	-C≡C- 4.73-493µm
350	3.99	206.6	95	2700	.364	2.80	0.57	-	-	-
371	15.96	60.3	80.35	2000	.375	3.0	0.3	0.56	-	-
383	18.62	44.3	79.3	1508	.386	3.2	-	0.5	0.75	-
458	13.3	62.04	83.3	2282	.450	4.0	-	-	0.25	0.80
410	12.37	75.05	85.2	2224	.465	4.45	-	-	-	0.60

5.7 Experimental procedure

The infrared spectroscopic study of the shock heated acetylene was carried out in the following sequence;

1) The shock tube was cleaned by unscrewing the end plate of the shock tube and running a long rod carrying cotton wool and kleen wipe tissue cloths many times through the entire length of the test section.
2) The diaphragm was placed in position and the tube evacuated to the appropriate vacuum levels (to 1.33×10^{-7} KN/m^2 in the test section and to 1.33×10^{-4} KN/m^2 in the driver section).
3) The scanning wheel was set in motion at the required speed.
4) The monochromator was set to the wavelength of interest.
5) Liquid nitrogen was added to the dewar vessel of the detector and the power switched on.
6) The shock tube was loaded to the appropriate pressures with hydrogen and nitrogen in the driving section and C_2H_2/argon mixture in the driven section.
7) The oscilloscope, speed counters, and all other electronic measuring devices were made ready.
8) The shutter of the camera - Shackmanm Polariod PL7A or the Zenit E - was opened.
9) The shock was fired.
10) The camera shutter was closed.
11) Reading of the microsecond chronometer counter recorded.
12) The photographic record was processed and analysed.

Large soot-like deposits were found in the shock tube after each run; the higher the acetylene content of the mixture, the more the quantity of this substance deposited in the tube. So the shock tube had to be cleaned thoroughly after each run. This procedure was made necessary since the accumulation of such deposits would considerably cut down the infrared radiation reaching the detector through the shock tube window.

The results were rechecked for reproducibility by repeating each run twice or more times under similar initial shock tube conditions. Repetition of the runs were necessary inorder to see whether the fluctuations normally associated with the bursting of the diaphragms and the problems of turbulence in the reflected shock region due to boundary layer formation were of any significance.

CHAPTER 6

RESULTS AND DISCUSSION OF PYROLYSIS OF ACETYLENE

6.0 Results and discussion of pyrolysis of acetylene

6.1 Infrared results at wavelength interval between 2.0 to 2.7μm from shock heated acetylene

Typical infrared records obtained in this spectral region are shown in figures 6.1 (a,b, and c). The emission was preceded by an induction period during which no detectable infrared signal was observed. The length of this period, τind, varied considerably depending on the experimental conditions. Table 6.1 shows the experimental conditions and results for three mixtures of acetylene (2%, 5% and 7%) in argon. It was observed that the induction time, τind was particularly sensitive to both the initial concentration of acetylene and the reaction temperature. Shown in tables 6.2 and 6.3 are some of the results which illustrate these properties. Increase in the initial partial pressure of acetylene at approximately constant reaction temperature (see table 6.4) results in decrease of the induction time. By keeping the initial acetylene concentration at approximately constant value (table 6.3), showed that increase in temperature also led to a significant reduction in the value of τind. Above certain temperatures the induction time became very short that it was not possible to obtain an accurate measurement. The temperatures at which the induction time became negligible decreased as the reaction mixture became richer in acetylene; these values were around 1900°K, 1720°K and 1680°K for C_2H_2 partial pressures of 0.266, 0.665 and 0.931 KN/m^2 respectively.

After the induction period the infrared signal rapidly rose to a maximum and slightly fell before rising again to

FIGURE 6.1: INFRARED EMISSION RECORDS FROM SHOCK-HEATED MIXTURES OF C_2H_2 IN ARGON AT 2.0 - 2.7μm . WAVELENGTH REGION.

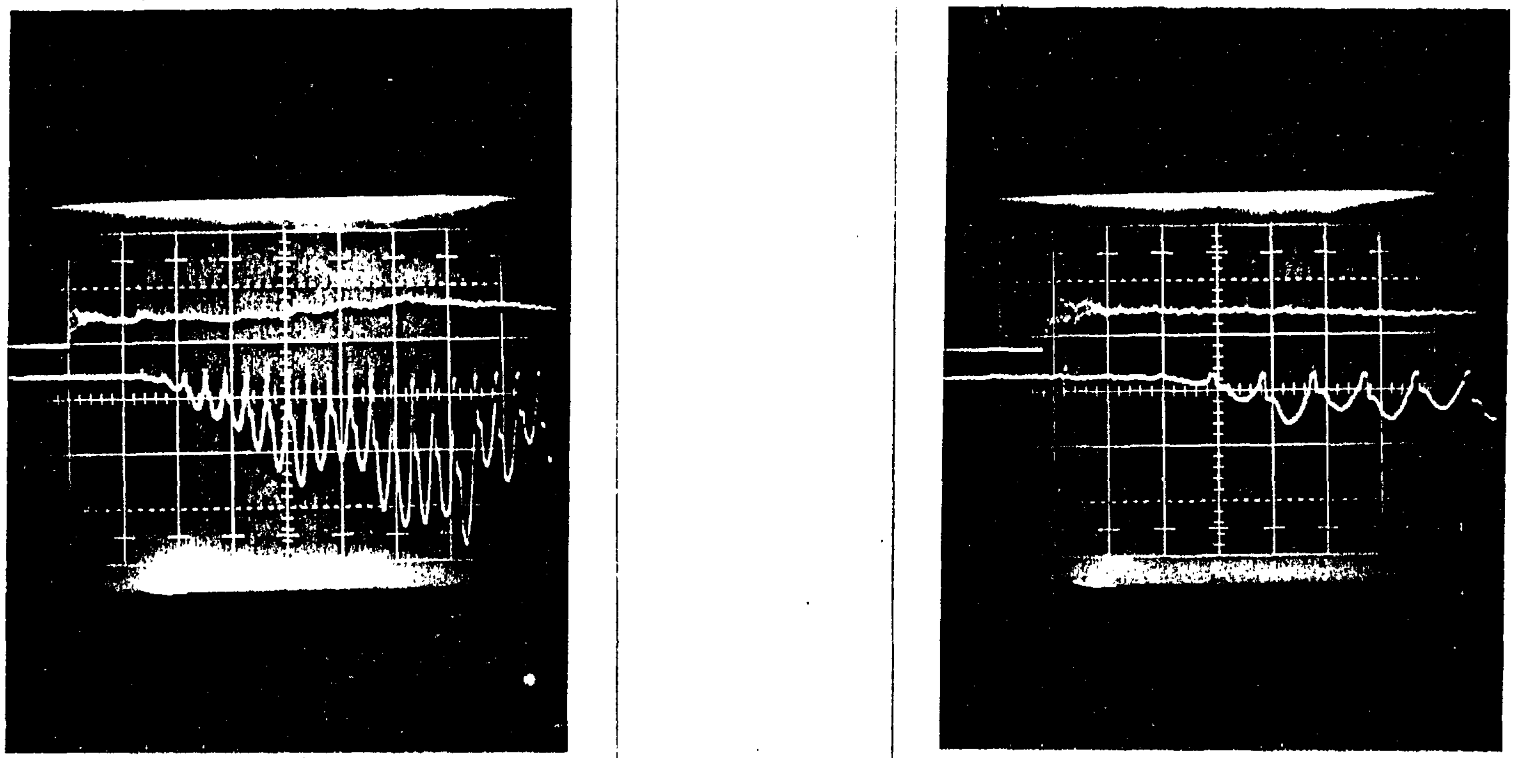

(b)

(a)

Run no. 348

Mixture - 2% C_2H_2/Ar .

Reflected Shock Temperature = 1524°K

Oscilloscope Graticule: Y = 0.5 V/cm

X = 0.5 ms/cm

Run no.349

Mixture - 2% C_2H_2/Ar.

Reflected Shock Temperature = 1676°K

Oscilloscope Graticule : Y = 0.5 V/cm

X = 0.2ms/cm.

FIGURE 6.1: CONTD.

(c)

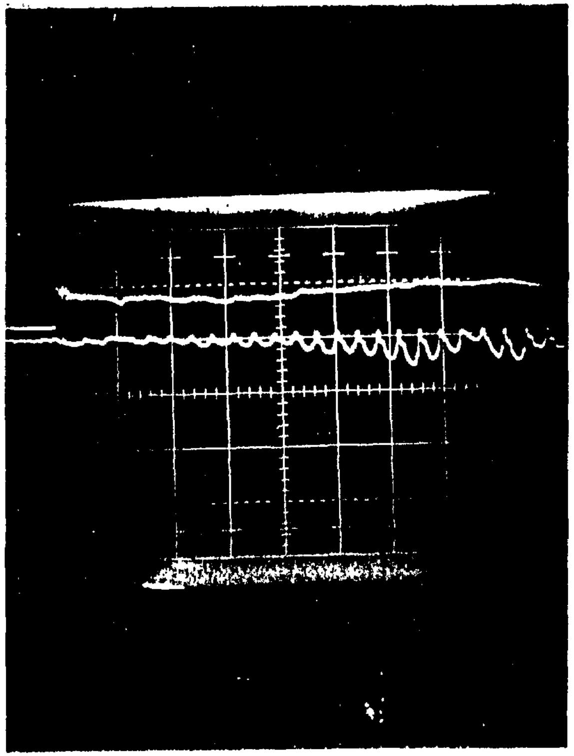

RUN NO. 344

P_1 = 10.24 KN/m^2 (2% C_2H_2/Ar)

REFLECTED SHOCK TEMPERATURE = 2103°K

OSCILLOSCOPE GRATICULE: Y = 0.5 V/cm.

X = 0.5ms/cm.

(d)

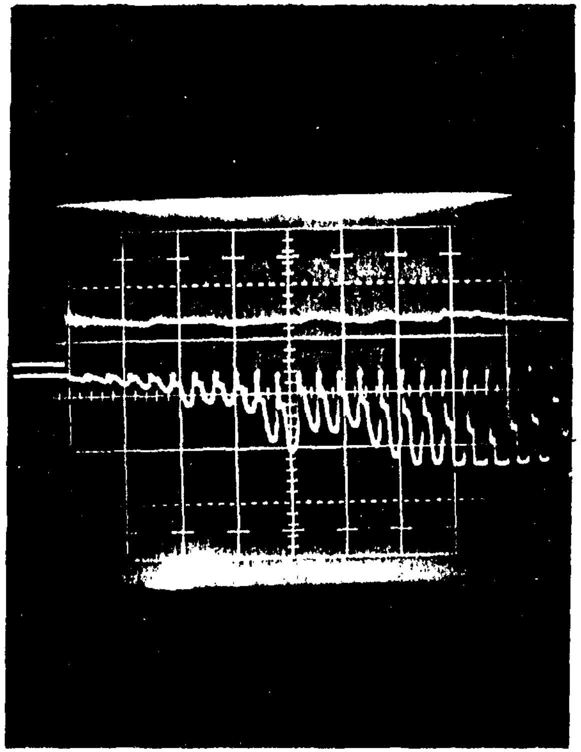

RUN NO. 350

P_1 = 10.64 KN/m^2 (5% C_2H_2/Ar)

REFLECTED SHOCK TEMPERATURE = 2028°K

OSCILLOSCOPE GRATICULE: Y = 0.5 V/cm.

X = 0.5 ms/cm.

Table 6.1: Experimental shock tube conditions for measuring the induction time, τ_{ind}

Run no.	Reaction mixture	Initial Partial pressure $P_{C_2H_2}$	P_{41}	H_2 in driver gas	shock velocity	Reflected shock temp., T_5	'scope graticule (vertical)	Induction time τ_{ind}	Density ratio ρ_{51}	$C_5 x 10^3$	$\log_{10} C_5 x \tau + 3$
		KN/m^2		%	mm/μs	^oK	V/cm	ms		moles/ litre	
301	A (5%C_2H_2/Ar)	0.732	49.35	77.14	0.776	1300	0.2	1.00	6.676	1.963	3.293
302		"	49.35	80.80	0.798	1360	0.2	0.80	6.908	2.031	3.211
303	"	"	51.70	78.18	0.804	1382	"	0.60	6.968	2.049	3.090
304	"	0.831	50.44	79.17	0.809	1395	0.1	1.00	7.010	2.342	3.369
305	"	0.765	53.95	79.58	0.819	1429	0.2	0.70	7.107	2.184	3.215
306	"	0.665	62.04	81.67	0.780	1316	0.2	0.80	6.727	1.798	3.158
309	"	"	"	81.70	0.822	1435	"	0.60	7.13	1.906	3.058
310	"	"	"	83.33	0.831	1463	"	"	7.209	1.927	3.063
311	"	"	"	85.83	"	"	"	0.40	7.209	1.927	2.887
312	"	"	"	86.70	0.856	1544	"	-	7.442	1.989	-
313	"	"	"	86.80	0.864	1567	0.2	0.50	7.507	2.006	3.00
314	"	"	"	89.20	0.921	1759	"	-	7.979	2.133	-
307	"	0.505	80.27	87.29	0.840	1491	"	0.30	7.298	1.482	2.648
308	"	0.466	88.63	88.33	0.974	1946	0.1	-	8.378	1.567	2.716
315	A	0.412	100.06	90.0	0.905	1703	"	0.40	7.853	1.301	

Table 6.1. contd.

Run no.	Reaction mixture	$P_{C_2H_2}$	P_{41}	H_2 in driver gas	shock velocity	Temp. T_5	V/cm	τ_{ind} ms	ratio ρ_{51}	$C_5 x10^3$	$\log_{10} C_{5x} + 3$
316	A	0.399	99.09	78.26	0.962	1902	0.2	0.40	8.288	1.329	2.725
317	"	0.266	103.4	92.5	0.953	1869	0.05	0.60	8.222	0.879	2.722
320	B (2%C_2H_2/Ar)	0.319	51.7	77.8	0.797	1320	0.5	1.95	6.120	0.785	3.185
343	"	0.293	56.4	80.0	0.819	1516	0.5	1.20	6.350	0.748	2.953
348	"	0.266	62.04	81.7	0.822	1524	0.5	1.0	6.364	0.680	2.833
321	"	0.327	67.3	81.3	0.842	1592	0.1	1.0	6.525	0.858	2.933
349	"	0.372	44.3	75.8	0.866	1676	0.5	0.72	6.696	1.001	2.870
322	"	0.239	68.9	75.0	0.868	1684	0.1	0.70	6.720	0.645	2.655
323	"	0.293	66.0	83.0	0.926	1896	0.1	0.70	7.115	0.838	2.768
324	"	0.154	88.6	87.2	0.956	2007	0.1	1.2	7.295	0.452	2.734
325	"	0.160	94.8	81.8	0.971	2066	0.1	1.0	7.390	0.475	2.677
326	C (7%C_2H_2/Ar)	0.931	51.7	86.5	0.817	1357	0.1	0.6	7.733	2.894	3.24
327	"	"	62.04	86.25	0.854	1465	0.1	0.6	8.111	3.035	3.26
328	"	"	64.62	84.0	0.868	1509	0.1	0.4	8.255	3.089	3.092
329	"	"	62.64	83.40	0.891	1580	0.1	0.32	8.476	3.172	3.010

Table 6.1. contd.

Run no.	Reaction mixture	$P_{C_2H_2}$	P_{41}	H_2 in driver gas	shock velocity	Temp., T_5	V/cm	τ_{ind} ms	ratio ρ_{51}	$C_5 x 10^3$	$\log_{10} C_5 x \tau + 3$
331	C	0.931	62.04	86.63	0.926	1691	0.1	0.20	8.805	3.295	2.819
333	"	"	59.4	87.4	0.974	"	"	0.2	9.205	3.295	2.838
334	"	"	58.9	87.4	0.986	1880	"	0.1	9.290	3.476	2.838

a higher maximum. At longer observations (> 3.0ms) there were irregularities in the pattern of the infrared emission (e.g. as in figure 6.1 (b)), and as such analysis of the results was confined to observation times under 2.5ms only. The distortions in the infrared signal could be due to effects of turbulence in the reflected shock region induced by the boundary layer, or a genuine chemical phenomenon reflecting the instability of the compounds emitting in this infrared region. However in all cases, the pressure trace was a useful guide in assessing the results obtained in this study. And both the pressure history behind the reflected shock wave and the pattern of the infrared emission observed at longer wavelength regions (to be discussed later) show vividly that changes in the infrared emission profile are due to chemical reactions involving unstable compounds.

Earlier investigators [24, 34, 41] high temperature pyrolysis of acetylene have detected the presence of several polyacetylenes. The results obtained by Bradley and Kistiakowsky[34], and those of Gay et al[41], using the time of flight mass spectrometer, showed that these polyacetylenes have complex structures up to C_6 and C_8 with considerably less hydrogen atoms. Bradley and Kistiakowsky and others[124] have suggested that these polyacetylenes may be intermediates in the formation of solid carbon. It is apparent from the experimental results given by these researchers[34, 41, 124] that the formation of these higher carbon content polymers (C_6, C_8 etc) was preceded by a short induction time. Unfortunately, there is relatively little known about the spectra of these higher polyacetylenes, especially in the wavelength region under 3.0µm because these compounds are very unstable. Also due to their structural

Table 6.2: The effect of initial concentration of acetylene on the length of induction time

Run no.	$P_{C_2H_2}$,	C_2H_2 in argon	P_{41}	H_2 in driver gas	shock velocity	reflected shock tempera-ture	induc-tion time, τ_{ind}
	KN/m^2	%		%	mm/µs	^oK	ms
321	0.327	2	67.25	81.25	0.842	1592	1.00
313	0.665	5	62.04	86.80	0.864	1567	0.56
329	0.931	7	64.64	83.4	0.891	1580	0.32

Table 6.3: The effect of temperature on induction time.

Run No.	$P_{C_2H_2}$	C_2H_2 in Ar.	P_{41}	H_2 in driver gas	Shock Velocity	Temperature	Density ratio, 51	Induction Time, τ_{ind}
	KN/m^2	%		%	mm/µs	^oK		ms
320	0.319	2	51.7	77.8	0.797	1320	6.120	1.95
343	0.293	"	56.4	80.0	0.819	1516	6.350	1.20
323	0.292	"	66.00	83.00	0.926	1896	7.115	0.700
306	0.665	5	62.04	81.67	0.78	1316	6.727	0.800
302	0.732	"	49.35	80.80	0.798	1360	6.908	0.800
313	0.665	"	62.04	86.80	0.864	1567	7.507	0.500
316	0.399	"	99.09	78.26	0.962	1902	8.288	0.400
326	0.931	7	51.7	86.5	0.817	1357	7.733	0.600
331	0.931	"	62.04	86.63	0.926	1691	8.805	.200

complexity overlapping in the emission bands of their different composite structural groups would be expected in this spectral region where the bands of $=CH_2$, $= CH-$, $\equiv CH$ and $- C \equiv C -$ and others lie very close to one another. Because of such overlapping of the different emission bands, and for the fact that other conjugated substances might also be present in the hot gas, the resultant emission would appear as a continuum[24]. And from the suggestion put forward by Aten and Greene[24] that the absorption (or emission) of polymerizing polyacetylenes appears as a continuum first in the ultraviolet and then in visible, it is then obvious that the appearance of the continuum in the infrared would be characterized by an induction period.

Though it is not possible from the observations at 2.0-2.7µm wavelength range to attribute such emission to any particular structural group actually present, however, it is obvious that the emitted radiation is predominantly from species whose formation takes place much later in the process of acetylene decomposition.

The appearance of emission continuum in the visible during the pyrolysis of hydrocarbons has always been attributed to the formation of carbon particles. Previous studies on the mechanism of carbon formation from acetylene[29, 31] have shown that the deposition of solid carbon particles is normally preceded by an induction time. Bradley and Kistiakowsky[34] have shown that there is a similarity between this induction time and the duration of the period prior to a sharp drop in the concentrations of the lighter polyacetylenes (e.g. C_4H_4) formed at the early stages of the acetylene pyrolysis. An attempt was therefore made to see how the present data fitted into the results of these earlier investigations, especially in relation to the kinetics of formation of the species emitting at this (2.0 - 2.7μm) spectral region. The result obtained from such comparison would lead to a better understanding of the relationship between the induction times at 2.0 - 2.7μm and those measured for incipient carbon formation in the visible; hence an insight might be gained as to the nature of species being formed during the induction period.

6.1.1. Correlation of induction time data

If the rate of formation of high polymeric substances depends on the acetylene concentration to the order n, then the rate expression will be of the form[29],

$$\frac{dC_s}{dt} = \text{constant}\left[\exp\left(-E_a/RT\right)\right]\left[C_2H_2\right]_o^n \qquad (6.1)$$

where C_s = the concentration of the high polymeric substances emitting at this wavelength range.

E_a = the activation energy in J/Mole

T = the reaction temperature, ^oK

R = molar gas constant in $Jmol^{-1}\ {^oK}^{-1}$.

$[C_2H_2]_o$ = initial concentration of C_2H_2.

If it is assumed that at the onset of infrared radiation in this wavelength range the minimum detectable amount of emission corresponds to equal amounts of the polymeric substances being formed for all conditions of temperature and pressure behind the reflected shock-wave, then equation (6.1), can be approximately expressed in the form[39]

$$(\Delta C_s)_{initial} = \text{constant}$$

$$= \text{constant}\left[\exp(-E_a/RT)\right]\left[C_2H_2\right]_o^n \Delta\tau \qquad (6.2)$$

where $\Delta\tau$ - the induction time in microseconds and ΔC_s is the amount of substance formed at time $\Delta\tau$.

By taking the logarithm of both sides, equation (6.2) reduces to

$$\log_{10}\Delta\tau = \frac{E_a}{2.3RT} - \log_{10}\left[C_2H_2\right]_0^n + \text{const.} \qquad (6.3)$$

which gives

$$\log_{10}\Delta\tau = \frac{E_a}{2.3RT} - n\log_{10}\left[C_2H_2\right]_0 + \text{const.} \qquad (6.3a)$$

From equation (6.3a) n can be readily evaluated at any constant temperature by plotting the logarithms of the various values of $\Delta\tau$ against those of their corresponding initial concentration of acetylene. The negative of the slope of the resultant straight line gives the value of n. This method is not particularly convenient when using the shock-tube technique because of the enormous task involved in trying to obtain exactly the same temperatures behind the shock-waves for different initial shock conditions. However, as shown in table 6.2, the reaction temperature was approximately constant at 1580°K, and by using these limited data, it was possible to obtain a rough value of n = 1.08 from figure 6.2. The plotted points in figure 6.2 are based on the values shown in table 6.4.

Table 6.4 Variation of induction time with initial concentration of acetylene at T = 1580°K

Run no.	$P_{C_2H_2}$, KN/m²	$C_0 \times 10^4$, moles/litre	$(\log_{10}C_0)+6$	$\Delta\tau$, μs	log $\Delta\tau$
321	0.327	1.315	2.119	1 000	3.00
313	0.665	2.673	2.427	500	2.699
329	0.931	3.74	2.573	320	2.505

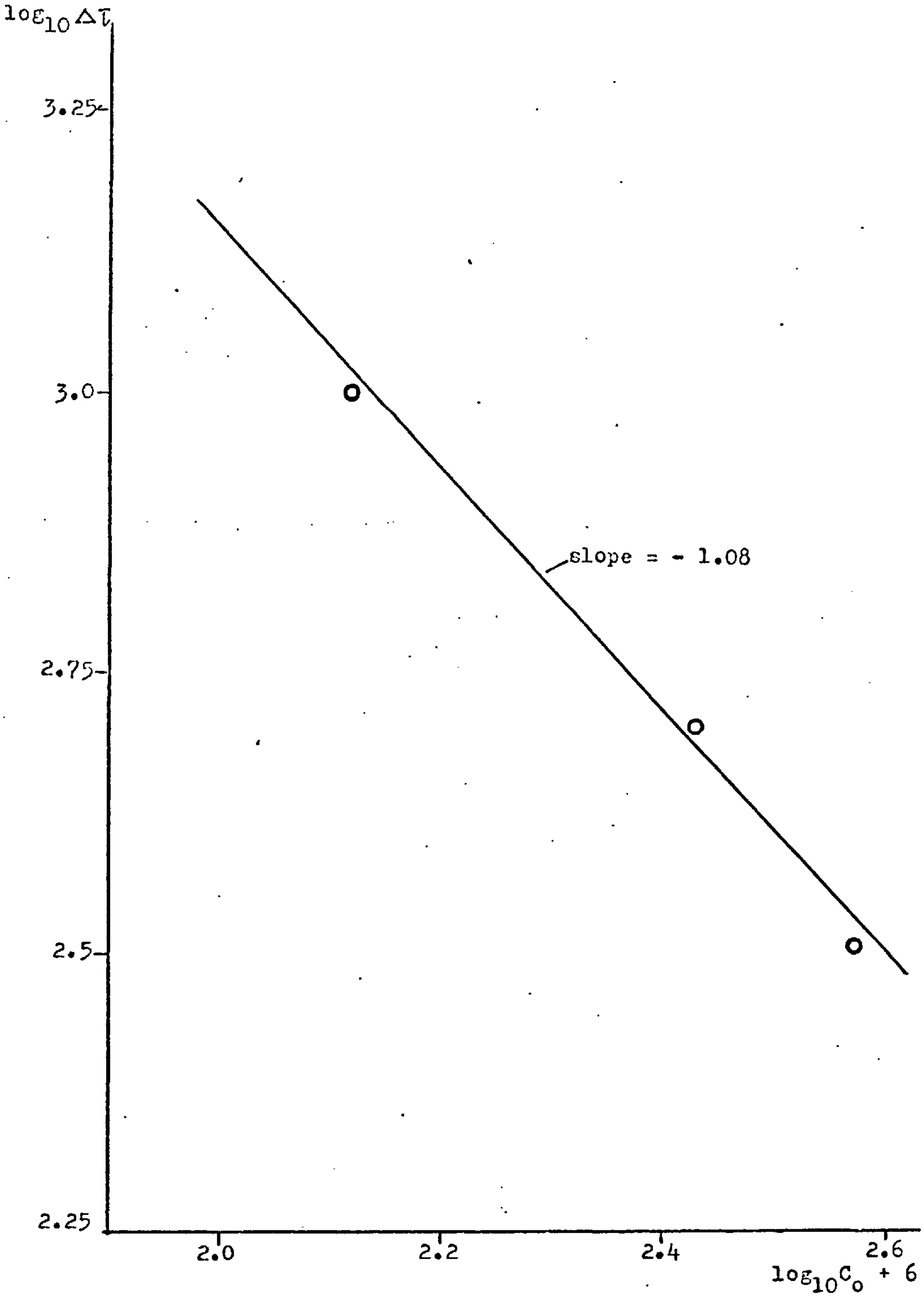

Figure 6.2: The determination of n - power dependence of induction time on initial acetylene concentration at T ≃ 1580°K

An alternative method which is very convenient for application in studies using the shock tube technique is the 'initial pressure differential' method; where measurements are made at constant initial reactant concentrations while the temperature is varied over the desired range. This method has been widely used by Lifshitz et al[27, 18] in modelling different kinds of chemical reactions behind the reflected shock waves. Inorder to determine the power dependence n, using this differential method, a group of experiments were conduted using two mixtures of acetylene in argon; mixture A contained 5% C_2H_2 in argon and mixture B contained 2% C_2H_2 in argon. By keeping the initial pressure of the two mixtures approximately constant (13.3 - 15.96 KN/m^2), n can then be evaluated since the initial concentration of acetylene in mixture A would be 2.5 times greater than as in mixture B. ∴ If equation (6.3) is specifically written for mixture A, it becomes,

$$\log_{10}\Delta\tau_A = \frac{E_a}{2.3RT} - \log_{10}\left[\bar{x}\,(C_2H_2)\right]_o^n + \text{const.} \qquad (6.4)$$

where $\bar{x}$ is the number of times the initial concentration of C_2H_2 in A is greater than that in B; and then for mixture B,

$$\log_{10}\Delta\tau_B = \frac{E_a}{2.3RT} - \log_{10}\left[C_2H_2\right]_o^n + \text{const.} \qquad (6.5)$$

By substracting (6.4) from (6.5), we have that

$$\log_{10}\Delta\tau_B - \log_{10}\Delta\tau_A = n\log_{10}\bar{x} \qquad (6.6)$$

hence

$$n = \frac{\log_{10}\Delta\tau_B - \log_{10}\Delta\tau_A}{\log_{10}\bar{x}} \qquad (6.7)$$

Inorder to evaluate the R.H.S. of equation (6.7), the logarithms of the induction times in both mixtures A and B are plotted

Table 6.5: Experimental conditions to evaluate n

Mixture	Run no	P_1	% H_2	Temp	$^1/_T$ x10^3	Induction time	log τ
		torr*		$^\circ$K		τ, μs.	
A (5% C_2H_2 in Ar)	301	110	77.14	1300	7.69	1000	3.0
	302	110	80.80	1360	7.35	800	2.903
	305	115	79.58	1429	7.03	700	2.845
	309	100	81.70	1435	6.97	600	2.778
	313	100	86.80	1567	6.38	500	2.699
B (2% C_2H_2 in Ar)	320	120	77.8	1320	7.58	1950	3.29
	343	110	82.8	1516	6.60	1200	3.079
	348	100	88.85	1524	6.56	1000	3.00
	321	123	81.25	1592	6.28	1000	3.00
	323	110	83.0	1896	5.27	700	2.845

* 1 torr = 0.133 kN/m^2

against 1/T,.

Table 6.5 shows the experimental conditions of this group of runs. And using the results obtained from this table figure 6.3 was plotted. Figure 6.3 shows that the plot of $\log_{10}\Delta\tau$ vs. 1/T for the two mixtures A and B; gave two parallel lines 'A' and B' which were obtained by the method of least squares.

It can be seen from table 6.5 that mixtures A and B differed in their C_2H_2 concentration by exactly a factor of 2.23; that is $\bar{x} = 2.23$; so that the vertical distance, h, between these two parallel lines, when divided by $\log_{10} 2.23$ should yield the value of n.

From figure 6.3, h = 0.343

$$\therefore \quad n = \frac{\log_{10}\Delta\tau_B - \log_{10}\Delta\tau_A}{\log_{10}\bar{x}}$$

$$= \frac{h}{\log_{10} 2.23} = \frac{0.343}{0.348}$$

$$= 0.985$$

The values of n determined by the two methods outlined above, is approximately unity. Hence the rate of formation of the polymeric substances shows a first order dependence on the initial concentration of acetylene. Using the value of n = 1, all other experimental induction time data, including data obtained from limited runs conducted with 7% C_2H_2 in argon (mixture C), were normalized by the initial C_2H_2 concentration.

Inorder to determine the value of the activation energy of the formation of these substances, E_{ind}, equation (6.3) was rewritten to:

$$\frac{E_{ind}}{2.3RT} = \log_{10}\Delta\tau\left[C_2H_2\right]_o^n$$

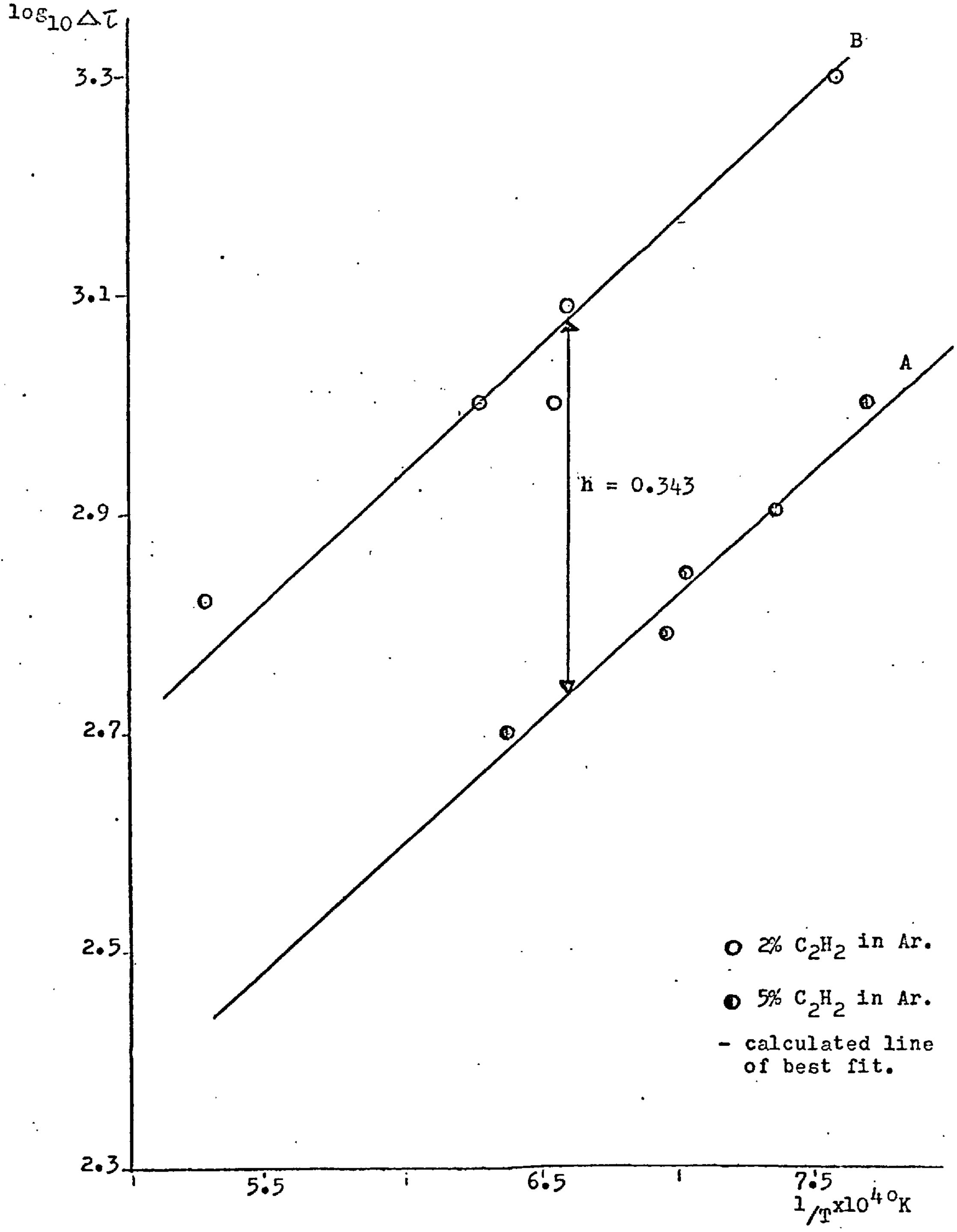

Figure 6.3: A plot of $\log_{10}\Delta\tau$ vs $^1/_T$ for mixture A and B for determining of dependence power, n

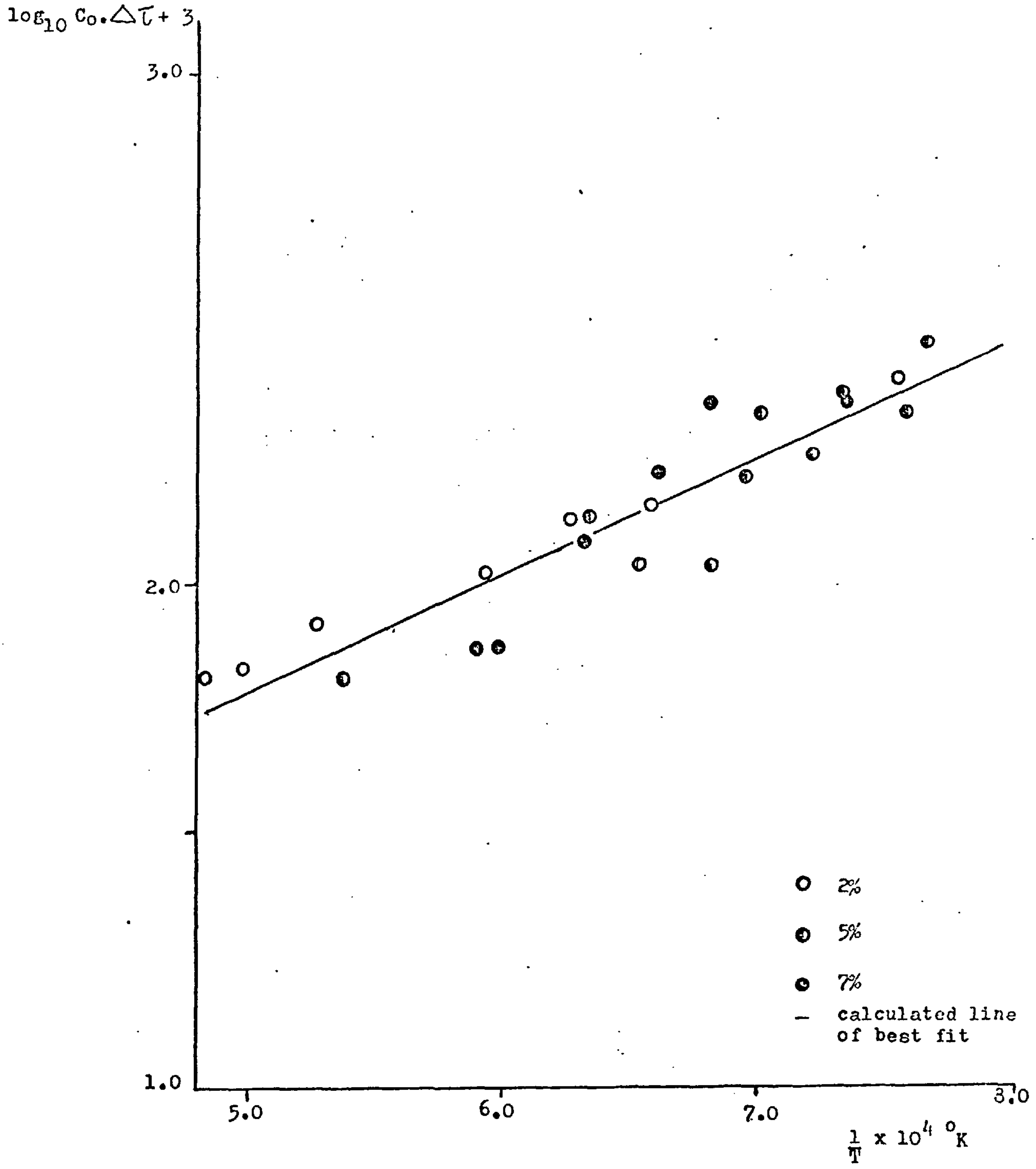

Figure 6.4: A plot of normalized induction time vs $\frac{1}{T}$ for the determining E_{ind}

And from the slope of the plot of $\log_{10} \Delta\tau \, [C_2H_2]_0^n$ vs $1/T$, with n = 1, the values of E_{ind} could be calculated. The details of the experimental conditions and the results for the three mixtures of C_2H_2 in argon are shown in table 6.6. Figure 6.4 shows a least square fit of all the experimental values, and all the points are seen to scatter along a single line.

$$\text{The slope of this line} = \frac{E_{ind}}{2.3R} = 0.229 \times 10^4$$

$$E_{ind} = 0.229 \times 2.3 \times 8.28 \times 10^4 \text{ J/mole}$$

$$= 43.6 \text{ KJ/mole.}$$

Hooker [29] had measured induction times in the visible spectrum from acetylene/argon mixtures for the incipient carbon formation. His results from a plot of the form in figure 6.4, yielded activation energy of the value E_{ind} = 41.8 KJ/mole which is in agreement to that obtained in the present study. Similar agreement has been reported by Bradley and Kistiakowsky[34], who had defined induction time as the time corresponding to the rapid decay of the C_4 polyacetylene formed during the pyrolysis of acetylene. It is therefore very likely that the substances whose infrared emission at 2.0 - 2.7µm was preceded by the induction time are indentical to carbonaceous materials whose formation might be as a result of the decomposition of other products formed in the early stages of acetylene pyrolysis. Large quantities of carbon deposits recovered from the shock tube after each run - especially in mixtures of high acetylene content - are expected to contribute significantly to the overall emission continuum observed in this spectral region. Further examinations at longer wavelength regions, where the resolution of the different structural groups is possible, might offer further explanations about the presence of the induction time.

6.2. Results at 2.60 - 3.08μm spectral region

Preliminary runs conducted in this region using mixtures of 5% acetylene in argon showed that generally the intensity of the emission was very strong, and in many cases the value of the intensity exceeded the saturation level of the detector's amplifier. The saturation effect was easily recognizable by the abrupt flattening-up of the infrared signal - this is illustrated in figure 6.5. As a safeguard against saturation the width of the exit slit was reduced to a value of 0.2mm. And even at this slit width the saturation effect was still occasionally observed, especially at high initial concentrations of acetylene in the test gas, but in all runs conducted using mixture B (2% C_2H_2/Ar) this effect was not observed.

Figures 6.6 (a,b,c,d) show the typical infrared records obtained at the stated conditions. These records show the presence of a peak shoulder to the left of the scan at ~ 3.03 μm. This corresponds[145,151] to the CH stretching frequency at 3300 - 3287 cm^{-1} of the terminal ≡ CH group in the acetylenes. No other peaks were noticed in this wavelength region within the temperature range studied.

The plots of the intensity of emission at 3.03μm against the observation time in the reflected shock region for different temperatures are shown in figures 6.7 (a and b).

FIGURE 6.5: INFRARED RECORD FROM SHOCK-HEATED 5% C_2H_2/Ar MIXTURE AT 2.60 - 3.08µm SHOWING THE SATURATION EFFECT.

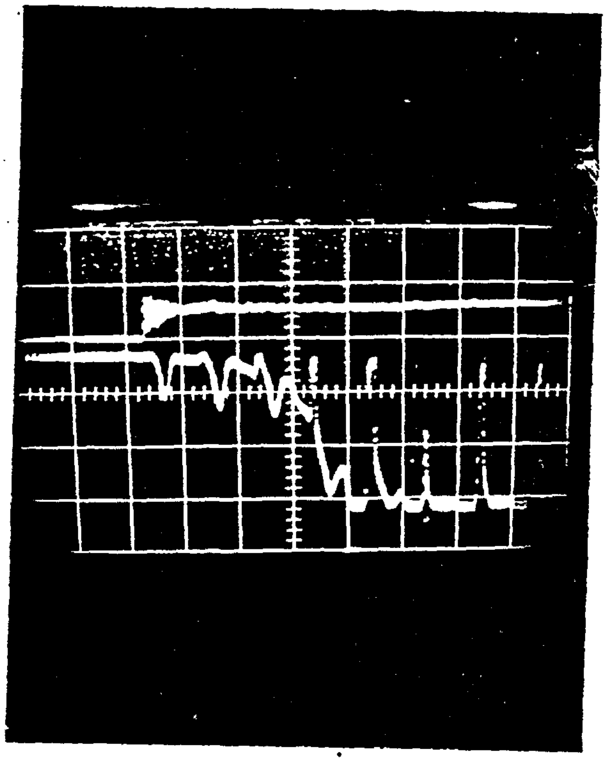

RUN NO. 369

$P_{C_2H_2}$ = 0.69 KN/m^2 . (5% C_2H_2/Ar)

P_{41} = 64.63

H_2 IN DRIVER GAS = 82.7 %

INCIDENT SHOCK VELOCITY = 0.977 mm/us

REFLECTED SHOCK TEMPERATURE = 1957°K

OSCILLOSCOPE GRATICULE: Y = 1.0 V/cm.

X = 0.2ms/cm.

FIGURE 6.6; CONTD.

(b)

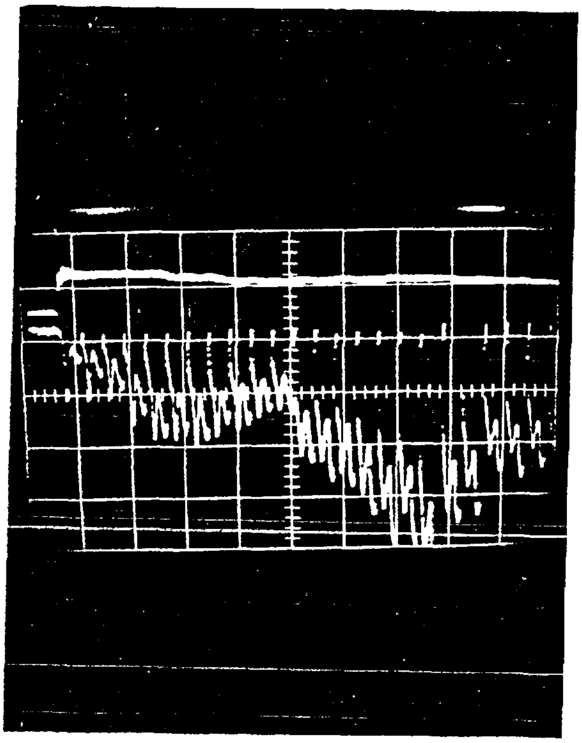

RUN NO. 375

P_1 = 13.3 KN/m^2 (2% C_2H_2/Ar)

REFLECTED SHOCK TEMPERATURE = 2290°K

OSCILLOSCOPE GRATICULE: Y = 0.2 V/cm.

X = 0.5ms/cm.

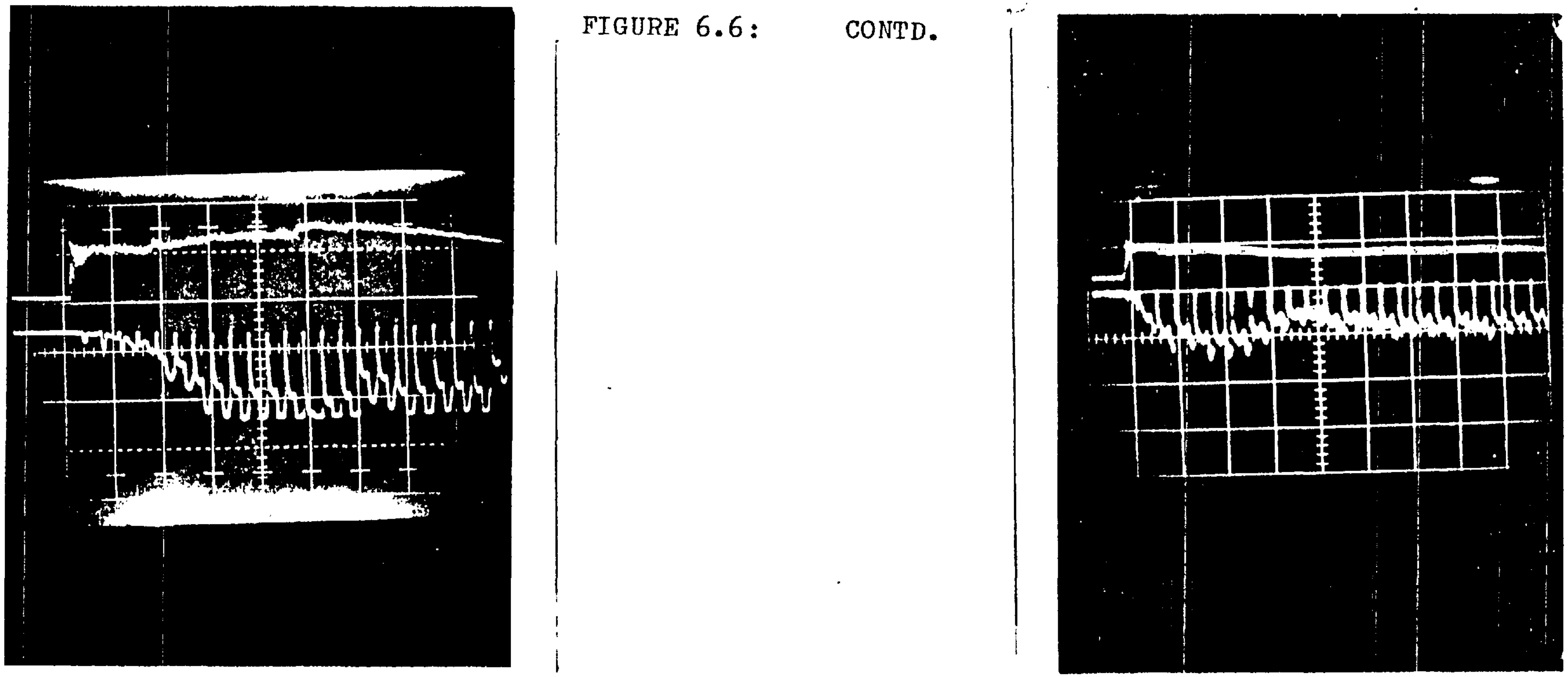

FIGURE 6.6: CONTD.

(c)

RUN NO. 360

P_1 = 17.96 KN/m^2 (5% C_2H_2/Ar)

REFLECTED SHOCK TEMPERATURE = 1395°K

OSCILLOSCOPE GRATICULE: Y = 0.5 V/cm.

X = 0.5ms/cm.

(d)

RUN NO. 365

P_1 = 15.96 KN/m^2 (5% C_2H_2/Ar)

REFLECTED SHOCK TEMPERATURE = 1902°K

OSCILLOSCOPE GRATICULE: Y = 1.0 V/cm.

X = 0.5ms/cm.

Figure 6.7(a), are plots of results obtained from mixture A (5% C_2H_2/Ar), while figure 6.7(b) are those from mixture B(2% C_2H_2/Ar). In tables 6.7 (a) and (b) are given the experimental shock tube conditions for each of the temperatures in these plots.

The intensity - time plots in figures 6.7 (a) and (b) show that emission was detected immediately following the reflection of the shock. This is expected since acetylene contains ≡ CH group and is present initially. However, the intensity of the emission increased with observation time - initially slowly at the lower temperature before rapidly rising to maximum and then decaying. At higher temperatures the rise was more rapid; at temperatures above 2250°K and longer observation times (greater than 2.2ms) the emission started to rise again after passing through the first maximum - thereby exhibiting two maxima (as can be seen in figure 6.6(b)).

In those runs where a substantial part of the first scan coincided with the onset of shock reflection it was observed that there was a slight drop in the intensity of the emission at the early stages of the reaction. This could not be measured in most cases as the time for the first scan (0.2ms) affected its value.

The intensity of the emission increased with temperature upto 1864°K, after which the intensity level decreased with increasing temperature. At temperatures above 2200°K the intensity immediately behind the reflected wave remained constant for a short time before it rose rapidly to maximum, decayed and rose to pass through the second higher maximum.

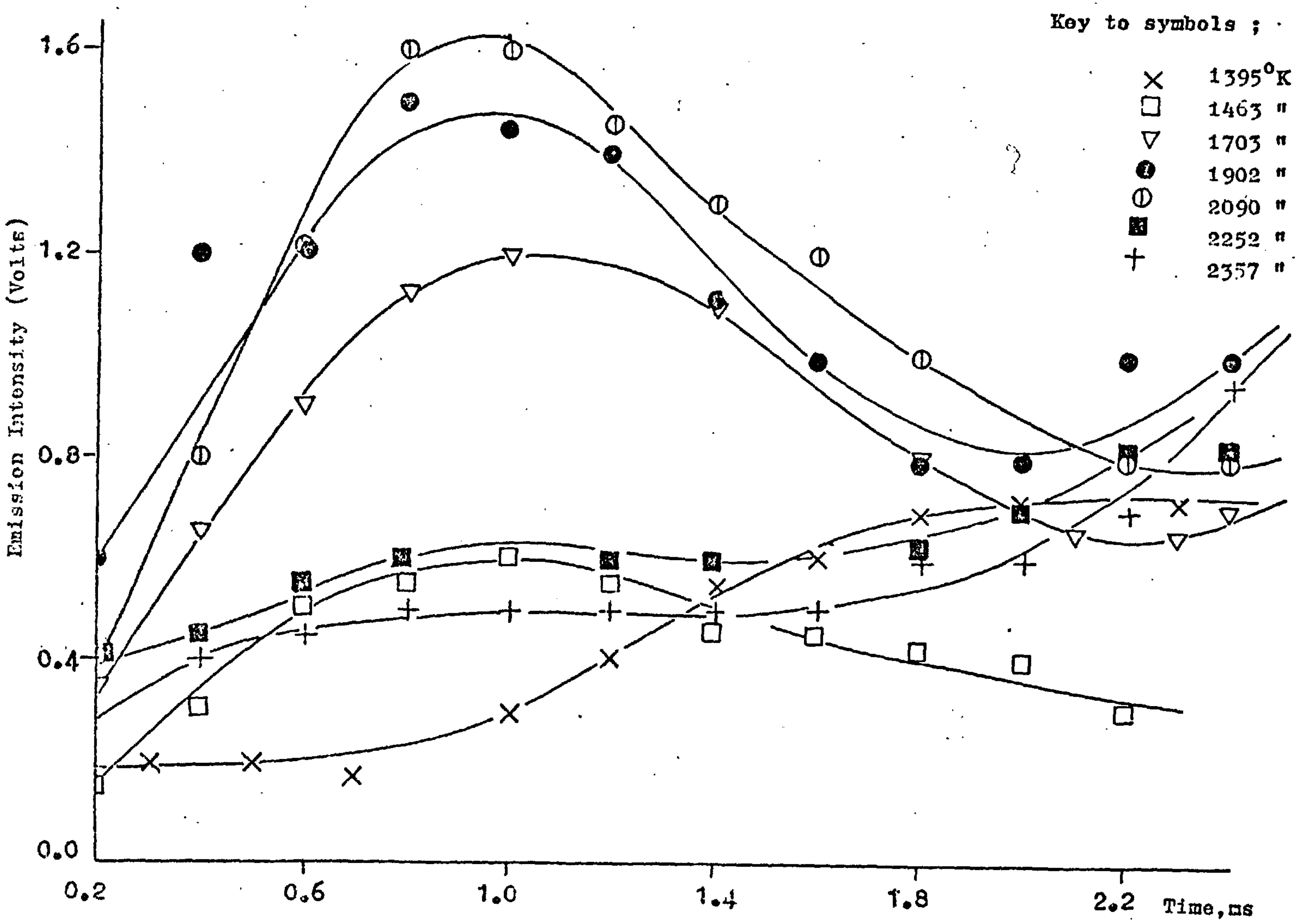

Figure 6. 7a: Emission - time plot at 2.60 - 3.08um for mixture A(5%C_2H_2/Ar)

Figure 6.7(b): Intensity - time plot for infrared emission from shock-heated 2% C_2H_2/Ar. mixture at 2.6 - 3.08µm

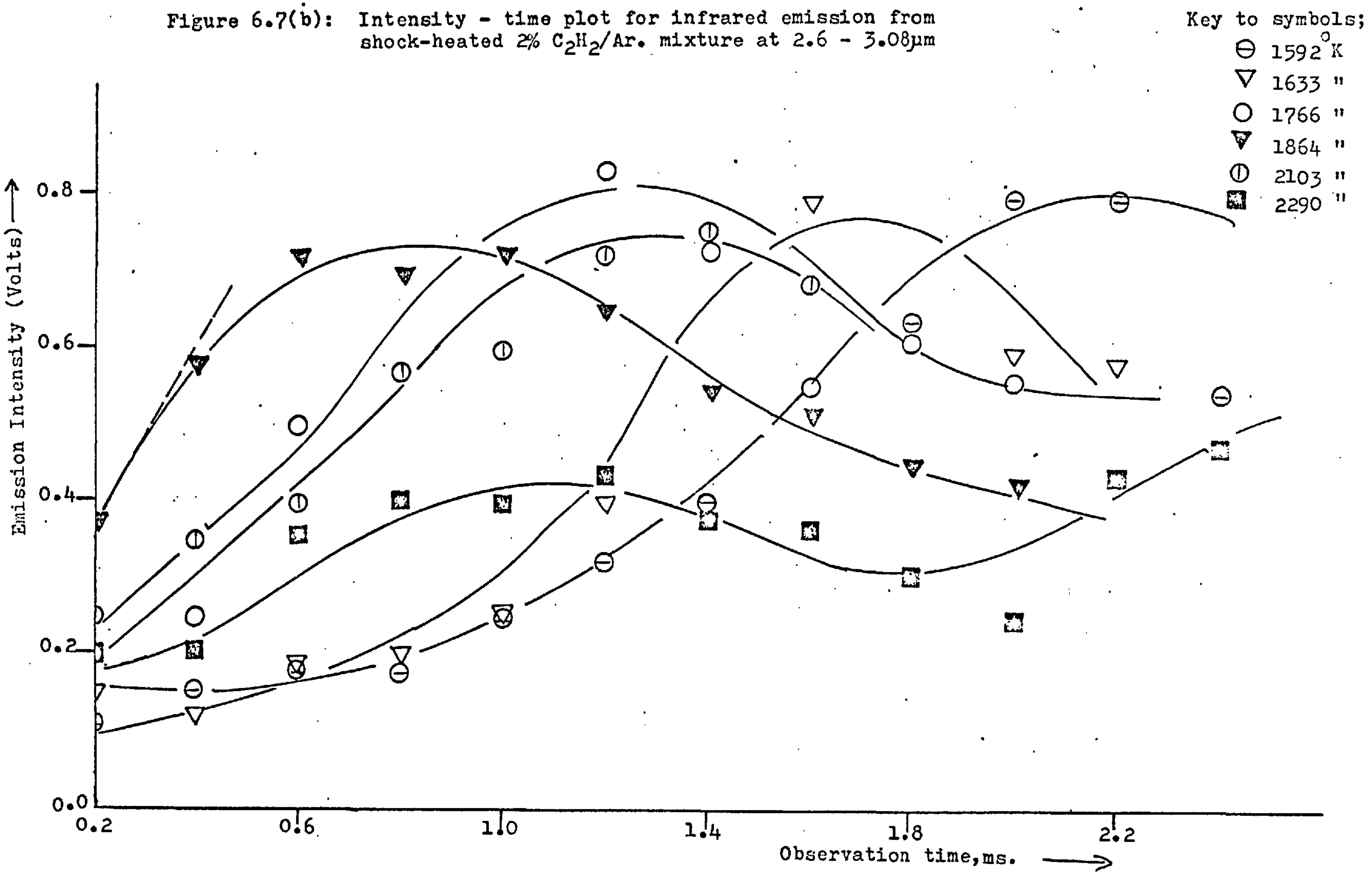

Table 6.7(a): Experimental shock tube conditions for shock heating a mixture of 5% C_2H_2/Ar at 2.6 - 3.08μm

Run no.	$P_{C_2H_2}$	Initial conc. of C_2H_2 in the test gas	Diaphragm Pressure Ratio, P_{41}	Hydrogen in driver gas	Incident shock velocity	Reflected shock Temperature	Reflected shock	
							Pressure ratio P_{51}	Pressure P_5
	KN/m^2	moles/litre(x10^4)		%	mm/μs	^{o}K		KN/m^2
360	0.898	3.608	45.96	75.0	0.808	1395	32.5	628
361	0.998	3.475	47.72	77.9	0.831	1463	35.0	699
364	0818	3.287	52.54	80.0	0.9045	1703	44.5	728
365	0.798	3.207	53.85	81.5	0.9620	1902	48.0	766
363	0.732	2.940	56.4	81.70	1.012	2090	60.0	878
366	0.599	2.405	68.93	83.3	1.055	2252	67.0	803
367	0.565	2.272	73.0	84.3	1.080	2357	71.0	802

Table 6.7(b): Experimental shock tube conditions for shock heating mixture of 2% C_2H_2/Ar at 2.60-3.08μm

Run no.	Initial Partial Pressure of C_2H_2, $P_{C_2H_2}$	Initial conc. of C_2H_2	Pressure Ratio Across the Diaphragm, P_{41}	Hydrogen in the driver gas	Incident Shock velocity	Reflected Shock temperature, T_5	Reflected shock	
							Pressure ratio P_{51}	Pressure P_5
	KN/m^2	moles/litre		%	mm/us	^oK		
371	0.372	1.497 x 10^4	48.0	77.69	0.842	1592	34.5	642
370	0.343	1.379 "	48.5	78.30	0.853	1633	35.6	611
372	0.330	1.325 "	50.0	85.8	0.890	1766	41.0	676
373	0.319	1.283 "	51.7	86.0	0.918	1864	43.6	696
374	0.306	1.229 "	58.44	87.2	0.980	2103	52.5	803
375	0.266	1.069 "	62.04	88.0	1.026	2290	59.0	771

The overall behaviour of the emission - time plots could be explained by either of the following reasons:

i) during the pyrolysis of acetylene two competing processes are taking place; (a) the decomposition of acetylene and (b) the formation of other acetylenic compounds. The observed slight decrease in the intensity of the emission at early stages of the reaction could be indicating that under 0.4ms, the rate of decomposition of acetylene is many times greater than the rate of formation of other polyacetylenes and related products which contain $\equiv$ CH. But the signal begins to rise immediately the rate of formation of these products exceeds that of acetylene decomposition. OR

ii) that the intensity of emission does not follow the concentration of any particular stable species present during acetylene pyrolysis but is caused by the formation of excited complexes in which the vibrations are at higher energy levels.

The complex pattern of the infrared emission at temperature above 2200^{o}K could be an indication that the reaction products emitting at this wavelength region are themselves very unstable; after their formation, they decompose and reform (or polymerize) to other related compounds. The presence of a period of time at which the intensity level remained constant before the it started to rise again at high temperatures (above 2100^{o}K) might suggest the possibility of a change in the reaction mechanism as it is known that acetylene becomes more stable at higher temperatures.

6.2.1. Dependence of emission intensity at 3.04μm from shock heated acetylene on reflected shock temperature

As the ≡ CH stretching frequence in C_2H_2 is known to have very strong intensity at 3.04μm further investigations were made at this wavelength by keeping the scan wheel stationary and examining the changes in the emission pattern with regard to temperature variation at approximately constant partial pressure of acetylene. The monochromator was set to 3.04μm. The scan wheel was positioned such that one of its slits which now served as the monochromator's entrance slit, was central with respect to the entrance aperture guide S1. The width of the exit slit was set at the same value as that of the disc (· 0.1mm).

When shocks were fired into a mixture of 2% C_2H_2 in argon the infrared signal rose very sharply to a high value and remained at this value for sometime before it gradually rose to pass through a broad maximum value. The final maximum level attained by the infrared signal was many times higher than the initial height of the signal following the shock wave reflection. The ratio of these heights, I_{max}/I_o as shown in figure 6.8, varied with temperature. In figure 6.8a these parameters (I_o, I_{max} and τ_f) have been defined. The ratio, I_{max}/I_o, is higher at lower temperatures than at high temperatures; but above 2000°K there was no change with ratio. It was also observed that the length of period before the commencement of the gradual rise in the intensity of the infrared signal decreased as the temperature increased.

At temperature of 1890°K and above, this period, at which the intensity level remained constant before rising, denoted as 'τ_f,' was either immeasurably small or totally absent and

Figure 6.8a: A schematic diagram of a typical infrared Emission Record at 3.04µm.

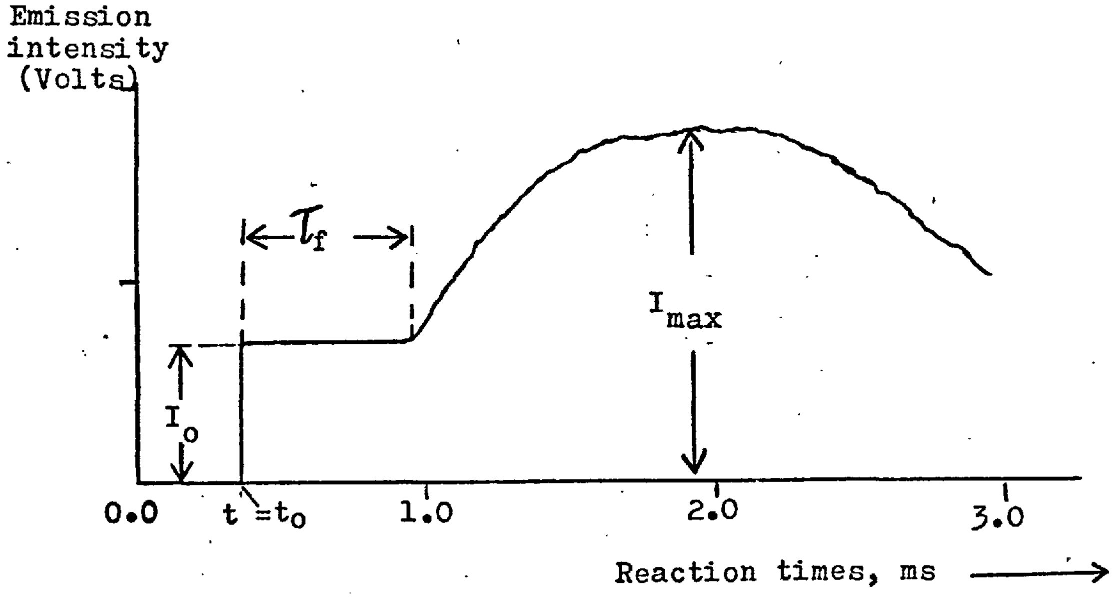

Figure 6.8: A plot of I_{max}/I_o versus reflected shock temperature at 3.04µm

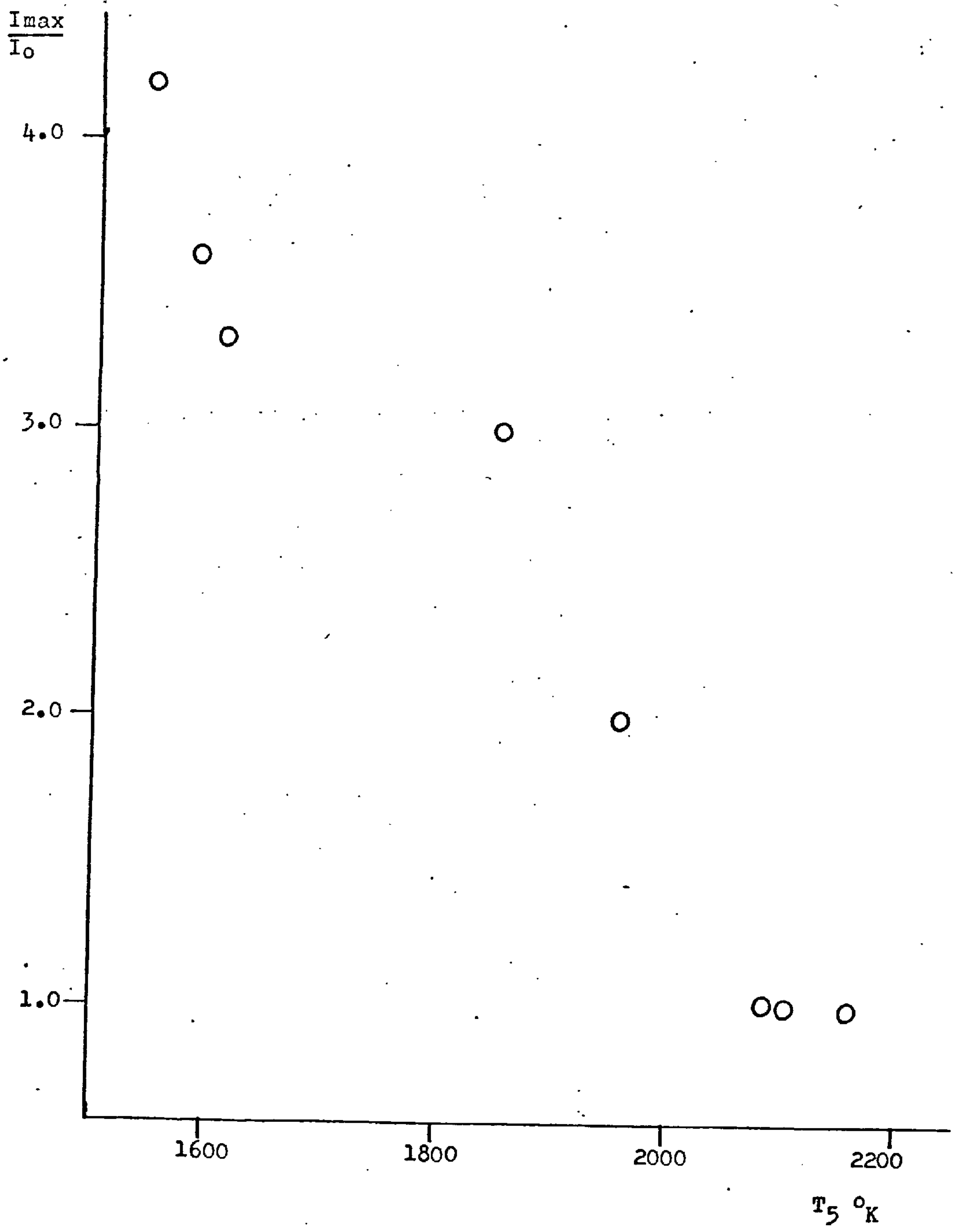

the infrared emission seemed to remain nearly constant throughout the experimental observation time. Also for runs conducted with mixture of 5% C_2H_2/Argon at initial pressures (P_1) above 100 torr, the value of τ_f was considerably shortened and in most cases it was zero.

Table 6.8 shows the effect of reflected shock temperature on τ_f and on the infrared emission intensities I_o and I_{max}; where I_o is the intensity at the onset of shock reflection and I_{max} is the maximum emission intensity recorded for the same run. The values given in the table 6.8 are those obtained at strictly the same observation conditions using mixture B. The values of I_o increased with temperature for a constant initial concentration of acetylene, whereas I_{max} changed only slightly.

Immediately following the onset of shock reflection (at t_o - reaction time = zero) all the acetylene is present as C_2H_2, whereas at other times, t greater than t_o, pyrolysis occurs and various reaction products contribute to the observed total emission. Thus at t = o, the intensity of the emission can be represented[42] by the expression;

$$I_o = g\left[\epsilon_{C_2H_2} \cdot C_o\right]\xi \qquad (6.8)$$

in which g represents the geometric factor of the optical and detecting system, ξ is the sensitivity of the photoconducting cell, C_o is the initial concentration of acetylene and ϵ represents the emissivity of the gas at the shock temperature.

Table 6.8: Dependence of initial emission intensity I_o, at 3.04μm on temperature.

Run no.	Initial Partial Pressure of acetylene, $P_{C_2H_2}$	Reflected shock temperature	Initial Height of IR, Signal, I_o	Maximum Intensity level after time, τ_f	Ratio, $\frac{I_{max}}{I_o}$	Length of τ_f
	KN/m^2	^oK	Volts	Volts		ms
S1	0.293	1553	0.25	1.05	4.2	0.65
S2	0.293	1592	0.25	0.85	3.6	0.50
S3	0.293	1616	0.30	1.10	3.3	0.45
S4	0.266	1855	0.40	1.20	3.0	0.30
S5	0.266	1962	0.41	0.80	1.95	0.20
S6	0.253	2090	0.23	0.23	1.0	-
S7	0.239	2167	0.16	0.16	1.0	-
S8	0.226	2167	0.16	0.16	1.0	-
S9	0.218	2103	0.11	0.11	1.0	-

The setting of the oscilloscope's graticule is:

Vertical, Y_{IR} = 0.5V/cm

Horizontal, X = 0.5ms/cm

except in run numbers S6 to S9 where the setting was

Y_{IR} = 0.2V/cm and X = 0.2ms/cm.

The blank spaces in the last column indicate that τ_f was either too small to be accurately measured or zero.

Preliminary calculation of the values of the emissivity of acetylene at $t = o$, for various temperatures was made using equation (6.8), under conditions such that the effects of both g and ξ were eliminated. This was achieved by taking measurements at constant wavelength, slit width and the sensitivity of the oscilloscope. Figure 6.9 shows the dependence of intensity of emission on reflected shock temperature. The plot of $\ln(I_o/P_{C_2H_2})$ versus $^1/_T$ gave a straight line whose equation is of the form,

$$I_o = 3.66\text{x}10^3 \exp(-10{,}625/RT)\, P_{C_2H_2}. \qquad (6.9)$$

Figure 6.9 is based on the values given in table 6.9. Equation 6.9 illustrates that in the experimental temperature range of 1600 to 2000°K, the exponential term showed a weak temperature dependence; hence

$$\epsilon_{C_2H_2} = 3.66\text{x}10^3 \exp(-10{,}625/RT),\ \text{mv/torr} \qquad (6.10)$$

6.2.2. Rate of rise of infrared emission at the wavelength interval 2.60 - 3.08µm.

Generally the rate of chemical reaction, R_a, in terms of product formation can be expressed as:

$$R_a = d(P)/dt = K[C_2H_2]_o^n \qquad (6.11)$$

where (P) is the concentration of the product, K is the reaction rate constant and n is the order of the reaction

Figure 6.9 : A plot of $\ln\left(I_o/P_{C_2H_2}\right)$ vs $1/T$ for evaluating the Emissivity of C_2H_2 at 3.04μ

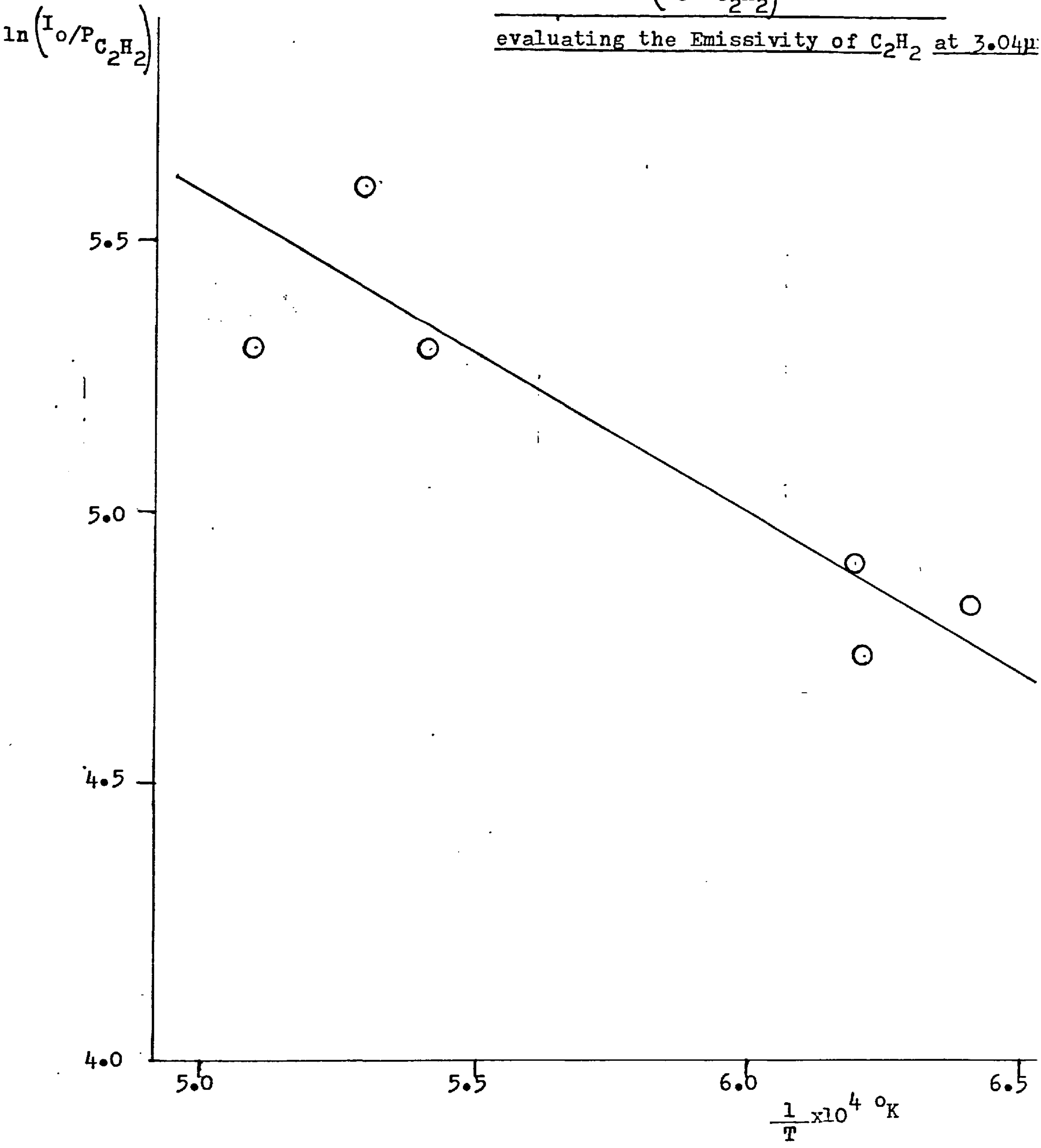

Table 6.9: Emissivity of shock heated acetylene at 3.04µm.

Temperature	$P_{C_2H_2}$	I_o	$I_o/P_{C_2H_2} = \epsilon$	$l_n\ (I_o/P_{C_2H_2})$
^oK	torr*	mv		
1553	2.0	250	125.0	4.83
1592	2.2	250	113.64	4.73
1616	"	300	136.36	4.915
1855	2.0	400	200.0	5.30
1896	2.2	600	272.73	5.61
1962	2.0	410	205	5.32
2090	1.9	230	121	4.80
2141	2.0	240	120	4.79

* 1 torr = 0.133 KN/m^2

with respect to the initial concentration of acetylene, $[C_2H_2]_o$.

For thermal emission measurements, the rate of rise of intensity is comparable to the rate of increase in the concentration of the emitting species, hence if the following relationship

$$I = \epsilon(P) \qquad (6.12)$$

holds for species emitting at a particular wavelength region, then combination of equations (6.11) and (6.12) yields

$$R_a = \frac{1}{\epsilon} dI/dt = d(P)/dt = K\,[C_2H_2]_o^n \qquad (6.13)$$

In applying the above expression for determining the reaction rate at wavelength regions where the emission intensity rises to a maximum and then starts to fall or remains constant after attaining the maximum value, the rate of increase in intensity ca be defined as the average rate of rise over a fixed period of observation time or fraction of reaction reached.

If it is supposed that the overall reaction leading to the emission at any particular wavelength region can be represented by a simple two step mechanism

$$n\,C_2H_2 \xrightarrow{k_1} (C_2H_2)_n^*$$

$$(C_2H_2)_n^* \xrightarrow{k_2} \text{product} \quad (+\,h\nu)$$

then applying steady state conditions for the thermally excited molecular species $(C_2H_2)_n^*$, we have

$$(C_2H_2)_n^* = \frac{k_1}{k_2} (C_2H_2)_o^n$$

And the rate of formation of product at that wavelength region is therefore;

$$\frac{d(P)}{dt} = k_2 (C_2H_2)_n^*$$

$$= k_1 (C_2H_2)_o^n \qquad (6.14)$$

where k_1 is the rate of decomposition of acetylene and equation (6.14) has the same form as (6.13).

In the present study, the reaction rate was determined for reaction time, $t << t_{max}$, where t_{max} is the time at which the intensity of the emission reached maximum, by evaluating the slopes of the intensity - time plots at the early stages of the reaction. Such rate constants were obtained in that stage of the pyrolysis of acetylene where the rate of polyacetylene formation is substantially equal to the loss of acetylene. A typical method for evaluating the slopes of the straight lines drawn to the intensity - time curves is shown in figure 6.7 for $T_5 = 1864^oK$.

The value of n, the reaction order, was assumed to be 2 since this is consistent with the findings by several[24,112,118] researchers that the rate of polymer formation from acetylene or acetylene decomposition is a second-order reaction.

Table 6.10: Rate of Rise of Infrared Emission at 3.04µm.

Temperature, ^{o}K	Slope ($\Delta I/\Delta t$)	R_a ($1/\epsilon \cdot \Delta I/\Delta t$)	$Log_{10}K$ $[log_{10}R_a/C_o^2]$
1592	0.33	0.907	7.411
1633	0.2	0.52	7.50
1703	1.5	3.576	7.52
1766	0.833	1.847	8.02
1864	1.24	2.48	8.178

Figure 6.10: Arrhenius plot for the Rate of Rise of Infrared Emission at 3.04μm.

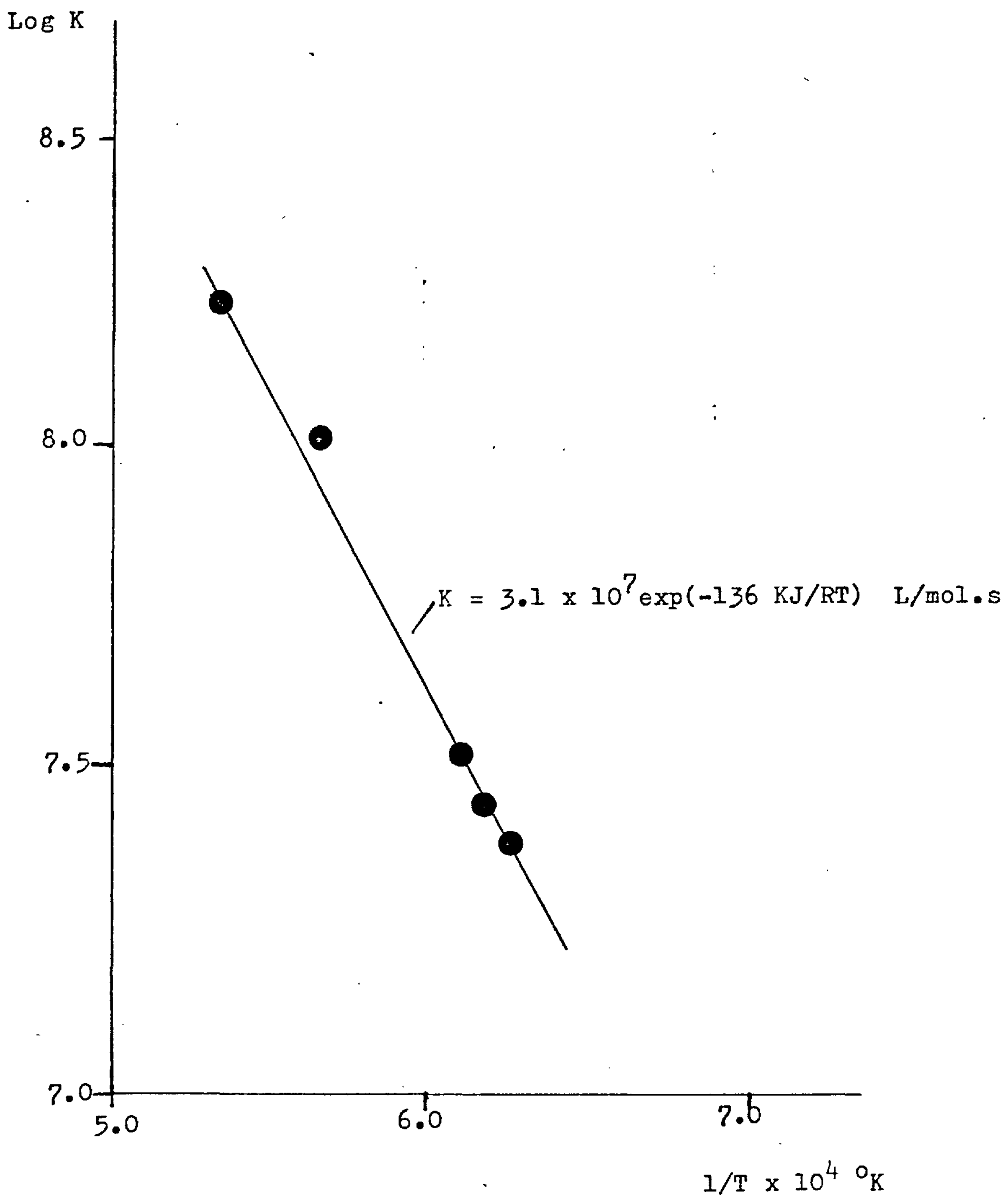

The results of such calculations are shown in table 6. 10. Experiments at higher temperatures than those shown in table 6. 10 were not particularly suitable for accurate measurements as the infrared emission became very weak and the conditions here were limited by the signal to noise ratio.

The Arrhenius plot using the values outlined in table 6.10 yielded a second order expression,

$$K = 3.1 \times 10^{7} \exp(-\ 136\ \text{KJ/RT})\ \text{litre/mol./sec.}$$

This value of E_a = 136 KJ/mole lies within the lower range of reported[23-25, 41, 110-112, 115] literature values (117 - 176 KJ/mole) of activation energy for second order disappearance of acetylene.

6.2.3. Discussion of Results at 3.04µm

The infrared radiation from shock-heated acetylene/argon mixtures at 3.04µm rose in two stages (figure 6.8a). The initial sharp rise to a constant value I_o, the magnitude of which depended on the temperature of the reflected shock wave, signified the onset of shock reflection and is thought to be due to the compression of the mixtures by the shock wave and the vibrational excitation of acetylene. The gradual rise in the radiation intensity after time τ_f signifies either the onset deactivation of some highly excited product molecules by repeated collisions with argon and acetylene molecules or decomposition in which the excess energy is used to break the chemical bond(s) to yield stable reaction products. Similar results have been obtained by Hooker[29] (at 3287 cm^{-1}) and Kuratani and Bauer[42] (at 3195 cm^{-1}) from the infrared radiations from shock-heated mixtures containing acetylene. Their results showed that infrared radiation started to rise a second time after an interval of time during which it had remained at a constant value.

Although it is not possible to say for certain what compounds or particular reation products are responsible for the increase in the emission intensity at 3.04µm after τ_f, but it is worth noting that at lower temperatures which favour the formation of higher molecular weight ploymers, the ratio of I_{max} to I_o is about four times higher than its value at the less favourable high temperature conditions. It is possible that the rise at the end of the period τ_f could be part of a radiation continuum from CH and/or 'carbon' particles which are beginning to be formed as the decomposition of acetylene becomes appreciably high. This is very likely to be the case since carbon formation from hydrocarbons are usually preceeded by an induction period [23, 29-31]. This suggestion is strengthened by fact[29] that carbon particles from shock-heated acetylene/argon mixtures do not start to absorb radiation (in the visible) until sometime after the infrared radiation had reached its equilibruim value; at this time a simultaneous increase in the radiation of the heated gases and a decrease in the intensity of the transmitted radiation occurs.

A comparison between the induction time, τ_{ind} measured at the wavelength region 2.0 - 2.7µm (see table 6.1) and the values of τ_f at different temperatures is shown in table 6.11. From this table it is seen that τ_f is approximately one-half the value for τ_{ind} at the comparable temperatures. The magnitude of the difference between τ_f and τ_{ind} ($\tau_{ind} \approx 2\,\tau_f$) indicates that the reaction immediately commencing after period τ_f is not the rate controlling step, and that substances emitting at wavelength region under 2.7µm are those products whose formation occur much later during the pyrolysis of acetylene. The period τ_f, between the onset of the reflection of the shock wave and the commencement of an accelerated rate of rise of the emission intensity, is thought to be connected in some manner with the time for the molecular vibrations of acetylene to become large enough to induce dissociation; while the rise in emission intensity after τ_f was caused by the formation of highly energized products or species which emit at frequencies very close to that of acetylene at 3287 cm^{-1}.

Table 6.11 Comparison between the induction time, τ_{ind} (at 2.0-2.7μm) and τ_f - time at which intensity remained constant at 3.04μm

Initial partial Pressure of C_2H_2 $P_{C_2H_2}$	Reflected shock Temperature	τ_{ind},	τ_f
KN/m^2	^oK	ms	ms
0.266	1524	1.0	-
0.293	1516	1.20	-
0.293	1553	-	0.65
0.293	1592	-	0.50
0.327	1592	1.0	-
0.293	1855	-	0.30
0.266	1896	0.70	-

6.3 Emission results at the wavelength interval between 3.05 to 3.49µm from shock heated acetylene

Figure 6.11 shows the typical infrared records obtained in this wavelength region. In this region it was observed that the emission has maximum intensity at 3.22µm. This corresponds[145,151] to = CH_2 vibrational frequency at 3105 cm^{-1} in compounds having vinyl group. Another peak shoulder is seen to the left of the more intense peak at 3.22µm. This second peak, though not well resolved, is thought to correspond[145] to -CH= vibrational frequency at 3030cm^{-1} (3.32µm) of vinyl group. Most of the previous workers[24,34,41] on high temperature pyrolysis of acetylene have found vinylacetylene, a compound which contains both =CH - and =CH_2 groups, to be present in the reaction products.

Figures 6.12 (a) and (b) show the plots of the intensity of the infrared emission at 3.22µm against the observation time in the reflected shock region for temperatures between 1508 - 2520°K. The experimental shock tube conditions for the results used for these plots are given in table 6.12.

The intensity - time records show that the infrared radiation was detected almost immediately following the onset of the reflection of the shock waves; and since the pyrolysing acetylene does not contain a double - bond in its structure, it is therefore to be suggested that the formation of product having double bond(s) in its structural composition takes place immediately as acetylene begins to pyrolyse. In general the intensity - time profile shows that there is an initial increase in emission - intensity with the observation time. The emission pattern reveals three

FIGURE 6.11: INFRARED EMISSION RECORDS FROM SHOCK-HEATED MIXTURES (2% & 5%) C_2H_2 IN ARGON AT 3.05 - 3.49µm WAVELENGTH REGION.

(a)

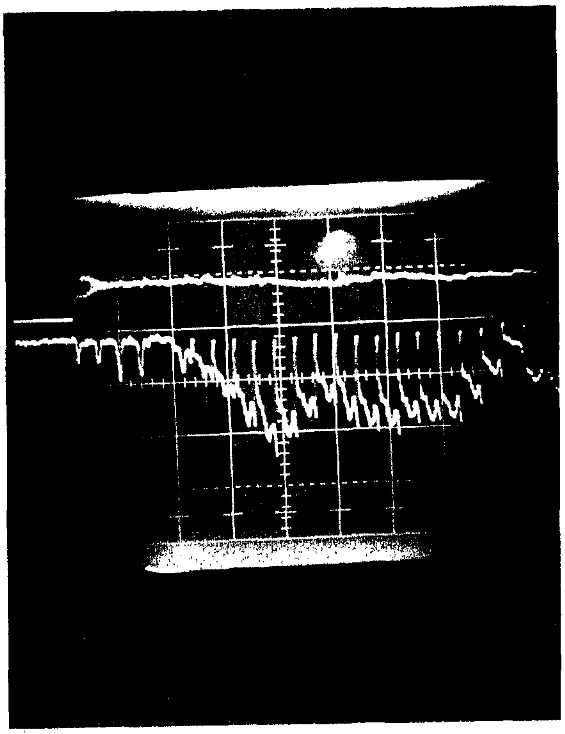

RUN NO. 384

P_1 = 17.96 KN/m^2 (2% C_2H_2/Ar)

REFLECTED SHOCK TEMPERATURE = 1585°K

OSCILLOSCOPE GRATICULE: Y = 0.2 V/cm.

X = 0.5ms/cm.

FIGURE 6.11: CONTD.

(b)

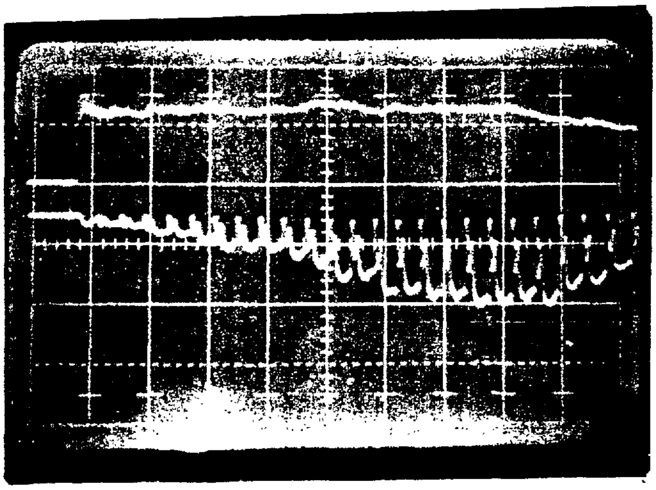

RUN NO. 429

P_1 = 8.25 KN/m^2 (5% C_2H_2/Ar)

REFLECTED SHOCK TEMPERATURE = 2520°K

OSCILLOSCOPE GRATICULE: Y = 1.0 V/cm.

X = 0.5ms/cm.

Fig.6.12(a): Intensity - time plot for infrared emission from shock-heated 2% C_2H_2/Ar. mixture at 3.05 - 3.49µm

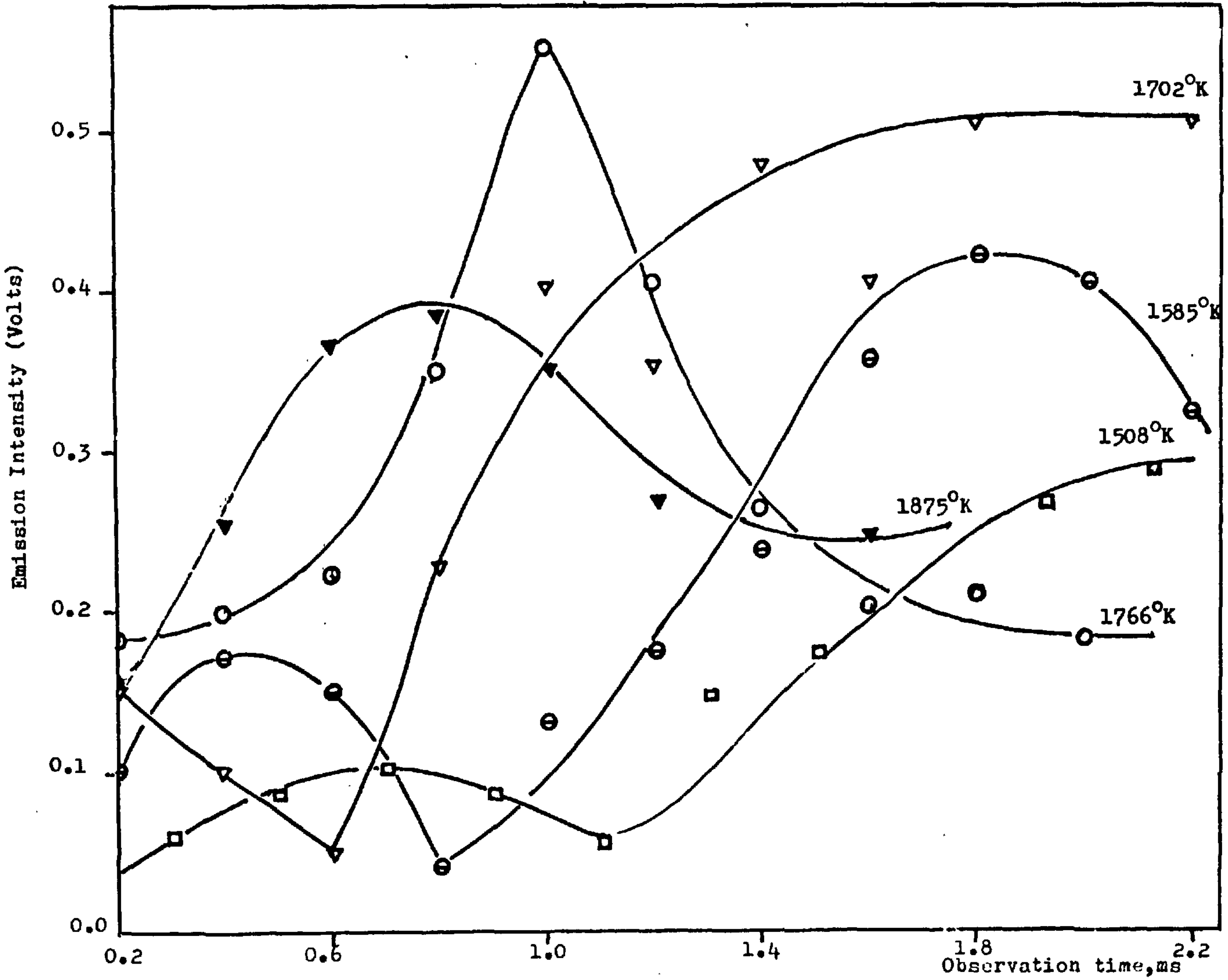

Figure 6.12(b) : Intensity - time plot for infrared emission from shock - heated 2% C_2H_2 / Ar. mixture at 3.05 - 3.49 µm.

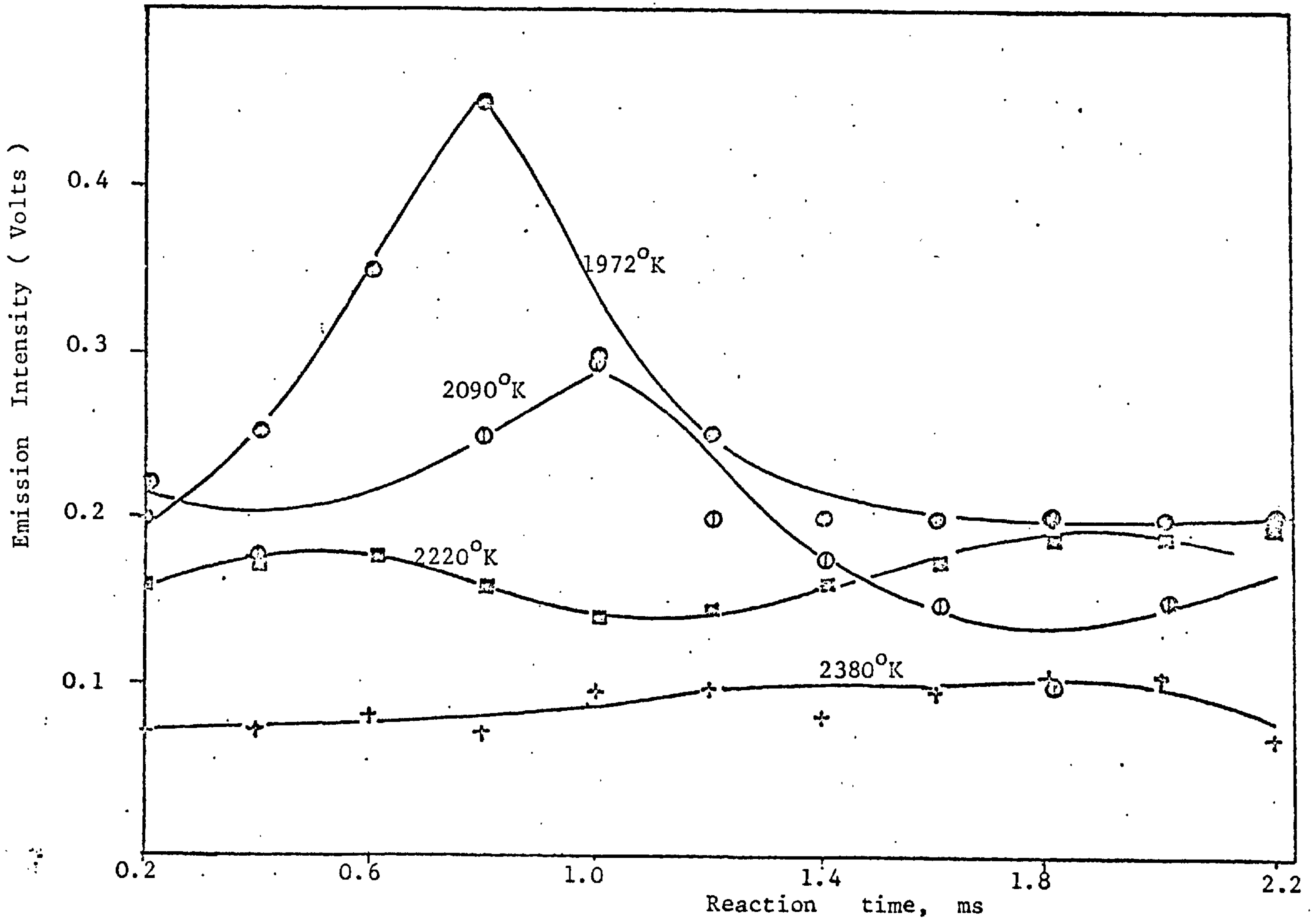

Table 6.12: The experimental shock tube conditions for runs at 3.05-3.49μm

Run No.	Initial partial pressure $P_{C_2H_2}$	Initial conc of C_2H_2	P_{41}	H_2 in driver gas	Shock Velocity	Reflected Shock Temp T_5	Density ratio ρ_{51}	P_{51}	Reflected Shock Pressure, P_5
	KN/m^2	mole/litre		%	mm/μs	°K			KN/m^2
383	0.372	1.497×10^{-4}	40.62	73.65	0.817	1508	6.336	31.80	592
384	0.359	1.443 "	45.96	77.50	0.840	1585	6.503	34.31	616
388	0.327	1.315 "	50.44	78.33	0.873	1702	6.750	38.26	626
381	0.317	1.272 "	52.13	80.00	0.891	1766	6.876	40.43	640
391	0.293	1.176 "	56.40	79.17	0.921	1875	7.074	44.17	646
390	0.277	1.112 "	59.65	80.83	0.947	1972	7.241	47.54	657
392	0.239	0.962 "	68.93	83.33	0.977	2090	7.426	51.67	618
395	0.215	0.855 "	77.55	85. 0	1.01	2220	7.611	56.26	599
386	0.207	0.834 "	79.54	86.67	1.047	2380	7.808	61.90	642
429	0.412	1.657 "	100.0	90.0	1.123	2520	9.299	77.98	643

temperature dependent characteristics. At lower temperatures the infrared intensity at 3.22µm rose gradually to a maximum and sharply decayed and the rose again to a much higher and broad maximum. The emission intensity increased with temperature up to around 1800°K and above this temperature the intensity of the emission started to decrease with increase in temperature and only one maximum was observed. At temperatures higher then 2100°K the emission intensity was very low and there was almost no change in the intensity level throughout the observation time behind the reflected shock wave for runs conducted with mixture B. With mixture A, the signal rose slowly at high temperatures.

A special feature peculiar only to the observations in this wavelength region, is illustrated in the infrared records at run numbers 381 and 383. As can be seen in figure 6.11 (a), the width of the scan increased immediately the intensity of the infrared emission had passed through a minimum value. Such increase in the scan width resulted in the broadening of the principal peak (at 3.22µm)and the appearance of another peak shoulder (at 3.32µm) to the left of the original one. The length of time before 'peak broadening' occurred decreased with increasing temperature.

Broadening of emission or absorption bands in infrared spectroscopy is normally associated with shift in the vibration frequencies of the functional groups in question. Conjugation effect due to the presence of multiple functional groups in a compound is mostly responsible for such shifts. In the present experimental circumstances the observed broadening effect is likely due to the result of increase in both the complexity and the concentrations of the emitters in this wavelength region. This is particularly so at the lower temperatures where the peak broadening was accompanied by an accelerated rise in the intensity of the infrared emission.

The formation of polyacetylenes and other related high molecular weight polymers during the pyrolysis of acetylene is particularly favoured at lower temperatures. These polymers, for example the homologues of vinylacetylene, contain multiple ($=CH_2$, $=CH-$, $-C\equiv C-$, etc)bonds and owing to conjugation effects displacement will occur in the positions of their vibrational frequencies; this will eventually lead to broadening in the emission bands.

Skinner and Sokoloski[118] and others[31,119] have identified vinylacetylene as the major primary product during the pyrolysis of shock-heated acetylene at lower temperatures while at higher temperatures (1400° - 2500°K) diacteylene is the only prominent hydrocarbon.[12,24] Cullis and Franklin[112] have observed that the vinylacetylene so formed at the initial stages of acetylene pyrolysis was gradually being converted to other products mostly diactylene. If one examines the present result in this light, then the emission-time profiles at 3.05 - 3.49µm wavelength region can thus be explained in terms of formation of two types of product - primary and secondary products. At lower temperatures($<1700^\circ$K) a primary product, probably vinylacetylene, is formed at the early stages of the reaction; higher polymers , for example vinyl-diacetylene (C_6H_4),[34] are formed later as a result of the consumption of the primary product. At higher temperatures the rate of consumption of the primary products becomes very fast and hence the secondary products become the major emitters.

This is particularly so since the time of decay (t_d) of the infrared emission following the initial rise in its intensity decreases with increase in reaction temperature. This is shown in table 6.13.

Table 6.13 Time for emission intensity to pass through minimum at wavelength interval 3.05-3.49µm.

Run no.	$P_{C_2H_2}$	Temperature,	Time of decay of intensity after initial rise.
	KN/m^2	^{o}K	t_d, ms.
383	0.372	1508	1.1
384	0.359	1585	0.8
388	0.327	1702	0.6

And also it can be seen from figure 6.12(a), e.g. at 1702^{o}K, the initial small maximum had already occurred before 0.2ms. At higher temperatures it can be assumed that the decaying process of the primary product is completed before 0.2ms and hence only the rising portion of the infrared signal corresponding to the formation of the secondary product are observed.

The start of formation of an appreciable amount of the secondary product is signified by the broadening of the peak. Table 6.14 shows the comparison between the times at which the peak broadening occurred and the induction period before the start of infrared radiation at 2.0 - 2.7µm spectral region.

Table 6.14: Comparison between induction time for emission at 2.0 - 2.7μm and time at which peak broadening occurred at 3.05 - 3.49μm

Run no.	Initial partial pressure of C_2H_2, $P_{C_2H_2}$	Reflected shock Temperature	Time for broadening	τ_{ind}
	KN/m^2	°K	ms	ms
383	0.372	1508	1.3	—
343	0.293	1516	-	1.20
384	0.359	1585	1.0	-
321	0.327	1592	-	1.0
322	0.239	1684	-	0.7
388	0.327	1702	0.6	-

As can be seen from the table, there is a good agreement between both times, and hence it could be suggested that the secondary product formed in this region(3.05 - 3.49μm) is identical, if not the same as those emitting at the infrared region under 2.7μm. As was mentioned earlier in section 6.8.1, the agreement between the value of the activation energy for the formation of these polymeric substances at (< 2.7μm), and the values obtained by both Hooker[29] and Bradley et al[34] for carbon formation, does suggest a similarity between these polymeric materials and carbon. In systems which produce soot, such as acetylene-oxygen flames, Homann, Mochizuki and Wagner[132], and Homann and Wagner,[152] have detected the presence of such radicals as $C_2H^\bullet$, $C_2H_3^\bullet$ and C_2 in the reaction zone, whilst Bonne, Homann and Wagner[124] have obtained evidence indicating considerable involvement of polyalkynes, such as diacetylene and vinylacetylene, in soot formation. In the light of the above observations and from their own investigation on the reaction of ethynyl radical with hydrocarbons, Cullis et al[130] suggested that the initial nucleus in carbon forming process is $C_2H^\bullet$ radical and that acetylene and polyacetylenes are the growth species. An example of such reactions has been given[130] as:

$$C_2H^\bullet + C_2H_2 \longrightarrow C_4H_2 + H^\bullet$$

and the diacetylene formed in the above equation now act as the growth species

$$C_2H^\bullet + C_4H_2 \longrightarrow C_8H_2 + H^\bullet$$

$$C_2H^\bullet + C_6H_2 \longrightarrow C_8H_2 + H^\bullet$$

Although the exact nature of the structural composition of most of these high polyalkynes are not precisely known, however one characteristic feature of these hydrocarbons is that they contain comparatively little hydrogen and that they have double and triple C - C bonds. Once they are formed, these polyalkynes are partly consumed by addition reactions such as[130]:

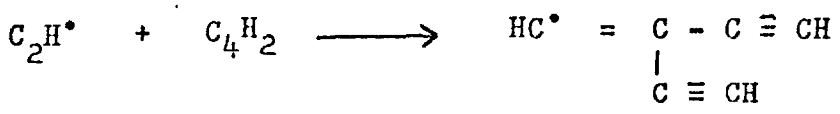

$$C_2H^{\bullet} + C_4H_2 \longrightarrow \begin{array}{l} HC^{\bullet} = C - C \equiv CH \\ \qquad\quad\;\; | \\ \qquad\quad\;\; C \equiv CH \end{array}$$

and

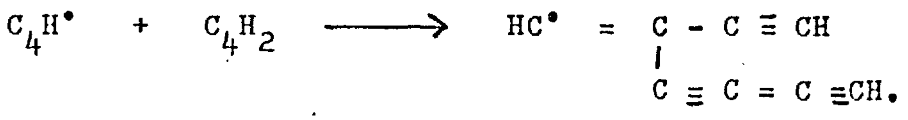

$$C_4H^{\bullet} + C_4H_2 \longrightarrow \begin{array}{l} HC^{\bullet} = C - C \equiv CH \\ \qquad\quad\;\; | \\ \qquad\quad\;\; C \equiv C = C \equiv CH. \end{array}$$

As has been pointed by Porter[77], the presence of double and triple bonds is very important since it enables such molecules to maintain their radical characteristics during further addition of smaller molecules such as acetylene and diacetylene. The striking similarity between the rapid rise in the infrared emission intensity at 3.05-3.49µm after the initial decay at lower temperatures, and the rapid increase in the concentration of the polyacetylenes in, say, the oxidation zone of acetylene-oxygen flames, tends to favour such reactions. And the last two reactions above actually show that peak broadening in the $=CH_2$ and = CH- had occurred because of conjugation with the triple bonds.

6.4 Emission results at wavelength interval between 3.5 - 5.3μm from shock heated acetylene.

In this spectral region, the strength of the infrared emission was very strong and like the intensity at 2.6 - 3.08μm region, it showed strong dependence on the initial concentration of the acetylene. However, unlike the observation at 2.6 - 3.08μm, no saturation effect in the detector output occurred at this wavelength region. Thus, this permitted experiments to be conducted using both 5% and 2% mixtures of acetylene in argon. The former was favoured since it gave a higher signal to noise ratio.

Typical infrared records obtained in this wavelength region are shown in figures 6.13 (a and b). In these photographs, the intensity of the emission is seen to reach maximum at 4.6μm and this corresponded to the position of a well resolved peak close to the end of the scan. Any peak here would correspond[145,151] to the -C≡C- vibrational frequency in polyacetylenes which usually occurs at 2100 - 2280cm^{-1} (4.43-4.76μm). As was mentioned earlier, almost all the gaseous products of acetylene pyrolysis at shock temperatures are acetylenic hydrocarbons - containing various numbers of carbon atoms, C_4, C_6, C_8, etc - and although the exact composition of some of them are unknown, however, by virtue of being alkynes, they all contain the characteristic triple bond(s). As such their -C≡C- stretching frequency will lie very close to each other since it is known that conjugation (including even cylic acetylene has only a small effect on the position

FIGURE 6.13: INFRARED EMISSION RECORDS FROM SHOCK-HEATED MIXTURE OF 5% C_2H_2 IN ARGON AT 3.5 - 5.3μm WAVELENGTH REGION.

(a)

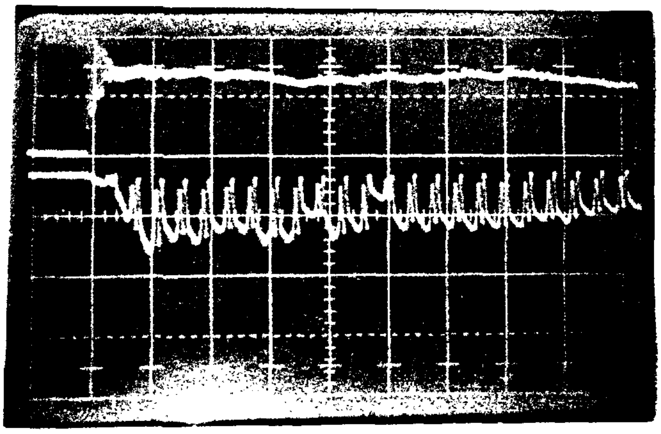

RUN NO. 455

P_1 = 13.3 KN/m^2

REFLECTED SHOCK TEMPERATURE = 1660°K

OSCILLOSCOPE GRATICULE: Y = 1.0 V/cm.

X = 0.5ms/cm.

FIGURE 6.13: CONTD.

(b)

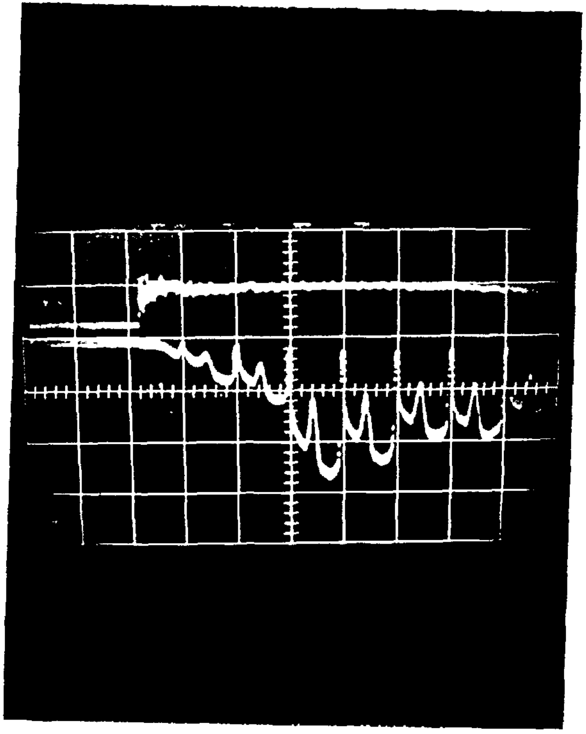

RUN NO. 403

P_1 = 13.3 KN/m^2

REFLECTED SHOCK TEMPERATURE = 2141°K

OSCILLOSCOPE GRATICULE: Y = 1.0 V/cm.

X = 0.2ms/cm.

of the -C≡C- bond. But the shape of the emission intensity to the right of the peak at 4.6µm (notably seen in figure 6.13 (b)) indicates that it is definitely a part of separate peak of probably another structure belonging either to the same or another compound. However, the ratio of the heights of these peaks was observed not to vary with increasing reaction time, thereby suggesting the likelihood that the two peaks could belong to the same compound. Therefore, the infrared emission - time profile here could be indicative of the time variation characteristics of the formation of any or the combination of these polyacetylenes.

Figure 6.14 (a and b) show the plots of the intensity of the infrared emission at 4.6µm against the observation time in the reflected shock region at reflected shock temperatures of 1400 - 2700^{o}K for various initial concentrations of acetylene. The corresponding experimental conditons for each of the runs used in the plot are stated in table 6.15. The intensity - time plots show that at all thetemperatures investigated, the intensity of the emission increased with observation time to maximuim and then started to decay; the intensity became progressively weaker as the temperature increased. The variation of the intensity of the emission at 4.6µm with time showed a regular pattern and those irregularities displayed by the intensity - time plots in the lower spectral region were minimum here. This might be due to the difference in the stretching modes of the terminal ≡CH and -C≡C- bands in the different alkynes, and moreover since -C≡C- band in acetylene itself is infrared inactive here, this would further lessen the complexity in the emission

Figure 6.14(a): Intensity-time plot for infrared emission from shock-heated 5% C_2H_2/Ar mixture at 3.53 - 5.3µm .

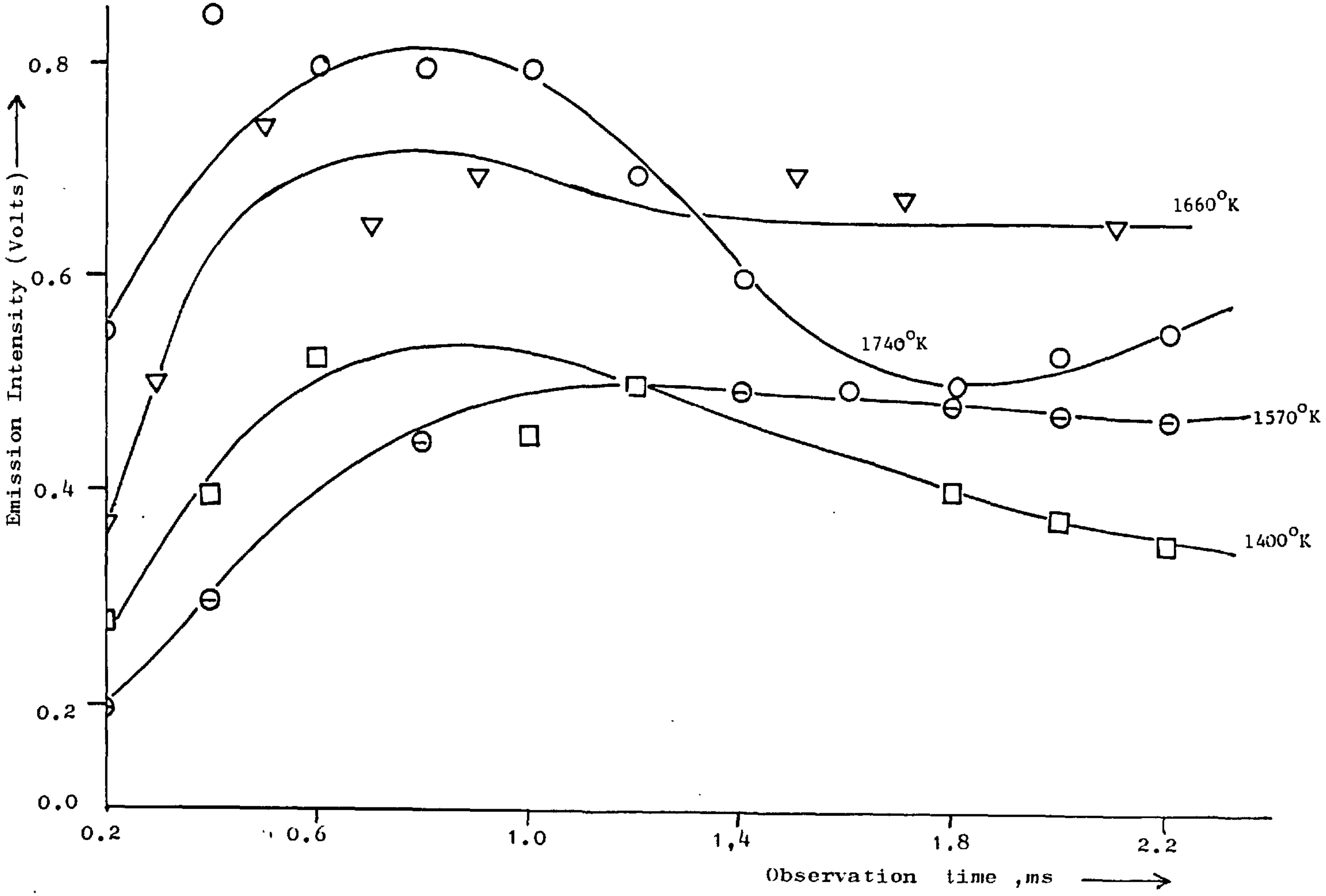

Figure 6.14(b): Intensity-time plot for infrared emission from shock-heated 5% C_2H_2/Ar. mixture at 3,53 - 5.3μm .

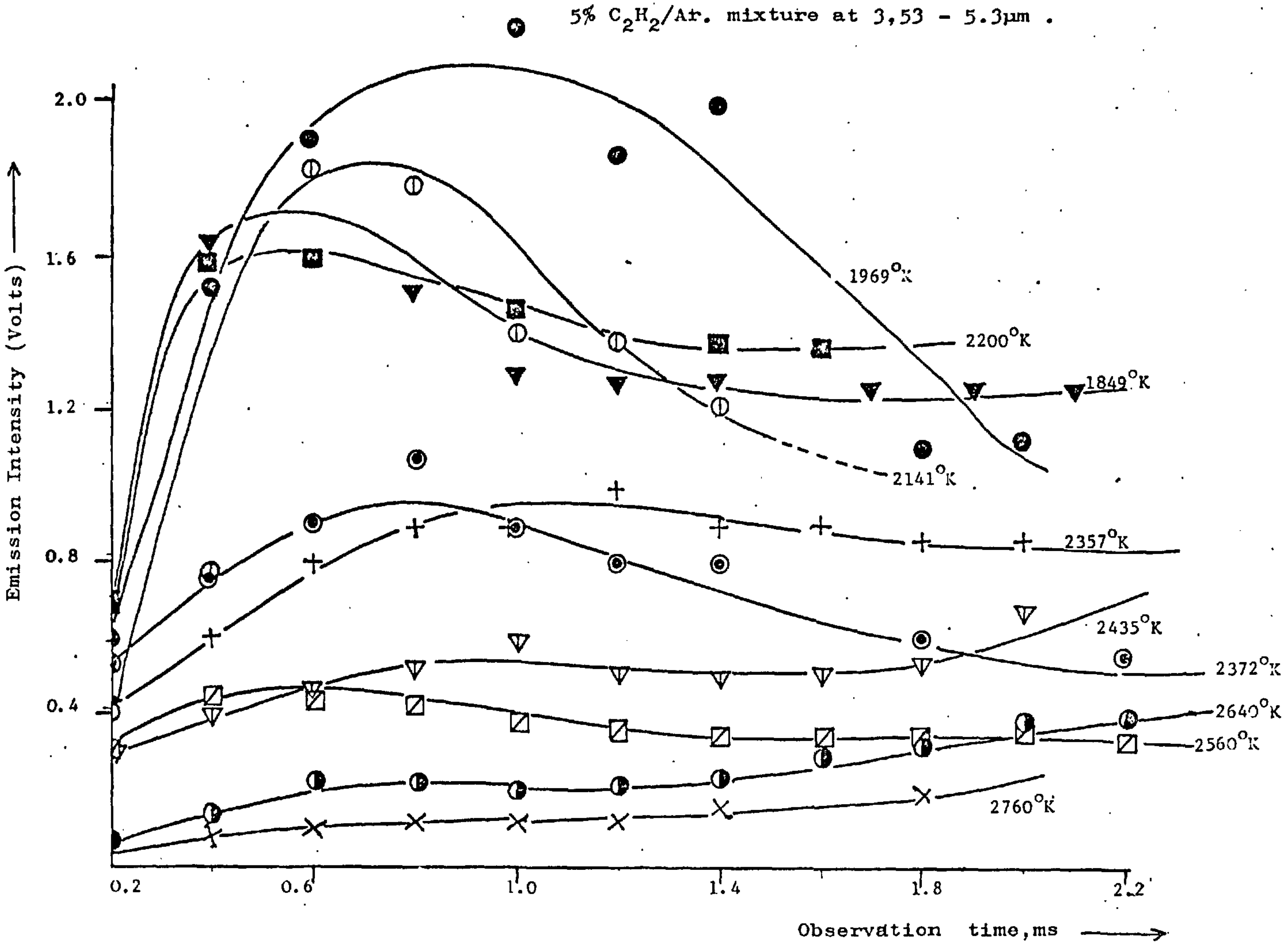

Table 6.15 Experimental condition for emission results at 3.5 - 5.3µm

Run on	Initial pressure $P_{C_2H_2}$	Concentration of C_2H_2	P_{41}	H_2 in P_4	Incident shock velocity	Density ratio, ρ_{51}	Reflected pressure ratio P_{51}	*Reflected shock pressure, P_5	Reflected shock Temperature
	KN/m^2	moles/litre		%	mm/msec			KN/m^2	^{o}K
451	0.930	$3.742\text{x}10^{-4}$	44.3	76.7	0.8085	7.010	32.536	606	1400
453	0.898	3.608 "	46.0	78.0	0.8635	7.507	39.166	703	1570
455	0.665	2.673 "	49.2	78.60	0.8912	7.740	42.734	568	1660
454	0.798	3.207 "	51.7	79.2	0.9153	7.932	45.956	733	1740
452	0.765	3.074 "	53.9	80.0	0.9466	8.175	50.323	770	1849
456	0.732	2.940 "	56.4	81.0	0.9801	8.413	55.185	807	1969
403	0.665	2.673 "	62.0	83.33	1.037	8.80	63.929	850	2141
457	0.698	2.806 "	59.1	81.25	1.04	8.817	64.495	901	2200
459	0.632	2.539 "	65.3	83.50	1.081	9.073	71.157	899	2357
461	0.599	2.405 "	68.91	84.2	1.085	9.096	71.827	860	2372
462	0.565	2.271 "	73.0	85.0	1.10	9.186	74.471	842	2435
463	0.532	2.138 "	77.6	85.8	1.116	9.269	77.263	822	2500
466	0.466	1.871 "	88.6	87.5	1.122	9.92	80.0	745	2640
467	0.412	1.657 "	100.1	89.0	1.135	10.60	82.2	656	2760

pattern. Such a circumstance would lend less confussion to the interpretation of the results at this spectral region than at particularly 2.6 - 3.08μm where the emission intensity of both acetylene and its reaction products are very strong.

While it is not possible from these measurements to know which of the polyacetylenes are present, however there seems to be a general concensus amongst majority of the previous investigators of acetylene pyrolysis at both ordinary and shock wave temperatures that C_4H_n (where n is 2 or 4) is the most abundant of the acetylenes that are found in the reaction products. Diacetylene, C_4H_2, is the most favoured product since other C_4 polyacetylenes tend to decompose further to diacetylene[112].

CHAPTER 7

ELUCIDATION OF THE MECHANISM OF ACETYLENE PYROLYSIS

7.0 Elucidation of the mechanism of acetylene pyrolysis.

7.1 Mechanism of acetylene pyrolysis

The pyrolysis of other hydrocarbons are known to result in an eventual production of acetylene, before finally decomposing to 'carbon ' and hydrogen. But the controversy over many decades now has centred on the last step leading to the final decomposition products (carbon) of hydrocarbons. It is in connection with this that the elucidation of the mechanism of acetylene pyrolysis is of considerable interest.

The decomposition of acetylene is complex and many suggestions have been put forward as to its nature; some of these have been discussed earlier in section (1.6). There is conflicting evidence as to the route by which acetylene decomposes. The product distribution of acetylene pyrolysis differs according to the temperature range investigated. For example, Bauer[153] studied the pyrolysis of acetylene in the shock tube between 1150 - 1450°K but detected neither vinylacetylene nor diacetylene at reaction times upto 1ms. In contrast Aten and Greene [23, 24] found small quantities of both in their investigation between 1400 - 2500°K. In addition shock tube studies utilizing the time of flight mass spectrometer[34, 41] have also detected higher polymers at temperatures between 1800°K and 2700°K; these polymers were found to decay to yield carbon. This strengthens further the argument of Gaydon and Wolfhard[154] that formation of solid carbon resulted from the cracking of rather higher polymers.

However, despite much controversy provoked by the mechanism of acetylene pyrolysis, certain features are now well established. A number of experimental results 25, 41,110 indicate that acetylene is consumed through a simple bimolecular polymerization reaction to form vinylacetylene and diacetylene; the former being the sole primary product at lower temperatures ($< 1500^{o}K$),

$$C_2H_2 \quad + \quad C_2H_2 \longrightarrow \quad C_4H_4$$

whereas the latter is favoured at high temperatures,

$$C_2H_2 \quad + \quad C_2H_2 \longrightarrow \quad C_4H_2 \quad H_2$$

At present, there is overwhelming evidence available in favour of a radical mechanism for the decomposition of acetylene. Many researchers 23, 24, 29-31, 115 have observed that the decomposition of acetylene is preceded by an induction period, which is greatly lengthened[111-2] by the addition of nitric oxide or eliminated[111] by the addition of radical generating substances. Several mechanisms have been proposed to explain these observations, and in particular a number of suggestions have been made as to the nature of the second-order initiation steps. Possible initiation reactions may include a bimolecular reaction of acetylene to give an excited molecule of acetylene in the triplet state or a triplet or biradical species [126 - 8], the bimolecular reaction to give the $C_4H_3^{\bullet}$ and $H^{\bullet}$ [41, 129, 130] and bimolecular disproportionation reaction of two molecules of acetylene to form an ethynyl ($C_2H^{\bullet}$) and a vinyl ($C_2H_3^{\bullet}$) radical [121, 131].

However, from the fact that nitric oxide inhibits, while the addition of rapid radical producing agents - diacetyl and ethylene oxide[111] - gives rise to acceleration of the reaction rate, it is therefore, established that a radical chain reaction actually takes place. In this study the induction period observed at 2.0 - 2.7μm confirms that a complex chain reaction is involved. Hence the discussion below is limited to radical mechanism.

7.1.1. Initiation step

For a free radical mechanism, the following initiation steps have been proposed for acetylene pyrolysis.

		ΔH
(7.1)	$C_2H_2 \longrightarrow C_2H^\bullet + H^\bullet$	478.8 KJ/mol
(7.2)	$C_2H_2 + C_2H_2 \longrightarrow C_4H_3 + H^\bullet$	190.9 KJ/mol
(7.3)	$C_2H_2 + C_2H_2 \longrightarrow C_2H^\bullet + C_2H_3^\bullet$	315 KJ/mol

where the heats of reaction, ΔH are calculated from the data of reference 125. If the initiation reaction were to be slower than all subsequent reactions and does not result in the setting up of a propagation chain, then the overall rate of the reaction will be equal to the rate of initiation. In such a situation, reaction (7.1) and (7.3) will be very much too endothermic; and whereas the activation energy of reaction (7.2) may be very close to that of the overall reaction, its pre-exponential factor will be certainly too low by a factor[75] as much as 100 to 1000. Hence it would appear that none of these initiation steps is involved in a rate determining fashion during acetylene decomposition, but rather they could be responsible for setting up propagation chains which would undoubted account for the high rate of acetylene consumption observed by many authors. For such circumstances, the overall rate of the reaction maybe less directly dependent on the rate of initiation and the assessement of their relative importance becomes difficult. However, for a generally accepted overall second order kinetics, step (7.1) becomes improbable and hence reactions (7.2) and (7.3) are more likely to occur. On this basis many authors[41, 112-3, 130] have favoured reaction (7.2) while Back[131] considers reaction (7.3) to be the actual initiation step on the grounds that reaction (7.2) could have occurred through the following steps;

$$C_2H_2 + C_2H_2 \longrightarrow {}^{\bullet}C_2H + {}^{\bullet}C_2H_3^{\bullet} \qquad (7.3)$$

$${}^{\bullet}C_2H_3 \longrightarrow C_2H_2 + H^{\bullet} \qquad (7.4)$$

$${}^{\bullet}C_2H + C_2H_2 \longrightarrow {}^{\bullet}C_4H_3 \qquad (7.5)$$

7.1.2. Propagation step

The propagation reactions are formulated on the basis of the detected reaction products. As has been outlined earlier, investigations similar to this current one have shown that diacetylene and sometimes vinylacetylene are the major higher acetylenes with some small amounts of hexatriyne (C_6H_2) and octatriyne (C_8H_2) and of course the inevitable 'carbon' particles. On the basis that diacetylene and sometimes vinylacetylene are the major high temperature products in the pyrolysis of acetylene, Cullis et al [130] have proposed a complete reaction scheme for temperature 1000 - 2500°K, consisting of 7 reaction steps, while Back[131] has set out a more complex scheme comprising upto 17 elementary reactions to account also for the formation of other products.

However, the complexity of Back's mechanism could be considerably simplified by grouping the reactions in the scheme into 3 different temperature regions - low, intermediate and high temperatures. At high temperature region there is not much difference between these two reaction schemes except for the different initiation steps. Identical propagation reactions have been suggested by references [41] and[124] to explain the formation of polyacetylenes. Some of these reactions include the followings:

a) those leading to the formation of diacetylene

$$C_2H^{\bullet} + C_2H_2 \longrightarrow C_4H_2 + H^{\bullet} \qquad (7.5b)$$

in which the propagation may also occur as a result of the reaction (7.6)

$$H^{\bullet} + C_2H_2 \longrightarrow C_2H^{\bullet} + H_2 \qquad (7.6)$$

$$C_4H_3^{\bullet} \quad (+M) \longrightarrow C_4H_2 + H^{\bullet} \ (+M) \qquad (7.7)$$

$$2C_2H^{\bullet} \longrightarrow C_4H_2 \qquad (7.8)$$

b) those leading to the formation of higher polyacetylenes,

$$C_2H_3^{\bullet} + C_2H_2 \longrightarrow C_4H_5^{\bullet} \qquad (7.9)$$

$$C_4H_5^{\bullet} \longrightarrow C_4H_4 + H^{\bullet} \qquad (7.10)$$

$$C_4H_3^{\bullet} + C_2H_2 \longrightarrow C_4H_4 + C_2H^{\bullet} \qquad (7.11)$$

$$C_4H_2 + C_2H^{\bullet} \longrightarrow C_6H_2 + H^{\bullet} \qquad (7.12)$$

$$C_6H_2 + C_2H^\bullet \longrightarrow C_8H_2 + H \qquad (7.13)$$

It is possible that some of these reactions occur through ways, such as:[130]

$$C_2H^\bullet + C_4H_2 \longrightarrow C_2H_2 + C_4H^\bullet \qquad (7.14)$$

$$C_4H^\bullet + C_2H_2 \longrightarrow C_6H_2 + H^\bullet \qquad (7.15)$$

and

$$H^\bullet + C_6H_2 \longrightarrow C_6H^\bullet + H_2 \qquad (7.16)$$

$$C_6H^\bullet + C_2H_2 \longrightarrow C_8H_2 + H^\bullet \qquad (7.17)$$

The participation of some highly unsaturated radicals such as $C_6H_3^\bullet$ and $C_8H_3^\bullet$ has been suggested by Gay et al[41] and Cullis et al [130], and it is thought [130] that their combination results in coagulation leading to the formation of carbonaceous materials.

The infrared emission results obtained in this investigation had shown the presence of $=CH_2$, $-C\equiv C-$ and $-C\equiv CH$ groups. If these groups were assigned to some stable molecules, then it is possible to formulate a chemical model on the basis of the reaction schemes outlined above and carry out various comparative analyses.

It is very difficult to visualize the effect that reactions in a scheme embodying reactions (7.1) to (7.17) will have on product formation. Steady-state analysis is precluded due to the complexity of the system and hence the computer method for solving the differential equations derived from such mechanisms was adopted. The principal advantage of this method is that no reactions need to be eliminated initially, but by assessing the effects of introducing or removing reaction steps, and/or changing their rate constants it is possible to predict the concentration time profiles of the various products and hence an appropriate mechanism is identified.

From the experimental results on the variation of the intensity of the infrared emission with time at the different wavelength regions, matching of the simulated concentration time profiles with the experimental intensity-time plots could be made by using the following characteristis features;

i) times for the intensity of the emission of the different groups to pass through a minimum or to reach a maximum, and

ii) induction period before the onset of emission at the lower (2.0-2.7µm) infrared region.

By examining the concentration time profiles of the different products (or that of a group of related products) predicted from the model, an assessment of the relationship between the experimentally obtained emission - time profile and the product distribution could be made.

7.2 Kinetic modelling of gas phase reactions

Studies of gas phase reactions particularly at high temperatures, often yield complex rate laws due to the contributions to the observed kinetics from several elementary steps. This is particularly evident in pyrolysis and combustion studies, where the fuel or fuel/oxidant can rapidly produce significant concentrations of reactive species. The purpose of numerical analysis of a kinetic model is to derive a concentration-time profile for radical and molecular species in a reaction simulating that in the shock tube. It is often difficult to decide beforehand on a method for predicting the course of a complex reaction or even being sure that the mechanism assumed is the only one possible. There maybe alternative reaction paths which can lead to the same kinetic observation. Therefore, in developing a theoretical model, one is usually faced with the problems of selecting the important reaction steps to include in the model and also in choosing accurate rate parameters for each step.

Semenov[155] has given a comprehensive survey of 'classical' methods (such as the application of steady-state hypothesis) used to determine mechanisms and rate constants in reaction mixtures. Applying such methods, an apparent rate law is derived for a particular reaction mechanism and compared to the experimental results. Further mechanisms are postulated until the desired rate law is predicted. For complex systems such as chain reactions, this usually leads to the determination of values for the ratios of groups of rate constants or to the formulation of rate constant in equalities. In this way, it is often possible to eliminate some of the proposed steps from the effective reaction mechanism for different limiting conditions. But in recent years, it has become fashionable to use computer simulation in the analysis of complex free radical mechanism by attempting to fit data to more detailed chemical models; in many of these, there is the mistaken belief that the ability to achieve such a fit is, of itself, an indication of the correctness of such model and that the parameters so obtained are of fundamental significance, rather than recognizing them as mere numerical fits which they are. This has resulted in the proliferation of misleading rate constants often seen in the literature. However the adoption of complex chemical models is necessitated by the inability of simplified models to adquately describe the complexity of the system being investigated; in so doing many hypothetical reaction steps are included and these often result in large errors. The large discrepancies in the values of reported rate parameters are apparent reflections on the compromise between choosing very complex models and the ability to achieve accurate analysis.

Byrne et al[158] have reviewed the various numerical methods for handling differential rate equations formulated from complex chemical models. The two most popularly used methods are the Snow's method[156] and that originated by Gear [159]. The Snow's method uses a standard numerical method to integrate the set of simultaneous rate equations derived from the model and often such methods incorporate procedures to fit rate constants to experimental product distributions. The main disadvantage of Snow's and other related methods is that they make use of a quasi steady-state approximation when one (or more) of the free radical intermediates becomes small. The errors inherent in this type of computational approach have become increasingly apparent over the years and have been reviewed by Edelson.[157]

At elevated temperatures, however, steady-state conditions may not be achieved and such methods are no longer applicable. In these circumstances, it becomes appropriate to simulate the observed changes accompanying the reaction by integrating sets of coupled differential equations, representing the rates of the individual elementary reactions. These equations are coupled because the rate of each step, and hence its contribution to the overall kinetics is a function of the concentration of the reactants; these may participate in more than one elementary step. For any given mechanism the rate of the jth reaction for the ith species is expressed as:

$$R_j = \left[K_j \sum_{i=1}^{NS} C_i^{\gamma_{ij}} \right] - \left[K'_j \sum_{i=1}^{NS} C_i^{P_{ij}} \right]$$

The net rate of consumption of species i is given by the differential equation:

$$\frac{dC_i}{dt} = \sum_{j=1}^{NR} (\gamma_{ij} R_j - P_{ij} R_j)$$

where

NR = number of chemical reactions

NS = number of chemical species

γ_{ij} = stoichiometric number of reactants for forward reactions

C_i = concentration of the specie i

P_{ij} = stoichiometric number of reactants for reverse reactions

K_j, K'_j = rate constants for forward and reverse reactions respectively.

for initial conditions, $C_i(o) = C_{io}$.

There the set of differential equations representing the entire reaction mechanism involving NR reactions and NS species can be written as in the form:

$$\dot{\underset{\sim}{C}} = f\,(c)$$

$$= \underline{A}\ \underline{C} \text{ for linear system.}$$

The function f(c) can be linear or non-linear in concentration depending on the formulated mechanism. $\underset{\sim}{A}$ represents the matrix of the rate constants, values of which are either experimentally determined or estimated by using thermochemical data table. Because of the large differences in the values of the rate constants for the individual elementary reactions, the elements of $\underset{\sim}{A}$ pose difficulty in obtaining a numerical solution. Such a difficult system to solve is termed[159] "stiff", and the degree of 'stiffness' is a measure of the time constants. The most serious problem posed by stiff differential equations is that of numerical stability. It is in respect to this that many workers in computational kinetics have increasingly turned to Gear's integration method[159]. The Gear's method works extremely well for these stiff equations and it is free of the problems associated with steady-state approximations.

The integration of these differential rate equations predicts the variation of some observable properties usually the concentration of chemical species with time, and this can be directly compared with experimental results. The values for the rate constants of the elementary steps are adjusted until a match between the two is obtained. Alternatively some other experimentally derived properties maybe compared to the computer prediction of the same properties instead of the detailed matching of the complete reaction profiles. For example, Bradley and Frend [26] using Gear's method have matched the apparent rate constant for the pyrolysis of ethane in a shock tube by adjusting both the reaction mechanism and the values of the rate constants. Bowman[170] in his study of the oxidation of methane behind the reflected shock waves, matched two experimental properties - the maximum concentration of O-atom and the time to reach this maximum - with the numerical computed values. By individually perturbing, the rate constants of each reaction in the proposed mechanism, he was able to determine to which reaction rate the O-atom concentration profiles was most sensitive.

However, the formidable task of computer fitting proceedures is somewhat simplified because of the availability of such computer programs as library subroutines, and also because the choice of possible rate constants is subjected to the constraints that:

i) some of them are known from literature

ii) the remainder can be reasonably estimated from similar known processes.

7.3 Computational method used in this work

In the reflected shock region the gas is brought abruptly to rest and maintained at a constant temperature until the arrival of the rarefaction waves. Hence homogeneity could be assumed and the reaction proceeds isothermally. In isothermal constant - volume pyrolysis the experiment is described by set of differential equations which are constructed by the rigorous application of mass-action principles. This set contains an equation for each chemical species in the model, and in each equation expresses the time derivative of of this species in terms of the usual mass-action products. By assigning numerical values to all the rate constants, and the initial concentration of the reactant known, this becomes an initial value problem in non-linear ordinary differential equation. As was pointed out in the last section (7.1), Gear's method offers both accurate and rapid solutions to initial value problems, and has been extensively used[26, 161] in kinetic modelling of hydrocarbon pyrolyses.

The computer program used in this work was based on the adaptation of Gear's method (available from the NAG library as a subroutine code named - DO2AJF), to the kinetic modelling of acetylene pyrolysis. The program makes use of methods of variable order upto a maximum of six, in which the order and the step-size are chosen automatically to try to obtain the required accuracy with minimum computation. A set of differential equations is formulated from the proposed mechanism(s) and incorporated to this library subroutine as an external routine. An outline of this numerical technique is described in the NAG Library Manual[162], while the details are available in the text by Gear[159].

An outline of the working procedure of this program as applied to the pyrolysis of shock-heated acetylene is given below (in section 7.3.1).

7.3.1 Computing procedure

1) A mechanism consisting of many elementary reactions was formulated and fed into the program.

2) Read in total number of reactions and species participating in the reaction; denote each chemical species by a number; for example, acetylene - 1, vinyl radical - 2, ethynyl radical - 3, vinylacetylene - 4, etc.

3) Values were assigned to the frequency - factors and the activation energies of reaction steps in the proposed scheme. These values were either literature values for the same reaction or estimated from known similar reactions.

4) Read in the experimental reaction temperature (T_5) and the initial concentrations of acetylene and argon corresponding to a particular shock tube condition; (the initial concentrations of other species at time, $t = 0$, are zero).

5) Set the error bound tolerance for each of the species.

6) Estimate a value for the initial step length; (this value will be automatically adjusted by the program if the assigned value is too high to enable numerical solution to be proformed within the error limit). The step length is a time interval which is a fraction of the total observation time for which the concentrations of the species are to be calculated.

7) Set an upper limit for the observation time (equal to total reaction time);

8) Calculate the rate constants at temperature (T_5) for each

step in the mechanism.

9) Call the Nag library subroutine D02AJF to integrate over the step length and calculate the concentration of each species. The subroutine checks whether the step length is sufficient to achieve the specified accuracy in the concentration of each species. If not, the step length is automatically adjusted.

10) At each successfully performed integration, calculate the rate of each elementary reaction.

11) Write out the reaction time, concentration of each species and rates of reaction.

12) Increase the reaction time by step length size and repeated the integration from step (9).

13) Steps (9) to (12) are repeated until the reaction time equals to the total observation time limit as in step (7).

14) Plot graphs of concentration versus reaction time for each species using a college subroutine.

7.4. Results of kinetic modelling

The infrared records obtained in the infrared region between 2.0µm to 5.3µm from shock-heated acetylene and discussed in chapter 6, do suggest that the pyrolysis of acetylene might involve complex kinetics.

The experimental results showed that the major structural groups that were present in the system are ≡CH, $=CH_2$, =CH- and -C≡C-. Both ≡ CH and -C≡C- detected at the wavelength intervals between 2.7 - 3.08µm and 3.5 - 5.0µm respectively are acetylenic bands, and since acetylene which is being pyrolyzed as well as the major hydrocarbon products of its decomposition all contain these functional groups, therefore, the comparison between the computed concentration profiles and the experimental results will be very difficult to achieve. Hence the following simple and straightforward procedure was adopted; the simulated concentration - time profiles for each stable reaction product were examined and compared individually to the experimental emission results. On this basis both the profiles of the product being examined and its concentration level relative to the other products had to be taken into consideration.

On the basis of the literature survey given in section 1.6.2.2, the major reaction products of acetylene pyrolysis at the temperatures covered in this study are known to be the following hydrocarbon, vinylacetylene, diacetylene, hexatriyne and polymeric (C_8) substances. Therefore, any reaction scheme to be proposed must account for the formation of these products. Various sets of reaction mechanism and their rate constants were compiled from literature and from these, on the whole two sets of reaction schemes (as in tables 7.0 and 7.1) emerged. These

Table 7.0: **Scheme I:** **Mechanism for the Pyrolysis of Acetylene**

	Reaction		Products	A	E_a (KJ/mole)	Reference
1.	$C_2H_2 + C_2H_2$	$\longrightarrow$	$C_4H_3^\bullet + H^\bullet$	10^{11}	185.2	130
2.	$C_4H_3^\bullet + C_2H_2$	$\longrightarrow$	$C_4H_4 + C_2H^\bullet$	10^{8}	41.8	130
3.	$C_4H_3^\bullet$	$\longrightarrow$	$C_4H_2 + H^\bullet$	10^{14}	250.8	130
4.	$C_2H_2 + C_2H^\bullet$	$\longrightarrow$	$C_4H_2 + H^\bullet$	10^{11}	0.0	169
5.	$C_2H_2 + H^\bullet$	$\longrightarrow$	$C_2H^\bullet + H_2$	$10^{11.3}$	79.4	130
6.	$C_4H_2 + C_2H^\bullet$	$\longrightarrow$	$C_6H_2 + H^\bullet$	10^{8}	12.5	130
7.	$C_2H_2 + H^\bullet$	$\longrightarrow$	$C_2H_3^\bullet$	10^{10}	27.2	130
8.	$2C_2H_3^\bullet$	$\longrightarrow$	Products (polymer)	$5\text{x}10^{8}$	30.66	167
9.	C_4H_4 (+M)	$\longrightarrow$	$C_4H_2 + H_2$ (+M)	10^{13}	209	* 173
10.	C_4H_2 + M	$\longrightarrow$	$C_2H_2 + C_2$ (+M)	$1.8\text{x}10^{17}$	77.2	* Estimated
11.	C_6H_2 + M	$\longrightarrow$	$C_6 + H_2$ + M	$2\text{x}10^{14}$	189	*168

Table 7.1: Scheme II - Using Back's Initiation step

		A	E_a (KJ/mole)	Reference
1.	$C_2H_2 + C_2H_2 \longrightarrow C_2H^{\bullet} + C_2H_3^{\bullet}$	5.0×10^{12}	70×4.2	131
2.	$C_2H^{\bullet} + C_2H_2 \longrightarrow C_4H_3^{\bullet}$	7.0×10^{8}	6.5×4.2	131
3.	$C_4H_3^{\bullet} + C_2H_2 \longrightarrow C_4H_4 + C_2H^{\bullet}$	10^{8}	41.8	130
4.	$C_4H_3^{\bullet} \longrightarrow C_4H_2 + H^{\bullet}$	10^{14}	44.0×4.2	131
5.	$C_2H_2 + H^{\bullet} \longrightarrow C_2H^{\bullet} + H_2$	$10^{11.3}$	79.4	130
6.	$C_2H_2 + H^{\bullet} \longrightarrow C_2H_3^{\bullet}$	10^{10}	27.2	130
6(b)	$C_2H_3^{\bullet} + M \longrightarrow C_2H_2 + H^{\bullet}\ (+M)$	7.94×10^{11}	31.5×4.2	167
7.	$C_4H_2 + C_2H^{\bullet} \longrightarrow C_6H_2 + H^{\bullet}$	10^{8}	12.5	130
8.	$C_2H^{\bullet} + H^{\bullet} \longrightarrow C_2 + H_2$	10^{-10}	35.6×4.2	171
9.	$C_4H_4 + M \longrightarrow C_4H_2 + H_2 + M$	10^{14}	209.0	*173
10.	$C_4H_2 + M \longrightarrow C_2H_2 + C_2 + M$	1.8×10^{17}	77.2	*Estimated
11.	$C_6H_2 + M \longrightarrow C_6 + H_2 + M$	2×10^{14}	189	* 168

were based on the extension of the mechanisms proposed by Cullis et al[130] and that due to Back[131] for high temperature regimes to include the formation of the various high polyacetylenes. These two mechanisms were extensively tested and examined by computer simulation. For more detailed analysis secondary reactions of the initial decomposition products and the formation of carbonaceous materials were also considered.

Numerical integration of the differential equations formulated were carried out for each trail sets of reaction mechanism. In each case, the experimental conditions - temperature and composition of the reactants - were used for integration according to the procedure outlined previously in section 7.3.1. Comparison of the calculated concentration - time profiles and the experimental emission results was accomplished with the aid of computer generated plots of concentration versus reaction time for all the stable products. Trial - and - error searches for successful combinations of different reactions and rate data to achieve profile matching were made. In order to overcome the observed discrepancies in profile matching, the technique of evaluating the effects of introducing or removing reaction steps was adopted so that an appropriate mechanism could be identified. After all the various possible reaction combinations have been examined, the following two sets of reaction mechanism - schemes I and II - emerged and are discussed below.

7.4.1. Scheme I: Using Cullis' initiation step.

This scheme is shown in table 7.0; it consists of 11 reaction steps in which the following initial step,

$$2\ C_2H_2 \longrightarrow C_4H_3^{\bullet} + H^{\bullet}$$

was used. Scheme I is a detailed version of the reaction mechanism proposed by Cullis et al[130] in which additional reactions involving the secondary reactions of the primary products, as well as the formation of higher polymers was examined. The rate constants for the reaction steps and the sources from which they were obtained are also given in the table. In cases where estimates of the rate constants had to made, the choice of those data had been based on those of very similar reactions; such rate constants are marked*.

7.4.1.1. Predicted concentration profiles of the stable products.

The typical computed results of the concentration - time profiles of acetylene and the major reaction products are shown in figures 7.1 to 7.4 at the specified reflected shock temperatures.

a) Acetylene

Figure 7.1 shows the predicted concentration profiles of acetylene from shock-heated mixture of C_2H_2 and argon. The concentration of acetylene decreased with increasing reaction time for all temperatures. The rate of decomposition was slower at the lower temperatures than at higher temperatures. On thermodynamic grounds the predicted decomposition rates at temperatures above 1900°K are too high and therefore unacceptable. Hence computations beyond this temperature needed modifications in the proposed scheme. This is discussed later.

Figure 7.1: Computed concentration profile for acetylene

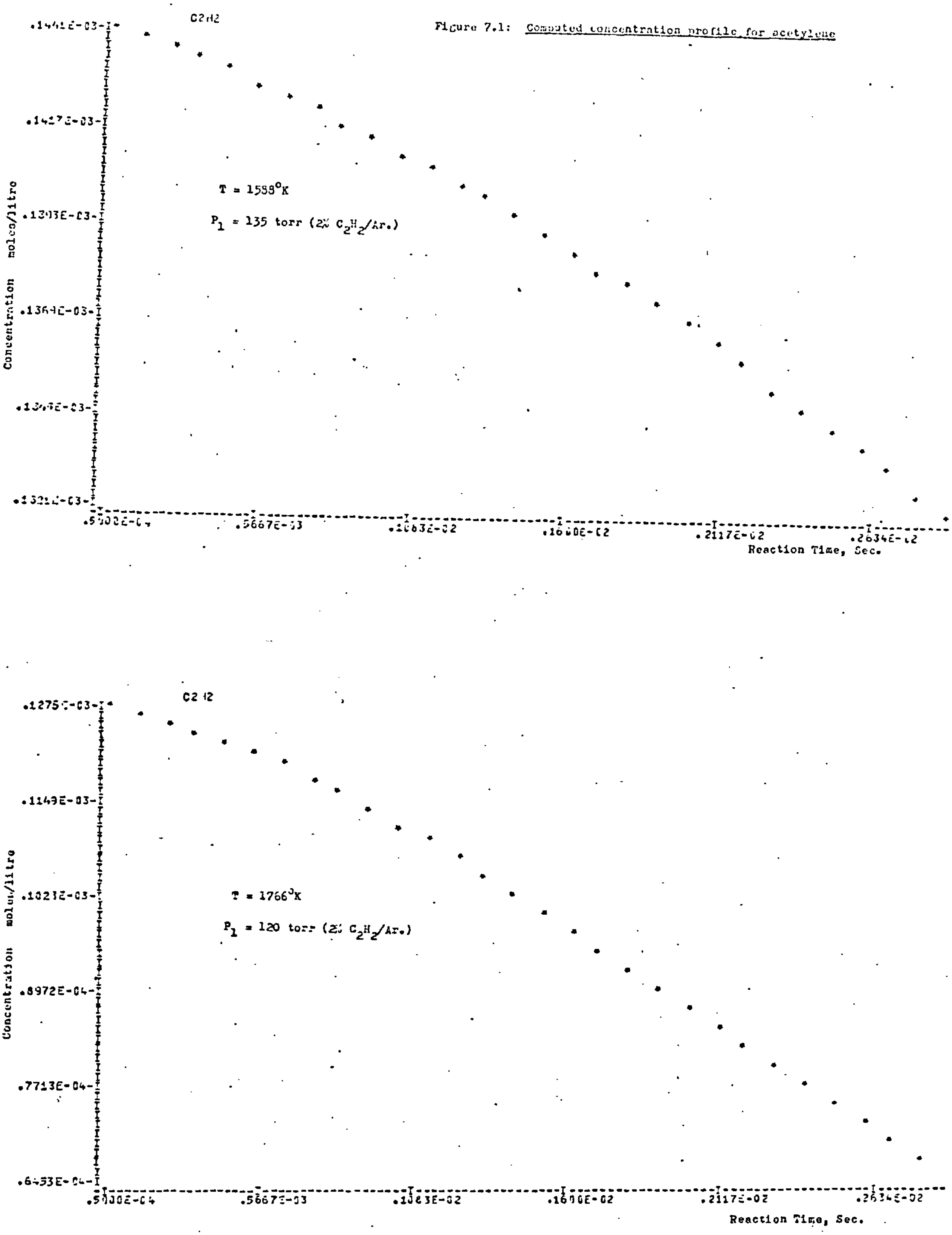

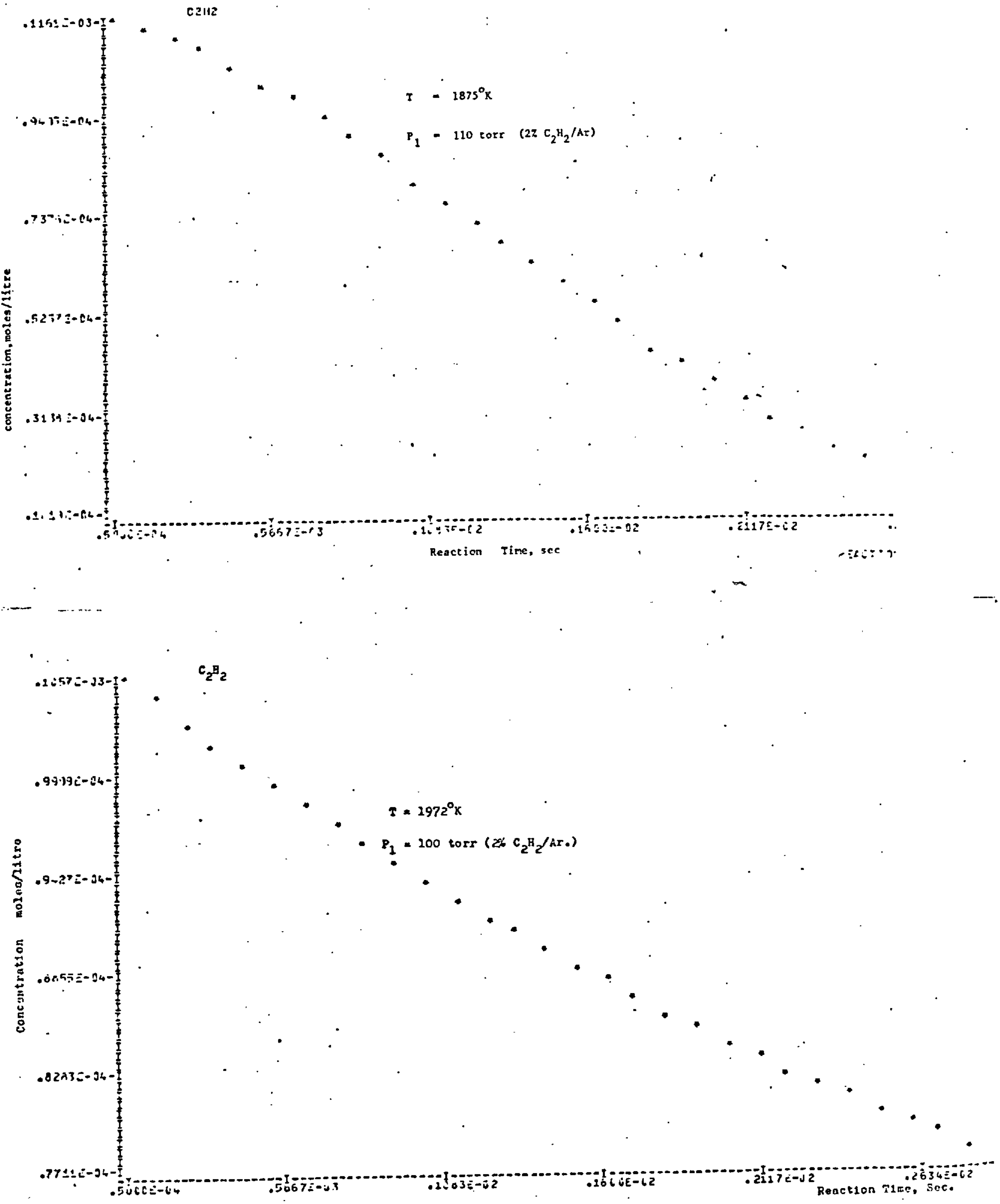

Figure 7.1: Contd.

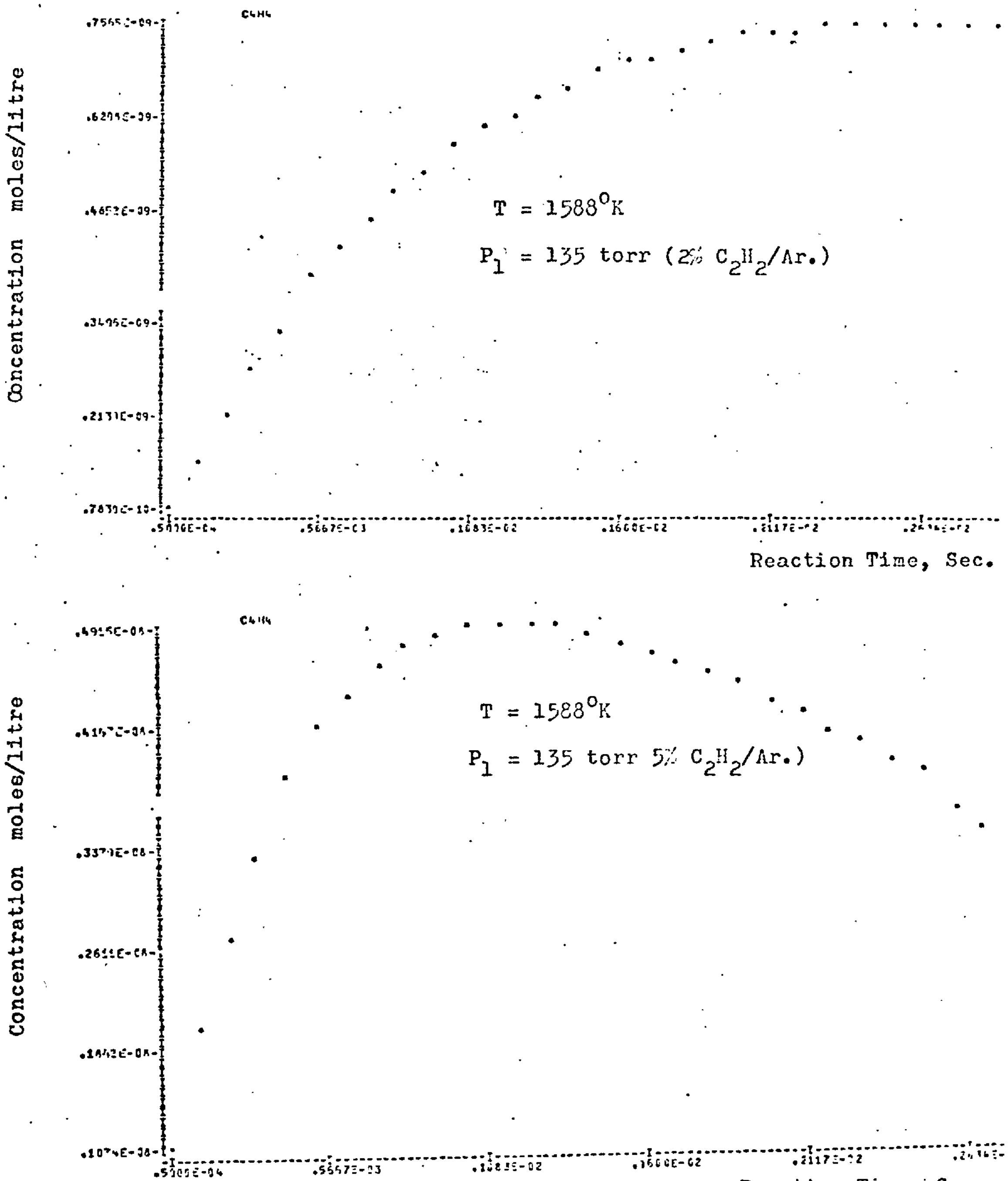

(a)

Figure 7.2: Computed profile of vinylacetylene, C_4H_4

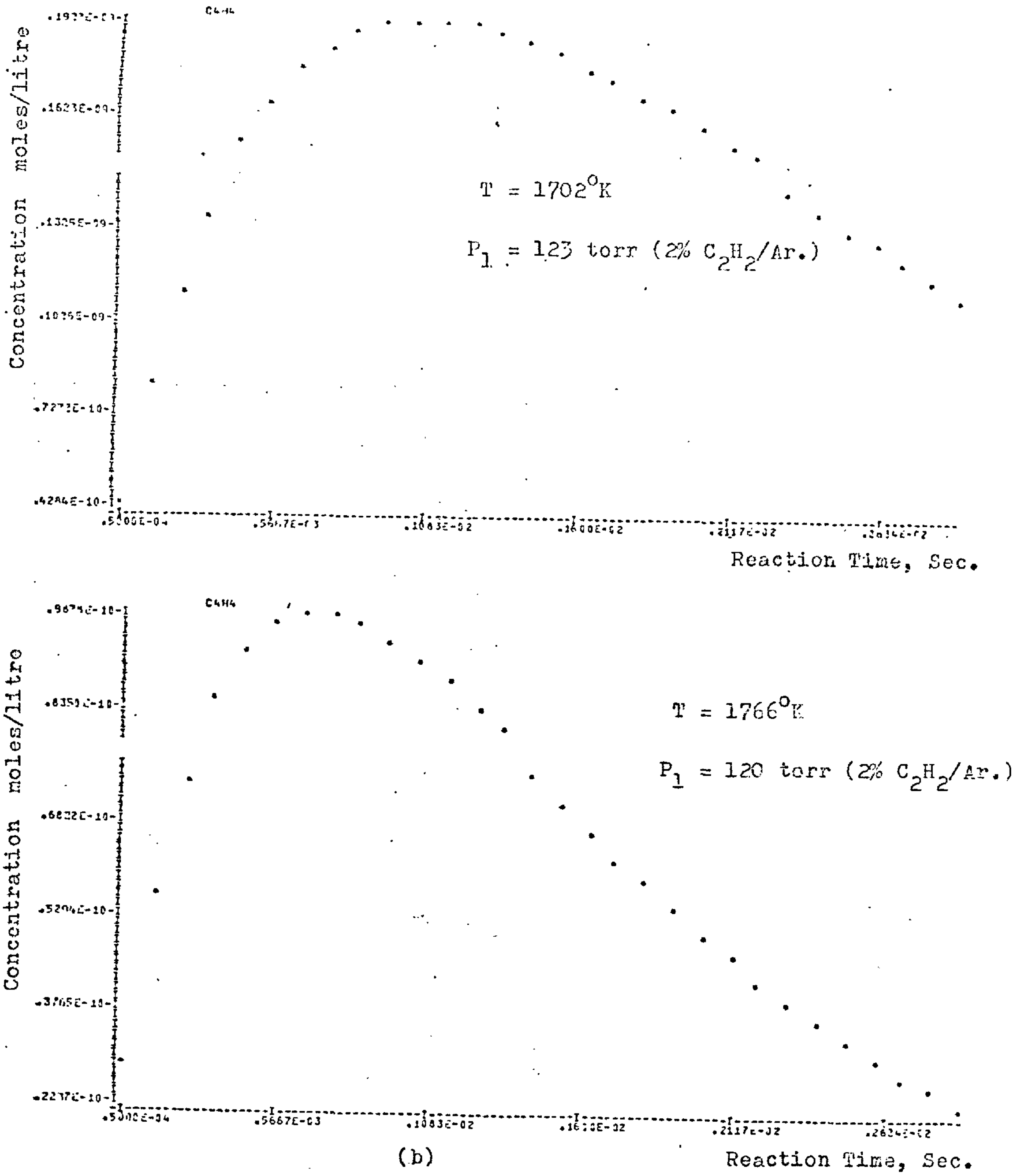

(b)

Figure 7.2: Computed profile of vinylacetylene, C_4H_4

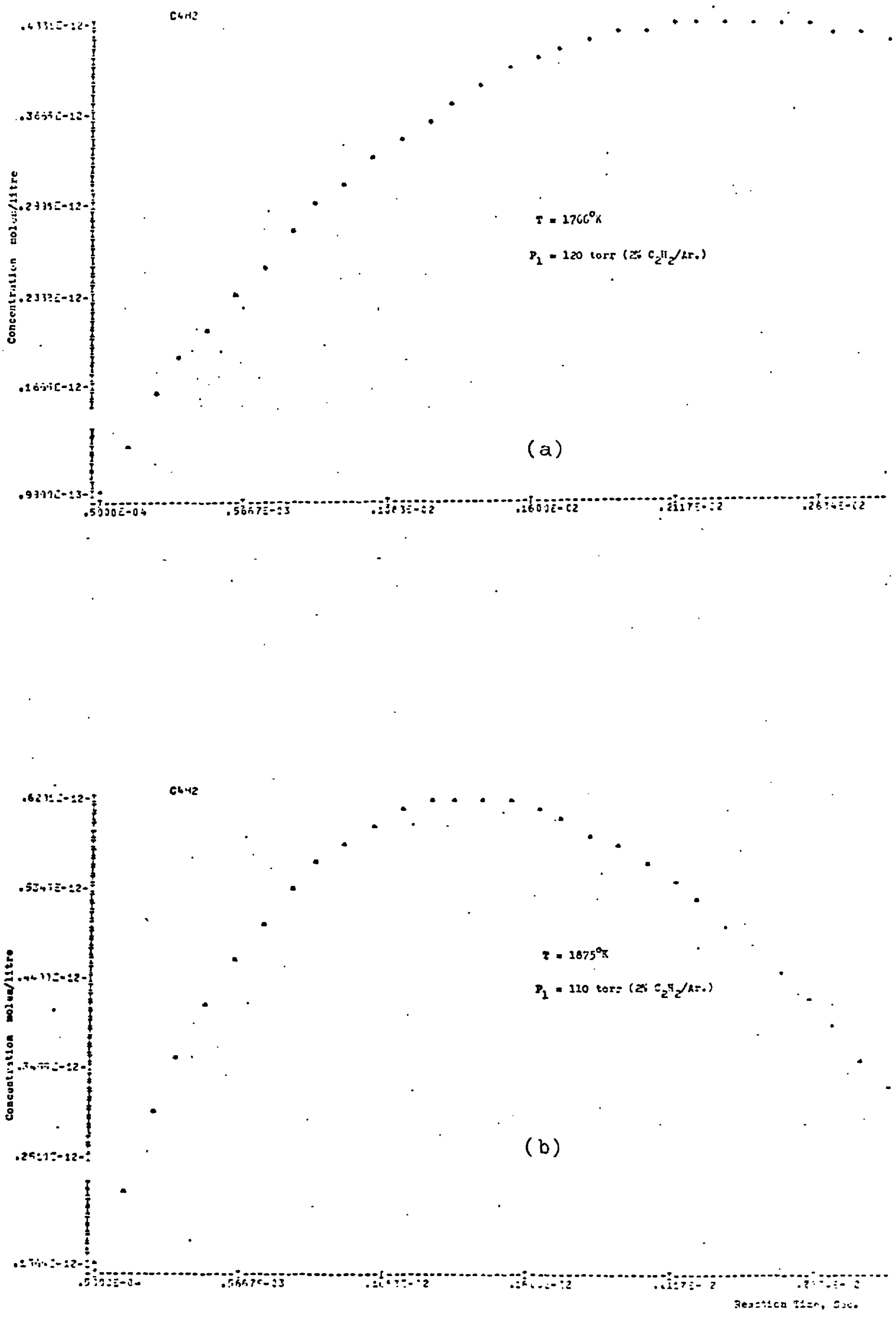

Figure 7.3: Computed profiles for diacetylene, C_4H_2

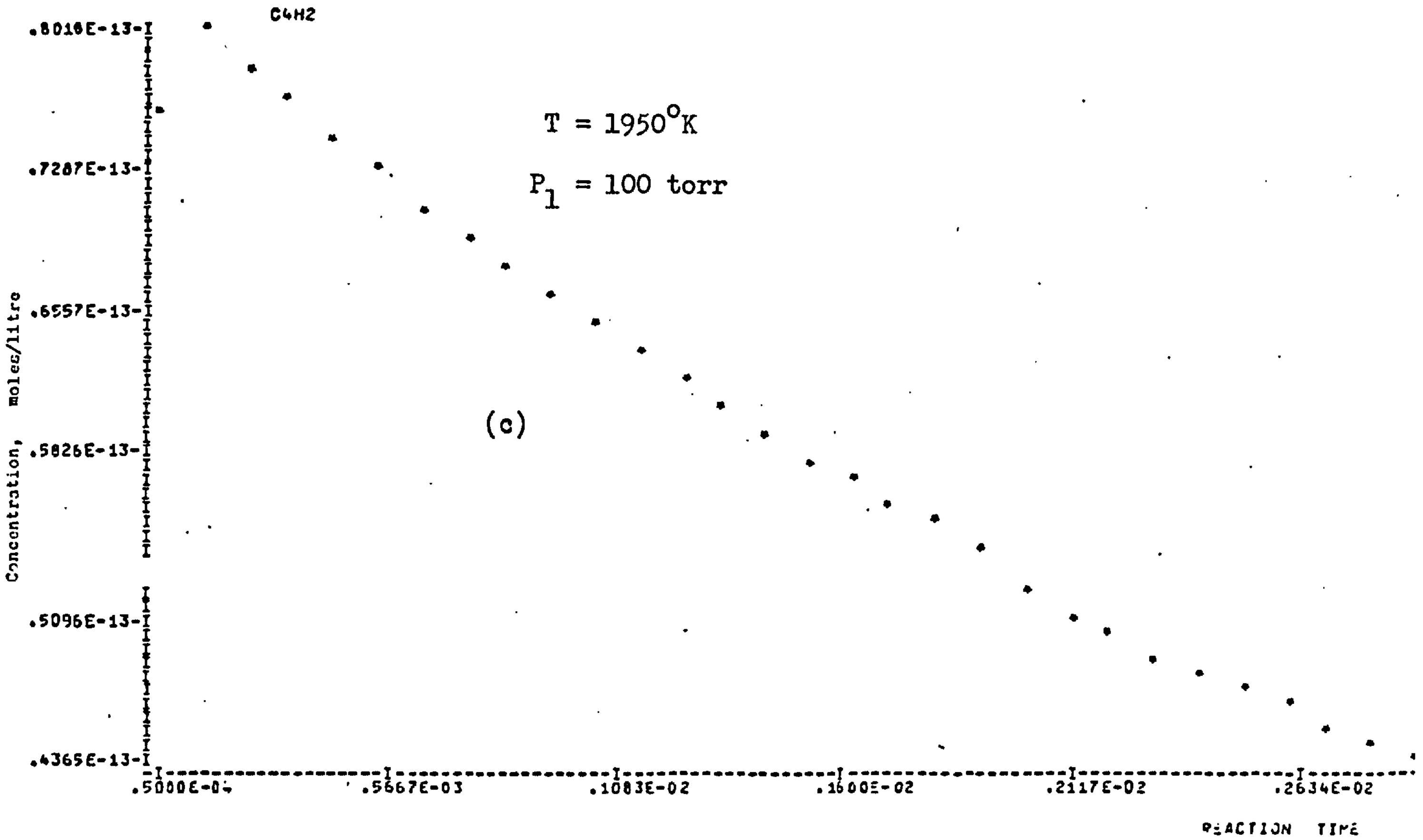

FIGURE 7.3 CONTD.

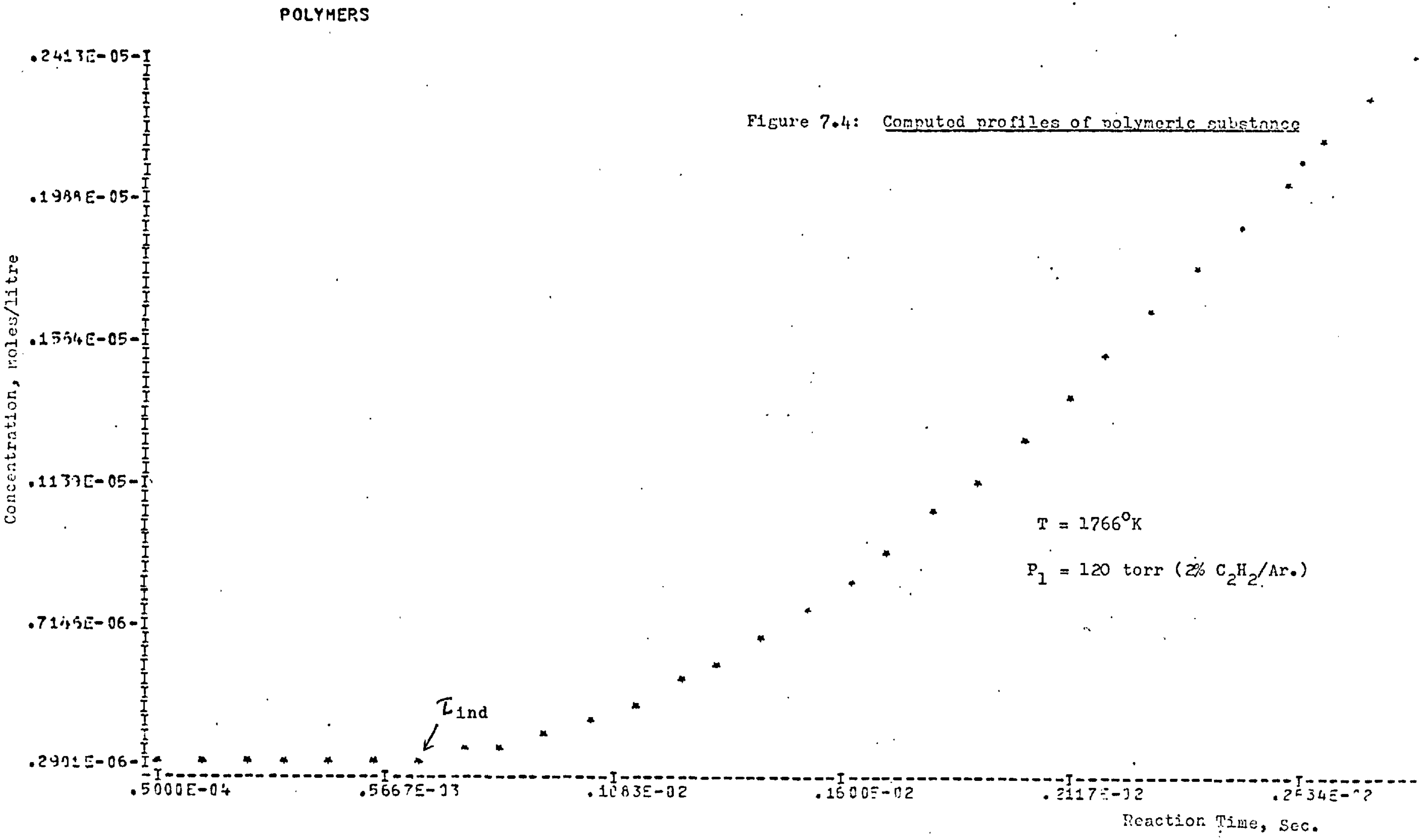

Figure 7.4: Computed profiles of polymeric substance

T = 1766°K

P_1 = 120 torr (2% C_2H_2/Ar.)

b) Vinylacetylene, C_4H_4

The concentration - time profiles for vinylacetylene is shown in figures 7.2. The concentration of vinylacetylene increased with reaction time to a maximum value and then started to fall, except for 2% C_2H_2/argon in where, at temperatures under 1590°K, the maximum value was not reached within the set computational time limit of 3.0ms. The time that elapsed before the maximum concentration was attained shortened progressively with increase in reaction temperature.

c) Diacetylene, C_4H_2

The concentration profiles of diacetylene (shown in figures 7.3 (a to c) were similar to those of vinylacetylene, except that in this case the maximum concentration was reached at much later reaction time; the time taken for the predicted concentration of C_4H_2 to pass through maximum also decreased with temperature ; this is illustrated by the following values in table 7.2 .

Table 7.2: Time, t_{max}, taken for the computed concentration of product to pass through maximum during the pyrolysis of 2% C_2H_2/Argon.

Reaction temperature , °K	Time, t_{max}, (ms)	
	C_4H_4	C_4H_2
1608	2.06	-
1702	1.08	3.3
1766	0.69	2.6
1875	0.49	1.40

The predicted concentration of vinylacetylene was generally higher than those of diacetylene by a factor of 10^3 at $T < 1875^{o}K$, but at $T > 1900^{o}K$, C_4H_4 rapidly builds up and decays, while the concentration of C_4H_2 increases and exceeds that of C_4H_4.

d) Polyacetylenes

The concentrations of C_6H_2 were insignificant relative to the other compounds, The computed concentrations of these polyacetylenes increased gradually from zero at the early stages of the reaction but later accelerated. The plot of the computed concentrations of the polymeric product formed by the recombination of two vinyl radicals to C_4H_6 denoted by 'polymer' is shown in figures 7.4 . These figures show that the plot displayed a characteristic induction period during which there was little change in the concentration levels of these products. The length of the induction period decreased with increasing temperature in the following manner for a reaction mixture of 2% acetylene in argon:

Temperature, ^{o}K	Induction time, ms (computed)
1508	1.255
1608	0.830
1875	0.600

The values predicted by this scheme showed that the concentrations these polymeric products and 'carbon' particles were quite substantial.

7.4.1.2. Comparison* of experimental with modelled results obtained by scheme I.

Comparison between the modelled profile and:

i) The acetylenic ≡CH and -C≡C- functional groups at the wavelength intervals 2.60 - 3.08μm and 3.5 - 5.3μm respectively.

The predicted concentration profiles of acetylene at all temperatures do not bear any resemblance to the emission profiles at any of the four spectral regions investigated. Since acetylene was present initially in the reaction mixture, it would be anticipated that at least, at the region 2.60 - 3.08μm, where the vibrational frequency of ≡CH group in acetylene is known to exist and is particularly strong, the infrared emission profile should have been identical to the predicted concentration - time profiles, for acetylene. This discrepancy has been discussed earlier in section (6.2.0) and the only possible explanation is that due to high rates of formation of other alkynes, the infrared emission follows the concentration profile of these products.

The predicted concentration profiles for both C_4H_4, and C_4H_2, are identical to the emission - time plots for ≡CH and -C≡C- group. However, there are discrepancies between the different times at which the computed concentration of these compounds passed through maximum and those for which the infrared emission reached maximum value before decaying. These times are shown in table 7.3.

The other compounds containing both ≡CH and -C≡C- groups are C_6H_2 and C_8H_2 but their predicted concentration profiles did not follow the pattern of the emission time plots, and

---

* This is based on the assumption [52] that the emission intensity is proportional to the concentration of the emitting species.

Table 7.3: Time taken to reach maximum value by emission due to ≡CH and -C≡C- groups and the computed concentrations of C_4H_4 and C_4H_2.

Reaction temperature, ^oK	% C_2H_2 in Argon	t_{max} (ms) for			
		Infrared emission due to		computed concentrations of	
		≡CH	−C≡C−	C_4H_4	C_4H_2
1395	5	2.2	2.0	No maxima	
1592	2	2.0	-	2.45	-
1583	5	-	1.4	1.18	3.04
1766	2	1.2	-	0.69	2.60
1740	5	-	0.8	-	1.42
1875	2	0.8	-	0.49	1.40

Table 7.4: Time taken for Experimental emission at 3.32μm and modelled concentrations of C_4H_4 to reach maximum value

Temperature, °K	Time taken to reach maximum (ms)	
	Experimental $=CH_2$ Emission	Predicted Conc. of C_4H_4
1588	1.8	2.45
1702	1.8	1.20
1766	1.0	0.69
1875	0.8	0.49
1972	0.8	0.40

moreover, even if they were formed, the predicted concentration levels for them are so minute relative to those of C_4H_4 and C_4H_2 as to have any significant influence on the intensity of the emission at these wavelength regions.

ii) $=CH_2$

The only major product in the model that contains double bond structure is vinylacetylene and C_4H_6 if it is assumed[118] that the product formed by the recombination of two vinyl radicals is butadiene. The predicted concentration profiles for both of these compounds from reaction scheme I did not precisely match the emission profiles at temperatures under 1702°K, especially the characteristic fall in the intensity of the infrared emission which preceeded the observed peak broadening phenomenon. But the general trend of increase in emission intensity with time to pass through maximum closely matched the profiles of C_4H_4. An example of such profile comparison is shown in figure 7.5 at T = 1875°K. Time taken for the emission intensity at 3.32µm to reach maximum is compared with the predicted t_{max} for the concentration of vinylacetylene and diacetylene in table 7.3.

iii) Polymers

The predicted concentration profiles of the polymeric product formed from the reaction

$$2C_2H_3 \longrightarrow \text{products}$$

showed a characteristic feature of induction time which closely matched the experimental induction time obtained at the wavelength interval 2.0 - 2.7µm. Since no other products

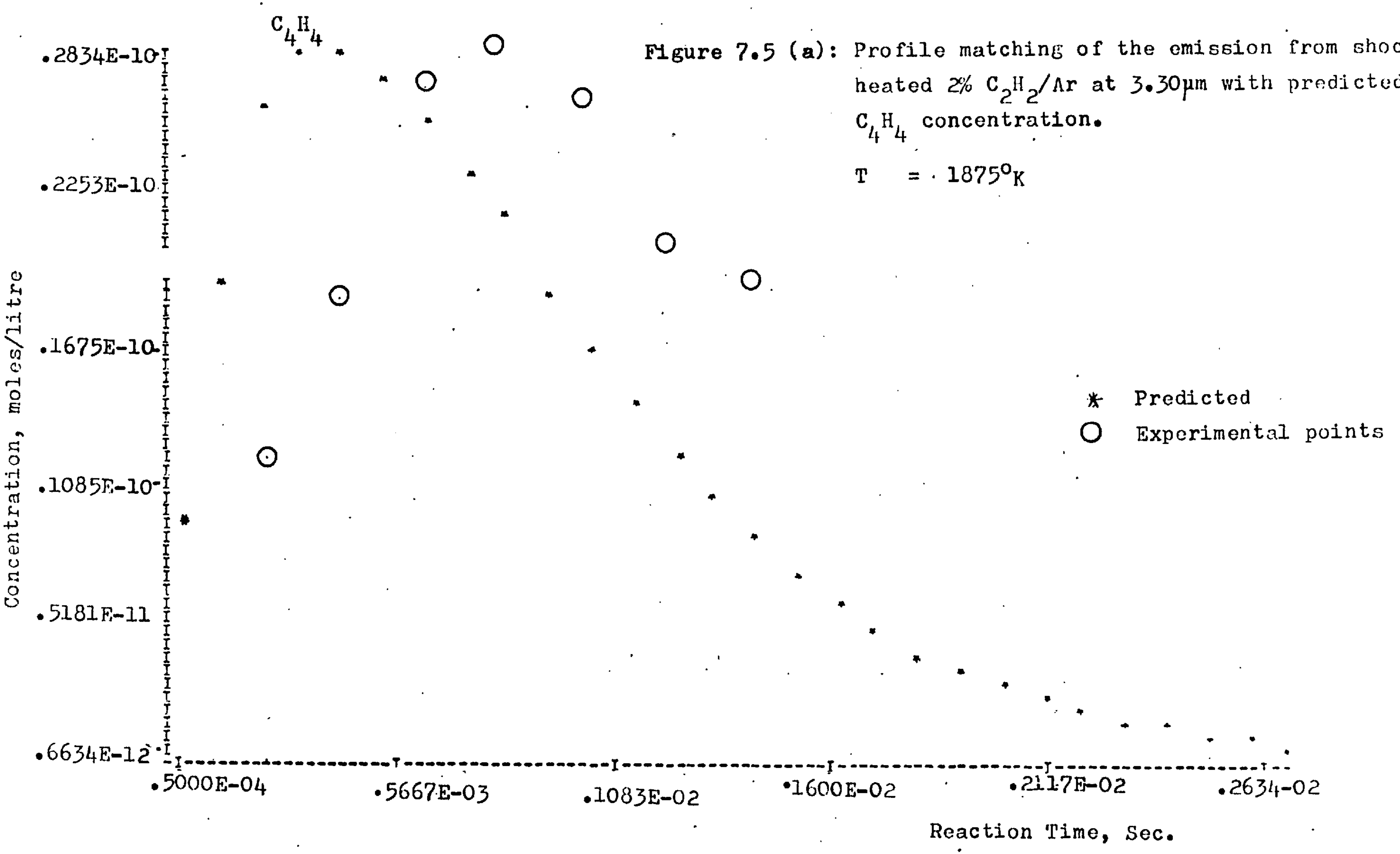

Figure 7.5 (a): Profile matching of the emission from shock-heated 2% C_2H_2/Ar at 3.30µm with predicted C_4H_4 concentration.

T = 1875°K

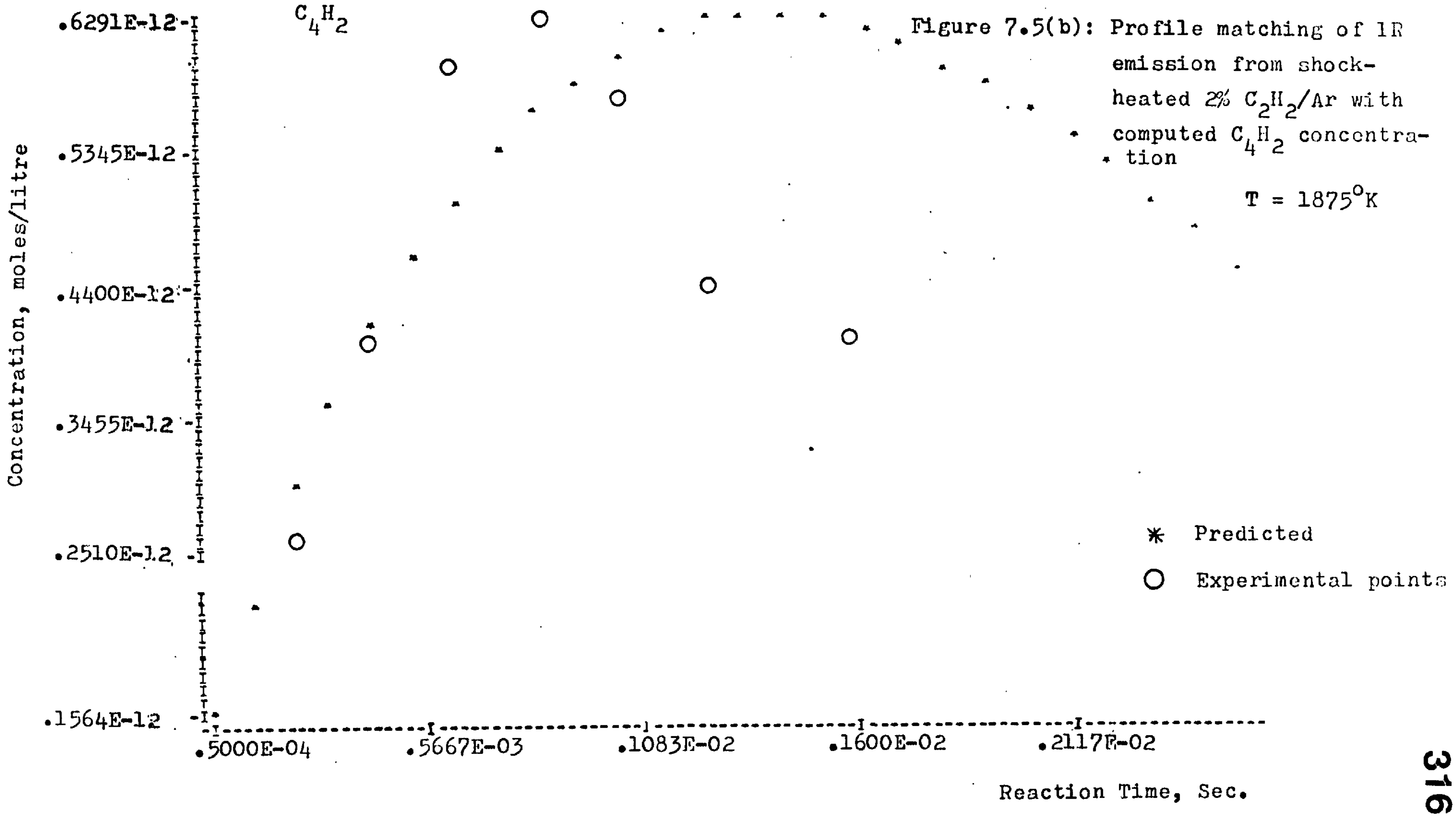

Figure 7.5(b): Profile matching of IR emission from shock-heated 2% C_2H_2/Ar with computed C_4H_2 concentration

$T = 1875^{o}K$

displayed such induction characteristics similar to the experimental induction time, it could be assumed that these polymers are responsible for the emission results at the wavelength region under 2.7µm. Table 7.5 illustrates this fact.

Table 7.5: Comparison between experimental and computed Induction times

Temperature, °K	Induction time, ms	
	Experimental	Computed.
1508	1.20	1.255
1592	1. 0	1. 0
1875	-	0.600
1896	0.70	-

At temperatures higher than 1975°K, the extended Cullis model failed to produce satisfactory concentration - time profiles for any of the products; at high temperatures and for reaction time as short as 0.5ms the predicted rates became too high, and the rates of consumption of these products exceeded the rates of their formation and hence computation beyond 0.5ms reaction time was not possible. The results modelled from scheme 1 and shown in tables (7.3 to 7.5) show that at temperatures under 1972°K, the predicted concentration-time profiles for C_4H_4, C_4H_2 and C_4H_6 were very similar to the experimental infrared emission records. But at higher temperatures the predicted rates became too high and the.

scheme failed to produce satisfactory concentration profiles for the major reaction products, and this necessiated the re-examination of certain reaction steps by observing the effects of their withdrawal from the scheme. Such tests proved that the secondary reactions involving the primary products are mandatory inorder to explain the observed profiles. Withdrawing such reactions as (R9-11) from the scheme shown in table 7.0 had significant effect on the concentration - time profiles of the reaction products; their profiles did not pass through maxima when the secondary reactions were not considered. The inclusion of reaction (9)

$$C_4H_4 \xrightarrow{K_9} C_4H_2 + H_2 \qquad (9)$$

was based on the experimental findings by Cullis and Franklin[112] at temperatures upto 1300°K and the suggestions by others[110,118] that vinylacetylene formed at the early stages of the reaction was being converted to diactylene. This reaction was assumed to be indentical to;

$$C_2H_4 \longrightarrow C_2H_2 + H_2$$

and the value of K_9 was estimated on this basis.

The participation of secondary reaction (10)

$$C_4H_2 \longrightarrow C_2H_2 + C_2 \qquad (10)$$

during the pyrolysis of acetylene has been suggested by Kozlov and Knorre[25] to be important at high temperatures. They have explained the decrease in the decomposition rate of acetylene at higher temperature in terms of two main reactions(a) and (10)

$$C_2H_2 + C_2H_2 \longrightarrow C_4H_2 + H_2 \qquad (a)$$

and

$$C_4H_2 \longrightarrow C_2H_2 + C_2 \qquad (10)$$

In which reaction (a) is the initial reaction at low temperatures. But as the temperature increases the rate of reaction (10) begins to exceed that of its acetylene formation; this leads to a transition in the high temperature regions and results in thermal decomposition of acetylene taking place mainly on the carbon participles.

Similar tests showed that the following reactions;

$$2C_2H_3^{\bullet} \longrightarrow \text{product } (C_4H_6)$$

$$C_6H_2 + C_2H^{\bullet} \longrightarrow C_8H_2$$

$$C_8H_2 \ (+\ M) \longrightarrow C_8 + H_2 \ (+M)$$

become less important at $T > 1900^{o}K$; their withdrawal enabled the computation to be carried out upto $2400^{o}K$. Computations performed with the exclusion of these reactions did not predict t_{max} for the formation of C_4H_4, while the concentration - time profiles of C_4H_2 and C_6H_2 were similar to experimental results. The concentration - time profiles for the different products using this modified version of scheme I are shown in figures(7.6 to 7.9). However, the predicted t_{max} at these temperatures were quite outside the experimental values. Therefore, alternative reaction steps were sought which could produce a better match between the

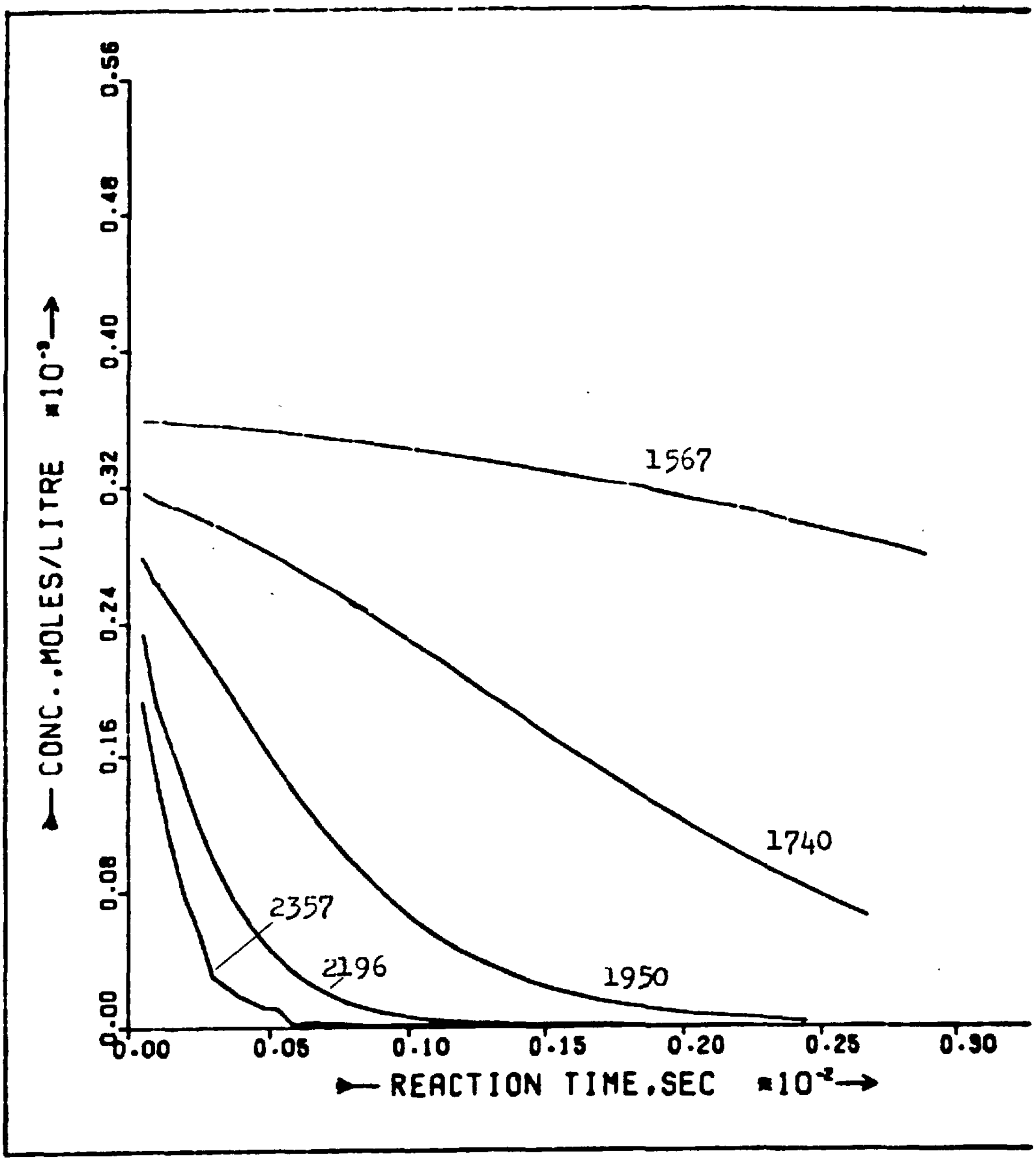

FIGURE 7.6: MODELLED CONCENTRATION - TIME PROFILES FOR C_2H_2 DURING THE PYROLYSIS OF 5% C_2H_2/Ar. MIXTURE USING SCHEME I.

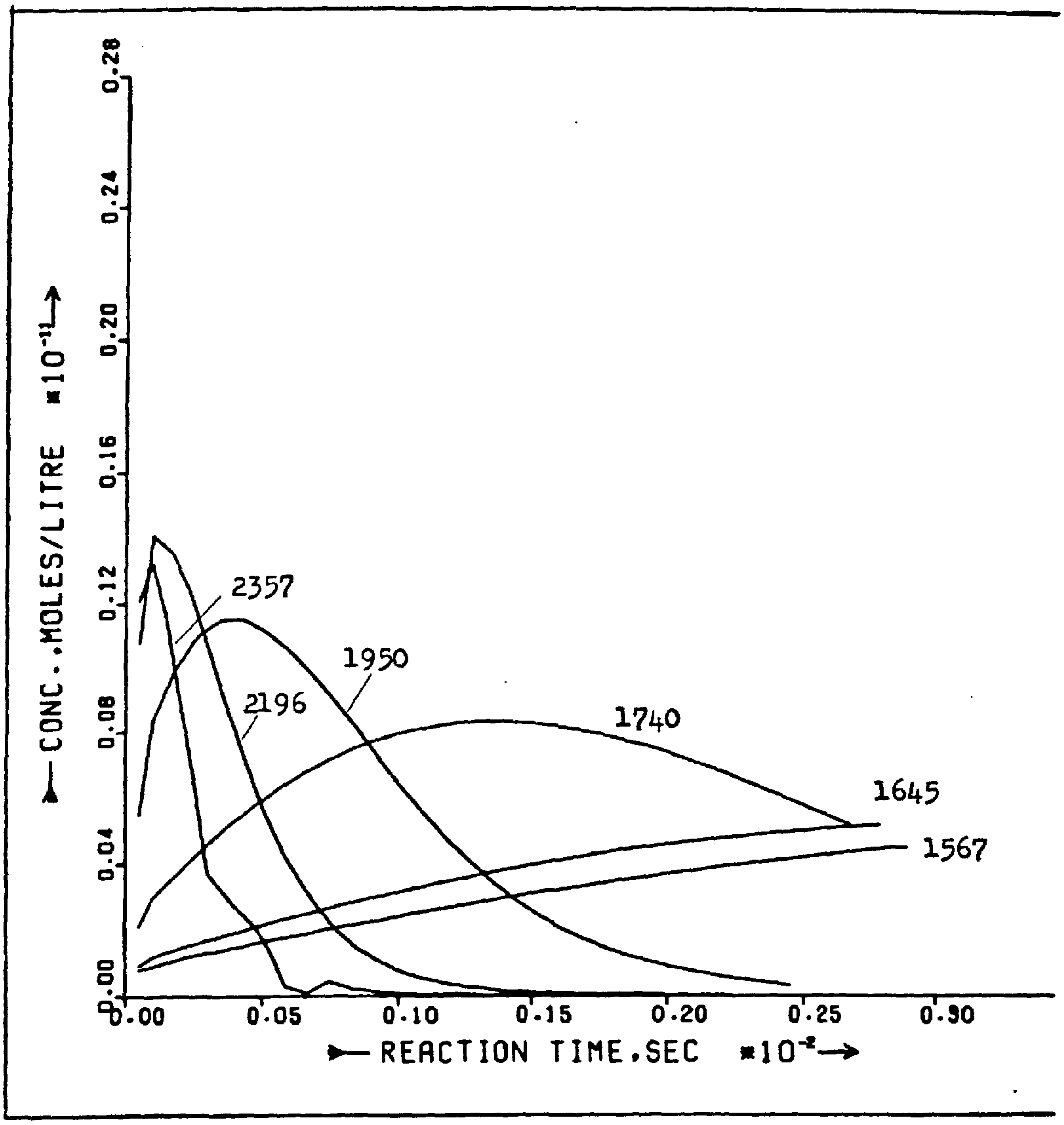

FIGURE 7.7: MODELLED CONCENTRATION - TIME PROFILES FOR C_4H_2 DURING THE PYROLYSIS OF 5% C_2H_2 IN ARGON, USING SCHEME I.(TABLE 7.0)

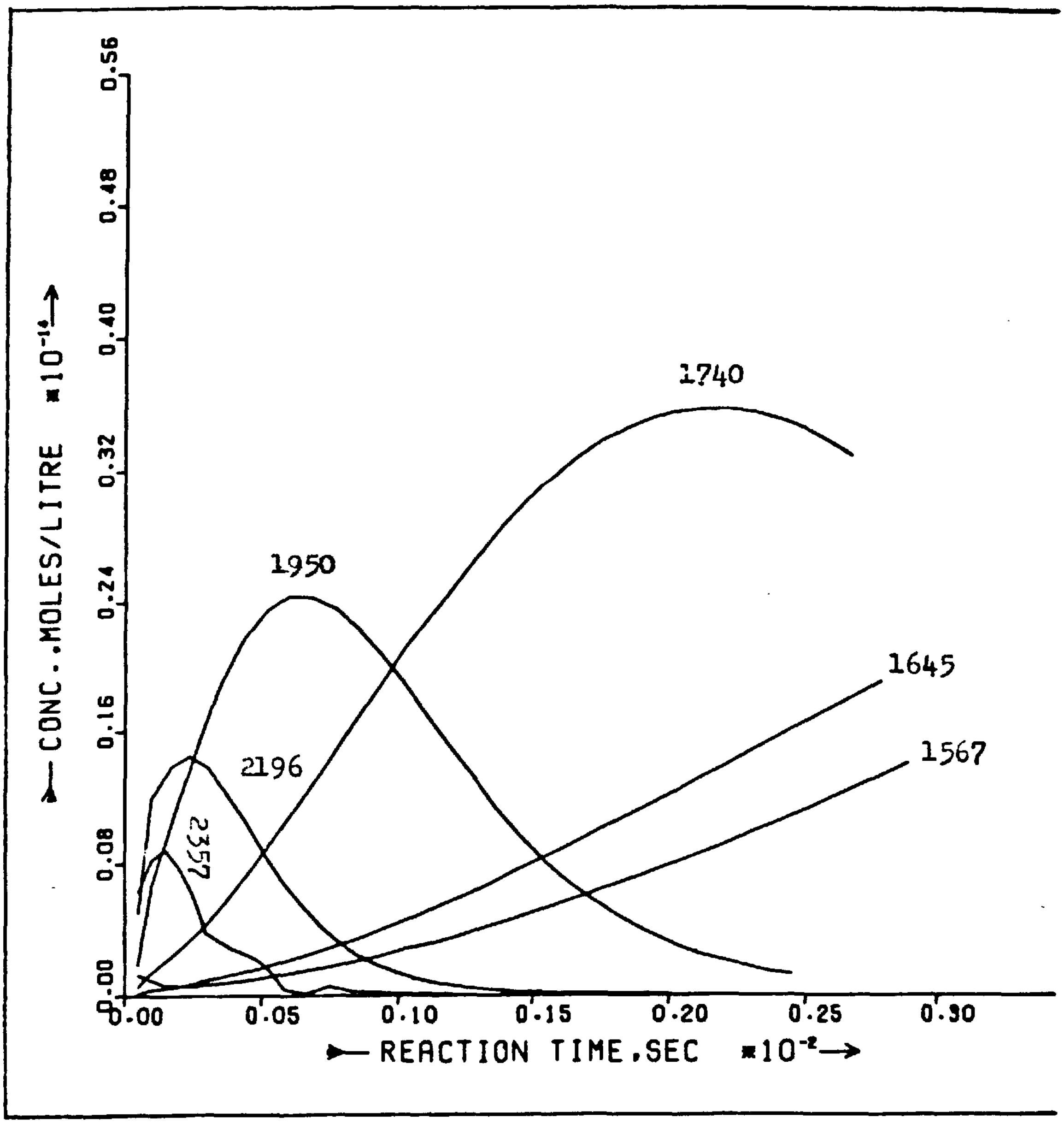

FIGURE 7.8: MODELLED CONCENTRATION - TIME PROFILES FOR C_6H_2 DURING THE PYROLYSIS OF 5% C_2H_2 IN ARGON, USING SCHEME I (7.0)

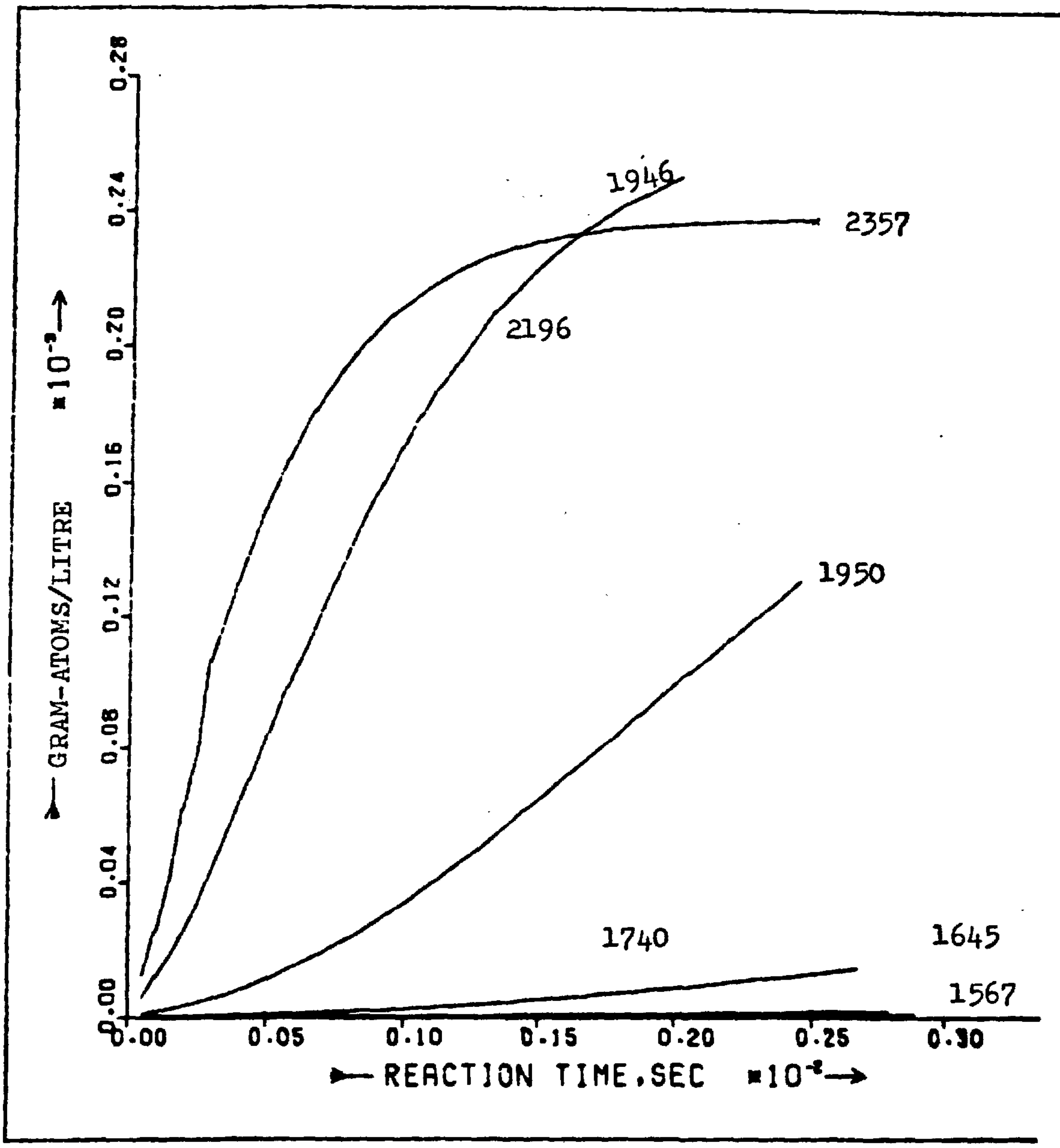

FIGURE 7.9: PREDICTED CONCENTRATION - TIME PROFILES FOR 'CARB FORM MECHANISM IN TABLE 7.0 (SCHEME I) FOR THE PYROLYSIS OF 5% C_2H_2/Ar.

predicted and experimental t_{max}. It was found that using the initiation step suggested by Back,[131]

$$2C_2H_2 \longrightarrow C_2H_3^{\bullet} + C_2H^{\bullet}$$

in the place of

$$2C_2H_2 \longrightarrow C_4H_3^{\bullet} + H^{\bullet}$$

due to Cullis et al[130], reasonable high temperature results were obtained. Alternative version of scheme I in which the Back's initiation reaction was used is designated as scheme II, and is discussed below in the next section.

7.4.2 Scheme II - Using Back's initiation step

In this scheme the initiation step in the decomposition is a bimolecular disproportion reaction to give $C_2H^{\bullet}$ and $C_2H_3^{\bullet}$ radicals [131]. The proposed reaction mechanism is shown in table 7.1 and as in scheme I, the secondary reactions were considered.

The computed concentration - time profiles of the major reaction products from this reaction scheme is shown in figures (7.10 to 7.14) at different reaction temperatures. As in scheme I, the predicted concentrations of C_4H_4, C_4H_2, C_6H_2 and carbon increased with reaction time and at temperatures from 1950°K and above these concentrations passed through maxima. The concentration profiles of acetylene decreased with time. At temperatures upto 1740°K, the rate of decrease was very small but the rate increased rapidly at higher temperatures. From temperatures around 2100°K, the computed results showed that C_2H_2 does not undergo any appreciable decomposition after about 2.0ms. Thus showing that scheme II is thermodynamically more feasible than scheme I.

The plots of the predicted concentration - time profiles of acetylene and the reaction products at various temperatures for reaction mixture of 2% and 5% of C_2H_2 in argon are shown in figures (7.10 to 7.14) and labelled as follows:

figures(7.10 a & b): showing the dependence of concentration time profiles of C_2H_2 on reflected shock temperature.

figures(7.11): showing the variation of concentration time profile of vinylacetylene with reaction temperature.

figures(7. 12 a & b): showing the concentration - time profiles for diacetylene at different temperatures.

figures(7. 13 a & b): showing the concentration - time profiles for hexatriyne.

figures(7. 14): showing the increase in quantity of carbon yield with temperature during pyrolysis of C_2H_2

A comparison between the emission time plots for both ≡CH and -C≡C- groups in figures (6.12 & 6.14) and the predicted concentration profiles in figures (7.10 a &b)for C_2H_2 do not show any similarity. And therefore like the previous reaction

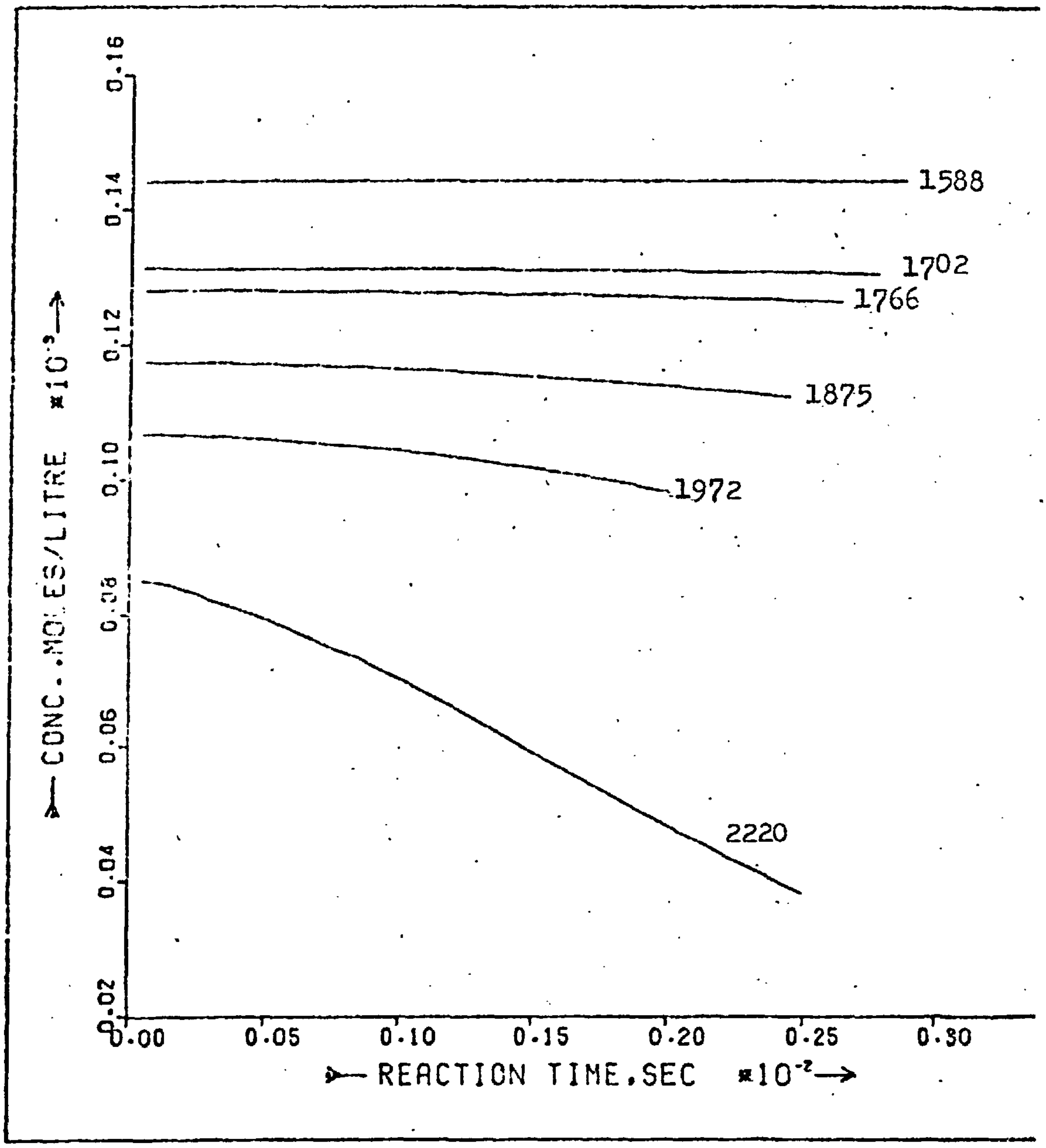

FIGURE 7.10(A): CONCENTRATION-TIME PROFILES FOR C_2H_2, DURING THE PYROLYSIS OF 2% C_2H_2 IN ARGON, MODELLED ACCORDING TO SCHEME II IN TABLE 7.1.

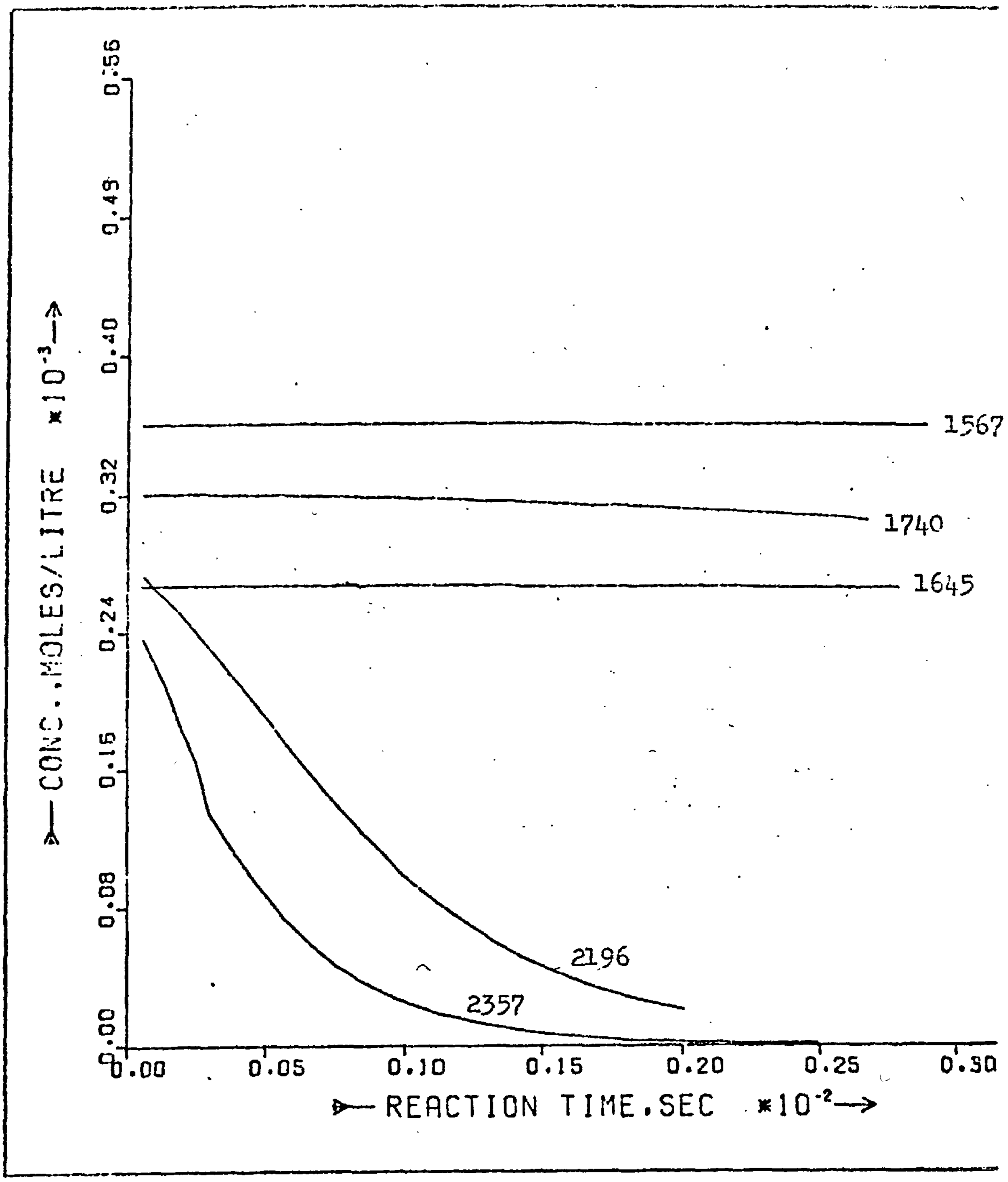

FIGURE 7.10(B): CONCENTRATION-TIME PROFILES FOR C_2H_2, DURING THE PYROLYSIS OF 5% C_2H_2 IN ARGON, MODELLED ACCORDING TO SCHEME II IN TABLE 7.1.

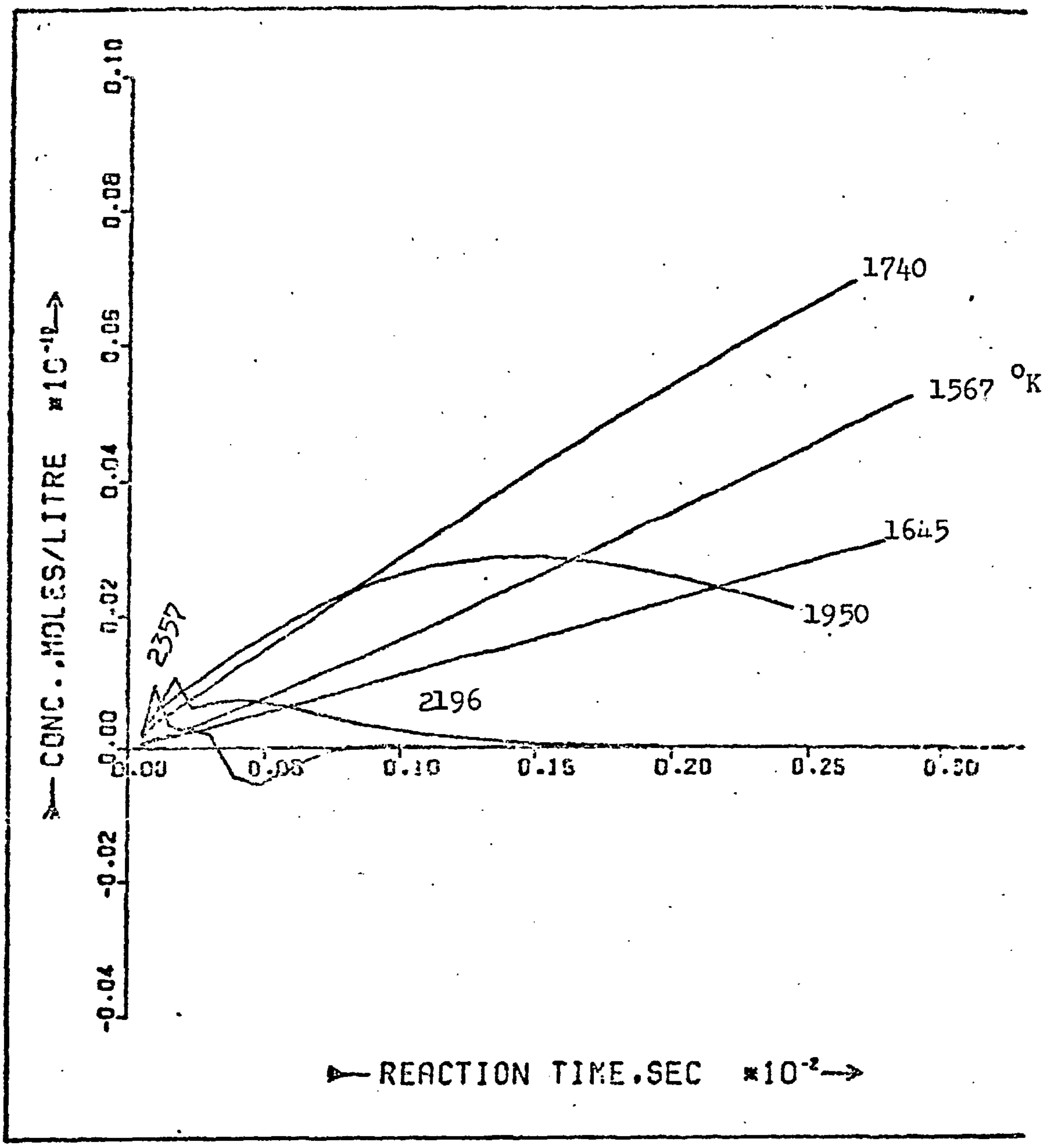

FIGURE 7.11: CONCENTRATION-TIME PROFILES FOR C_4H_4 PREDECTED FROM THE PYROLYSIS OF 5% C_2H_2 IN ARGON. USING BACK'S INITIATION STEP.

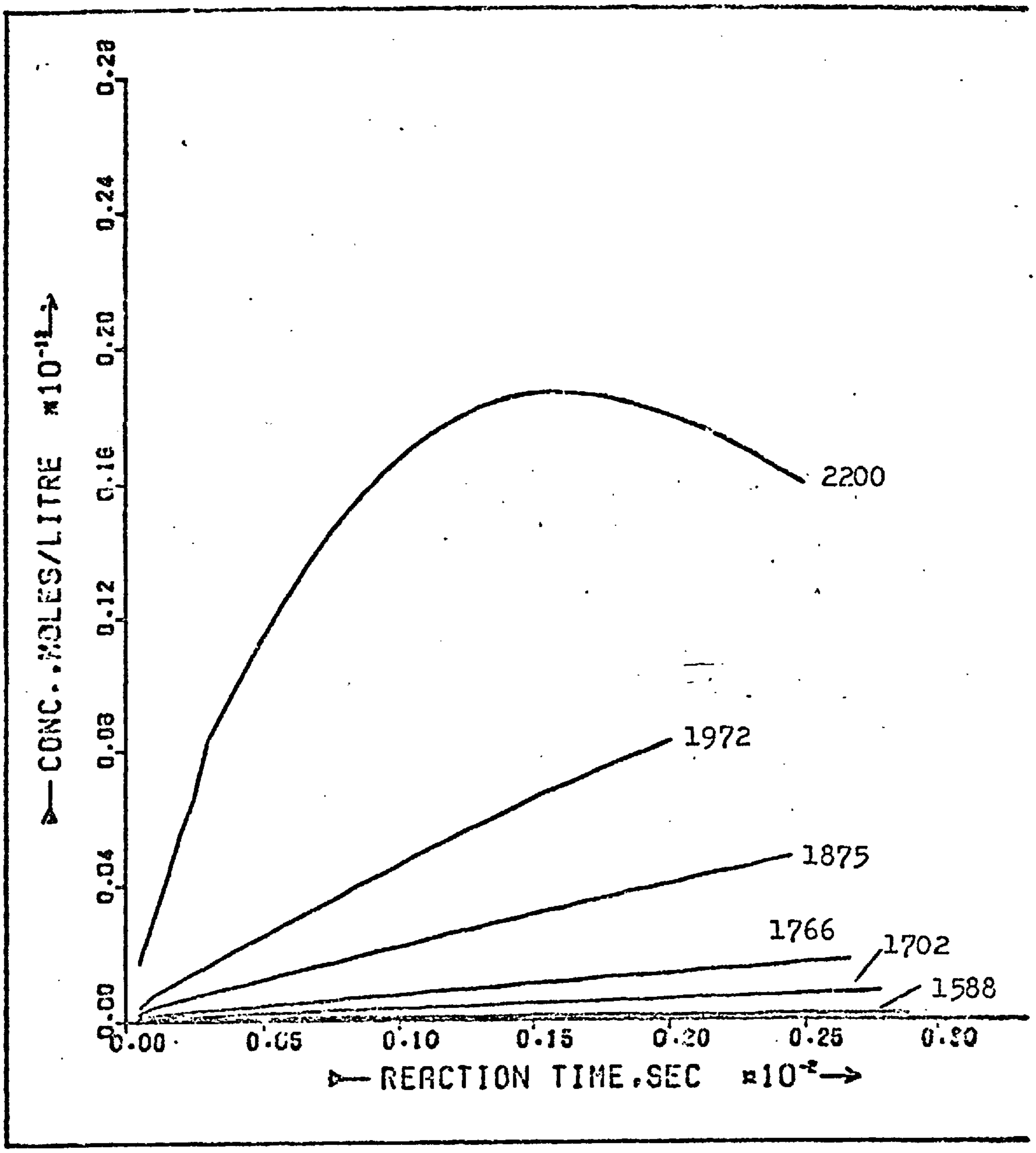

FIGURE 7.12(A): COMPUTED CONCENTRATION-TIME PROFILES FOR C_4H_2, DURING THE PYROLYSIS OF 2% C_2H_2 IN ARGON, MODELLED FROM SCHEME II.

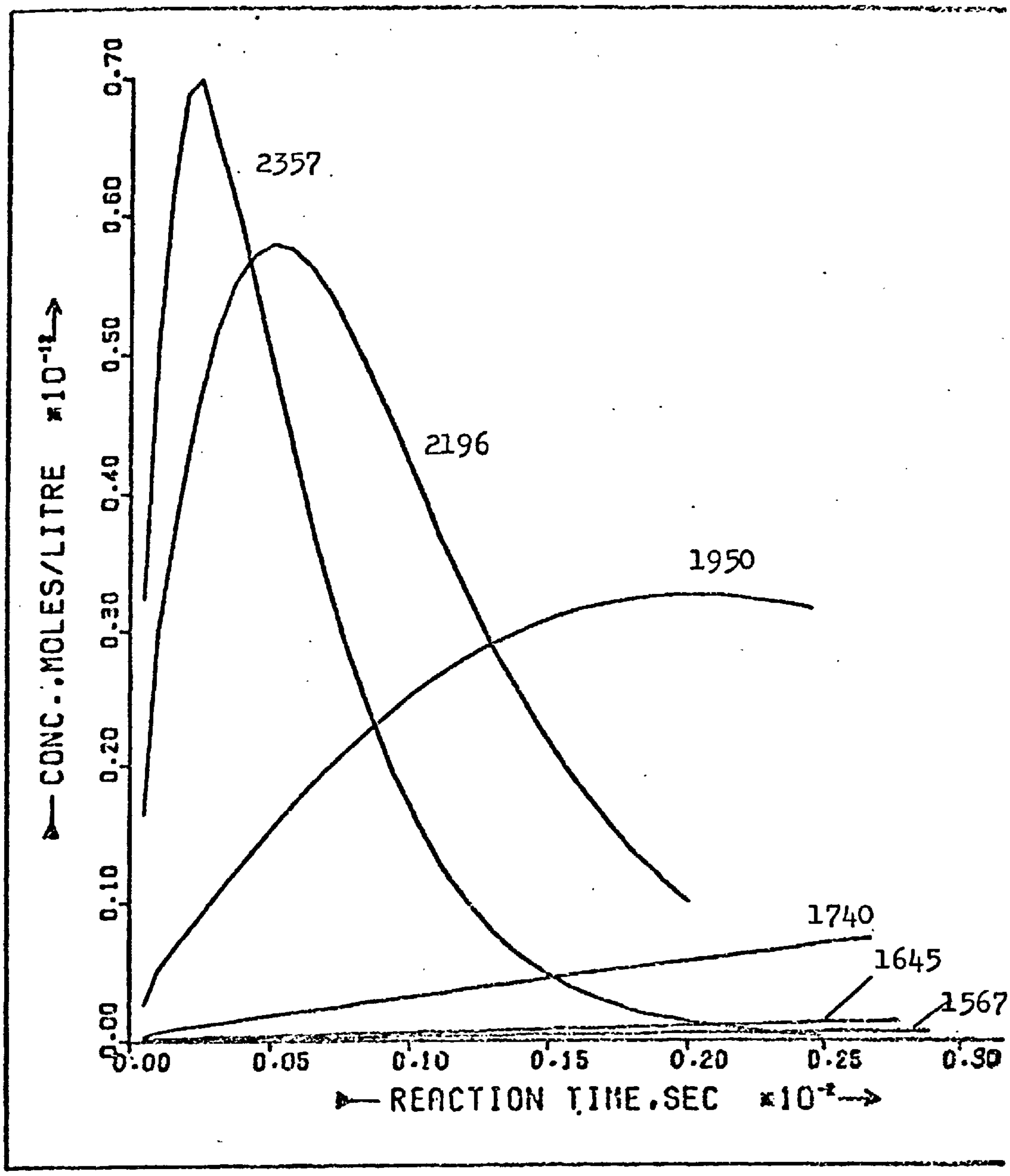

FIGURE 7.12(B): COMPUTED CONCENTRATION-TIME PROFILES FOR C_4H_2, DURING THE PYROLYSIS OF 5% C_2H_2 IN ARGON, MODELLED ACCORDING TO THE MECHANISM IN TABLE 7.1. USING BACK'S INITIATION.

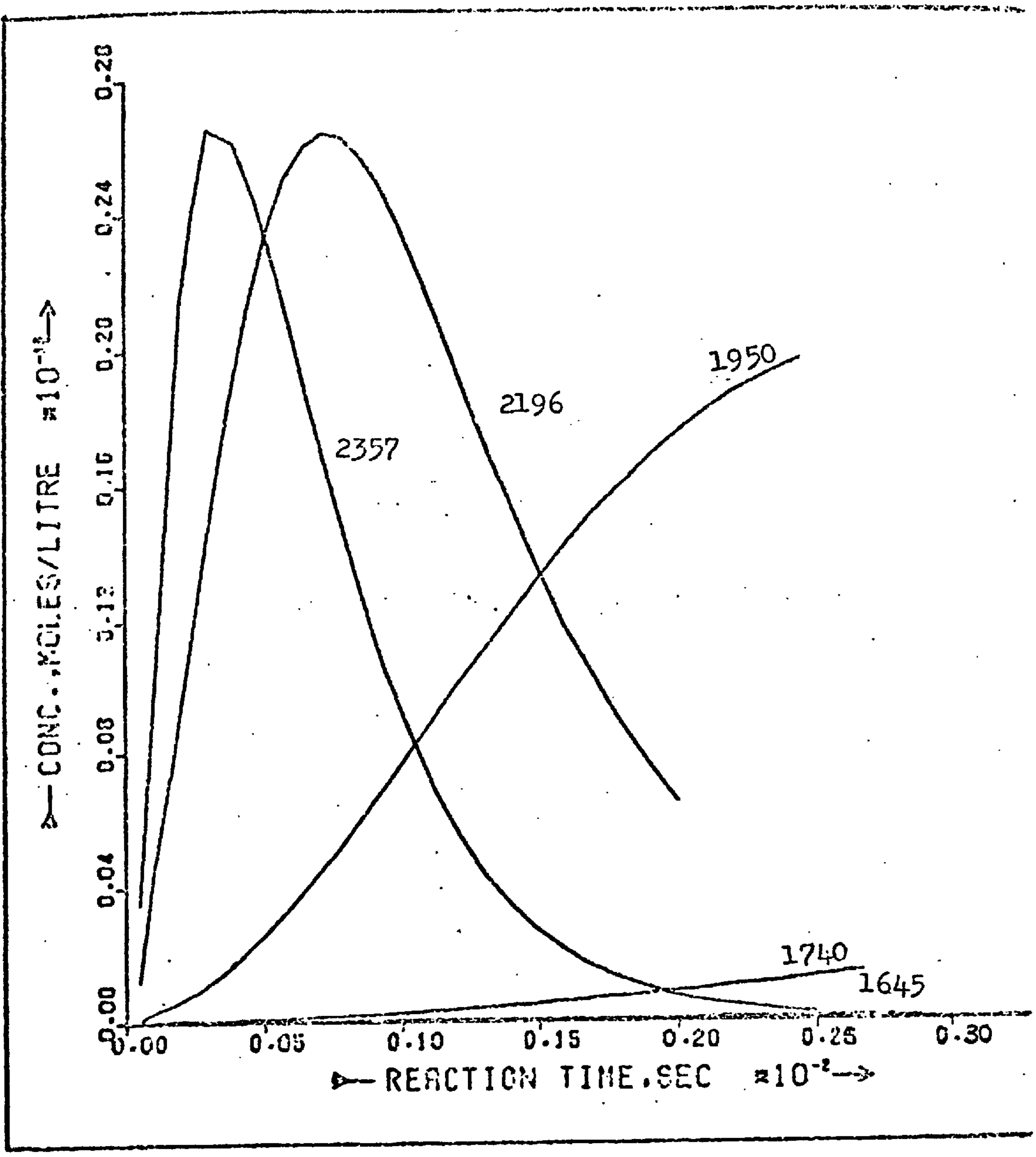

FIGURE 7.13(A): CONCENTRATION-TIME PROFILES FOR C_6H_2. DURING THE PYROLYSIS OF 5% C_2H_2 IN ARGON, MODELLED ACCORDING TO THE MECHANISM IN TABLE 7.1 USING BACK'S INITIATION STEP.

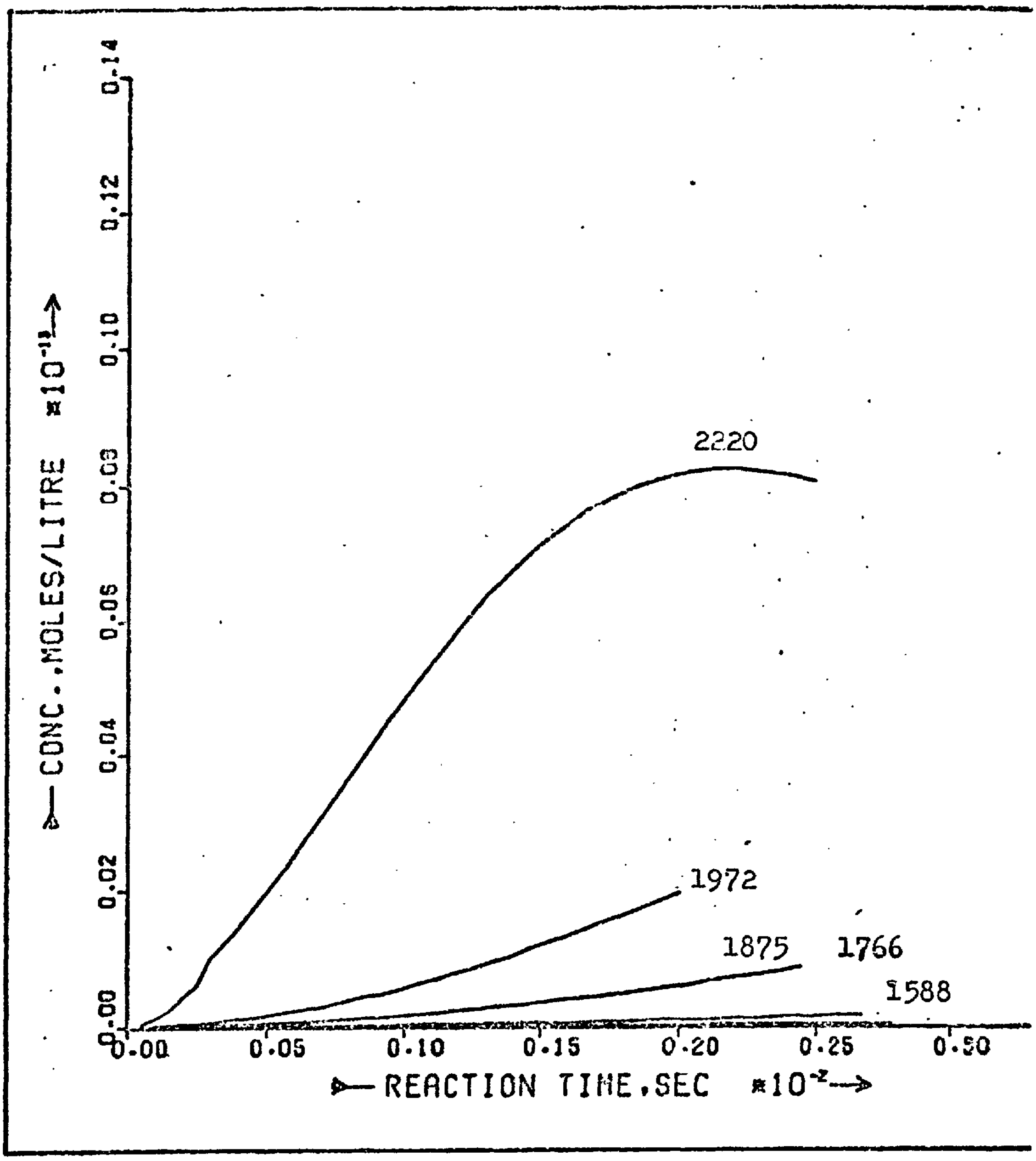

FIGURE 7.13(B): COMPUTED CONCENTRATION-TIME PROFILES FOR C_6H_2, DURING THE PYROLYSIS OF 2% C_2H_2 IN ARGON, MODELLED FROM SCHEME II.

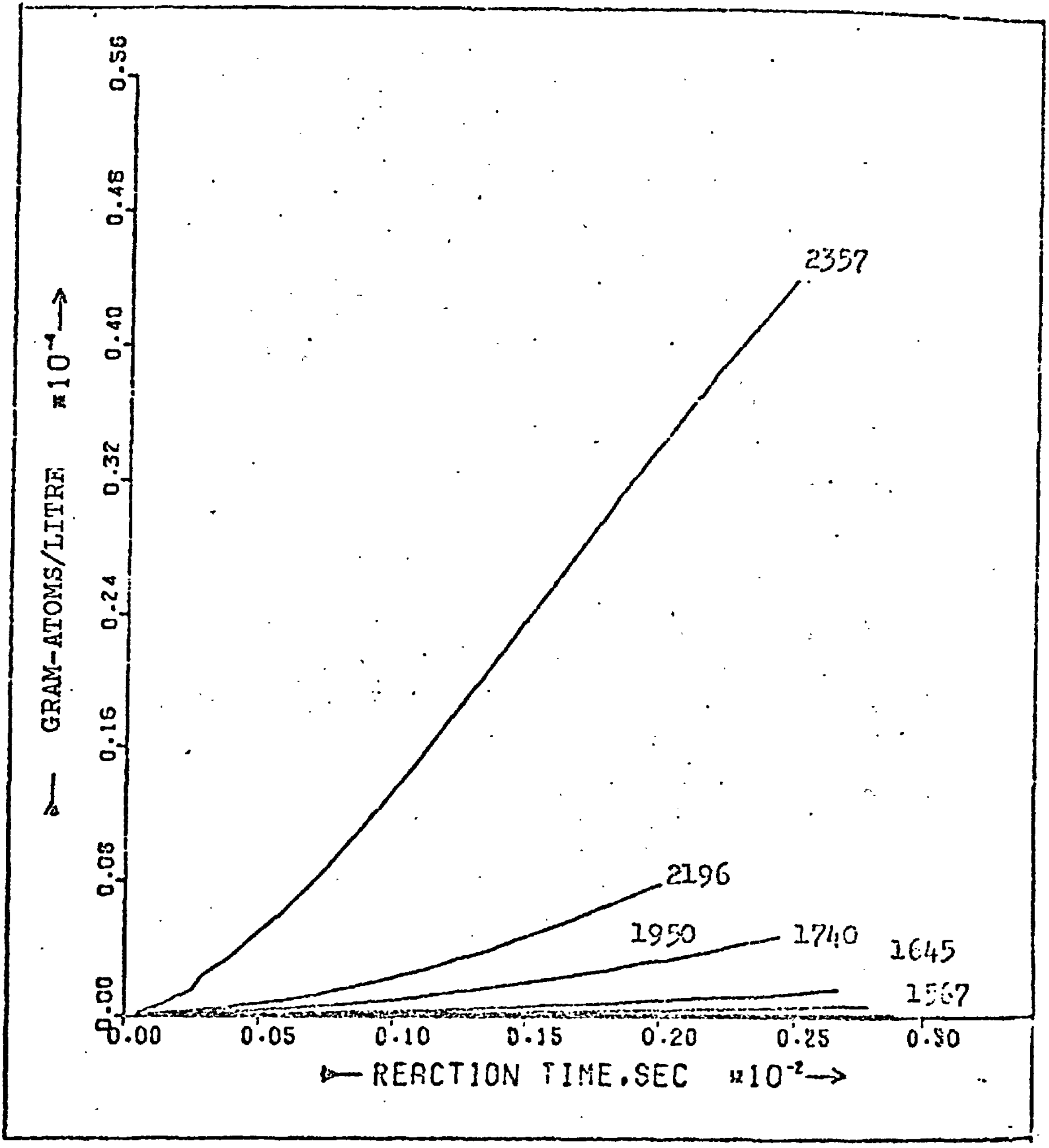

FIGURE 7.14: COMPUTED CARBON PROFILES DURING THE PYROLYSIS OF 2% C_2H_2 IN ARGON, MODELLED ACCORDING TO THE MECHANISM IN TABLE 7.1. USING BACK'S INITIATION.

mechanism (scheme I - table 7.0) the concentration profiles of C_2H_2 during its pyrolysis modelled according to scheme II, assuming Back's initiation step, does not indicate any agreement with the infrared results.

At temperatures under 1950°K, the results modelled according to scheme II for the major reaction products shown figure 7.11-14 did not pass through maxima for the average computation time of 3.0ms; this is contrary to the experimental observations at the wavelength regions between 2.75 - 5.2μm in which the infrared emission from the different structural groups were seen to pass through maxima. But at higher temperatures, the predicted variation of concentration with time for vinylacetylene and diacetylene exhibited the same profiles as the experimental emission - time plots - that is rising to a maximum and then decaying.

At temperatures upto 1900°K, the rate of formation of C_6H_2, as shown in figure (7. 13), was slow but it rapidly accelerated at higher temperatures to display similar concentration - time profiles as C_4H_2. The predicted yield of 'carbon' was characterised by a very slow initial rate of formation for all temperatures except at $T > 2357°K$, where the build-up in its concentration started at very short reaction time (figure 7. 14). The results of computational simulation using the reaction scheme II predicts that for all temperatures modelled the maximum level in the concentrations of diacetylene and hexatriyne increased with temperature and as a result the highest concentration levels of these products were obtained at the highest temperatures. On the contrary for vinylacetylene, further increase in temperature beyond 1760°K, led to a decrease its concentration levels, and as a result above 2000°K, the formation of vinylacetylene was negligible.

Comparison between the experimental and the computed results obtained from scheme II is summarized in table (7. 6).

Table 7.6: Comparison of experimental & results modelled from II

Reaction temperature, °K	%C_2H_2 in argon	Time Taken to Reach Maximum, ms				
		Experimental		computed concentration		
		≡CH	- C ≡ C-	C_4H_4	C_4H_2	C_6H_2
T<1950				N O M A X I M A		
1950	5	0.80	1.0	1.47	2.06	-
2100	2	1.40	-	1.96	2.55	-
2141	5	-	0.80	6.30	0.80	1.08
2200	2	0.6	-	1.27	1.67	-
2209	5	-	0.80	0.20	0.54	0.75
2370	5.0	-	0.60	-	0. 4	0.60
2500	5.0	-	0.4	-	0.30	-
		= CH_2 and		C_4H_4		
1702	2	1.8		-		
1972	2	0.8		3.5		
2090	2	1.0		1.96		
2220	2	0.6		1.08		

7.5. Discussion of the kinetic models

In general there are lots of discrepancies between the computed results of the concentration - time profiles of the individual hydrocarbons and the infrared emission plots. This is an indication that other reactions are undoubtedly occurring during the simultaneous polymerization and dehydrogenation of acetylene. Apart from those reactions leading to the formation of the products considered in schemes I and II, other side reactions resulting in the formation of some other products, unaccounted for in these models cannot be ruled out. For example, Bradley and Kistiakowsky[34] have found high acetylenic polymers of molecular weight $(C_2H_2)n$, n upto 4, during the pyrolysis of acetylene at temperatures between 1800°K and 2700°K. However, because the detailed knowledge of the structural somposition of these polymers are not well-known, it was therefore not possible to include some of them in the models, and this makes it very difficult to explain the complex pattern of the infrared emission plots. Hence the discrepancies between the modelled and the experimental results, outlined in table (7.7) and figures 7.1- 16 could be largely due to this reason.

From the comparison given in table (7.7), it is apparent that the results obtained from the model using scheme I gave a better approximation to the experimental results at temperatures upto 1900°K, than the prediction obtained from scheme II. At temperatures above this, the results from scheme II were closer to the experimental infrared profiles. This is illustrated in figure 7.16 in which the

TABLE 7.7: Comparison between modelled and experimental results

	Scheme I	Scheme II
a)	= CH_2 emission plots and the predicted concentration-time profiles for C_4H_4.	
i) At $T \leqslant 1766$°K:	The results modelled from both schemes (I&II) were not capable of predicting the observed initial decay of the infrared emission at 3.32 µm, which was accompanied by the broadening of the peak width. But the time for the infrared signal to pass through the secondary maximum (that is the highest value of t_{max}) was predicted from scheme I. Scheme II did not predict any maxima at these temperatures.	
ii) T = 1875 - 2220°K.	The predicted, concentration-time profiles upto 1972°K, for C_4H_4 had similar contours to the experimental emission results. Figure 7.5 a) shows such profile matching. Beyond 1972°K the predicted rates of consumption of C_4H_4 largely exceeded its rate of formation.	No t_{max} predicted at lower temperature, the concentration-time profiles did not pass through maxima at temperatures under 1900°K. At temperatures above 1900°K, the predicted t_{max} was very much longer than the experimental value.

Table 7.7 Contd.

b) ≡ CH and the computed profiles for C_4H_4, C_4H_2 and C_6H_2

The predicted t_{max} for these products using scheme I was closer to the experimental results than those predicted from scheme II. At temperatures upto 1900°K, the predicted time (t_{max}) for C_4H_4 was closest to the experimental results than the tmax for C_4H_2 and C_6H_2. At 2220°K, the predicted tmax for C_4H_2 and C_6H_2 were nearer to the experimental value as the concentration of C_4H_4 because negligible.

c) <u>- C ≡ C - and C_4H_4, C_4H_2 and C_6H_2</u>

	Cullis' initiation (scheme I)	Back's initiation (scheme II)
i)	1740°K; Predicted t_{max} for C_4H_4 was slightly higher but nearest to the experimental value than the correspondings for C_4H_2 and C_6H_2.	The predicted concentration-time profiles for C_4H_4, C_4H_2 and C_6H_2 did not reach maximum at $t \leq 3.0$ms.
ii)	1950°K; Predicted t_{max} for C_6H_2 was near to the experimental value and was followed by that for C_4H_2; tmax for C_4H_4 was very small.	t_{max} for C_4H_4 was higher than the experimental but nearer to it than t_{max} for C_4H_2, C_6H_2 did not reach maximum at this temperature.
iii)	2141°K; Predicted t_{max} very much lower than the corresponding experimental values for C_4H_4, and C_6H_2.	Predicted t_{max} for C_4H_2 equal to the time for -C≡C- emission to reach maximum before decaying. T_{max} for

Table 7.7 Contd.

	C_6H_2 was higher than experimental.
iv) 2196°K; same as in (iii)	Predicted t_{max} for C_6H_2 and C_4H_2 closer to the experimental.
v) 2357°K; same as in (iii)	Predicted t_{max} for C_6H_2 equal to the experimental. value.
d) polymeric Substances	
Induction times predicted matched the experimental emission profile at 2.0 - 2.7 µm wavelength region at lower temperatures.	Also predicted induction time at lower temperatures, but did not match with the experimental values.

FIGURE 7.15 ; Profile matching at 1508°K between the predicted conc. - time profiles for polymers (C_6H_2 & product from $2C_2H_3^{\bullet}$) from scheme I and Emission intensity time plot at wavelength region under 2.70 µm.

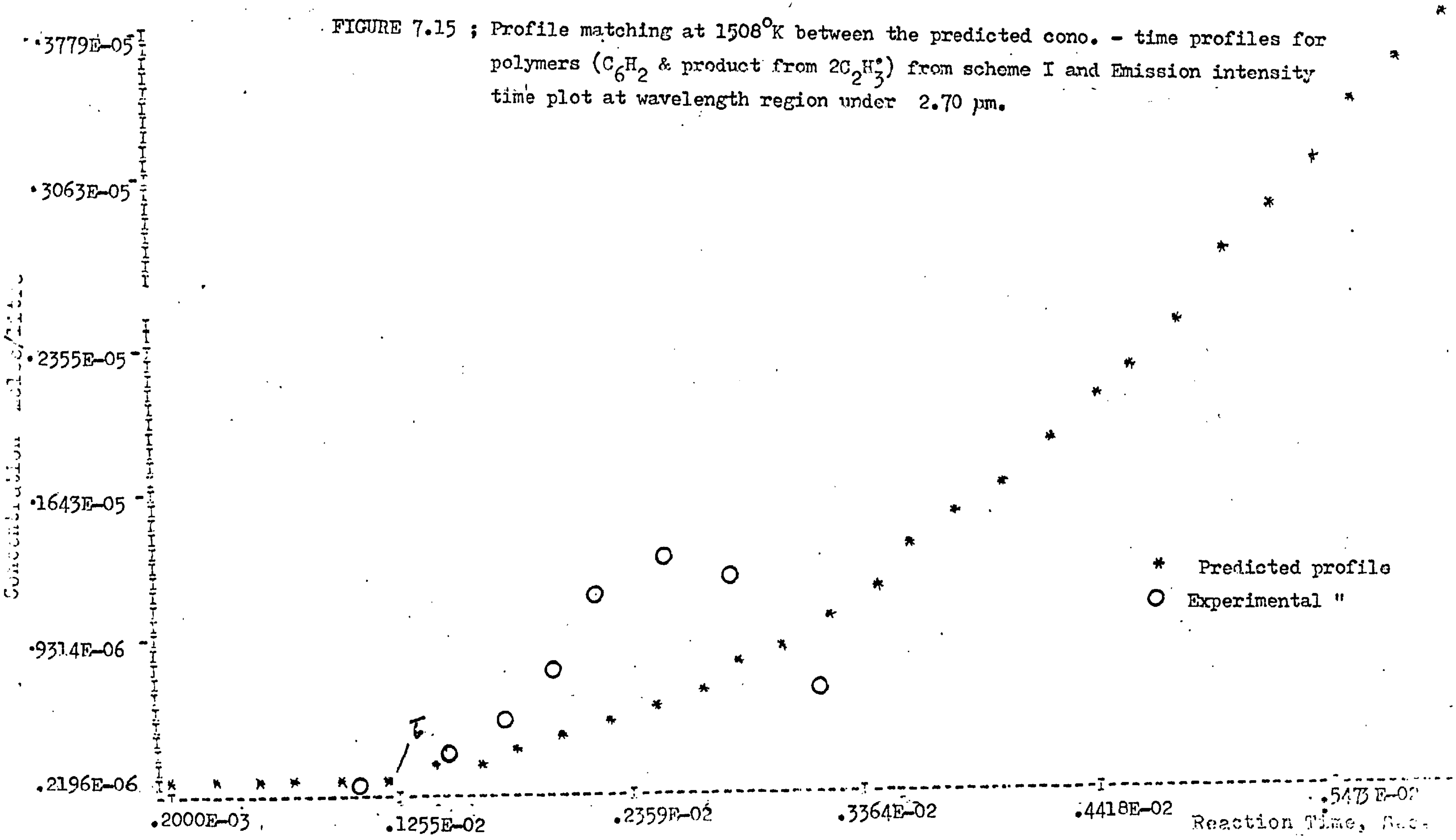

Figure 7.16: Comparison at 2141°K between the intensity-time plot for -C≡C- at 3.5-3.5μm and the computed concentration-time profile for C_4H_2 from scheme II.

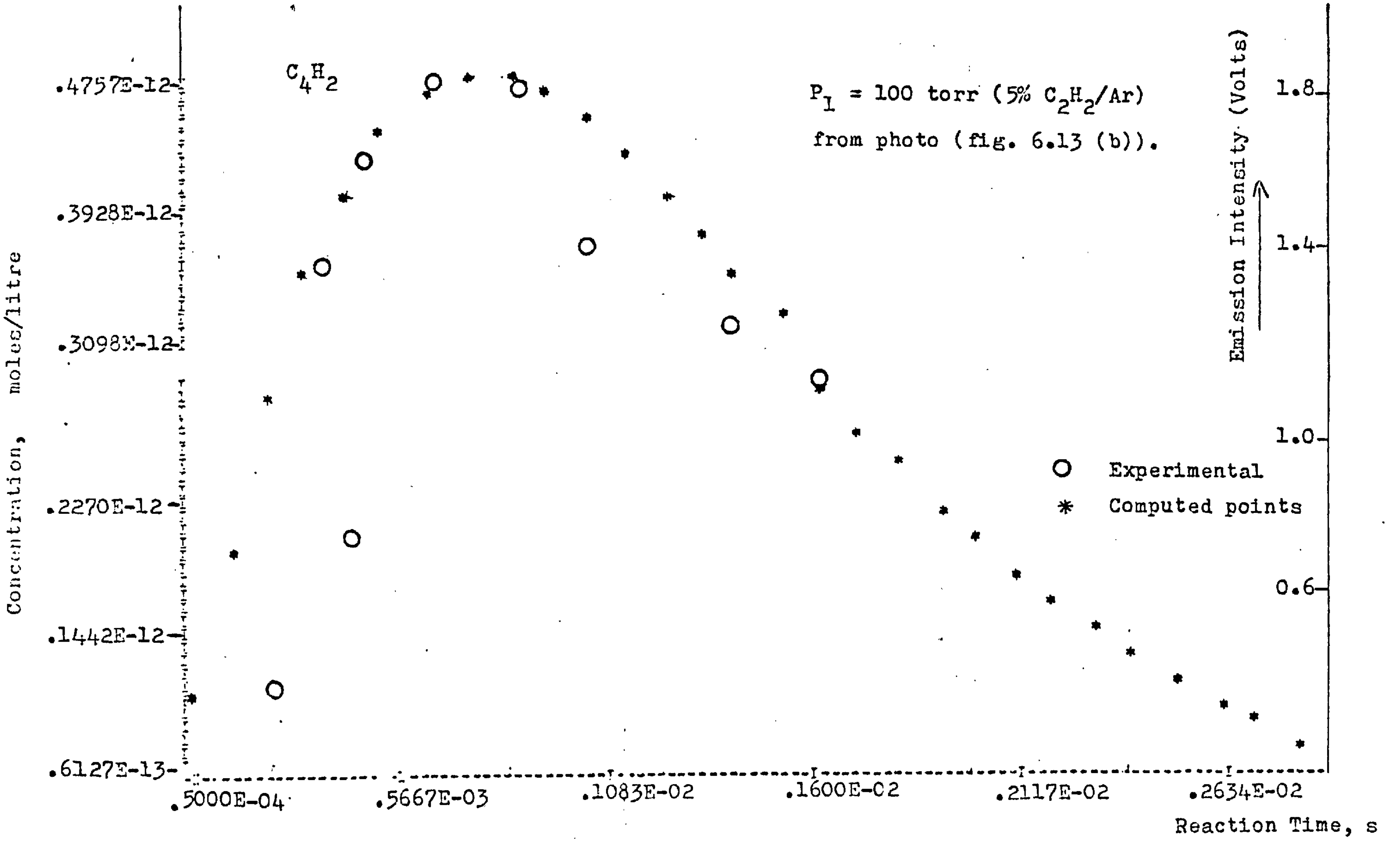

computed concentration profile of diacetylene at 2141°K has been compared with the infrared emission records in figure 6.13(b) for -C≡C- group at 3.5 - 5.3µm. There is excellent agreement between the computed results from scheme II and the experimental infrared record, in which the t_{max} predicted by the model using Back's initiation step coincided with the experimental time at which the intensity of the emission passed through maximum. In order to facilitate visual comparison figure 7.16 was plotted by appropriately scaling the data, that is by equating the maximum concentration of the product to the maximum intensity of the emission at the same conditions of temperature and initial acetylene concentration.

The modelled results show that of all the acetylenic hydrocarbons formed at temperatures under 1900°K, the vinylacetylene profile gave the nearest match to the experimental data for both the ≡CH and -C≡C- emission plots. But at T> 1900°K, the predicted concentration - time profiles for diacetylene and hexatriyne, C_6H_2, were approximately similar to the emission - time plots due -C≡C- stretching. Generally, the computed profiles for C_4H_4, C_4H_2, and C_6H_2 were closely matched to the emission plots for -C≡C- than for those due to ≡CH at 3.04µm. It is thought that the significant contributions to the emission at the latter wavelength position by acetylene was responsible for such differences.

The emission intensity at 3.22µm and 3.32µm due =CH_2 and =CH- stretchings was assumed to be entirely due to the presence of vinylacetylene, but the computed results do show that this might not be exactly so especially at temperatures under 1766 °K, where the experimental observation showed that two maxima were present - the first one being a smaller maximum and its decay was followed by the broadening of the peak width. It is believed that this phenomenon, as has been discussed earlier in section (6.8.3), is an indication that, at least at lower temperatures, other compounds having either multiple double bonds or other complex structures, whose stretching frequencies lie very close to 3.22μm, are formed. The presence of such other compounds would result in a shift in the position of the peak due to conjugation effect. More weight is added to this suggestion by the results of the kinetic modelling which confirmed that the formation of higher polymeric compounds are preceeded by an induction period, the length of which accurately matched the experimental induction time, τ_{ind}, at the near infrared region. And as was pointed out in the discussion on the results of the emission records at 3.05 - 3.49μm there was an agreement between τ_{ind} and the time for the secondary rise in the intensity of infrared emission corresponding to the point of the start of peak broadening. One of such compounds is thought to be the polymeric product formed by the recombination of two vinyl radicals - probably C_4H_6, a compound which has multiple (two) double bonds.

The discrepancies in the modelled results from the two schemes at low and high temperature regions could be as a result of changes in the concentrations of the radicals. At high temperatures $C_4H_3^{\bullet}$ and other higher radicals will become largely dissociated and the chain will be carried by hydrogen atoms and smaller - $C_2\overset{\bullet}{H}_3$, $C_2H^{\bullet}$ radicals. This relative concentration of $C_2H_3^{\bullet}$ and $C_2H^{\bullet}$ radicals becomes a complex function of a number of competing reactions. High temperatures will favour the formation of $C_2H^{\bullet}$ radicals, which is formed by abstraction from acetylene, while addition reactions to $C_2H_3^{\bullet}$, either by hydrogen atoms or of larger radicals followed by decomposition having a lower activation energy will become more pronounced as the temperature is lowered. This might explain the reason why the termination reaction,

$$2\,C_2H_3^{\bullet} \longrightarrow \text{product}$$

becomes less important at high temperatures. As has been noted earlier, the rates predicted by scheme I become too high at high temperatures and therefore not capable of predicting the high temperature product distributions, while the converse is true for scheme II. It would, therefore, seem that there are two possible initiation steps which take place during the pyrolysis of acetylene over such a wide temperature range. One initiation step

$$2\,C_2H_2 \longrightarrow C_4H_3^{\bullet} + H^{\bullet}$$

which is thermodynamically favoured, together with reactions in scheme I being capable of adquately explaining the kinetics of the system upto about 1900°K; while at higher temperatures, an alternative initiation step

$$2\,C_2H_2 \longrightarrow C_2H^{\bullet} + C_2H_3^{\bullet}$$

and the reactions in scheme II give a better description of the reaction kinetics than the first scheme. This suggestion is quite feasible, because when two competiting reactions occur simultaneously the one with higher, not the lower, activation energy tends to become dominant at high temperature. Although the initiation steps might not be kinetically distinguishable, on the basis that either would lead to an overall second order reaction for the pyrolysis of acetylene, nevertheless, it is likely that several changes in the mechanism must occur over such a wide temperature range embodied in this investigation. And the reactions outlined in schemes I and II can account for such changes at different temperature regions without altering the main kinetic characteristics.

However, although it is possible that changes in the modelled product distribution with temperature follow the change in the relative concentration of these radicals, but a lot of the discrepancies also arose due to the lack of the exact knowledge of the values of the rate constants for the elementary reactions involved. Large errors are definately introduced not only in the estimated rate data, but also in the rate constants of most of the elementary reactions since most of the data available in the literature are based on low temperature investigations.

CONCLUSIONS

Conclusions

From the results on propane pyrolysis and the corresponding discussions, it maybe concluded that:

1) the thermal decomposition of propane behind the reflected shock waves at temperatures between 1200 - 2800°K and total reaction zone pressures of 5 - 15 atm (505.4 - 1516 KN/m^2) yielded a first order kinetic expression, $k = 1.79 \times 10^8 \exp(-176.2 KJ/RT)\ s^{-1}$.

2) At the stated experimental conditions very high percentage of propane decomposition was maintained between reaction times of 0.2 to 3.5ms.

3) Increasing the temperature of the pyrolysis of propane, increased propane decomposition, and at temperatures above 2000°K, total decomposition of propane was achieved.

4) The major reaction products are acetylene, ethylene and methane, in the order of decreasing importance.

5) Small quantities of ethane and propylene were detected only at temperatures below 1500°K.

6) The product distribution showed a marked difference from those reported by other investigators (mostly at temperatures lower than those covered in the present study). Acetylene, which has been always described as a 'minor' reaction product at lower temperatures becomes the principal gaseous product at temperatures above 1700°K.

7) The appearance of C_2H_2 amongst the reaction products corresponded to those temperature range at which the

yields of propylene and ethane, and to a lesser extent that of ethylene, showed rapid decline.

8) The yield of acetylene reached maximum at the temperature range where the yields of ethylene and methane were minimum.

9) At constant reflected shock pressures, conversion of propane into methane, ethylene and acetylene were sensitive to simultaneous variation of reaction time and temperature.

10) Maximum conversion of propane to methane (15 - 20%) was obtained at temperatures between 1450 - 1650°K independent of reaction times (at least upto 3.5ms).

11) Outside the above temperature region the conversion of propane to methane decreased and became sensitive to reaction time. The rate of decrease being steeper towards the higher temperatures.

12) Maximum conversion of propane into ethylene (40 - 50%) was obtained at temperature range between 1380 - 1500°K, for reaction times upto 3.0ms; outside this temperature/reaction time range propane conversion into ethylene dropped and became sensitive to reaction time variation.

13) At lower propane conversion to acetylene ($< 30\%$), acetylene yield was not very sensitive to changes in reaction time for $t > 1.5$ms; but at higher conversions the yield of acetylene become very sensitive to prolonged reaction time ($t > 0.8$ms), and its value decreased with increase in time.

14) The yield of carbonaceous materials calculated from mass balance deficit showed similar trend as the dependence of the yield of acetylene on temperature. The yield of 'carbon' increased with increase temperature.

15) Addition of ethane to propane/argon mixtures accelerated the decomposition of propane at temperatures above 1200°K.

16) At temperatures under 1000°K, ethane does not appreciably accelerate the pyrolysis of propane.

17) The accelerating influence of the addition of ethane on the pyrolysis of propane increases with increase in temperature. This is due to changes in the level of concentrations of the chain carriers.

18) Increase in the quantity of ethane added to propane/argon mixture does not result in equal increase in its accelerating influence on propane decomposition.

19) The presence of ethane in the reacting propane/argon mixture did not change the overall trend of the dependence of the average rates of formation of the major reaction products on temperature.

20) The rate of conversion of propane to methane and ethylene in the presence of ethane, relative to the same rate in its absence, decreased with increase in temperature after about 1550°K. The extent of the decrease increased with rise in reaction temperature.

21) Rate of conversion of propane to acetylene in the presence of ethane increased relative to the same

rate in pure propane/argon mixture at all temperatures.

22) The effects of the addition of ethane on the pyrolysis of propane could be explained in terms of increase in the concentration levels of the free radicals - methyl, ethyl radicals and hydrogen atom; especially the latter two which respectively account for the formation of acetylene and reduction of propane's self-inhibiting characteristics.

23) It is thought that at lower temperatures (around 1000°K) ethane will be present in largely an undissociated state relative to propane and hence the much needed chain propagating radicals in propane pyrolysis will be mainly consumed by reactions with ethane instead. Thus interfering with the chain reactions.

24) At higher temperatures, ethane also decomposes to increase the concentrations of hydrogen atoms and the free radicals which will reduce inhibitions and thus accelerate propane consumption.

25) Total reaction (reflected shock) pressure has negative effect on the optimum conversion of propane to acetylene. Increased reaction pressure at constant reaction time (for any $t > 0.5$ms) decreases the conversion of propane into acetylene.

26) At short reaction time (≤ 0.4ms) increased reaction pressure over 3-folds produces less than 10% change in the propane conversion to acetylene.

27) At constant pressure, the longer the reaction time, the lower the conversion of propane into acetylene.

28) For optimum conversion of propane to acetylene, it is necessary to conduct the experiments at short reaction times (under 0.5ms.) and at total reaction pressure under 550 KN/m^2.

(b) From infrared spectroscopic studies it may be concluded:-

1) The ultrarapid scan spectrometer has been used to investigate the pyrolysis of acetylene at 1400 to 2760 °K by observing the infrared emission profiles at the wavelength region between 2.0µm to 5.3µm. In this wavelength range peaks, whose intensity reached maximum at 3.04µm, 3.22µm (and 3.30µm), and 4.6µm, were observed. These peaks indicate the presence of ≡CH, $=CH_2$ (and =CH-), and -C≡C- groups respectively.

2) These structures (≡CH, $=CH_2$, =CH-, and -C≡C-)were thought to be predominantly due to the presence of C_2H_2 , C_4H_4 C_4H_2 and C_6H_2 .

3) Infrared emissions from shock-heated mixtures of C_2H_2 and argon at wavelength range between 2.0 - 2.7µm were proceeded by a well-defined induction period during which no detectable infrared signal was observed.

4) The induction time varied inversely as the initial concentration of acetylene.

5) Increase in reaction temperature decreased the value of the induction time.

6) The temperatures at which the length of induction period became negligible decreased as the mixture became richer in acetylene; these were 1900°K, 1720°K and 1680°K for initial partial pressures of acetylene of 0.266, 0.665 and 0.931 KN/m^2 respectively.

7) A good correlation was found to exist between the induction time at 2.00 - 2.70µm and the time for incipient formation of 'carbon particles'.

8) The rate of formation of the species emitting at low infrared region (2.0 - 2.70µm) obtained by induction time measurements has an activation energy of 43.6 KJ/mole. This is more in agreement with Hooker's[29] results than those of others.

9) At temperatures under 1702°K, there was a shift in the peak position at 3.30um towards a lower wavelength (3.22µm). This occurred immediately the intensity of the emission at 3.30µm had past through a minimum value. The shift in the peak position was accompained by a broadening of the peak width.

10) The length of the induction time corresponded quite well to the time, t_b, at which broadening of the peak at 3.30µm occurred.

11) The shift in peak position immediately after t_b is a result of the formation of secondary reaction products different from the primary one(s), although both may contain similar functional groups.

12) The rate of acetylene decomposition can be determined indirectly from the rate of rise of intensity of infrared emission at the early stages of the reaction.

13) Arrhenius expression for second-order rate of acetylene disappearance was obtained as:-

$$k = 3.1 \times 10^{7} \exp(- 136 \text{ KJ/mole}), \text{ mole}^{-1}.\text{litre}.s^{-1}.$$

14) The obtained value for the activation energy for acetylene decomposition, E_a = 136 KJ/mole, falls within the lower range of the values quoted in literature; showing that with the method of ultrarapid scan infrared spectroscopy useful kinetic results can be obtained.

15) The results of the infrared emission experiments for shock-heated acetylene indicated that the mechanism for the pyrolysis of acetylene is a complex process. Two kinetic models were proposed to explain the mechanism of acetylene pyrolysis between 1500 to 1900°K and 1900 to 2400°K respectively.

16) Secondary reactions involving the decomposition of the primary products -C_4H_4 and C_4H_2 are manadatory inorder to obtain computed concentration profiles which matched the emission-time plots.

17) Concentration-time profiles for the various reaction products were successfully simulated using the Gear's[159] integration method which is devoid of steady state limitiations.

18) At temperatures upto 1900°K, the experimental results were better explained by kinetic model based on the extension of that proposed by Cullis et al[130], in which the initiation step is $2C_2H_2 \longrightarrow C_4H_3^{\bullet}$ and $H^{\bullet}$. Above this temperature, the predicted rates became too

high and the scheme fails to produce suitable concentration-time profiles to match the emission profiles at any wavelength region studies.

19) At temperatures above 1900°K some reactions became unimportant and reactions in scheme II (table 7.1) based on the initiation step suggested by Back[159] were capable of producing concentration - time profiles which matched the experimental emission profiles.

20) Comparison between the experimental results and the computed concentration-time profiles for the reaction species indicated that the likely products of acetylene pyrolysis are C_4H_4 and C_4H_2 and polymeric substances - C_6H_2 , C_4H_6 and carbonaceous materials.

REFERENCES

References

1. Vieille,P; C.P. acad. Sci, Paris 129, 1228, 1899.
2. Payman,W; and Shepherd, W.C.F., Proc. Roy.Soc.A158, 348,1934.
3. Glick,H.S; Squire,W. and Hertzberg,G., 5th Symp. (Intern) combust. 335, 1955.
4. Bradley,J.N., "Shock Waves in Chemistry and Physics". Methuen, London, 1962.
5. Gaydon, A.G. and Hurle, I.R., "The Shock Tube in High Temperature Chemical Physics". Chapman, London, 1963.
6. Greene, E.F. and Toennies, J.P. "Chemical Reactions in Shock Waves". Arnold, 1964.
7. Bauer,S.H., Ann. Rev. Phys. Chem. 16, 245, 1965.
8. Bradley, J. N., Ind. Chem., p.557, Nov. 1962.
9. Belford,R.L. and Strehlow R.A., Ann. Rev. Phys. Chem. 20, 247, 1969.
10. Hertzberg,A., Smith,W.E., Glick, H.S; and Squire,W; Corned Aero, Lab. Reports No. AD-789-A-2; and AEDC-TN-55-15, 1955.
11. Wittliff, C.E., Wilson,M.R. and Herzberg,A., J.Aero.Sci. 26, No.4 219, 1959.
12. Greene,E.F., Taylor,R.L. and Patterson,W.L., J.Phys. Chem. 62, 238, 1958.
13. Lifshitz,A. and Bauer, S.H., J.Chem. Phys. 38, 2056, 1963.
14. Ref. (5) page 243.
15. Tsang, W., J.Chem. Phys. 40, 1171, 1964.
16. Tsang, W., J. Chem. Phys. 41, 2487, 1964.
17. Johnston,H.S. and Tschuikow-Roux,E., J.Chem. Phys. 36, 463, 1962.
18. Lifshitz,A. and Schechner, P., Isr.J.Chem. 12, 729,1974.

19. Tschuikow - Roux, E. Phys. Fluids, 8, 821, 1965.

20. Simmie, J., Quiring, W.J., and Tschuikow - Roux, E., J. Phys. Chem. 73, 3830, 1969.

21. Evans, P.J., Ichimura, T., and Tschuikow - Roux, E., Int. J. Chem. Kinet. 10, (No. 8), 854, 1978.

22. Napier, D.H. and Subrahmanyam, N., J. Appl. Chem. and Biotechn. 22, 303, 1972.

23. Aten, C.F., and Greene, E.F., Disc. Farad, Soc. 22, 162, 1956.

24. Aten, C.F. and Greene, E.F., Combust. Flame 5, 55, 1961.

25. Kozlov, G.I., and Knorre, V.G., Combust. Flame 6, 253, 1962.

26. Bradley, J.N., and Frend, M.A., J. Phys. Chem. 75, 1492, 1971.

27. Lifshitz, A., Scheller, K. and Bucrat, A., Proc. 9th. Intern. Shock Tube Symp., Stanford Univ. p.690, 1973.

28. Fairbairn, A.R., and Gaydon, A.G., Proc. Roy, Soc. A239, 464, 1957.

29. Hooker, W.J., 7th Symp. (Intern.) Combust, 949, 1959.

30. Gosling, A.J., Lampard, D. and Fussey, D.E., Combust. Inst. European Symp. p. 388, 1973.

31. Mar'yasin, L. and Nabutovskii, Z.A., Kinetics and Catalysis (English translation), 14, 139, 1973.

32. Jacobs, T.A., 8th Symp. (Intern.) Combust. p.151, 1962.

33. Napier, D.H. and Simonson, J.R., J. Am. Rocket Soc. 32, 1736, 1962.

34. Bradley, J.N. and Kistiakowsky, G.B., J. Chem. Phys. 35, 264, 1961.

35. Hay,A.J. and Belford,R.L., J.Chem. Phys. 47, 3944, 1967.

36. Windsor,M., Davidson,N. and Taylor,R., 7th Symp. (Intern.) Combust. p. 80, 1959.

37. Jacobs, T.A., J. Phys. Chem. 67, 665, 1963.

38. Hartig,R., Troe,J. and Wagner,H. Gg. 13th Symp. (Intern.) Combust. p.147, 1971.

39. Wray,K.L. and Feldman,E.V., J. Chem. Phys. 54, 3445, 1971.

40. Bott,J.F. and Jacobs,T.A., J. Chem. Phys. 50, 3850, 1969.

41. Gay,I.D., Kistiakowsky,G.B., Michael,J.V. and Niki,H., J. Chem. Phys. 43, 1720, 1965.

42. Kuratani,K. and Bauer,S.H., J. Am. Chem. Soc. 87, 150, 1965.

43. Grillo,A. and Slack,M.W., Combust. Flame 27, 377, 1976.

44. Cooke,D.F. and Williams,A., Ibid. 24, 245, 1975.

45. Bullock,B.W. and Silverman,S., J. Opt. Soc. Am. 40, 608, 1950.

46. Daly,E.F., Nature 166, 1072, 1950.

47. Wheatly,P., Vincent,E., Rotenberg,D. and Cowan, G., J. Opt. Soc. Am. 41, 665, 1951.

48. Brown,D.A.H. and Roberts,V., J. Sci. Instr. 30, 5, 1953.

49. Tanner,K.N., and King,R.L., Nature 181, 963, 1958.

50. Dmitrievskii,O.D., Neporent,B.S. and Nikitin,V.A., Optika i Spektroskopiya 3, 180, 1957.

51. Bethke,G.W., J.Opt. Soc. Am. 50, 1054, 1960.

52. Sproul,D.G.S., PhD. Thesis Univ. of London, 1973.

53. Duff,R.E., Phys. Fluids. 4, 1463, 1961.

54. Mirrels,H., NACA TN 3401, Washington, 1955.

55. Mirrels,H., Phys. Fluids, 6, 1201, 1963.

56. Mirrels, H; Proc. 8th Intern. Shock Tube Symp; London, paper 6, 1971.

57. Belles, F.E. and Brabbs,T.A., 13th Symp. (Intern) Combustion, P.165. 1970.

58. Brabbs, T.A. and Belles,F.E., Proc. 8th Intern. Shock Tube Symp., London, paper 24, 1971.

59. Strehlow, R.A. and Cohen, A; J. Chem. Phys. 28, 983, 1958.

60. Cowperthwaite,M., and Bauer,S.H; J. Chem. Phys. 36, 1743, 1962.

61. Strehlow, R.A., and Belford, R.L., AAE. Techn. Report, No. 69-1, Univ. Illnois, Urbana, 1969.

62. Warshay, M., NASA TND - 3502, 1966.

63. Warshay, M., NASA TND - 4795, 1968.

64. Glick, H.S., 7th Symp. (Intern) Combustion, p.98, 1957.

65. Skinner, G.B. and Ball, W.E., J. Phys. Chem. 64, 1025,1960.

66. Porter, G.,Comb. Researches and Rev., p.108, AGARD, Butterworth, London, 1955

67. Tiedge, W.F. and Caskey,F.E., Encycl. Ind. Chem. Anal; 4, 126, 1967.

68. Miller, S.A., "Acetylene; its properties, manufacture and uses". Vol. 2, Benn, London, 1965 - 1966.

69. Handie, D.W.F., "Acetylene: manufacture and uses" Oxford Univ. Press, London, 1965.

70. Goldstein,R.F. and Waddams,A.L. "The Petroleum Chemical Industry". p.99, Spon, London, 1967.

71. Rice,F.O., Johnson,W.R. and Evening, B.L., J.Am. Chem. Soc. 54, 3529, 1932.

72. Rice, F.O., Herzfeld,K.F., J. Am. Chem.Soc. 56, 284, 1934.

73. Goldfinger,P. Lefort,M. and Niclause,M.,"Contribution a l'Etude de la Structure moleculaire", Victor Henri commemorative Vol. pg. 283, Desoe Liege, 1943.

74. Laidler, K.J.,"Reaction Kinetics " Vol.I pergamon, 1963.

75. Benson, S.W., "The Foundation of Chemical Kinetics". Mcgraw - Hill 1960.

76. Frost, A.A. and Pearson, R.G., "Kinetics and Mechanism" 2nd Ed., John Wiley, New York, 1965.

77. Bamford, C.H., and Tipper, C.F.H., "Comprehensive Chemical Kinetics", Vol. 5, chapt. one., 1972

78. Napier, D.H., Private Communication.

79. Laidler, K.J; Sagent,N.H. and Wojeiechowski,B.W., Proc. Roy. Soc. A 270, 242, 1962.

80. Laidler,K.J; Sagent, N.H. and Wojeiechowski, B.W., Ibid, A 270, 254, 1962.

81. Leathard,D.A. and Purnell,J.H., Ibid., A 306, 553, 1968.

82. Leathard,D.A. and Purnell,J.H., Ibid., A 305, 517, 1968.

83. Papic, M.M. and Laidler,K.J., Can J.Chem. 49, 535, 1971.

84. Papic, M.M. and Laidler,K.J.,Ibid 49, 549, 1971.

85. Kunugi,T., Tominaga, H., S. Abiko, and Namatame,A., Int. Chem. Eng. 7, 550, 1967.

86. Kershenbaum, L.S. and Martin,J.J., A.I. Ch. E. J. 13, 148, 1967.

87. Kershenbaum, L.S., PhD thesis Univ. of Michigan, 1968.

88. Buekens,A.C., and Froment,G.F., Ind. Eng. Chem. Process Des. Dev. 7, 435, 1968.

89. Crynes,B.L., and Albright,L.F., Ibid 8, 25, 1969.

90. Herriott,G.E., Eckent,R.E. and Albright,L.F., A.I.Ch. E. J. 18, 84, 1972.

91. Murata,M., Takeda,N., and Saito, S., J. Chem. Eng. Japan 7, 286, 1974.

92. Benson,A.M., A.I. Ch.E. J. 13, 903, 1967.

93. Steacie,E.W.R., "Atomic and Free Radical Reaction", 2nd Ed. p. 90 - 103, Reinhold, New York ,1954.

94. Volkan,A.G., and April,G.C., Ind. Eng. Chem. Process Des. Dev. 16, 429, 1977.

95. Pease,R.N. and Durgan,E.S., J.Am. Chem. Soc. 52, 1262, 1930.

96. Steacie,E.W.R. and Puddington,I.E., J.Res. B. 16, 176, 1938.

97. Mareck,L.F. and Mcluer,W.B., Ind. Eng. Chem. 23, 878, 1931.

98. Ingold,K.U., Stubbs,F.J. and Hinshelwood,C.F.J., Proc. Roy. Soc. A.203, 486, 1950.

99. Staveley,L.A.K., Proc. Roy. Soc. A.162, 557, 1937.

100. Hobbs,J.E. and Hinshelwood,C.N., Proc. Roy. Soc. A.167, 447, 1938.

101. Poltcnak,V.A., Leitis,L.Ya., Voevoaskii,V.V., Russ. J. Phys. Chem. 33, 379, 1959.

102. Martin,R., Niclause,M., Dzierzynski,M., Compt. Rend. 254, 1786, 1962.

103. Fusy,J., Scacchi,G., Martin,R., Combes,A., Niclause,M., Comp. Rend. 261, 2223, 1965.

104. Lifshitz, A. and Frenklach,M., J.Phys. Chem. 79, 686, 1975.

105. Besthy, B.S., PhD. Thesis, Univ. of London, 1978.

106. Shirotsuka,T., Hirata,A., Cawasaki,K. and Chao Mu-ken. Kagaku Kogaku 33, 7, 662, 1969.

107. Frend, M.A., PhD Thesis, Univ. of Essex, 1969.

108. Knox, K., Norrish, R.G.W., and Porter, G., J. Chem. Soc. 2038, 1952.

109. Steacie, E.W.R., - 'Atomic and Free Radical Reactions'; 2nd. Ed., p. 172, Reinhold, N.Y. 1954.

110. Silcocks, C.G., Proc. Roy. Soc. A 242, 411. 1957.

111. Cullis, C.F., Minkoff, G.F. and Nettleton, M.A., Trans. Farad. Soc., 58, 1117, 1962.

112. Cullis, C.F. and Franklin, N.H., Proc. Roy. Soc. A 280, 139, 1964.

113. Read, I.A., PhD. Thesis, Univ. of London, 1968.

114. Munson, M.S.B. and Anderson, R.C., Carbon I, 51, 1958.

115. Frank - Kamenetsky, D.A., Acta. Phys. Chem. USSR, 18, 148, 1943.

116. Minkoff, G.J., Newitt, D.M. and Rutledg., J. Appl. Chem. 7, 406, 1957.

117. Bone, W.A. and Coward, H.F., J. Chem. Soc. 93, 1197, 1908.

118. Skinner, G.B. and Sokoloski, E.M., J. Phys. Chem. 64, 1952, 1960.

119. Mar'yasin, I.L. and Nabutovskii, Z.A., Kinetics and Catalysis, Engl. Transl. 11, 706, 1970.

120. Bauer, S.H., Waelbrock, F, and Tsang, W., 135th, Nat. meeting Am. Chem. Soc. Boston, 1957.

121. Stehling, F.C., Frazee, J.D. and Anderson, R.C., 8th Symp.(Intern.) Combust. p. 774, 1962.

122. Parker, W.G. and Wolfhard, H.G., J. Chem. Soc. 2038, 1950.

123. Gaydon, A.G. and Fairbiarn, A.R., 5th Symp.(Intern.) Combust. p.324, 1955.

124. Bonne, U., Homann, A.H. and Wagner, H.Gg; 10th Symp. (Intern.) Combust. p. 503, 1965.

125. Cottrel,T.D., 'Strength of Chemical Bonds', Butterworth, London, 1958.

126. Minkoff,G.J., Can. J. Chem. 36, 131, 1958.

127. Minkoff,G.J., and Tipper,C.F.H., "Chemistry of Comb. Reactions", p. 250, Butterworth, London, 1962.

128. Palmer,H.B. and Dormish,F.L., J. Phys. Chem. 68, 1553, 1964.

129. Cullis,C.F. and Read,I.A., Trans. Farad. Soc. 66, 920, 1970.

130. Cullis,C.F., Hucknall,D.J. and Shepherd,J.U., Proc. Roy. Soc. London A. 335, 525, 1973.

131. Back,M.N., Can. J. Chem. 49, 2199, 1971.

132. Becker,R., Zeit. Physik. 8, 321, 1922.

133. Napier,D.H. and Simonson,J.R., Unpublished work.

134. Stull,D.R. and Prophet,H., JANAF Thermodynamical Tables, NSRDS - NBS 37, 1971.

135. Wolfson,B.T. and Dunn,R.G., Wright - Patterson Air Force Base, Ohio, Report Number ARI 62 - 390.

136. Palmer,H.B. and Knox,B.E., Am. Rocket Soc. J. 31, 826, 1961.

137. Trass,O. and Mackay,D., A.I.A.A. Journal I, 2161, 1963.

138. Collins, R.H., and Napier, D.H., J. Sci. Instr., 41, 567, 1964.

139. Napier, D.H., Nettleton, M, Simonson, J.R. and Thackeray, D.P.C., A.I.A.A. 2. 1136, 1964.

140. Kimber, G.M., Mayo, G.T., Napier, D.H. and Smith, D.H. J. Sci. Instr., 42, 44, 1965.

141. Lavrovskii, K.P., World Petrol. congress, Proc. 8th., Moscow (1971)

142. Barabanov, N.L., Mukhina, T.N., Polonskaya, I.D., Intern. Chem. Engr. 15, 740, 1975.

143. Martin, A.E., "Infrared Instrumentation and Techniques". Elsevier, 1966.

144. Skinner, G.B., Lifshitz, A., Scheller, K. and Bucrat, A., J. Chem. Phys., 56, 3853, 1972.

145. Petrov, A.A., Porfiryeva, Yu.I. and Semenov, G.I., J. Gen. Chem. USSR. 27, 1250, 1957.

146. Wotiz, J.H., and Miller, F.A., J.Amer. Chem. Soc. 71, 3441, 1949.

147. Sheppard, N., and Simpson, D.M., Quart. Rev. 6, 1, 1952.

148. Blomquist, A.T. and Liu, L.H., J. Am. Chem. Soc., 75, 2153, 1953.

149. Blomquist, A.T. and Liu, L.H., Ibid. 73, 5510, 1951.

150. Photoconductive cell ORP 13, Mullard, February, 1966.

151. Hertzberg, G., "Infrared and Raman Spectra", D. Van. Nostrand Co, 1956.

152. Homann, K.H., and Wagner, H.G., Ber Bunsenges. Phys. Chem. 69, 20, 1965.

153. Bauer, S.H., 11th Symp. (Intern.) combustion, p.105, 1967.

154. Gaydon,A.G. and Wolfhard,H.G., "Flames" chp.VIII,Chapman & Hall,197

155. Semenov, N.N., "some problem of Chemical Kinetics and reactivity", Vol.I and II, 1958, 1959, Pergamon Press.

156. Snow, R.H. - J. Phys. Chem. 70, 2780, 1966.

157. Edelson, D. and Allara, D.L., A.I. CH. E. Journal 19 638, 1973.

158. Byrne, G.D., Hindmarsh, C.A., Jackson, K.R. and Brown,H.G., comput. Chem. Eng. 1, 133, 1977.

159. Gear, C.W., - "Numerical Initial Value Problems in ordinary Differential Equations", Prentice Hall, Chapter 9, 1971.

160. Dean, A.M., Kistiakowsky, G.B., J. Chem. Phys. 53, 830, 1970.

161. Allara, D.L. and Edelson, D., Int. J. Chem. Kinetics 7, 479, 1975.

162. NAG Library computer program manual.

163. Chapell, G.A. and Shaw, H., J. Phys. Chem. 72, 4672, 1968.

164. Haitt, R., and Benson, S.W., J. Am. Chem. Soc. 94, 25 and 6886, 1972.

165. Mogel, G. and Eremin, E.N., Russ. J. Phys. Chem. 44 (10), 143, 1970.

166. Ibberson, V.J. and Sen, M., Trans. Inst. Chem. Engrs. 54(4), 265, 1976.

167. Benson, S.W. and Hougen, G.R., J. Phys. Chem. 71, 1735, 1967.

168. Shaviv, A. and Bar-nun, A, Int. J. Chem. Kinetics 7, 661, 1975.

169. Jachimowski, C.J., Comb. Flame 29, 55, 1977.

170. Bowman, C.T., 15th Symp. (Intern.) Combust. 869, 1974

171. Jensen, D.E., Comb. Inst. European Symp. p. 382, 1973.

172. Paul, R.E. and Marek, L.F., Ind. Eng. Chem. 26, 454, 1934.

173. Gay, I.D., Kern, R.D., Kistiakowsky, G.B., H.Nike, J. Chem. Phys. 54, 2371, 1966.

Appendix A1 & 2

List of Symbols

a - the speed of sound in the gas

A - the frequency factor

C_i - concentration of specie, i

c - concentration of the reactant molecule.

C_p - specific heat of gas at constant pressure

C_v - specific heat of gas at constant volume

CS - contact surface

d - hydraulic diameter of the tube.

E_a - the activation energy.

E - internal energy.

f - the fraction of the experimental gas in the driven section of the test tube.

H - enthalpy of gas

I_o - initial intensity of infrared emission (that is emission intensity at $t = o$).

I_t - intensity of infrafed emission at time, t

J - mechanical equivalent of heat.

K - reaction rate constant

L - length of the driven section of the shock tube.

M - molecular weight of the gas

M_s - shock mach number

n - order of reaction

N_R - number of chemical reactions

N_s - number of chemical species

P - shock pressure (the subscripts defined the shock region being considered).

r_{ij} - stoichiometric number of reactants for forward reactions.

R - the universal gas constant

R_o - initial rate of reaction

R_j - rate of the jth reaction

S_1 - incident shock front ST - transmitted shock front.

S_R - reflected shock front.

t - reaction time, ms

τ_f - time at which the emission intensity remained constant at to.

t_1 - the laboratory time

t_p - the actual observation time.

T - shock temperature (the subscripts give the shock region in question).

U - velocity of gas relative to the shock front.

V - the actual velocity of the gases in the shock tube.

W - end wall of the shock tube.

W_s - velocity of the shock front relative to the shock tube.

W_R - velocity of the reflected shock front.

X - fraction of hydrogen in the driver gas.

ρ - density of the gas - the subscript defines the shock region being considered.

γ - specific heat ratio

μm - wavelength

Subscripts

1. - Undisturbed test gas ahead of the shock wave.

2. - incident shock wave.

3. - driver gas after the passage of the rarefaction fan.

4. - driver gas before the passage of the rarefaction fan.

5. - reflected shock wave.

R - reflected shock

S - incident shock.

APPENDIX A3

A3.1. Calculation of composition from peak areas.

Let a standard mixture contain the following composition in mole %:

$$\begin{array}{ll} C_n & Y_1\ \% \\ C_m & Y_2\ \% \end{array}$$

let the peak area of compound C_n be A_1 at a given attenuation. and the area for C_m be A_2 at the same attenuation.
Let the sensitivity, or calibration constant, for C_n, which is used as a reference, be equal to unity, and for C_m equal to S, then:

$$\frac{A_{1/1}}{(A_{1/1}) + (A_{2/S})} = Y_1$$

and

$$\frac{A_{2/S}}{(A_{1/1}) + (A_{2/S})} = Y_2$$

which simplifies to

$$\frac{A_2\ Y_1}{A_1\ Y_2} = S.$$

A3.2. Calibration for product composition

Pure samples of the anticipated components of the reaction products were injected into the columns at the optimum analytical conditions (as stated in section 3.4.2) and their retention times noted. For different volumes of a particular gas injected into the column, the corresponding peak areas at different attenuations were measured.

Standard mixtures supplied by B.O.C. were used to determine the calibration constants for methane, ethylene, propylene and hydrogen. The standard mixtures had the following compositions in moles %;

Mixture A

CH_4
C_2H_4) 4% of
C_3H_8) each
C_3H_6
balance N_2.

Mixture B	
CH_4	5.4
C_2H_4	6.1
C_3H_8	4.0
C_3H_6	4.6
H_2	4.4
N_2	balance

The calibration constants for acetylene and ethane were obtained by mixing different amounts of ethane and acetylene with the standard mixtures. For example, a typical such made up mixture 'C' had the following composition:-

C_2H_6	3.5%
C_2H_2	2.5%
mixture B	94%

This gives an overall composition of mixture 'C' as followings in mole %:-

CH_4	5.08
C_2H_6	3.50
C_2H_4	5.73
C_2H_2	2.50
C_3H_8	3.76
C_3H_6	4.32
H_2	4.14
N_2	70.97

APPENDIX A3 CIRCUITS FOR PLATINUM FILM GAUGE AMPLIFIER AND POWER SUPPLY[52]

FIGURE A 3·1

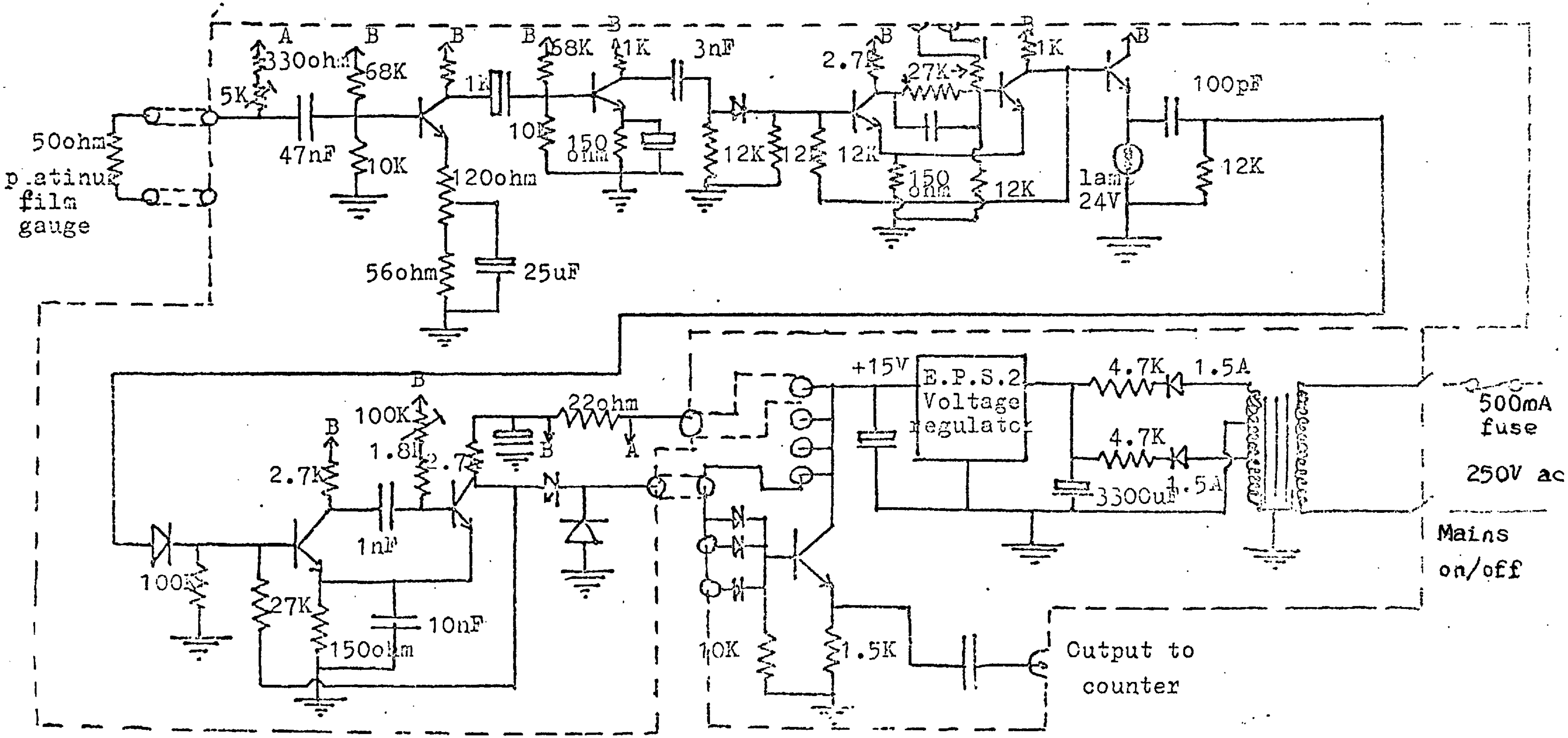

APPENDIX A3 CALIBRATION CURVE FOR TUNGSTEN RIBBON LAMP USED IN C_2 REVERSAL TEMPERATURE MEASUREMENTS[52]

FIGURE A3.2

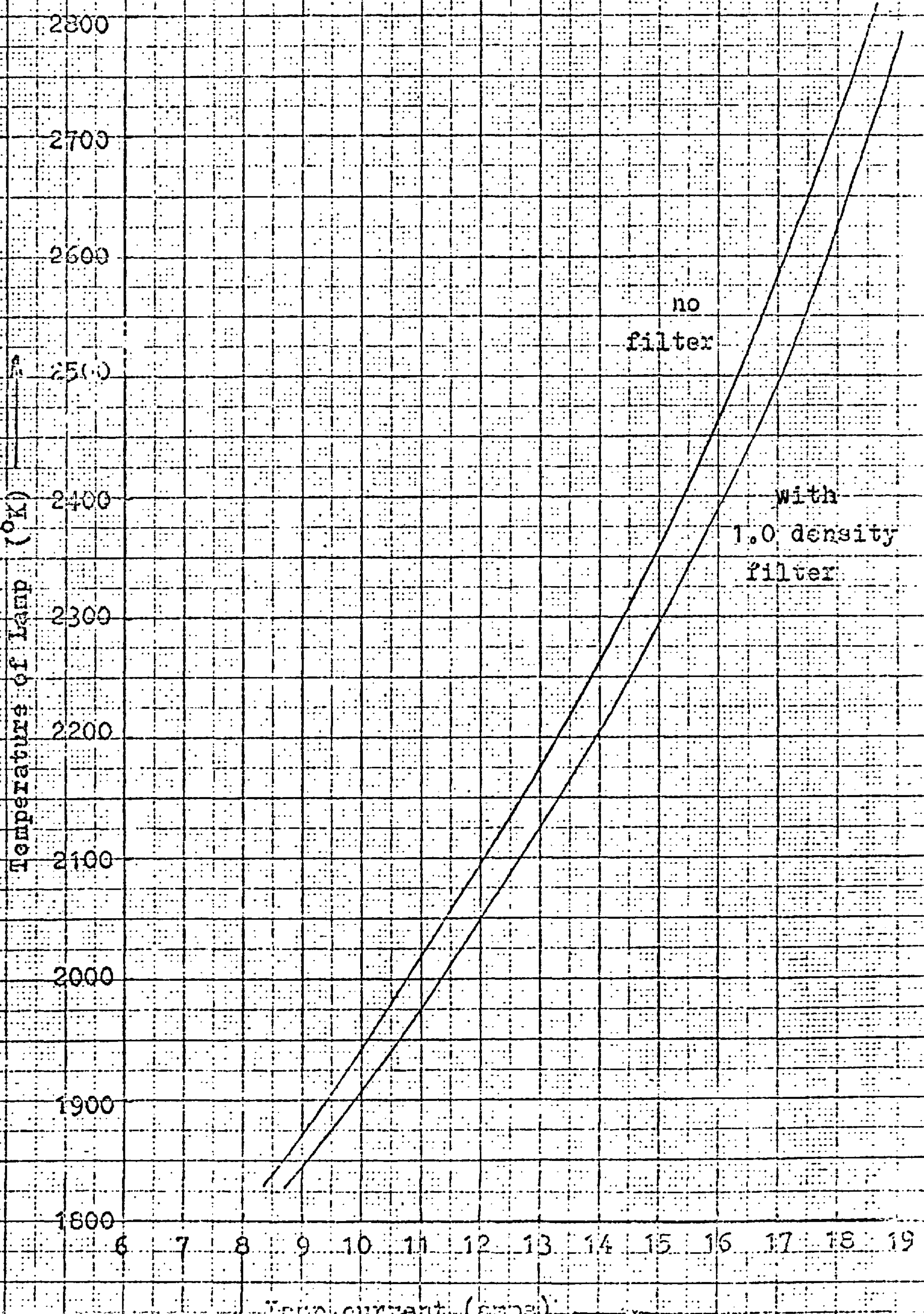

APPENDIX A4

Sample calculation of product distribution

In this appendix, is outlined two sets of sample calculation showing the method used in analysing the raw experimental data to yield the results tabulated in tables 4.1.

The first set of calculation (a) below was carried out for the reaction mixture recovered from pyrolysing pure C_3H_8 in argon, while the second set was performed for mixed feed when propane was diluted with small quantities of ethane. Table A 4.1 shows the raw experimental data used in these calculations.

Table A 4.1: RAW EXPERIMENTAL DATA

Run no.	Composition of pyrolysing mixture			P_1 torr	Temp. °K	Reaction time	Composition of shock treated mixture						
	C_3H_3	C_2H_6	Ar				CH_4	C_2H_6	C_2H_4	C_2H_2	H_2	C_3H_6	C_3H_8
91	4	-	96	250	1300	0.2	1.6	0.19	2.0	0.12	1.6	0.4	3.7
223	3.9	0.1	96	95	1450	0.1	1.16	0.20	2.10	0.18	1.6	0.3	0.9

a)

For each run, the material balance was performed on the recovered products (as shown in Tables A 4.1) and the hydrogen to carbon ratio determined. The formation of free 'carbon' was estimated from the balance deficit.

From table A 4.2, it can be seen that the ratio

$H/C = \frac{20.02}{7.08} = 2.83$, which is more than for pure propane ($8/3 = 2.67$). Thus, free "carbon" is formed in the pyrolysis. Let x be the atoms of free carbon formed, then the material

Table A.4.2: MATERIAL BALANCE TO DETERMINE H/C RATIO FOR RUN 91

Run no.	Component	Recovered gas analysis mole %	Material Balance		Moles of product per 100 moles of reacted C_3H_8
			C	H	
91	CH_4	1.26	1.26	5.04	50.4
	C_2H_6	0.19	0.38	1.14	7.6
	C_2H_4	2.0	4.0	8.0	80.0
	C_3H_6	0.4	1.2	2.4	16.0
	C_2H_2	0.12	0.24	0.24	4.8
	C_3H_8	3.7	-	-	-
	H_2	1.6	-	3.2	64.0
	Rest (Ar,N_2)	Rest	-	-	-
			Σ7.08	Σ20.02	

balance on carbon basis becomes 7.08 + x. By equating, the new hydrogen to carbon ratio to 2.67, the value of x could be determined.

Hence,

$$\frac{20.02}{7.08 + x} = 2.67$$

$$x = \underline{\underline{0.418}}$$

On this basis the amount of propane reacted, z =

$$\frac{7.08 + 0.418}{3.0} = \frac{20.02}{8.0} = \underline{\underline{2.50}}$$

and then, the number of moles of each product formed per 100 moles of reacted propane can be calculated, for example, the production of methane is,

$$\frac{1.26}{2.50} \times 100 = \underline{\underline{50.4}}$$

while the free 'carbon' atoms formed is,

$$\frac{0.418}{2.50} \times 100 = \underline{\underline{16.72}} \text{ g - atom per 100 moles of propane reacted.}$$

The percentage of propane decomposition is,

$$\frac{2.50}{2.5 + 3.7} \times 100 = 40.3$$

Yield of products, defined as mole % of C_3H_8 converted to product, is obtained by multiplying with a factor f_c. Where

$$f_c = \text{C atoms in product/(C atoms in test gas)}$$

For methane, f_c = 1/3 and ethane f_c = 2/3.

Hence yield of CH_4 = 50.4 x 1/3 = $\underline{\underline{16.8}}$

Product yield calculated on this basis was used in compiling table 4.1

b) Similar material balance was performed for run 223. For reaction mixture containing 3.9% C_3H_8, 0.1% C_2H_6 and 96.0 % argon, the H/C ratio for propane based on 100 moles of gas recvered after shock-heating will be

$$\frac{\Sigma H - 6y}{\Sigma C - 2y} = 8/3$$

where y is the amount of ethane in 100 moles of the feed. In this case y = 0.1

$\therefore$ H/C ratio is $\dfrac{\Sigma H - 0.6}{\Sigma C - 0.2}$ and from table A4.3 ,

$$H/C = \frac{19.6 - 0.6}{7.02 - 0.2} = 2.79.,$$ which

is more than 2.67 for propane. Thus free 'carbon ' is formed and can be estimated as before,

$$\frac{19.0 - 0.6}{(7.02 - 0.2) + x} = \frac{19.0}{6.82 + x} = 2.79, \quad x = 0.3$$

Hence z , moles of propane converted is

$$\frac{19.0}{8} \approx \frac{7.12}{3} = 2.38$$

Therefore % propane decomposed $= \dfrac{2.38}{2.38 + 0.9} \times 100 = 72.5$

Moles of product formed per 100 moles of propane reacted is calculated as before, for example,

$$\text{acetylene produced} = \frac{0.18}{2.38} \times 100 = 7.56$$

The amount of C_2H_6 formed from propane pyrolysis is (0.2 - 0.1) i,e (0.1/2.38) x 100 = 4.2 moles.

Product yield was obtained as before by multiplying by f_c, in this case f_c for CH_4 is 1/5, and 2/5 for C_2H_4 , etc.

Table A4.3: Material balance for determining H/C ratio for Run 223.

Run no.	Component	Recovered gas analysis moles %	Material balance		Moles of product per 100 moles of C_3H_8 reacted.
			C	H	
223	CH_4	1.16	1.16	4.64	48.73
	C_2H_6	0.2	0.4	1.20	4.2
	C_2H_4	2.10	4.20	8.4	88.2
	C_3H_6	0.3	0.90	1.80	12.6
	C_2H_2	0.18	0.36	0.36	7.56
	C_3H_8	0.9	-	-	
	H_2	1.6	-	3.2	67.2
	Rest(Ar,N_2)	Rest	-	-	
			$\sum$ 7.02	$\sum$ 19.6	

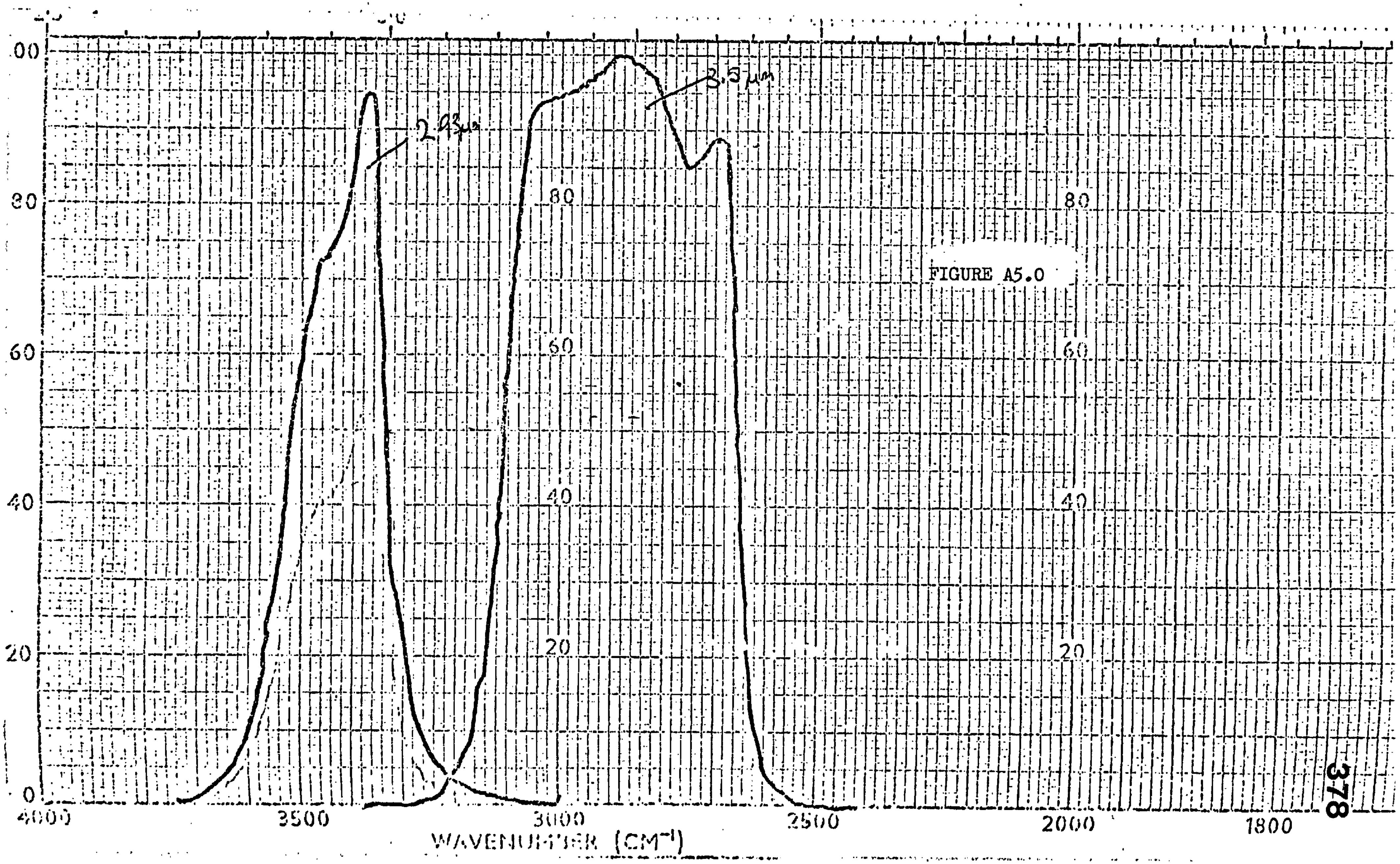

100
80
60
40
20
0
80
60
40
20
80
60
40
20
2.93μm
3.5μm
4000
3500
3000
2500
2000
1800
WAVENUMBER (CM^{-1})

FIGURE A5.0

THIN FILM PRODUCTS
WALTHAM, MASSACHUSETTS

Filter No. 3.1
Date 6-26-85
Calibration (1) ccs @ 3.167 Polystyrene
Full Scale 100 Ambient Temp 25°C
Instrument Beckman IR- 4

FIGURE A5.0 CONTD.

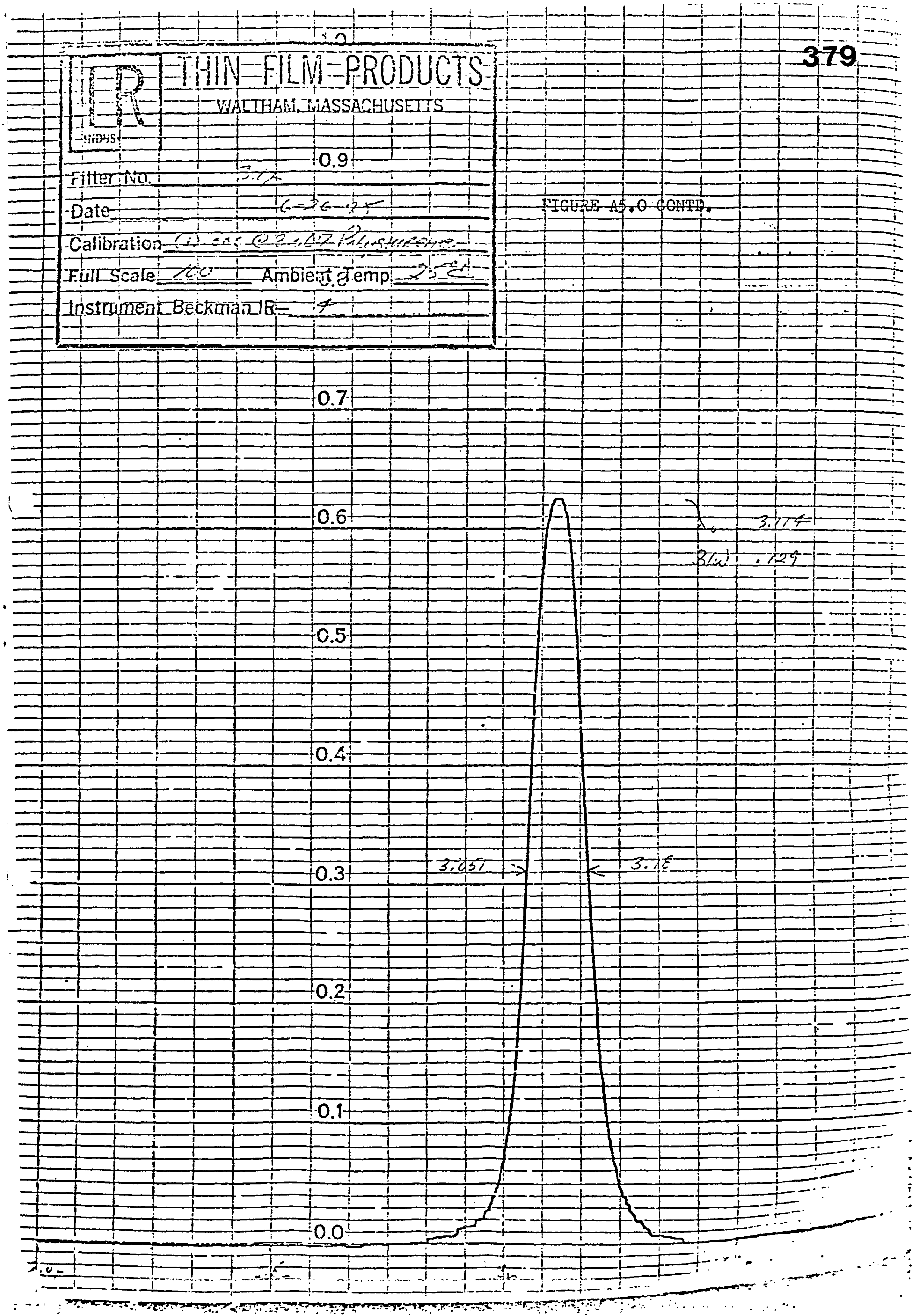

λ₀ 3.114
BW .129

IR THIN FILM PRODUCTS
WALTHAM, MASSACHUSETTS

Filter No. [illegible]
Date 6-26-65
Calibration [illegible]
Full Scale 100 Ambient Temp. 25°C
Instrument Beckman IR- 4

FIGURE A5.0 CONTD.

λ	B/W	Half
2.93	0.16	2.85 → 3.01
3.114	0.13	3.051 → 3.18
3.28	0.15	3.205 → 3.355

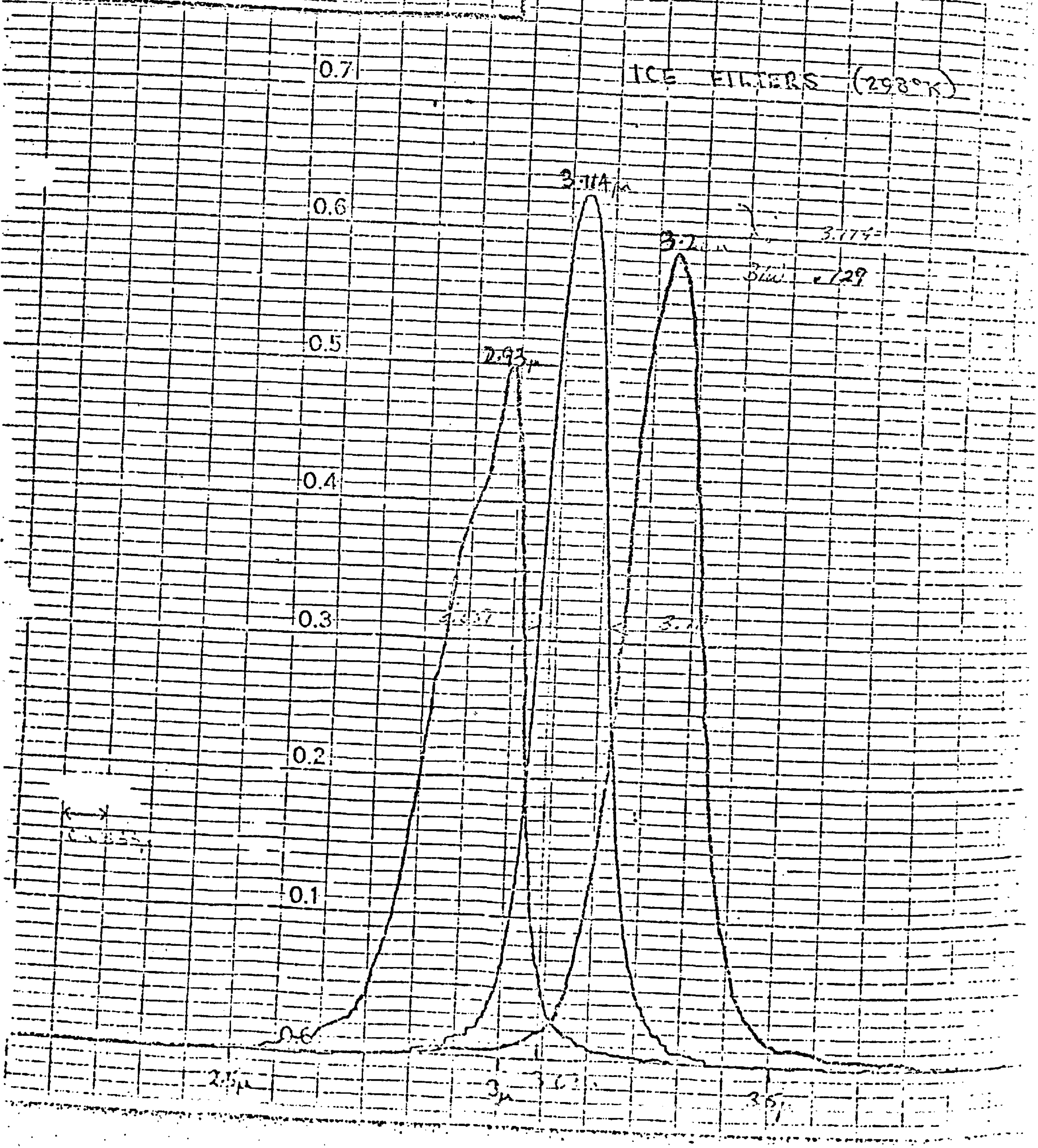

APPENDIX A5 CIRCUIT OF D.C. AMPLIFIER FOR ORP. 13 PHOTOCONDUCTIVE CELL FIGURE A5.1

GAIN = 430 for INPUT IMPEDANCE = 47K

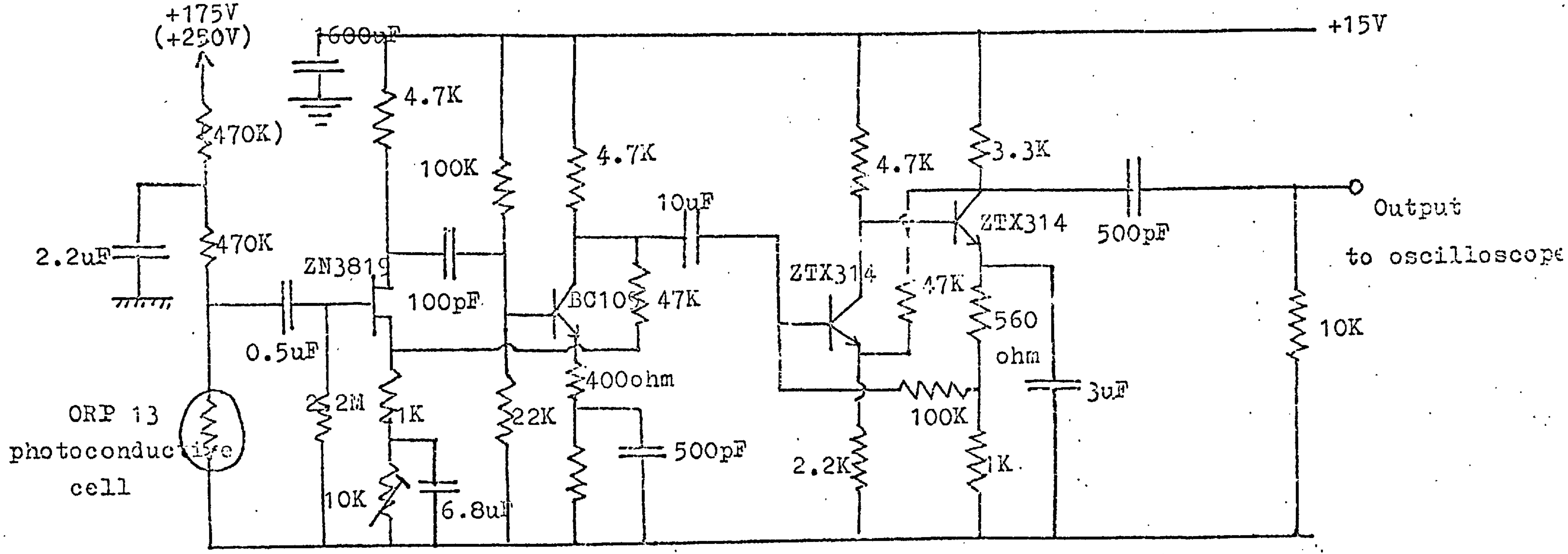

ERRATA

Page 46, 6th line

Insert; There are also extensive studies ....

Page 79, Equation (2.1.6)

FOR $\rho_1 U_1^2 = \rho_2 U_2^2$

READ $P_1 + \rho_1 U_1^2 = P_2 + \rho_2 U_2^2$

Page 85, Equation (3.3.6)

FOR P_5 READ ρ_5

Page 138, 2nd paragraph 10th line

FOR methane READ 'carbon'

Page 149, last line

FOR table 4.1 READ table 4.3

Page 169, Table 4.5 2nd column 4th line

FOR 500 READ 5000

Page 207, Table 5.1, 2nd column 1st line

FOR As compound READ As in compound

Page 272

FOR

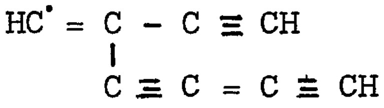

$$\begin{array}{l} HC^{\bullet}=C-C\equiv CH \\ \phantom{HC^{\bullet}=}| \\ \phantom{HC^{\bullet}=}C\equiv C=C\equiv CH \end{array}$$

READ

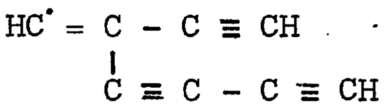

$$\begin{array}{l} HC^{\bullet}=C-C\equiv CH \\ \phantom{HC^{\bullet}=}| \\ \phantom{HC^{\bullet}=}C\equiv C-C\equiv CH \end{array}$$

Page 335, Table 7.6, 5th column at $T = 2141^{\circ}K$

FOR 6.3 READ 0.3

Page 352 , conclusion 9)

FOR at 3.30µm towards ....,READ to 3.30µm from......,

Page 373, Appendix A4 , Table A4.1, 8th column for Run No. 91

FOR 1. 6 READ 1.26

Erratum

Page 48, ~~3rd~~ 5th line in the 3rd paragraph

They observed that the activation energy increases with increasing propane conversion.

Page 194

(ii) two dreschel bottles (B1,B2) containing concentrated (70%) sulphuric acid to remove PH_3 and other hydride impurities (AsH_3, H_2S, etc) from the acetone-free gas from (i).

(iii) one dreschel bottle (B3) containing aqueous (15%) potassium hydroxide solution to remove CO_2 and acidic impurities; and bubbler (B4) containing potassium permanganate solution to oxidise ~~oxide~~ further any impurities - especially non-metallic hydrides - not removed in (ii).